

**STUDIES ON THE ELECTRICAL PROPERTIES OF  
SOME CRYSTALLINE ORGANIC COMPOUNDS  
AND CONDUCTING POLYMERS**

**N. C. SANTHAKUMARI**

Thesis submitted to  
Cochin University of Science and Technology  
in partial fulfilment of the requirements  
for the Award of the Degree of  
**DOCTOR OF PHILOSOPHY**  
in the Faculty of Science

**DEPARTMENT OF PHYSICS  
COCHIN UNIVERSITY OF SCIENCE AND TECHNOLOGY  
COCHIN - 682 022**

**FEBRUARY 1992**

**TO MY PARENTS**

**CERTIFICATE**

Certified that the research work presented in this thesis is based on the original work done by Mrs.N.C.Santhakumari under my guidance in the Department of Physics, Cochin University of Science and Technology, and has not been included in any other thesis submitted previously for the award of any degree.



**Prof.(Dr.) C.P.Girijavallabhan  
Supervising Teacher**

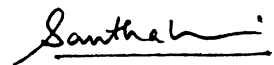
Cochin 682 022

15th Feb., 1992

**DECLARATION**

I hereby declare that the work presented in this thesis is based on the original work done by me under the supervision of Prof.(Dr.)C.P.Girijavallabhan, in the Department of Physics, Cochin University of Science and Technology and no part of this thesis is included in any other thesis previously submitted for the award of any other degree.

Cochin 682 022  
15th Feb., 1992



**N.C.Santhakumari**

## CONTENTS

	<u>Page</u>
PREFACE	i
ACKNOWLEDGEMENT	vii
 <b>PART I: STUDIES ON THE ELECTRICAL PROPERTIES OF SOME ETHYLENEDIAMMONIUM SALTS</b>  	
<b>Chapter 1</b>	<b>IONIC CONDUCTION IN SOLIDS—AN OVERVIEW</b>
1.1	Introduction
1.2	Theory of ionic conductivity
1.3	Ionic conductivity of crystals containing aliovalent impurities
1.4	Dielectric properties
1.5	Phase transitions in solids
1.6	Protonic conductors
1.7	Mechanism of protonic conduction
1.8	Protonic conduction in ammonium salts
1.9	Protonic conduction in substituted ammonium salts
1.10	Applications of protonic conductors
1.11	References
<b>Chapter 2</b>	<b>EXPERIMENTAL METHODS</b>
2.1	Introduction
2.2	Preparation of materials
2.3	A shielded cell for electrical measurements
2.4	Methods of measurement
2.5	Differential scanning calorimetry
2.6	References

<b>Chapter 3</b>	<b>ELECTRICAL CONDUCTIVITY AND DIELECTRIC CONSTANT IN ETHYLENEDIAMMONIUM DICHLORIDE CRYSTALS</b>	55
3.1	Introduction	56
3.2	Experimental	58
3.3	Experimental results	59
3.4	Discussion	65
3.5	References	74
<b>Chapter 4</b>	<b>ELECTRICAL PROPERTIES AND PHASE TRANSITIONS IN ETHYLENEDIAMMONIUM DINITRATE</b>	76
4.1	Introduction	77
4.2	Experimental	79
4.3	Experimental results	81
4.4	Discussion	88
4.5	Conclusions	103
4.6	References	104
<b>Chapter 5</b>	<b>ELECTRICAL CONDUCTIVITY, DIELECTRIC PROPERTIES AND PHASE TRANSITIONS IN ETHYLENEDIAMMONIUM SULPHATE SINGLE CRYSTALS</b>	107
5.1	Introduction	108
5.2	Experimental	108
5.3	Experimental results	111
5.4	Discussion	121
5.5	References	132
<b>Chapter 6</b>	<b>TEMPERATURE DEPENDENT VARIATION OF ELECTRICAL PROPERTIES IN ETHYLENEDIAMMONIUM ACID PHOSPHATE</b>	135
6.1	Introduction	136
6.2	Experimental	138

6.3	Experimental results	140
6.4	Discussion	148
6.5	References	158
<b>Chapter 7</b>	<b>A COMPARATIVE STUDY OF EXPERIMENTAL RESULTS FOR ETHYLENEDIAMMONIUM SALTS AND CONCLUSIONS</b>	<b>160</b>
7.1	Choice of materials	161
7.2	dc conductivity	162
7.3	ac conductivity	170
7.4	Dielectric constant	170
7.5	Phase transitions in ethylenediammonium salts	171
7.6	Conclusions	172
7.7	References	174
 <b>PART II: STUDIES ON THE ELECTRICAL PROPERTIES OF POLY(META-TOLUIDINE) AND POLY(ANILINE CO-META-TOLUIDINE)</b>		
<b>Chapter 8</b>	<b>CONDUCTING POLYMERS--AN OVERVIEW</b>	<b>176</b>
8.1	Introduction	177
8.2	Types of conducting polymers	177
8.3	Polyaniline	179
8.4	Substituted polyaniline	183
8.5	Theories of electrical conduction in conducting polymers	185
8.6	Applications of conducting polymers	191
8.7	References	196

<b>Chapter 9</b>	<b>EXPERIMENTAL METHODS ADOPTED FOR THE STUDY OF CONDUCTING POLYMERS</b>	<b>204</b>
9.1	Introduction	205
9.2	Synthesis of polymers	206
9.3	Purification of polymer base	208
9.4	Doping	209
9.5	Characterisation of the material	210
9.6	References	212
<b>Chapter 10</b>	<b>ELECTRICAL CONDUCTIVITY AND DIELECTRIC CONSTANT OF POLY(META-TOLUIDINE)</b>	<b>214</b>
10.1	Introduction	215
10.2	Experimental	217
10.3	Experimental results and discussion	219
10.4	References	237
<b>Chapter 11</b>	<b>ELECTRICAL PROPERTIES OF POLY(ANILINE CO-META-TOLUIDINE)</b>	<b>238</b>
11.1	Introduction	239
11.2	Experimental	240
11.3	Experimental results and discussion	244
11.4	Conclusions	291
11.5	References	292
<b>Chapter 12</b>	<b>SUMMARY AND CONCLUSIONS</b>	<b>296</b>

\* \* \*

## PREFACE

Solid electrolytes for applications like chemical sensing, energy storage, and conversion have been actively investigated and developed since the early sixties. Although of immense potential, solid state protonic conductors have been ignored in comparison with the great interest that has been shown to other ionic conductors like lithium and silver ion conductors. The non-availability of good, stable protonic conductors could be partly the reason for this situation. Although organic solids are better known for their electrical insulating character, ionic conductors of organic origin constitute a recent addition to the class of ionic conductors. However, detailed studies on such conductors are scarce. Also the last decade has witnessed an unprecedented boom in research on organic "conducting polymers". These newly devised materials show conductivity spanning from insulator to metallic regimes, which can be manipulated by appropriate chemical treatment. They find applications in devices ranging from rechargeable batteries to "smart windows".

This thesis mainly deals with the synthesis and investigations on the electrical properties of (i) certain

organic protonic conductors derived from ethylenediamine and (ii) substituted polyanilines.

The dissertation is divided into two parts. Part I deals with the synthesis, characterisation, electrical properties and phase transitions of four ethylenediammonium salts viz., ethylenediammonium dichloride (EDC), ethylenediammonium dinitrate (EDN), ethylenediammonium sulphate (EDS) and ethylenediammonium acid phosphate (EDAP). The objective was to assess the influence of the anions on their electrical properties and to evolve an understanding of the conduction mechanism in these organic solid state protonic conductors.

Part II of the thesis describes the synthesis of poly(meta-toluidine) and copolymers of aniline with meta-toluidine formed under different monomer feed ratios and a comparative study of the electrical properties of carefully purified poly(meta-toluidine) and poly(aniline co-meta-toluidine) at different levels of proton doping.

Part I of the dissertation is divided into six chapters. The First Chapter is an overview of the electrical conduction in ionic solids with special

reference to protonic conduction in ammonium salts. The Second Chapter outlines the synthesis of materials, formation of single crystals and the methods of measurements. The results of the studies of the thermal and electrical properties of EDC form the content of the Third Chapter. Chapter 4 presents the preparation and measurement of electrical properties of EDN. Chapters 5 and 6 contain results of the studies on EDS and EDAP respectively. The influence of the nature of anion on the electrical properties of EDC, EDN, EDS and EDAP are discussed in Chapter 7.

Part II of the thesis consists of five chapters, beginning with Chapter 8, which describes the present status of research on organic conducting polymers, with special reference to polyaniline. The methods of synthesis, purification and doping of poly(meta-toluidine) and poly(aniline co-meta-toluidine) are outlined in Chapter 9. The characterization of poly(meta-toluidine) by dc and ac electrical conductivities, dielectric constant, DSC, and infrared and UV-Visible spectroscopy is presented in Chapter 10. Chapter 11 embodies the methods of synthesis, and characterization of poly(aniline co-meta-toluidine) prepared under different monomer feed ratios by DSC, dc and ac electrical conductivities and

dielectric constant. Chapter 12 is the last chapter of the thesis and is a comparison of properties of poly(meta-toluidine) and poly(aniline co-meta-toluidine). In interpreting the results of electrical measurements, efforts were made to elucidate the mechanism of conduction in insulating as well as in conducting materials described in the foregoing chapters.

Part of the results presented in this thesis have been published/presented/communicated in form of the following papers:

1. dc electrical conductivity studies in pure, doped and deuterated potassium acid phthalate  
Hazeena George, N.C.Santhakumari, R.Navilkumar and C.P.G.Vallabhan  
Proceedings of the XIX National Seminar on Crystallography, Mahatma Gandhi University, Kottayam, Paper No.D-15 (1987).
2. dc electrical conductivity of polyaniline conducting plastic  
N.C.Santhakumari and C.P.G.Vallabhan  
Proceedings of the National Symposium on Current Trends in Pure and Applied Physics, Cochin University of Science and Technology, Paper No.M-34 (1988).

3. Fabrication and performance of a micro-gas coulometer for the detection of protonic conduction in solids.  
N.C.Santhakumari and C.P.G.Vallabhan  
Proceedings of the National Seminar on Instrumentation, Cochin University of Science and Technology, Cochin, Paper No.P-33 (1989).
  
4. Electrical conductivity and phase transition in ethylenediammonium dichloride  
N.C.santhakumari, R.Navilkumar and C.P.G.Vallabhan  
Proceedings of the Solid State Physics Symposium, Indian Institute of Technology, Madras, Paper No.P-19 (1989).
  
5. High temperature phase transition in ethylenediammonium sulphate single crystals  
N.C.Santhakumari, R.Navilkumar and C.P.G.Vallabhan  
Proceedings of the Second Annual General Meeting of the Materials Research Society of India, National Physical Laboratory, New Delhi (1991).
  
6. Dielectric studies of ethylenediammonium acid phosphate single crystals.  
N.C.Santhakumari, R.Navilkumar and C.P.G.Vallabhan

Proceedings of the Second Annual General Meeting of the Materials Research Society of India, National Physical Laboratory, New Delhi (1991).

7. Electrical properties and phase transitions in ethylenediammonium dinitrate.

N.C.Santhakumari and C.P.G.Vallabhan

Solid State Ionics, **45** (1991) 329.

8. Electrical conductivity, dielectric properties and phase transition in ethylenediammonium sulphate single crystals.

N.C.Santhakumari and C.P.G.Vallabhan

Journal of Physics and Chemistry of Solids (in press).

## ACKNOWLEDGEMENT

The work presented in this thesis was carried out in the Solid State Electronics Laboratory, Department of Physics, Cochin University of Science and Technology during 1988-91 under the supervision of Prof.(Dr.)C.P.Girijavallabhan. But for his invaluable guidance, unflinching support and constant encouragement, successful completion of this work would not have been possible. I have great pleasure to express my sincere gratitude to him for giving me an opportunity to work with him and for his inspiring guidance throughout the course of this work.

I am extremely thankful to Prof.(Dr.)M.G.Krishna Pillai, former Head of the Department and Prof.(Dr.)K.Babu Joseph, Head of the Department of Physics for their keen interest in my work.

I am also grateful to Prof.(Dr.)K.L.Sebastian and Prof.(Dr.)P.Madhavan Pillai for granting me permission to use the computer and laboratory facilities of the Department of Applied Chemistry.

An undertaking of this type requires the cooperation and help of many individuals. I sincerely acknowledge the timely help offered by the following persons:

- Dr.R.Navilkumar for his valuable suggestions and unflinching support,
- Mr.Edwin Xavier and Mr.K.Vidyalal for their kind cooperation,

- Dr.P.S.Harikumar, Mr.P.Narayanan, Mr.K.C.Philip and Miss K.Sumithra for their help during my work in the Applied Chemistry Laboratory,
- the administrative and technical staff of the Department of Physics for their prompt action, and
- the engineers and technicians of the USIC for the fabrication and timely repair of the instrumental facilities.

I would like to acknowledge my deepfelt gratitude to Sri K.P.Narayana Panicker, General Secretary and Sri N.Sivasankaran Nair, Education Secretary of the N.S.S.College's Central Committee for granting me deputation to pursue these studies.

I am thankful to Prof.P.Chandrasekharan, former Principal, Prof.P.R.C.Nair, Principal, N.S.S.Hindu College, Changanacherry and to my colleagues in the Department of Physics for their keen interest and kind cooperation in my research work.

The grant of a Teacher Fellowship under the Faculty Improvement Programme by the University Grants Commission, New Delhi is gratefully acknowledged.

Finally I would like to thank Mr.K.P.Sibiraj for neatly typing this thesis.

**N.C.SANTHAKUMARI**

PART I

STUDIES ON THE ELECTRICAL PROPERTIES OF SOME  
ETHYLENEDIAMMONIUM SALTS

## Chapter 1

### IONIC CONDUCTIVITY IN SOLIDS - AN OVERVIEW

#### Abstract

This chapter outlines briefly the theory of ionic conductivity in solids. Effect of phase transitions on the electrical properties of ionic solids is discussed at some length. Occurrence of protonic conductivity in different materials has been reviewed exhaustively. Special reference has been made to protonic conductivity in ammonium salts. The major applications of solid state protonic conductors have been summarised to project their importance in modern technology.

## 1.1 INTRODUCTION

The demand for materials showing high ionic conductivity for various applications in devices has given a new impetus to research in solid state ionic conductors. Our present knowledge of these materials is based on the early work of Schottky [1], Wagner [2], and Mott and Littleton [3,4]. It was found that the transference of mass and charge occurring in alkali halide crystals is mainly by means of ionic processes. Later the subject of ionic conductivity was expounded at length by Lidiard [5-7], Fuller [8-13], Barr [14,15] and Franklin [16]. In addition to these some other notable works [17-34] can also be found in the literature.

Most of the earlier work in ionic conductivity is centred around the alkali halides. The results of Kelting and Witt [35] can be considered as typical for the behaviour of conductivity as a function of temperature. The principal feature of their results is a straight line variation of  $\log \sigma$  against  $1/T$  for the high purity case and an approximate straight line for a low temperature highly doped case. The first of these regions is referred to as the intrinsic region since the conduction properties are those of chemically pure crystal, the second region

is called extrinsic since the conductivity depends on the nature and concentration of impurities. An approximate empirical relation for the conductivity can be written as

$$\sigma = \sigma_e + \sigma_i \quad (1.1)$$

$$= \sigma_{oe} \exp(-E_e/kT) + \sigma_{oi} \exp(-E_i/kT) \quad (1.2)$$

where  $E_e$  and  $E_i$  are the conduction activation energies for the extrinsic and intrinsic regions respectively. The constant  $\sigma_{oe}$  depends on the impurity content while  $\sigma_{oi}$  depends only on the host crystal. One would therefore expect  $\sigma_{oe}/\sigma_{oi}$  to be much less than unity, and of the order of impurity fraction; this is borne out experimentally. It is also found from experiment that  $E_e/E_i \approx \frac{1}{2}$ ; this is explained by noting that  $E_e$  should be the activation energy for the motion of extrinsically introduced defects, while  $E_i$  contains in addition the activation energy for creation of the defect within the originally perfect crystal.

The simplest type of thermally generated lattice defects which are used to explain the conductivity of ionic solids are Frenkel and Schottky defects. In the formation of a Frenkel defect an ion, which is originally at a site

of the perfect lattice moves to an interstitial position, the net result of the process is to generate two imperfections—a vacant lattice site and an interstitial ion. A Schottky defect is formed by the migration of an ion which was originally at a site of the perfect lattice to a surface position, the net result of this is to generate only one imperfection—the vacant lattice site. The other type of defects usually found in ionic crystals are: impurity ions, impurity-vacancy complexes and impurity-vacancy pairs.

## 1.2 THEORY OF IONIC CONDUCTIVITY

Consider the case of ionic conductivity in a sodium chloride lattice in which vacancies are made to move under an applied electric field. In a one dimensional model the vacancies migrating in the lattice do so by a series of jumps of distance 'a' from one position to the next over a potential barrier. The potential barriers are all the same and equilibrium positions are equivalent. It can be shown from classical statistical mechanics [5] that the probability per unit time for a vacancy to make the transition to a neighbouring equilibrium position is given by

$$\omega = \nu_0 \exp(-\Delta g/kT) \quad (1.3)$$

where  $\nu_0$  is a frequency which is interpreted as the vibrational frequency of the ions surrounding the vacancy and  $\Delta g$  is the Gibb's free energy of activation. The Gibb's free energy can be written in terms of the corresponding enthalpy  $\Delta h$  and entropy  $\Delta s$  as

$$\Delta g = \Delta h - T\Delta s \quad (1.4)$$

Now consider the case of a cation vacancy (effective charge  $-e$ ) moving from one equilibrium position to another in the presence of a uniform field  $F$  directed along the  $x$ -axis (Fig.1.1), the effect of the field is to add a term  $eFa$  to the potential energy. A jump in the direction of the field now takes place with a decreased probability.

$$\omega' = \nu_0 \exp[(\Delta g + eFa/2)/kT] \quad (1.5)$$

and jump against the field with increased probability

$$\omega'' = \nu_0 \exp[-(\Delta g - eFa/2)/kT] \quad (1.6)$$

The mean drift velocity  $u$  (in the direction of positive current flow) is therefore given by

$$\begin{aligned} u &= a(\omega'' - \omega') \\ &= a \nu_0 \exp(-\Delta g/kT) \times 2 \sinh(eFa/2kT) \end{aligned} \quad (1.7)$$

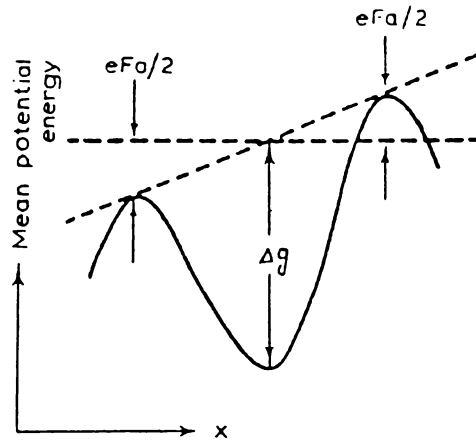


Fig.1.1 Schematic representation of the mean potential energy of a cation vacancy with an electric field in the  $x$ -direction.

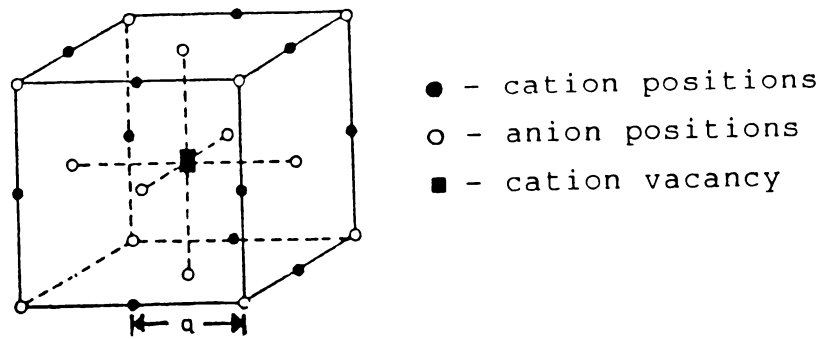


Fig.1.2 Illustration of the possible jumps for a cation vacancy to the nearest neighbour cation positions in an NaCl-type lattice.

For low field strength, we assume  $eFa \ll kT$  and we get

$$u = (a^2 e \gamma_0 / kT) \exp(-4g/kT) \quad (1.8)$$

which corresponds to mobility

$$\mu = (a^2 e \gamma_0 / kT) \exp(-4g/kT) \quad (1.9)$$

Equation (1.8) holds for a one dimensional model. For the motion of a cation vacancy in a three dimensional model we refer to Fig.1.2. Consider the electric field to be applied in (100) direction. The central cation vacancy can jump to any one of the twelve nearest neighbour cation sites, each of which is at a distance of  $a\sqrt{2}$  away from the vacancy. The electric field makes no change in the energy requirement for a jump in the transverse direction, nor do these jumps cause any flow of current. Of the remaining eight possible jumps, four are in the field direction. The only change in the equations (1.7), (1.8) and (1.9) is therefore the appearance of a factor 4.

Hence equation (1.9) will now read

$$\mu = (4a^2 e \gamma_0 / kT) \exp(-4g/kT) \quad (1.10)$$

Now the discussion on the density of mobile species falls into two parts viz., those corresponding to intrinsic and extrinsic regions of conduction.

If  $n_{AV}$  and  $n_{CV}$  be the densities of the anion and cation vacancies respectively and  $N$  be the density of possible vacancy sites, then from statistical thermodynamics,

$$(n_{AV}/N)(n_{CV}/N) = \exp(-g_s/kT) \quad (1.11)$$

where  $g_s$  is the Gibb's free energy of formation of a pair of Schottky defects.

Now the intrinsic conductivity can be written as

$$\sigma_i = n_{AV} e \mu_{AV} + n_{CV} e \mu_{CV} \quad (1.12)$$

$$= \frac{4N a^2 e^2}{kT} \exp(-g_s/kT) \times [ \mu_{AV} \exp -(\Delta g_{AV}/kT) + \mu_{CV} \exp - (\Delta g_{CV}/kT) ] \quad (1.13)$$

Considering  $\Delta g_{CV} \ll \Delta g_{AV}$ , so that to a high degree of approximation, only the cation vacancies move. Making

approximate definitions of Gibb's free energy in terms of enthalpy and entropy

$$g_s = h_s - TS_s \quad (1.14)$$

and

$$\Delta g_{CV} = \Delta h_{CV} - T\Delta S_{CV} \quad (1.15)$$

we have

$$\sigma_i = \frac{4Nae^2 \nu_{CV}}{kT} \exp[(4S_{CV} + S_s/2)/k] \times \exp[(\Delta h_{CV} + h_s/2)/kT] \quad (1.16)$$

Equation (1.16) is valid only for cubic crystals of alkali halide type. If both anions and cations are mobile, then the approximation made in deriving equation (1.16) from (1.13) is not valid. In comparison with the experimental data, it is possible that contributions to current from all sources except Schottky defects have been ignored.

### 1.3 IONIC CONDUCTIVITY OF CRYSTALS CONTAINING ALIOVALENT IMPURITIES

In ionic crystals, there is an opportunity to create a rather unique defect complex by the introduction

of aliovalent impurities, i.e., impurity ions which differ in charge from the corresponding solvent ion. When such impurities are introduced, additional defects (either vacancies or interstitial ions) must accompany the aliovalent ion in order to achieve charge compensation, the defect possessing an effective charge equal but opposite to that of impurity ion.

We shall consider the effect of divalent cationic impurities in an ionic crystal of the alkali halide type. The conductivity in the impurity sensitive region can be called extrinsic conductivity ( $\sigma_e$ ). In equation (1.11)  $n_{AV}$  and  $n_{CV}$  are no longer equal but are subject to the condition

$$n_{CV} = n_{AV} + n_I \quad (1.17)$$

where  $n_I$  is the density of divalent cationic impurities.

Hence knowing equation (1.11)

$$\frac{n_{CV}}{N} \frac{(n_{CV} - n_I)}{N} = \exp(-g_s/kT) \quad (1.18)$$

which is a quadratic equation in  $n_{CV}$  whose solution is

$$n_{CV} = \frac{n_I}{2} \left[ 1 + \left\{ 1 + \frac{4N^2 \exp(-g_s/kT)}{n_I^2} \right\}^{\frac{1}{2}} \right] \quad (1.19)$$

The conductivity is therefore given by

$$\sigma_e = n_{AV} e \mu_{AV} + n_{CV} e \mu_{CV} \quad (1.20)$$

$$= Ne(\mu_{AV} + \mu_{CV}) \exp(-g_s/2kT) \times$$

$$\left[ \left\{ 1 + \frac{n_I^2}{4N^2 \exp(-g_s/kT)} \right\}^{\frac{1}{2}} + \right.$$

$$\left. \frac{n_I}{2N \exp(-g_s/kT)} \frac{\mu_{CV} - \mu_{AV}}{\mu_{CV} + \mu_{AV}} \right] \quad (1.21)$$

from equations (1.18) and (1.19). Recalling that the intrinsic conductivity (1.13) is equivalent to

$$\sigma_i = Ne(\mu_{AV} + \mu_{CV}) \exp(-g_s/kT) \quad (1.22)$$

We have from (1.21)

$$\sigma_e = \sigma_i \frac{n_I}{N \exp(-g_s/kT)} \frac{\mu_{CV}}{\mu_{CV} + \mu_{AV}} \quad (1.23)$$

In deriving equation (1.23) we assumed that

$$n_I \gg 2N \exp(-g_s/2kT)$$

If we assume that  $\mu_{CV} \gg \mu_{AV}$ , equation (1.23) reduces to

$$\sigma_e = n_I e \mu \quad (1.24)$$

which is a quite obvious result in view of approximations. Using equations (1.10) and (1.24) we obtain

$$\sigma_e = \frac{4n_I a^2 e^2 \mu_{CV}}{kT} \exp\left(\frac{\Delta S_{CV}}{k}\right) \exp(-\Delta h_{CV}/kT) \quad (1.25)$$

which is approximately of the empirical form

$$\sigma_e = \sigma_{oe} \exp(-E_e/kT). \quad (1.26)$$

A comparison of equations for the intrinsic and extrinsic conductivities [equations (1.16) and (1.25)] is very much useful for explaining the experimentally observed orders of magnitude of the ratios  $\sigma_{oe}/\sigma_{ie}$  and  $E_e/E_i$ .

#### 1.4 DIELECTRIC PROPERTIES

The dielectric properties of a material depends on its interaction with an applied electric field at the electronic, atomic and molecular level. Polarisation and dielectric loss are the phenomena of interest and usually studied as a function of frequency.

When an electric field is applied to a dielectric material, the dipole moments of separate kinetic elements or atomic groups will tend to orient in the field direction. If the field is removed after a certain time, induced polarisation of the sample will diminish to zero as a result of thermal motion of separate kinetic elements, and the system will return to its previous equilibrium (or quasi-equilibrium) state. Such a process of reverting to equilibrium is called dielectric relaxation. It is characterised by the relaxation time  $\tau$ .

If an alternating electric field is applied to the material, the dielectric properties will depend on the frequency of the applied potential and the dielectric relaxation time  $\tau$ .

The dielectric properties of a material can be expressed by its complex dielectric constant (relative permittivity)

$$\epsilon^* = \epsilon' - i\epsilon'' \quad (1.27)$$

where  $\epsilon'$  and  $\epsilon''$  are the real and imaginary parts of the complex dielectric constant.  $\epsilon''$  is also known as the dielectric loss factor. The ratio

$$\frac{\epsilon''}{\epsilon'} = \tan \delta \quad (1.28)$$

is the dielectric loss tangent. It characterises the phase shift between the ac signal applied across a capacitor with the sample as the dielectric and the current passing through it.

If the dielectric relaxation can be described by a single relaxation time, then

$$\epsilon' = \epsilon_{\infty} + \frac{\epsilon_0 - \epsilon_{\infty}}{1 + \omega^2 \tau^2} \quad (1.29)$$

$$\epsilon'' = \frac{(\epsilon_0 - \epsilon_{\infty})\omega\tau}{1 + \omega^2 \tau^2}, \quad \text{and} \quad (1.30)$$

$$\tan\delta = \frac{(\epsilon_0 - \epsilon_\infty) \omega \tau}{\epsilon_0 + \epsilon_\infty \omega^2 \tau^2} \quad (1.31)$$

where  $\epsilon_0$  is the dielectric constant at  $\omega = 0$  and  $\epsilon_\infty$  the dielectric constant at  $\omega = \infty$

If  $\epsilon_0$  is the static dielectric constant,  $\epsilon_r$  the relative permittivity,  $\omega$  the angular frequency and  $\tan\delta$  the loss tangent, the ac conductivity  $\sigma_{ac}$  may be expressed [36]

$$\sigma_{ac} = \epsilon_0 \epsilon_r \omega \tan\delta \quad (1.32)$$

## 1.5 PHASE TRANSITIONS IN SOLIDS

Phase transformations in solids are often accompanied by prominent changes in their physical properties. The two important thermodynamic variables in the study of phase transitions are temperature and pressure. Any study of a phase transition therefore involves measurement of properties as a function of temperature or pressure. Several techniques are employed to investigate phase transitions depending on the nature of the solid and the properties of interest. A wide range of techniques like X-ray

diffraction, thermal, optical and electrical measurements are available to study phase transitions [37-43].

A solid phase is characterised by its uniformity in structure and composition and is separated from other phases by sharp boundaries. At the boundary a discontinuity occurs to the uniform structure or composition or both. At phase transition, a particular phase of the solid becomes unstable. A change in free energy at the phase transition is associated with the structural and compositional changes.

During phase transition the free energy of the system remains continuous. However, other thermodynamic quantities like entropy, heat capacity, volume etc. undergo discontinuous changes. Depending on the nature of discontinuous change undergone by the thermodynamic quantity, and the Gibb's free energy function, phase transitions may be classified [44] as follows.

According to the classification proposed by Ehrenfest [44], a phase transition has the same order as the derivative of the Gibb's free energy which shows a discontinuous change at the point of phase transition.

Gibb's free energy is given by,

$$G = H - TS = E + PV - TS \quad (1.33)$$

Hence

$$dG = dE + PdV + VdP - TdS - SdT \quad (1.34)$$

$$= VdP - SdT$$

The first and second derivatives of G may be written as

$$\left(\frac{\partial G}{\partial P}\right)_T = V \quad (1.36)$$

$$\left(\frac{\partial G}{\partial T}\right)_P = -S \quad (1.37)$$

$$\left(\frac{\partial^2 G}{\partial P^2}\right)_T = \left(\frac{\partial V}{\partial P}\right)_T = -V\beta \quad (1.38)$$

$$\left(\frac{\partial^2 G}{\partial P \partial T}\right) = -\left(\frac{\partial V}{\partial T}\right)_P = V\alpha \quad (1.39)$$

$$\left(\frac{\partial^2 G}{\partial T^2}\right)_P = -\left(\frac{\partial S}{\partial T}\right)_P = -\frac{C_P}{T} \quad (1.40)$$

Here  $C_p$ ,  $\alpha$  and  $\beta$  are the heat capacity, volume thermal expansivity and compressibility respectively. We see that transformations in which a discontinuous change occurs in heat capacity, thermal expansivity and compressibility belong to the second order. Third and higher-order transitions involve further differential quantities.

A first-order transition involving discontinuous change in entropy is represented graphically in Fig.1.3. In Fig.1.4 a similar first order pressure transition involving discontinuous change in volume at constant temperature is shown.

A large number of examples of both thermal and pressure transformations in inorganic solids belonging to the first order are known [45-48]. Phase transitions of the first order generally exhibit hysteresis which may also be taken as a characteristic of these transitions [49-50]. In first-order transitions, the high temperature phases having high internal energy and low density will also have higher entropy. In fact, the high temperature structures are generally of higher symmetry and higher disorder than the low temperature structures.

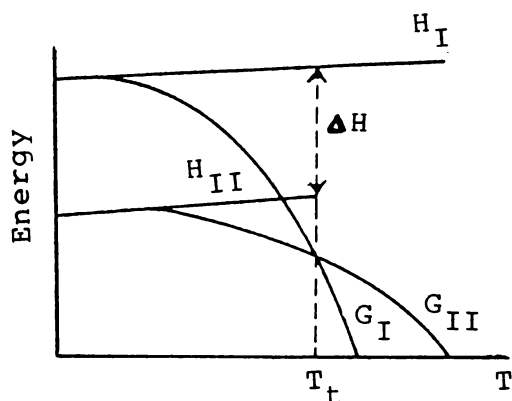


Fig.1.3 Variation of enthalpy and free energy with temperature in a first order phase transition.

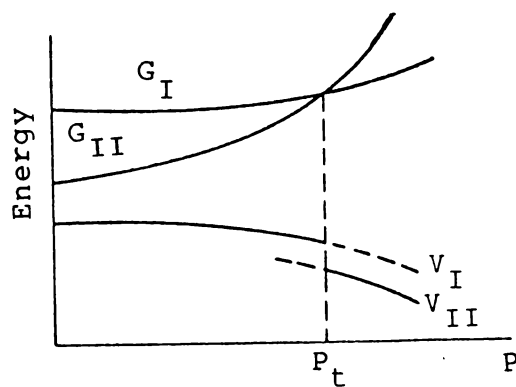


Fig.1.4 Variation of volume and free energy with pressure in a first order phase transition.

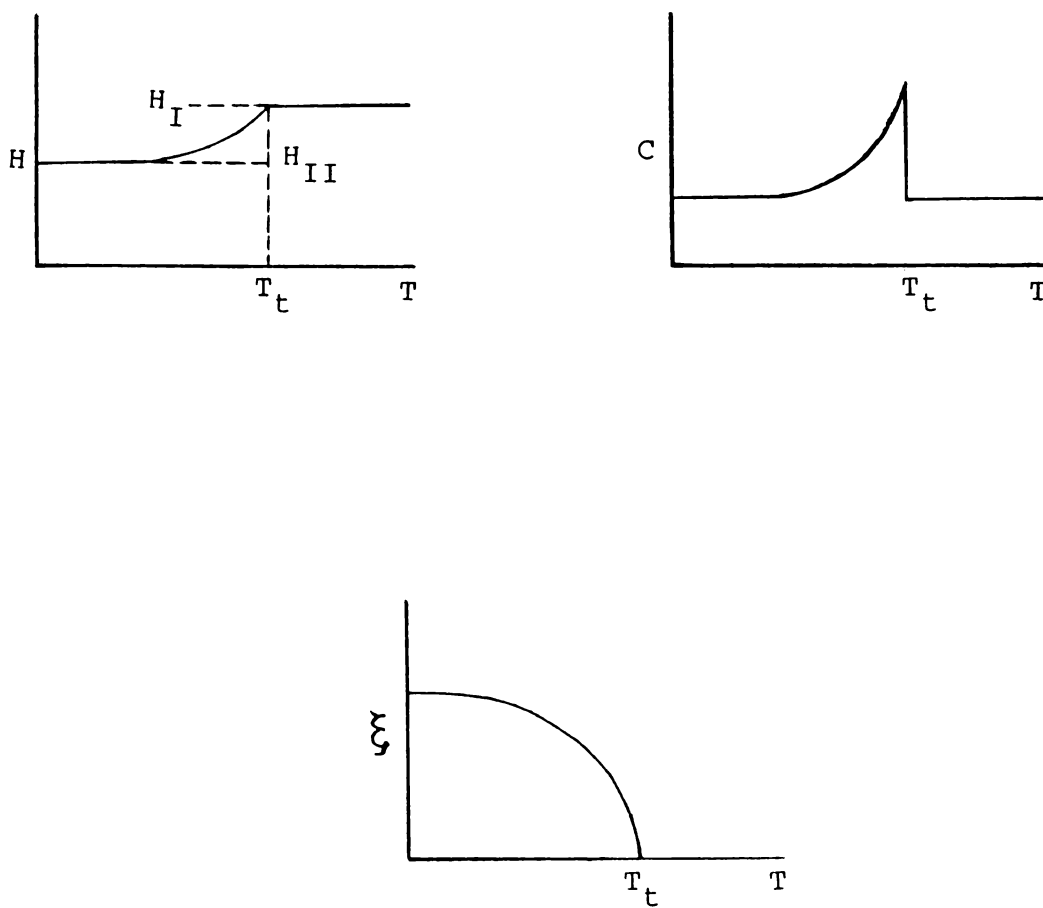


Fig.1.5 Variation of enthalpy, specific heat and order parameter in a second order transition.

In Fig.1.5 variations of enthalpy, heat capacity and the 'order parameter', with temperature during a second-order transformation are depicted. Transformation belonging to the second order are almost always associated with some kind of disordering process [49,50]. The disordering (or randomization) can be in terms of position or orientation.

A large number of transitions which are often incorrectly referred to as second order transitions are actually lambda transitions. In these transitions the heat capacity tends to infinity at the phase transition temperature.

## 1.6 PROTONIC CONDUCTORS

Majority of the superionic conductors reported in which monovalent cations act as charge carriers are based on silver and lithium. Those based on protons have been studied in any detail only in a few cases [51,52]. Protonic conductors assume significance in fuel cells, high energy density batteries, and in sensors. This recent interest has initiated detailed investigations on thermally stable protonic conductors [53,54].

The existence of proton as a conductor in a medium is not that simple as it appears to be. An unsolvated proton has a very small radius. Such free protons are not found in materials under equilibrium conditions. Hydrogen atom is covalently bonded to electronegative atoms such as carbon, nitrogen or oxygen. Hydrogen has the rare capability for expanding its covalency forming additional bond (hydrogen bond) which is characterised by directional properties. Oscillations of the hydrogen atom in such situations would effectively lead to a shift in its equilibrium position. This is equivalent to the transport of a proton. Since the hydrogen bond has directional characteristics, transport of a proton across a hydrogen bond has different magnitudes along different crystal axes depending upon the lattice structure.

## 1.7 MECHANISM OF PROTON CONDUCTION

### 1.7.1 Liquid-like transport

Certain protonic conductors with layered structure contain intercalated water molecule, eg.,  $\alpha$ - $[\text{Zr}(\text{PO}_4)_2\text{H}_2]\text{H}_2\text{O}$ , H-Al montmorillonite etc. In these layered materials, water molecules present in the interlayer space form a liquid-like network permitting

high protonic conductivity [55]. In pellicular materials with adsorbed moisture, the water present on the surface and in the interpellicular space can also act as a liquid transport medium eg.,  $ZrO_2 \cdot n H_2O$  [56].

### 1.7.2 Proton jump followed by reorientation of hydrogen bonds

Proton jump is often possible by a process of tunnelling through a hydrogen bond. In effect, a reorientation of the hydrogen bond occurs. This mechanism operates in hydrated salts, ammonium salts and organic acids. The probable modes of transport are described below.

#### (i) Polyatomic ion migration (Vehicle mechanism)

This conduction mechanism operates in strongly acidic media containing water where  $H_3O^+$  species is dominantly present. e.g.,  $H_3O^+$  -  $\beta$ -alumina [57], phosphomolybdic acid ( $H_3PMo_{12}O_{40} \cdot 29H_2O$ ) [58]. In these cases  $H_3O^+$  species migrates, thus effectively transporting  $H^+$ . A layered configuration of the anions facilitates this type of vehicular transport. Since the transport involves migration of massive polyatomic ions, the activation energy of the process is fairly high.

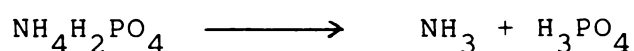
(ii) Co-operative proton transfer (Grothus mechanism)

Conduction can also occur due to proton exchange across a continuous chain or network of hydrogen bonds. This occurs in some layered hydrates which are weakly acidic or basic. The activation energy in such cases will be due to the barrier for the reorientation of the hydrogen bond and will be low in magnitude.

### 1.8 PROTONIC CONDUCTION IN AMMONIUM SALTS

Electrical properties of ammonium salts such as  $\text{NH}_4\text{Cl}$  and  $\text{NH}_4\text{Br}$  have been extensively investigated by various workers [27,59-66]. Herrington and Staveley [27] made a comparative study of the electrical conductivity of  $\text{NH}_4\text{Cl}$ ,  $\text{NH}_4\text{Br}$ ,  $\text{NH}_4\text{I}$ ,  $(\text{NH}_4)_2\text{SnCl}_6$  and  $\text{NH}_4\text{PF}_6$ . They concluded that protons play a dominant role in charge transport in these ammonium salts. Later investigations on  $\text{NH}_4\text{Cl}$  [59-64] and  $\text{NH}_4\text{Br}$  [65,66] support the observations of Herrington and Staveley. Murti and Prasad [63(c)] have probed phase transition using electrical conductivity measurements. They ascribed the excess conductivity observed at the phase transition to the release of protons from freely rotating ammonium ions. This well fits into the proton transport mechanism proposed by Herrington and Staveley.

A survey of the literature reveals that  $\text{NH}_4\text{H}_2\text{PO}_4$  (ADP) is an ammonium compound thoroughly investigated by several research groups [67-72]. Harris and Vella [69] have unambiguously proved that ADP dissociates according to the scheme.



The process was detected at all temperatures above  $40^\circ\text{C}$ . Thus the proton transport mechanism invoked to explain the conductivity in  $\text{NH}_4\text{Cl}$  is applicable here also.

Vallabhan et al have investigated a number of ammonium salts like  $(\text{NH}_4)_2\text{SO}_4$ ,  $\text{LiNH}_4\text{SO}_4$ ,  $\text{NH}_4\text{H}_2\text{PO}_4$ ,  $(\text{NH}_4)_3\text{H}(\text{SO}_4)_2$ ,  $(\text{NH}_4)_2\text{HPO}_4$  and  $(\text{NH}_4)_2\text{Cr}_2\text{O}_7$  [73-84] by dc and ac electrical conductivity and ionic thermocurrent measurements.

### 1.9 PROTONIC CONDUCTION IN SUBSTITUTED AMMONIUM SALTS

Takahashi et al [85] have investigated protonic conduction in certain substituted ammonium compounds like triethylenediammine sulphate containing triethylene-diammine and sulphuric acid in the mole ratios 1, 1.5 and 2. The highest conductivity observed was in  $\text{C}_6\text{H}_{12}\text{N}_2 \cdot 1.5\text{H}_2\text{SO}_4$ . Abrupt changes in conductivity were

observed at phase transitions which were confirmed by DTA. Electrolytic and emf measurements confirmed the role of protons in charge transport. Investigations by the same authors [85] on hexamethylene tetramine sulphate also provided comparable results. The work on these materials have thrown light on a new class of compounds of high protonic conductivity.

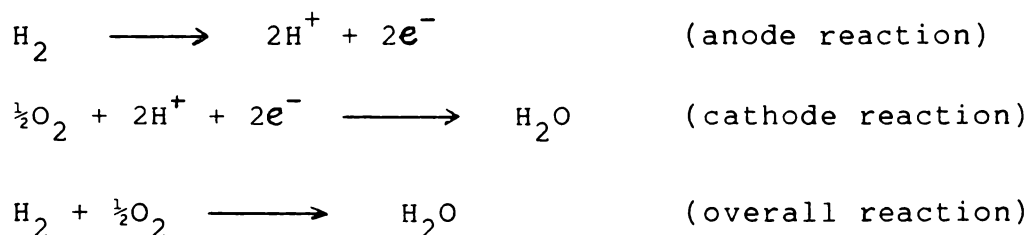
#### 1.10 APPLICATIONS OF PROTONIC CONDUCTORS

An era of active research in solid state protonic conductors was opened up by the energy crisis in early seventies. From the energy point of view major application of solid state protonic conductors is as electrolytes in fuel cells meant for stand-alone power systems, heavy duty automobile traction and electricity storage by the hydrogen route. Other applications include hydrogen concentration cells, batteries and sensors.

##### 1.10.1 Fuel cells

Electrochemical cells in which the free energy change of the chemical reaction is transformed directly into electrical energy are classified as fuel cells. Batteries have the reacting components stored in the electrode itself. In fuel cell the active chemical is

supplied from an external store. Power generation by fuel cells is free of pollution. The conversion of free energy into electrical energy has high efficiency. For these reasons storage of hydrogen as a fuel and its conversion to electricity are technically feasible and environmentally acceptable. The electrode reaction and the overall cell reaction in hydrogen-oxygen fuel cell can be represented,



### 1.10.2 Hydrogen concentration cells

When hydrogen at two different activities  $a_1$  and  $a_2$  are separated by a solid state protonic conductor, emf of the resulting concentration cell is given by the Nernst equation,

$$|E| = \left| \frac{RT}{nF} \ln \frac{a_1}{a_2} \right|$$

where  $R$  is the gas constant,  $T$  is the absolute temperature (K),  $n$  is the number of electrons involved in the reaction and  $F$  is the Faraday unit. The difference in activity may

be the result of different hydrogen ion concentrations or of different hydrogen partial pressures. Such cells can act as energy converters and also as sensors. A temperature difference in the metal hydride compartment (hydrogen reservoir) raises the partial pressures in that compartment by releasing hydrogen. The low partial pressure in the other compartment drives the electrode reactions thus generating power in the external circuit. The operating voltage,

$$V_c = \frac{\Delta H}{2F} \epsilon_{id}$$

where  $\epsilon_{id}$  is the ideal efficiency which is the Carnot efficiency. When  $\Delta H$  and  $\Delta S$  are temperature independent,

$$\epsilon_{id} = \frac{\Delta G_c - \Delta G_h}{T_h \Delta S_h} \cong \frac{T_h - T_c}{T_h}$$

Since the device works on pressure difference, liquid electrolyte is not suitable. Although the proposition seems attractive, capital cost for the cell and the hydride storage are the major obstacles to its commercialisation.

### 1.10.3 Batteries

When one of the metal hydride reservoirs in the hydrogen concentration cell is replaced by an oxygen or

air electrode, the system turns out to be a battery. The technological details remain more or less the same as those for the fuel cells. A working model of such a battery using hydrogen uranyl phosphate tetrahydrate (HUP) has been studied in detailed by Kahil et al. [86].

#### 1.10.4 Sensors

Solid state protonic conductor-based hydrogen sensors fall into two categories: (i) those used in the measurement of hydrogen ion concentration (pH) in solution, and (ii) those used in the measurement of hydrogen partial pressures. In a pH measuring cell, SSPC separates two solutions of  $\text{pH}_1$  and  $\text{pH}_2$ . One is the test solution and the other is a solution of known pH. The cell is schematically shown,



EMF of this cell is given by,

$$|E| = \left| 2.303 \frac{RT}{nF} \frac{\text{pH}_1}{\text{pH}_2} \right|$$

Such sensors have the advantage that they are compact and they can perform instantaneous in-line monitoring without interfering with the process in industrial installations.

**1.11 REFERENCES**

- [1] W.Schottky, Z. Phys. Chem. Abt. B **29** (1935) 335.
- [2] C.Wagner, Z. Phys. Chem. Abt. B **38** (1938) 325.
- [3] N.F.Mott and M.J.Littleton, Trans. Faraday Soc. **34** (1938) 485.
- [4] N.F.Mott and R.W.Gurney, Electronic Process in Ionic Crystals, 2nd ed. Oxford Press, London (1948).
- [5] A.B.Lidiard, Handbuch der Physik. Vol.20, p.246 (1957).
- [6] A.B.Lidiard, Phys. Rev. **94** (1954) 29.
- [7] I.Boxwara and A.B.Lidiard, Phil. Mag. **16** (1967) 805.
- [8] R.G.Fuller, C.L.Marquardt, M.H.Reilly and J.C.Wells Jr., Phys. Rev. **176** (1968) 1036.
- [9] R.G.Fuller and H.B.Rosenstock, J. Phys. Chem. Solids **30** (1969) 2105.

- [10] R.G.Fuller and M.H.Reilly, Phys. Rev. Lett. **19** (1967) 113.
- [11] R.G.Fuller, Bull. Am. Phys. Soc. **15** (1970) 384.
- [12] R.G.Fuller and M.H.Reilly, J. Phys. Chem. Solids **30** (1969) 457.
- [13] R.G.Fuller and F.W.Patten, J. Phys. Chem. Solids **31** (1970) 539.
- [14] L.W.Barr and A.B.Lidiard, Defects in Ionic Crystals, in Physical Chemistry: An Advanced Treatise, Vol.X, Academic Press, New York (1970).
- [15] D.K.Dawson and L.W.Barr, Phys. Rev. Lett. **19** (1967) 844.
- [16] W.Franklin, Phys. Rev. **180** (1969) 682.
- [17] G.Shannon, Diffusion in Solids, McGraw-Hill, New York (1963).
- [18] H.R.Glyde, Rev. Mod. Phys. **39** (1954) 373.

- [19] E.Pitts, Proc. Roy. Soc. A 217 (1953) 43.
- [20] C.Ramasastri and Y.V.G.S.Murti, Proc. Roy. Soc. 305 (1968) 441.
- [21] F.A.Kroeger, J. Chem. Phys. 51 (1969) 4025.
- [22] S.Chandra and J.Rolfe, Can. J. Phys. 48 (1970) 397.
- [23] S.Chandra and J.Rolfe, Can. J. Phys. 48 (1970) 412.
- [24] V.C.Nelson and R.J.Friauf, J. Phys. Chem. Solids 31 (1970) 825.
- [25] P.L.Read and E.Katz, Phys. Rev. Lett. 5 (1960) 466.
- [26] Y.V.G.S.Murti and P.S.Prasad, Proc. Nuclear Phys. and Solid State Phys. Symp. (India) 17C (1974) 67.
- [27] T.M.Herrington and L.A.K.Staveley, J. Phys. Chem. Solids 25 (1964) 921.
- [28] Y.V.G.S.Murti and C.S.N.Murthy, J. de Physique 34 (1973) 9.

- [29] D.Mapother, N.N.Crooks and R.J.Maurer, *J. Chem. Phys.* **18** (1950) 1231.
- [30] D.Patterson, J.A.Morrison and G.S.Rose, *Phil. Mag.* **1** (1956) 393.
- [31] G.Arai and J.G.Mullen, *Phys. Rev.* **143** (1966) 663.
- [32] A.M.Karo and J.R.Hardy, *Phys. Rev.* **B3** (1971) 3418.
- [33] H.Rabin and C.C.Klick, *Phys. Rev.* **117** (1960) 1005.
- [34] N.L.Peterson and S.J.Rothman, *Phys. Rev.* **177** (1969) 1329.
- [35] H.Kelting and H.Witt, *Z. Phys.* **126** (1949) 697.
- [36] F.C.Brown, *The Physics of Solids*, Chapter 7, Benjamin, New York (1967).
- [37] H.D.Megan, *Ferroelectricity in Crystals*, Methuen and Co., London (1957).

- [38] C.N.R.Rao and M.Natarajan, Crystal Structure Transformations in Binary Halides, NSRDS-NBS Monograph 41, Washington D.C. (1972).
- [39] C.N.R.Rao and G.V.Subba Rao, Transition Metal Oxides: Crystal Chemistry, Phase Transitions and Related Aspects, NSRDS-NBS Monograph 49, Washington D.C. (1974).
- [40] C.N.R.Rao, B.Prakash and M.Natarajan, Crystal Structure Transformations in Inorganic Nitrites, Nitrates and Chromates, NSRDS-NBS Monograph 53, Washington D.C. (1975).
- [41] C.N.R.Rao and B.Prakash, Crystal Structure Transformations in Inorganic Sulphates, Chromates, Phosphates and Perchlorates, NSRDS-NBS Monograph 56, Washington D.C. (1975).
- [42] C.N.R.Rao and K.P.R.Pisharody, Progress in Solid State Chemistry, Pergamon Press, Oxford, Vol.10 (1975).
- [43] J.B.Goodenough and J.M.Longo, Crystallographic and Magnetic Properties of Perovskite and Perovskite Related Compounds, Landolt-Bornstein New Series, Group III, Vol.4a, Springer-Verlag, Berlin (1970).

- [44] P.Ehrenfest, Proc. Amsterdam Acad. **36** (1963) 153.
- [45] W.Paul and M.Warschauer (ed.), Solids Under Pressure, Mc-Graw Hill, New York (1963).
- [46] K.J.Rao and C.N.R.Rao, J. Mater. Sci. **1** (1966) 238.
- [47] C.J.M.Rooymans, Philips Research Reports Supplement, No.5 (1968).
- [48] C.N.R.Rao and K.J.Rao, Progress in Solid State Chemistry, ed. H.Reiss, Vol.4, Pergamon Press, Oxford (1967).
- [49] A.R.Ubbelohde, Quart. Rev. (London), **11** (1957) 246.
- [50] Reactivity in Solids, ed. J.H.de Boer, Elsevier, Amsterdam (1961).
- [51] L.Glasser, Chem. Rev. **75** (1975) 21.
- [52] J.Bruinink, J. Appl. Electrochem. **2** (1972) 239.

- [53] Solid State Protonic Conductors III, (ed.) J.B. Goodenough, J.Jensen and A.Potier, Odense University Press, Denmark (1985).
- [54] S.Chandra, Superionic Solids—Principles and Applications, North Holland, Amsterdam (1981).
- [55] G.Alberti, M.Casciola and U.Costantino, in Solid State Protonic Conductors III, (ed.) J.B.Goodenough, J.Jensen and A.Potier, p.215, Odense University Press, Denmark (1985).
- [56] W.A.England, M.G.Cross, A.Hammnett, P.J.Wiseman and J.B.Goodenough, Solid State Ionics 1 (1980) 231.
- [57] G.C.Farrington and J.L.Briant, Mat. Res. Bull. 13 (1978) 763.
- [58] O.Nakamura, T.Kodama, I.Ogino and Y.Miyake, Chem. Lett. (1979) 17.
- [59] F.A.Kroeger, J. Chem. Phys. 51 (1969) 4025.

- [60] R.G.Fuller and P.W.Patten, J. Phys. Chem. Solids **31** (1970) 1539.
- [61] A.Kessler, Solid State Commun. **12** (1973) 697.
- [62] Y.V.G.S.Murti and C.S.N.Murthy, J. Physique **34** (1973) C9.
- [63] Y.V.G.S.Murti and P.S.Prasad, (a) Physica, **77** (1974) C9; (b) Solid State Commun. **15** (1974) 1619; (c) Physica **79B** (1975) 243.
- [64] F.Elkabbany, Appl. Phys. Commun. **6** (1986) 57.
- [65] Y.Berteit, A.Kessler and T.List, Z. Phys. **B24** (1976) 15.
- [66] B.E.Taylor and A.L.Lasker, Physica Status Solidi(b) **101** (1980) 423.
- [67] E.J.Murphy, J. Appl. Phys. **35** (1964) 2609.
- [68] J.M.Pollock and M.Sharan, J. Chem. Phys. **51** (1969) 3604.

- [69] L.B.Harris and G.J.Vella, *J. Chem. Phys.* **58** (1971) 4550.
- [70] S.Vasudevan and P.Ramasamy, *Ind. J. Pure and Appl. Phys.* **23** (1985) 432.
- [71] S.C.Subharwal and B.Ghosh, *Physica Status Solidi (a)* **89** (1985) K 83.
- [72] J.K.Rath and S.Radhakrishna, *J. Mater. Sci. Lett.* **6** (1987) 929.
- [73] U.Syamaprasad and C.P.G.Vallabhan, *Solid State Commun.* **34** (1980) 899.
- [74] U.Syamaprasad and C.P.G.Vallabhan, *J. Phys. C: Solid State Phys.* **14** (1981) L571.
- [75] U.Syamaprasad and C.P.G.Vallabhan, *J. Phys. C: Solid State Phys.* **14** (1981) 1865.
- [76] U.Syamaprasad and C.P.G.Vallabhan, *Solid State Commun.* **38** (1981) 555.

- [77] U.Syamaprasad and C.P.G.Vallabhan, Solid State Commun. **41** (1982) 169.
78. U.Syamaprasad and C.P.G.Vallabhan, Phys. Lett. **89A** (1982) 37.
- [79] U.Syamaprasad and C.P.G.Vallabhan, Phys. Rev. B. **26** (1982) 5941.
- [80] V.K.Subhadra, U.Syamaprasad and C.P.G.Vallabhan, J. Appl. Phys. **54** (1983) 2593.
- [81] R.Navilkumar and C.P.G.Vallabhan, J. Phys.: Condens. Matter **1** (1989) 6095.
- [82] R.Navilkumar and C.P.G.Vallabhan, Physica Status Solidi (a) **112** (1989) K113.
- [83] N.C.Santhakumari and C.P.G.Vallabhan, Solid State Ionics **45** (1991) 329.
- [84] N.C.Santhakumari and C.P.G.Vallabhan, J. Phys. Chem. Solids (in press).

- [85] T.Takahashi, S.Tanase, O.Yamamoto and S.Yamauchi,  
J. Solid State Chem. **17** (1976) 353.
- [86] H.Kahil, M.Forestier, J.Guitton, in Solid State  
Protonic Conductors III, (ed.) J.B.Goodenough,  
J.Jensen and A.Potier, Odense University Press,  
Denmark (1985).

## Chapter 2

### EXPERIMENTAL METHODS

#### Abstract

The experimental technique employed and the measuring systems used in the present investigations are described in this chapter. The procedure for the synthesis of materials, conditions for growing single crystals and preparation of single crystals for measurement are also given. The design and fabrication of a shielded cell which can be used for the measurement of dc and ac electrical conductivity and dielectric constant over the temperature range 80 to 530 K are outlined. The salient features of the instruments used in acquiring the data on electrical and thermal properties are also included in this chapter.

## 2.1 INTRODUCTION

The results presented in the following chapters in Part I of the thesis were obtained from a systematic investigation on single crystals of a series of ethylenediammonium salts viz., ethylenediammonium dichloride (EDC), ethylenediammonium dinitrate (EDN), ethylenediammonium sulphate (EDS) and ethylenediammonium acid phosphate (EDAP) using well established techniques. A brief description of the procedures for preparing the materials and their single crystals and the details of the design and fabrication of a shielded cell, and the experimental systems are presented in the following sections.

## 2.2 PREPARATION OF MATERIALS

### 2.2.1 General methods for the synthesis of ethylenediammonium salts

Ethylenediammine of 99.5% purity (Glaxo laboratories) was distilled from an all glass distillation apparatus immediately before use. Since ethylenediammine is volatile and fumes in air, a 6 molar solution was used in the synthesis. An appropriate volume of this solution was neutralised with a stoichiometric amount of the acid

diluted with water. Since the neutralisation reaction is highly exothermic the reaction mixture was cooled during neutralisation. The salt solutions were evaporated on a water bath. The microcrystals were separated by filtration and were purified by recrystallisation from double distilled water. The stoichiometry of the final product was determined by chemical analysis.

### **2.2.2 Methods for growing crystals**

In view of the evergrowing importance of single crystal devices in solid state electronics and optics, very efficient methods have been developed for growing defect-free crystals. These include growth from solution, growth from melt, growth from vapour, flux growth, epitaxial growth etc. The crystals used in the present study were grown from solutions since this method is the simplest and the only suitable method for growing crystals which decompose below their melting point.

### **2.2.3 Crystal growth from solution**

A saturated solution of the material in a moderately volatile solvent was used for growing the crystal. The solution was taken in a clean beaker and mounted in a water bath thermostated in the temperature

range 35 to 60°C depending on the material. The temperature of the bath was maintained at  $\pm 0.1^\circ\text{C}$  of the set temperature. The solution was protected from dust and air draught using baffles. Moderately sized single crystals of EDC, EDN, EDS and EDAP could be grown from aqueous solution by this technique.

Doped single crystals were grown by adding an appropriate amount of the dopant into the solution of the pure materials. Deuterated samples were prepared by repeated recrystallisation using heavy water (99.5% isotopic purity, BARC, Bombay). The incorporation of deuterium was confirmed from the infrared spectrum.

#### 2.2.4 Preparation of samples for electrical measurements

Single crystals of good transparency which were devoid of any visual defect as observed under a magnifying glass were used for measurements. Samples of typical size  $5 \times 5 \times 1 \text{ mm}^3$  were obtained by cleaving and cutting the slices. The specimen plates were polished using a crystal polishing kit (Perkin-Elmer). The broad faces of the specimen were cleaned and vacuum coated with silver to provide good electrical contact.

### 2.3 SHIELDED CELL FOR ELECTRICAL MEASUREMENTS

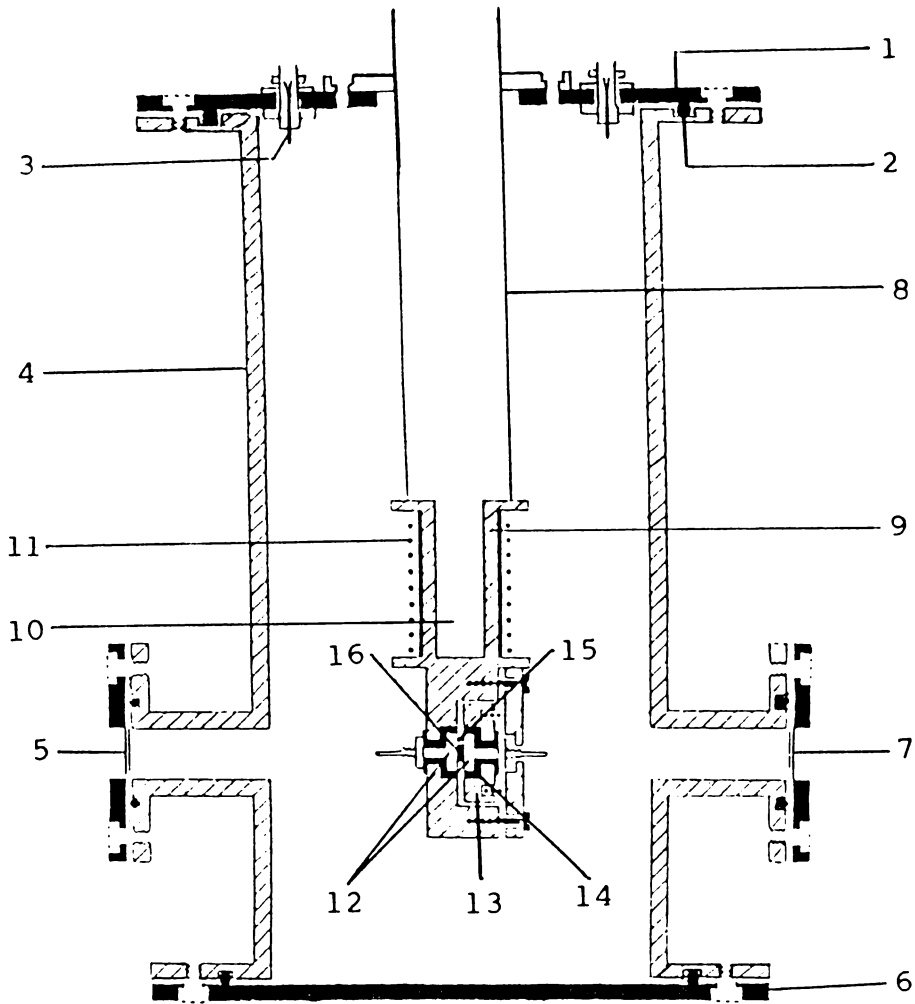
The reproducibility of electrical measurements on materials which have a tendency to adsorb moisture depend to a large extent on the atmosphere in which the studies are carried out. It is observed that maintaining a dynamic vacuum in the sample cell and annealing the sample at an elevated temperature help to acquire reproducible data. Moreover, at subambient temperatures most of the samples used in the present investigations turn out to be highly resistive. This leads to small amplitude signals in ac techniques which are easily affected by electromagnetic pick up. For these reasons it became necessary to use a specially designed cell having the following features for electrical measurements.

- i) The cell must be capable of operating over a wide temperature range.
- ii) It must be capable of providing a linear heating rate with proper heater controls.
- iii) The measuring cell and leads must be electromagnetically shielded and earthed.

iv) It must be possible to maintain a steady dynamic vacuum in the cell.

Depending upon the nature of measurement required, several cell designs have been described in the literature [1-7]. A schematic diagram of the variable temperature cell fabricated for the present study is shown in Fig.2.1.

The cell assembly has a cylindrical nickel plated MS body which acts as an EM shield. The ends of the MS cylinder are permanently fitted with MS flanges which are provided with grooves to accommodate neoprene O-rings for vacuum sealing. One of the flanges rests on the bottom plate. The top cover plate carries insulated electrical terminals for heater, thermocouple and the leads for electrical measurements of the sample. The terminals for output signal are provided with BNC connectors. The top cover carries a stainless steel tube into which liquid nitrogen can be poured. At the end of the SS tube a solid copper cylinder is brazed in. This acts as a cold finger. The other end of the copper cylinder is machined to a block of dimensions 30x30x20 mm. One of the circular copper electrode is accommodated



- |                    |                            |
|--------------------|----------------------------|
| 1. Top plate       | 9. Copper cold finger      |
| 2. Neoprene O-ring | 10. LN <sub>2</sub> cavity |
| 3. BNC             | 11. Heater coil            |
| 4. MS body         | 12. Electrodes             |
| 5. View port       | 13. Dismountable ram       |
| 6. Base plate      | 14. Teflon insulation      |
| 7. To vacuum       | 15. Thermocouple           |
| 8. SS tube         | 16. Sample                 |

Fig.2.1 Schematic diagram of the variable temperature cell used for the measurement of electrical properties of solids.

through a teflon insulator in a cavity drilled in this block. The thermocouple head isolated by a thin sheet of mica rests on this electrode. The second electrode is fixed on the detachable ram made of copper through teflon insulation. This assembly is spring loaded on the static block. This configuration ensures rapid thermal equilibration of the sample placed between the electrodes. The copper cold finger is provided with a heater winding which is also insulated by a thin mica sheet. The heater is powered by a programmed dc supply.

The salient features of this cell design are the following:

- i) Measurement can be made in the temperature range 80 to 530 K.
- ii) A dynamic vacuum down to 1 m torr can be maintained over the sample throughout the experiment.
- iii) By virtue of the special design of the liquid nitrogen holder, the consumption of liquid nitrogen is much lower than that in conventional commercial devices.

- iv) ac and dc electrical conductivities, dielectric constant and dielectric loss can be measured in the same cell with excellent sensitivity.
- v) Sample mounting and setting up the system for measurement can be accomplished rapidly.

## 2.4 METHODS OF MEASUREMENT

The experimental data on a number of electrical properties like ac and dc electrical conductivity, dielectric constant and dielectric loss are employed to extract information on the suitability of materials for technological applications. The above informations are also useful to interpret the mechanism of the electrical transport and other physical properties of the sample. A brief outline of the techniques used in this study is presented in the ensuing section.

### 2.4.1 dc electrical conductivity

Inorganic and organic single crystals, in general, show relatively low conductivity at ambient temperatures. At sub-ambient temperatures these materials show still lower conductivities, thus necessitating the use of an electrometer of high current sensitivity. We

have used Keithley electrometers model 642 and 617 for measuring the dc currents at an applied bias of 10 to 100 volts dc. The bias voltage was obtained from the programmable voltage source output of the Keithley electrometer model 617. This electrometer is capable of making current measurements down to 10 fA. It was confirmed that no polarization occurs at the electrodes for the applied voltage in this range. The samples are usually mounted in the sample holder of twin electrode design, the two identical circular electrodes being in good contact with the flat parallel surfaces of the specimen of well defined geometry (section 1.2.3).

#### 2.4.2 ac measurements

Hewlett Packard Impedance Analyzer model 4192 A was used for the measurement of ac conductance  $G$ , capacitance  $C$  and dielectric loss factor  $\tan\delta$ . In the lowest range of measurements the instrument gives a readability of 1 nS for  $G$ , 1 pF for  $C$  and 0.001 for  $\tan\delta$ . Using this instrument, measurement could be effected in the frequency range 10 Hz to 13 MHz.

The dielectric constant was calculated from the measured value of capacitance of a parallel plate condenser formed with the specimen as the dielectric.

This method suffers from the disadvantage that it is difficult to account for the contribution of lead and fringe capacitances towards the measured value of capacitance. One of the methods commonly employed to evaluate the lead and fringe capacitance is to set the assembly with an air gap equal to the thickness of the specimen and to measure the capacitance [8]. The cell used in the present investigations was not suitable to apply this method. Hence the method suggested by Ramasastry and Syamasudara Rao [9] was employed. In this method, the capacitance  $C$  of a set of samples of the same cross sectional area  $A$ , but of varying thickness  $d$  are measured. A plot of  $A/d$  vs.  $C$  (Fig.2.2) gives a straight line. The intercept on the capacitance axis gives the lead and fringe capacitance. There is slight shift in lead and fringe capacitance with frequency, as can be seen from Fig.2.2. However, this does not affect the qualitative nature of the data acquired at different frequencies.

## 2.5 DIFFERENTIAL SCANNING CALORIMETRY

Differential scanning calorimetric measurements of the materials were carried out on a Perkin Elmer DSC 7 instrument. Finely powdered, accurately weighed samples

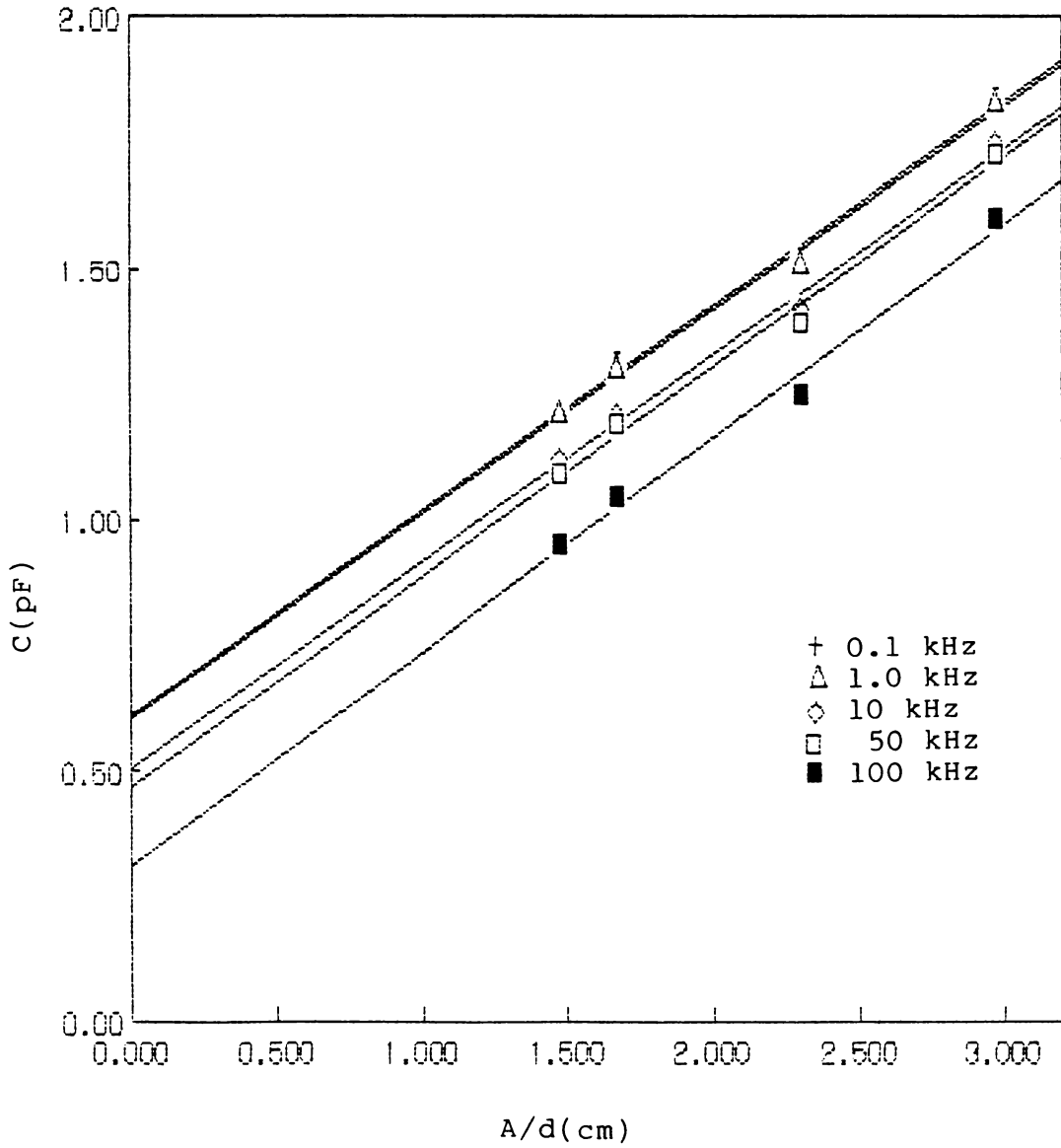


Fig.2.2 Plot of  $C$  vs.  $A/d$  at different frequencies for the evaluation of lead and fringe capacitance.

(3-5 mg) were used. In special cases flawless single crystal samples were used as mentioned in the text. Energy flow was noted against blank aluminium pans of identical nature. A dynamic nitrogen atmosphere was maintained over the sample by passing nitrogen at the rate of 3 ml per minute. The scan rate was set at 10 K per minute. The data were processed by the standard software provided by the manufacturer. The instrument has provisions for integrating the peaks and expressing the enthalpy change ( $\Delta H$ ) for the phase transition. It also gives the onset and peak temperatures for transitions. The onset of thermal anomaly is reported as the phase transition temperature.

## 2.6 REFERENCES

- [1] R.D.Gretz, Rev. Sci. Instrum. **38** (1967) 112.
- [2] F.E.Card and J.J.Galen, Rev. Sci. Instrum. **32** (1961) 858.
- [3] V.Kopane and V.E.Shubin, Instrum. Exp. Tech. **19** (1976) 1228.
- [4] R.K.Chaudhary and L.Kishore, Cryogenics **17** (1977) 419.
- [5] H.Abachi, J.Molenat and P.Malbrunot, J. Phys. E: Sci. Instrum. **12** (1979) 706.
- [6] H.Gobrecht and D.Hoffmann, J. Phys. Chem. Solids **27** (1966) 509.
- [7] E.B.Podgovsak and P.R.Moran, Phys. Rev. B. **8** (1973) 3405.
- [8] Annual Book of ASTM Standards 1975, Part No.40, Designation D 150-749, Am. Soc. for Testing Materials, Philadelphia.
- [9] C.Ramasastri and Y.Syamasundara Rao, J. Phys. E: Sci. Instrum. **12** (1979) 1023.

## Chapter 3

### ELECTRICAL CONDUCTIVITY AND DIELECTRIC CONSTANT IN ETHYLENEDIAMMONIUM DICHLORIDE CRYSTALS

#### Abstract

The results of the studies carried out on the electrical properties of ethylenediammonium dichloride are presented in the present chapter. The dc and ac conductivities, dielectric constant and dielectric loss factor have been measured as a function of temperature. The activation energies of conduction in different temperature ranges have been evaluated from the Arrhenius plots. An anomaly observed at 403 K in the electrical properties corresponds to a phase transition. This is also confirmed by the DSC measurements. The electrical conductivity in this material is explained in terms of proton transport. The enhancement of the electrical properties at the phase transition is probably due to the reorientation of the  $\text{-NH}_3^+$  group and the concomitant release of protons by the rearrangement of the hydrogen bonds.

### 3.1 INTRODUCTION

Protonic conductors assumed significance about two decades ago. The investigations on solid materials for probable protonic conduction was only a scientific curiosity. One of the simplest of compounds to be investigated by early workers to establish protonic conduction was  $\text{NH}_4\text{Cl}$ . The choice of this and related compounds was judged by a fair understanding of their crystal structures and simplicity of the methods for preparing crystals of pure samples.

The first detailed investigation on the electrical properties of ammonium salts was made by Herrington and Staveley [1]. Their investigation conclusively proved the participation of proton in charge transport mechanism in ammonium containing crystals. They also suggested a possible mechanism for the transport of protons. Murti and Prasad [2] extended the measurement of electrical properties to higher temperatures. They detected a high temperature phase transition at about 140 K by electrical conductivity measurements. They ascribed the conductivity anomaly observed at the phase transition to the onset of free rotation of  $\text{NH}_4^+$  ions and the release of  $\text{H}^+$ .

The major limitation of  $\text{NH}_4\text{Cl}$  is its volatility which persists even at ambient temperatures [1]. If the ammonium ion is substituted by a bulky group, its volatility can be curtailed. Moreover, the introduction of substituent can influence the hydrogen bonding which though weak, does exist in ammonium salts.

Ethylenediammonium dichloride,  $\text{H}_3\text{NCH}_2\text{CH}_2\text{NH}_3\text{Cl}_2$  (EDC), is a well characterized substituted ammonium salt. Ashida and Hirokawa [3] have elucidated the crystal structure of EDC in detail. Other investigations carried out in this material include infrared spectral studies [4-6], X-ray diffraction [7] and NMR spin-lattice relaxation measurements [8].

EDC belongs to the monoclinic system with  $a = 9.95$ ,  $b = 6.89$ ,  $c = 4.42 \text{ \AA}$  and  $\beta = 90.7^\circ$ . The space group is  $P2_1/a$ . The unit cell contains two ethylenediammonium ions and four chloride ions. The ethylenediammonium ions are hydrogen bonded to the surrounding anions in the lattice. In this respect it is similar to ammonium chloride except that it has a much bulkier substituted ammonium ion.  $\text{NH}_4\text{Cl}$  is one of the best understood materials in terms of its structure and

electrical properties. A comparison of the two compounds provides an opportunity to unravel the influence of substitution of the ammonium group with an organic moiety on the electrical properties, conduction mechanism and phase transition. The NMR spin-lattice relaxation measurements [8] show that when EDC is warmed a drastic increase in  $T$ , from 28 ms to 9 s occurs at 410 K. No attempt has so far been made to study any of the electrical properties of EDC. In this chapter we report the results of the studies carried out on the electrical properties of pure and  $\text{SO}_4^{2-}$  doped single crystals of EDC.

### 3.2 EXPERIMENTAL

EDC was prepared by mixing distilled ethylenediamine and hydrochloric acid in 1 : 2 mole ratio. The microcrystals were recovered and recrystallised using double distilled water. Large single crystals were grown by the evaporation of the aqueous solution at room temperature. The crystals thus grown were needle shaped and elongated along c-axis. A marked cleavage occurs perpendicular to c-axis as reported by Ashida and Hirokawa [3].  $\text{SO}_4^{2-}$  doped single crystals were grown by the same method as in the case of pure crystals from aqueous solution of EDC containing 0.1 mole % of EDS (ethylenediammonium sulphate). Specimens ( $5 \times 5 \times 1 \text{ mm}^3$ ) for electrical

measurements were cut and polished with their broad faces parallel to and perpendicular to the cleavage plane, so that electrical measurements could be made along  $c$  and  $c^*$ -axes. Evaporated films of silver was deposited on the broad faces to make good electrical contact.

dc and ac conductivities, dielectric constant and dielectric loss were measured as a function of temperature in the range 100 to 420 K as described in Chapter 2. Unless otherwise, stated all the measurements are reported here along  $c^*$ -axis. DSC thermograms were recorded using single crystals as well as powdered samples.

### 3.3 EXPERIMENTAL RESULTS

The variation of dc electrical conductivity with temperature in the range 300 to 420 K in single crystal samples of EDC along  $c$  and  $c^*$ -axes are presented in Fig.3.1. In the temperature range 100 to 320 K the conductivity does not show any significant variation. From 320 to 369 K the plot shows a linear rise with temperature. The activation energy in this region is 0.90 eV ( $c^*$ -axis). From about 369 K it shows a continuous curvature, and a  $\Lambda$ -shaped anomaly is observed at 403 K. The

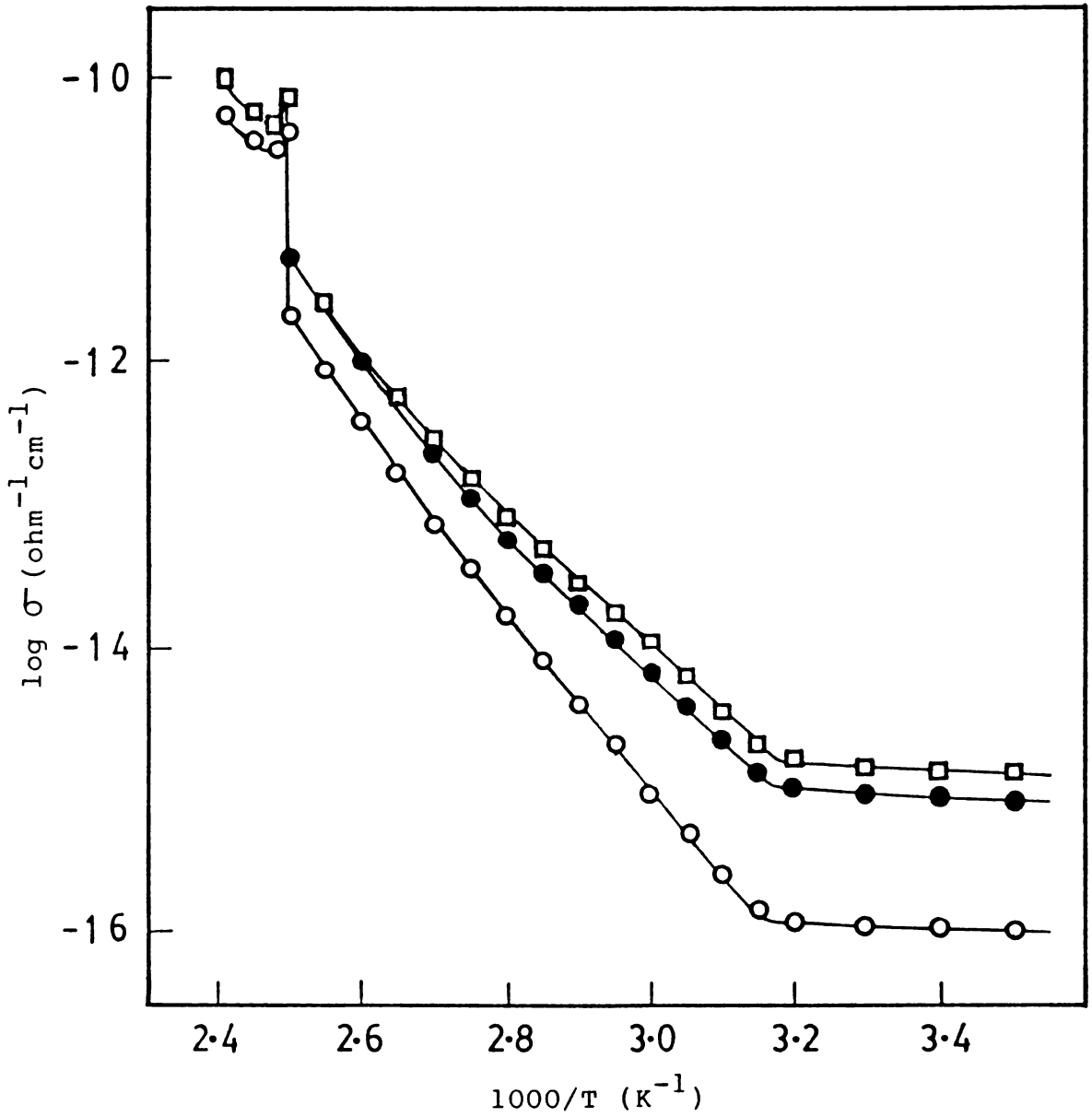


Fig.3.1:  $\log \sigma_{dc}$  vs  $1/T$  plots for EDC.  $\square$  - along  $c^*$ -axis for pure sample,  $\bullet$  - along  $c^*$ -axis for sulphate doped sample,  $\circ$  - along  $c$ -axis for pure sample.

conductivity of the  $\text{SO}_4^{2-}$  doped single crystals is found to be slightly lower than that of pure crystals. There is only slight difference in the activation energy for conduction in pure and doped crystals. The conductivity measured along the axis perpendicular to the cleavage plane (c-axis) is about one order of magnitude less than that along the  $c^*$ -axis at ambient temperature. This difference decreases as the temperature increases. The activation energy values evaluated from the Arrhenius plots are presented in Table 3.1.

The magnitude of ac conductivity in single crystals of EDC remains at a steady low value upto about 400 K. Above this temperature it shows a sharp increase resulting in a  $\Lambda$ -shaped anomaly as displayed in Fig.3.2. The variation of  $\tan\delta$  (at 1 kHz) with temperature in the temperature range 365 to 420 K is also depicted in Fig.3.2. The variation and anomaly in  $\tan\delta$  with temperature are analogous to those for ac conductivity.

The dielectric constant shows significant variations only at temperatures around the phase transition. Fig.3.3 is a typical plot of the frequency and temperature dependence of dielectric constant in the

Table 3.1: Activation energies for dc conduction in EDC.

Sample	Temperature range (K)	Activation energy (eV)	Reference
EDC (c-axis)	320 to 369	1.27	Present work
	369 to 392	1.37	
EDC (c*-axis)	320 to 369	0.90	Present work
	369 to 392	1.21	
EDC (SO <sub>4</sub> <sup>2-</sup> doped (c-axis))	320 to 369	0.98	Present work
	369 to 392	1.21	
NH <sub>4</sub> Cl	312 to 439	1.15	[1]
NH <sub>4</sub> Cl	313 to 448	1.23	[2]
NH <sub>4</sub> Br (pellet)	345 to 425	0.83	[1]
NH <sub>4</sub> Br	313 to 408	1.37	[2]
	453 to 573	0.83	
NH <sub>4</sub> Br	280 to 400	1.14	[9]
NH <sub>4</sub> I (pellet)	253 to 407	1.23	[1]

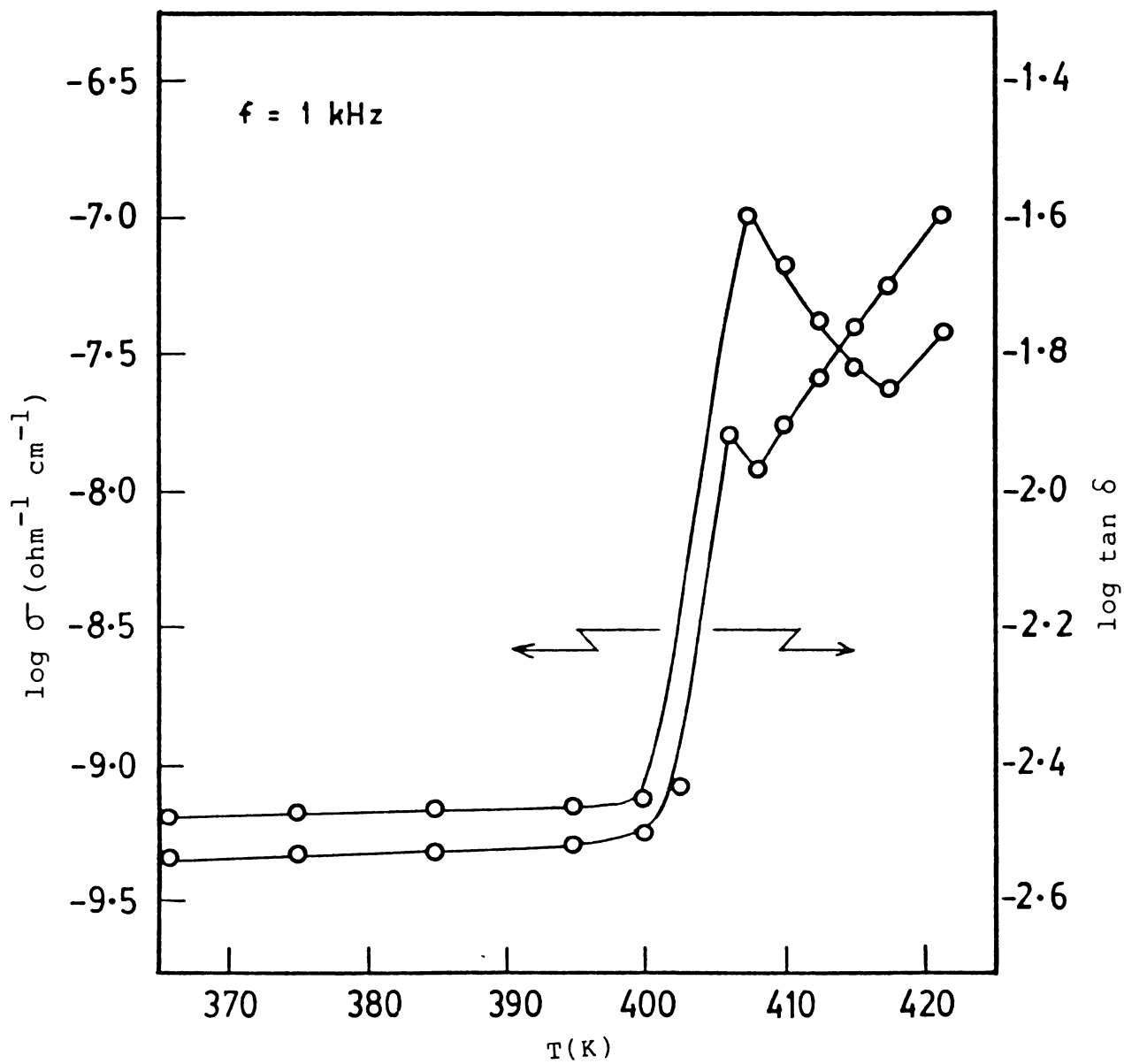


Fig.3.2: Variation of  $\sigma_{ac}$  and  $\tan \delta$  with temperature along  $c^*$ -axis.

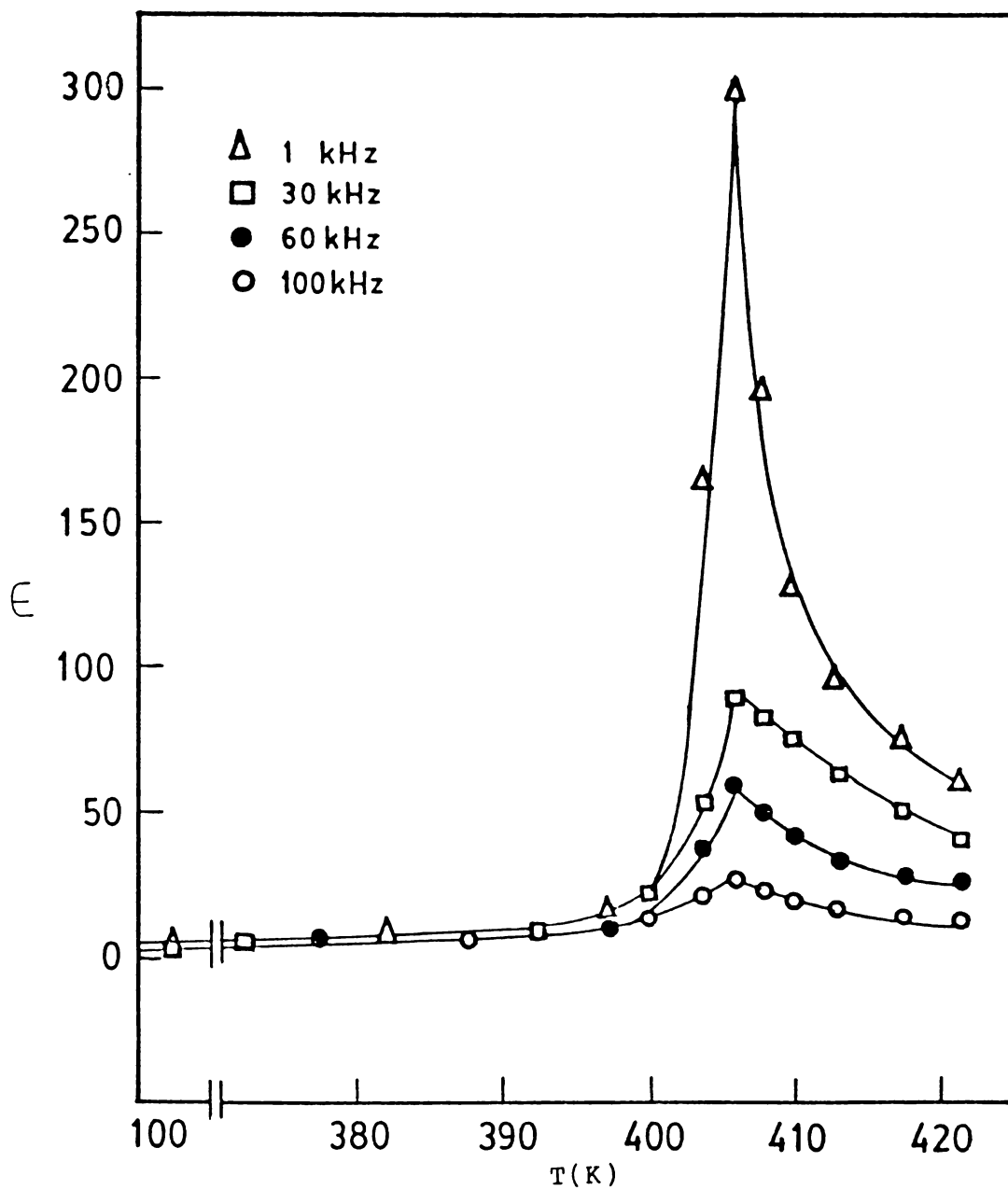


Fig.3.3: Dielectric constant of EDC as a function of temperature at different frequencies along  $c^*$ -axis.

temperature range 365 to 420 K. The temperature for the onset of  $\Lambda$ -shaped anomaly in the dielectric constant (403 K) is independent of frequency. However, the peak height decreases as the frequency increases.

The DSC thermograms recorded for EDC in nitrogen atmosphere are depicted in Fig.3.4. Powdered samples (5 mg) show a broad peak with onset at 405 K, followed by a sharp peak with onset at about 590 K. The latter endothermic peak is due to melting of the sample. This is accompanied by the decomposition of the sample. The DSC thermogram taken with small flawless single crystal sample of the same mass shows that the broad peak at 403 K has changed to a sharp peak with onset at the same temperature. The rest of the thermogram is identical with that taken with powdered samples.

### 3.4 DISCUSSION

Ethylenediammonium dichloride is one of the substituted ammonium compounds well understood in terms of its crystal structure [3]. A detailed consideration of the structure of this material will be helpful in understanding the mechanism of charge transport. The projections of the crystal structure of EDC on the (010)

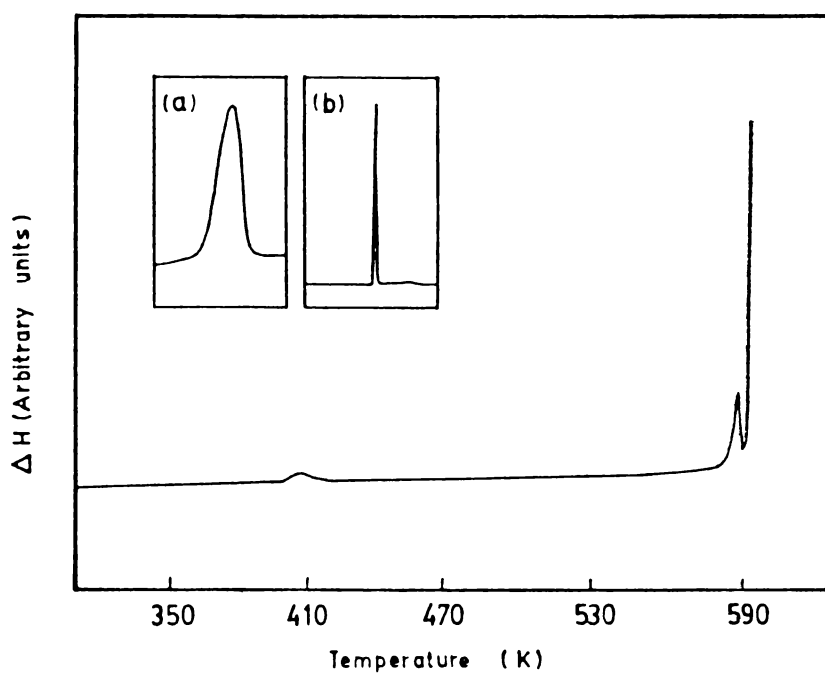


Fig.3.4: DSC traces for EDC. Inset: (a) peak at 403 K using powdered sample, (b) peak at 403 K using single crystal sample.

and (001) planes are shown in Figs.3.5 and 3.6. The three nearest chloride ions of nitrogen atom are Cl(1), Cl(2) and Cl(3). The corresponding N-H...Cl distances are 3.20, 3.22 and 3.14 Å respectively.

These short contacts are attributed to hydrogen bonds. The shortest Cl-Cl distance is 3.88 Å. Thus the three N-H...Cl hydrogen bonds bind the organic ions and the chloride ions making infinite two dimensional network perpendicular to the c-axis. The forces combining these layers along the c-axis are the van der waals' forces together with weak electrostatic forces. The low, almost temperature independent, dc conductivity of EDC at ambient and sub-ambient temperatures may be due to the strong hydrogen bonding between ethylenediammonium and chloride ions. It is anticipated that as the temperature of the specimen is raised above room temperature the hydrogen bonds become progressively weaker [8]. It seems appropriate to conceive a proton transport mechanism to explain the conductivity of EDC single crystals above 320 K. The activation energy values obtained from the conductivity plots of EDC show very good agreement with the values for protonic conduction in ammonium halides (Table 3.1). To explain the mechanism of conduction in

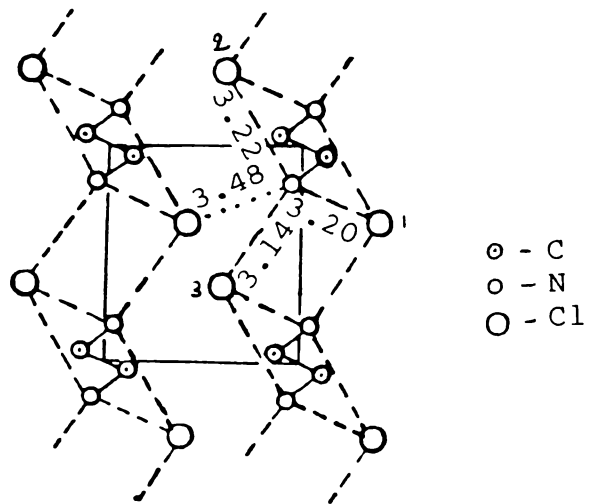


Fig.3.5: Structure of EDC projected on (010).

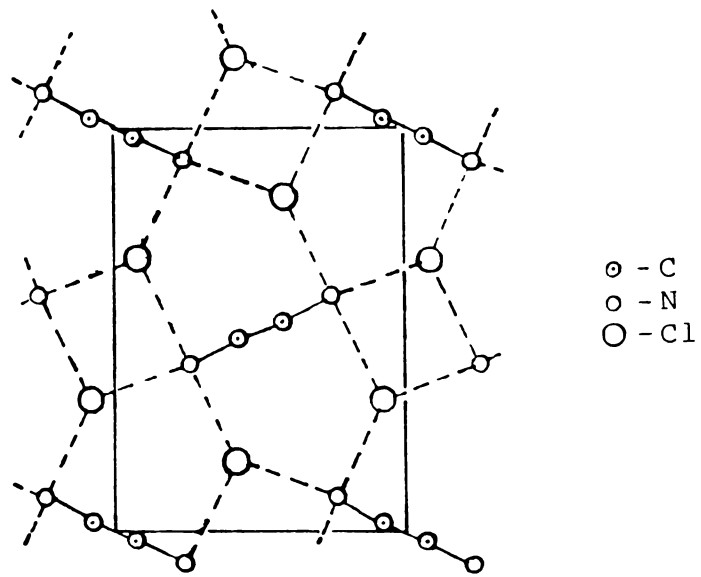


Fig.3.6: Structure of EDC projected on (001).

ammonium chloride, Herrington and Staveley [1] have proposed a three stage proton switch mechanism. This has been further supported by Fuller and Pattern [10] and Taylor and Lasker [9]. The proton switch mechanism seems to be applicable here to explain the mechanism of charge transport in EDC in which the cations and anions are connected by hydrogen bonds. The first step in the transport process can be the breaking of hydrogen bonds and the transfer of the protons directly to the neighbouring chloride ions where it is held by Coulomb attraction of the anion. In the second step, the neutral HCl molecules may fall into a neighbouring vacancy. In the third and final step, a reversal of the first step occurs forming the original structure.

Doping of EDC with sulphate ion slightly decreases the magnitude of conductivity in the low temperature region (Fig.3.1). The conductivity curves for the pure and doped samples (along  $c^*$ -axis) merge together above 369 K. The reduction in the value of electrical conductivity in doped samples can be explained in terms of the disturbance caused in the smooth hydrogen bonded network by the dopant ions. The hydrogen atoms of the ethylenediammonium ions are hydrogen bonded to the neighbouring chloride ions, the participating ionic moieties

being in the same two dimensional network. The introduction of divalent sulphate ion into the lattice displaces some of the chloride ions thus disturbing the original network of hydrogen bonds. The transport mechanism envisaged to be operative, viz., proton switch mechanism has a different potential energy barrier and hence a different frequency of occurrence in these disturbed regions of the crystal lattice.

The higher conductivity observed along the  $c^*$ -axis may be due to the shorter distance between the neighbouring atoms along this axis [3]. A proton switch mechanism can be more facile in the plane in which the hydrogen bonded network lies.

The continuous curvature of the  $\log\sigma$  vs.  $1/T$  plot in the temperature range 369 to 400 K may represent a continuously variable activation energy barrier [11] arising from a gradual loosening of the crystal lattice prior to a structural phase transition. The large increase in conductivity occurring at the phase transition may be due to the release of excess charge carriers during the rearrangement of the crystal lattice at the phase transition point. Such variations in conductivity at phase transition have been reported by earlier workers [2,12-15].

The ac conductivity versus temperature plot depicted in Fig.3.2 has some distinct features. At low temperatures the magnitude of electrical conductivity is low and remains steady upto 400 K. A sharp  $\Lambda$ -shaped anomaly with onset at 403 K is observed. This is a typical indication of a phase transition. Log  $\tan\delta$  versus temperature plot (Fig.3.2) also has similar features.  $\tan\delta$  remains almost steady upto 400 K. An inflection occurs in  $\tan\delta$  at about 403 K confirming a phase transition at this temperature.

The increase in dielectric constant with temperature is extremely small upto 400 K, which is typical of ionic materials [15]. Thereafter it rises rapidly and then falls off gradually. The value of  $\epsilon$  at room temperature is 8.12 (at 1 kHz) which rises to a peak value of 330 during the phase transition. The peak height is found to be dependent on the frequency of measurement. Such variations in dielectric constant are usually due to the contribution of the orientational polarization of the ions in the lattice. In EDC it is logical to anticipate that as the temperature of the specimen increases the hydrogen bonds become progressively weaker. At lower temperatures the  $-\text{NH}_3^+$  groups are in a state of torsional

oscillation. At sufficiently high temperature they change over to a state of free rotation with concomitant scission of the hydrogen bond. The onset of free rotation and loosening of the hydrogen bond significantly contribute to the orientational polarization of the ions in the lattice.

The anomalous variations in the electrical parameters, viz., dc and ac electrical conductivities, dielectric loss factor and dielectric constant indicate the occurrence of a structural reorientation with onset around 403 K.

An interesting feature observed in the results of DSC measurements is the dependence of the shape of the endothermic peak at 405 K on the nature of the sample. When single crystal samples are used a very sharp peak is observed at 405 K which turns out to be broad and suppressed when finely powdered samples of identical mass are used. The DSC thermograms further confirm the occurrence of a phase transition with onset temperature at 405 K, which is slightly above the value obtained in electrical measurements. The slight non-coincidence of temperature with the DSC thermogram may be due to higher heating rate and hence an apparent temperature lead in the DSC measurement.

### 3.5 REFERENCES

- [1] T.M.Herrington and L.A.K.Staveley, *J. Phys. Chem. Solids* **25** (1964) 921.
- [2] Y.V.G.S.Murti and P.S.Prasad, *Physica* **79 B** (1975) 243.
- [3] T.Ashida and S.Hirokawa, *Bull. Chem. Soc. Japan* **36** (1963) 704.
- [4] D.B.Powell, *Spectrochim. Acta* **16** (1960) 241.
- [5] J.Bellanato, *Spectrochim. Acta* **16** (1960) 1344.
- [6] R.J.Mureink and W.Robb, *Spectrochim. Acta* **24** (1968) 377.
- [7] C.H.Koo, M.I.Kim and C.S.Yoo, *Chem. Abs.* **61** (1964) 6485.
- [8] C.I.Ratcliffe, *J. C. S. Faraday II*, **76** (1980) 1196.
- [9] B.E.Taylor and A.L.Lasker, *Phy. Stat. Sol.(b)* **101** (1980) 423.

- [10] R.G.Fuller and F.W.Patten, J. Phys. Chem. Solids 31 (1970) 1539.
- [11] S.Chandra and N.Singh, J. Phys. C 16 (1983) 3081.
- [12] U.Syamaprasad and C.P.G.Vallabhan, Solid State Commun. 38 (1981) 555.
- [13] U.Syamaprasad and C.P.G.Vallabhan, Solid State Commun. 34 (1980) 899.
- [14] V.K.Subhadra, U.Syamaprasad and C.P.G.Vallabhan, J. Appl. Phys. 54 (1983) 2593.
- [15] R.Navilkumar and C.P.G.Vallabhan, J. Phys.: Condens. Matter 1 (1989) 6095.
- [16] C.P.Smith, Electrical Behaviour of Solids, p.132, Mc Graw-Hill, New York (1955).

## Chapter 4

### ELECTRICAL PROPERTIES AND PHASE TRANSITIONS IN

### ETHYLENEDIAMMONIUM DINITRATE

#### Abstract

The results of measurements of dc and ac electrical conductivities, dielectric constant and dielectric loss factor in single crystals of ethylenediammonium dinitrate (EDN) made axiswise as a function of temperature are reported in this chapter. All the above properties exhibit anomalous variations at 404 K thereby confirming the occurrence of a phase transition in EDN at this temperature. The DSC measurements carried out with EDN are in complete agreement with the above conclusion. The loss of nitric acid from the material above the phase transition temperature is established by chemical analysis. The activation energies for electrical conduction in various phases have been calculated. The mechanism of electrical conduction in the material has also been discussed in detail.

#### 4.1 INTRODUCTION

Electrical properties and phase transitions in crystals containing ammonium ions have been extensively studied with special reference to protonic conduction in them [1-6]. However, only rarely substituted ammonium compounds have been investigated in a detailed manner. Takahashi et al [7] have studied the ionic conductivity in triethylenediammonium sulphate and established protonic conductivity in them. Ethylenediammonium dinitrate,  $(\text{H}_3\text{NCH}_2\text{CH}_2\text{NH}_3)(\text{NO}_3)_2$ , (EDN) belongs to the category of organic solid ion conductors. The ethylenediammonium ion  $\text{H}_3\text{N}^+\text{CH}_2\text{CH}_2\text{NH}_3^+$  is structurally interesting since it can exist in the non-centrosymmetric gauche conformation or in the planar trans conformation of  $\text{C}_{2h}$  symmetry. Ethylenediammonium dichloride [8,9] and majority of the tetrahalide complexes crystallise in the monoclinic system with ethylenediammonium ion in the trans conformation [10,11]. In ethylenediammonium sulphate the cation exists in the gauche conformation [12].

The crystal structure of ethylenediammonium dinitrate (EDN) has been elucidated by Mylrajan and Srinivasan [13]. At room temperature, the crystal belongs to the triclinic space group  $\bar{P}1$  with  $z = 1$  with one

molecule in the unit cell having dimensions  $a = 5.068(2)$ ,  $b = 5.514(3)$ ,  $c = 7.173(3)$  Å,  $\alpha = 104.93(3)$ ,  $\beta = 90.16(4)$  and  $\gamma = 93.65(4)^\circ$ .

Investigations of the Raman and infrared spectra of EDN and its deuterated derivative have been done by Mylrajan and Srinivasan [12] in the temperature range 90 to 430 K. Temperature dependent vibrational frequencies and line widths revealed the existence of three phases below its melting point (463 K) viz.,



The C-N stretching and  $-\text{NH}_3$  rocking modes were found to be sensitive to phase transitions. It was also concluded that the trans form of  $\text{CH}_2$  group still prevails in the high temperature phases. No attempt has so far been made to study the electrical properties of EDN. In this chapter we report the results of a detailed investigation of the temperature dependent variations of dc and ac electrical conductivity, dielectric constant and dielectric loss in single crystals of EDN along c-axis and perpendicular to it ( $c^*$ -axis) in the temperature range 100 to 420 K. We have confirmed and accurately identified the

high temperature phase transition and evaluated the activation parameters for the electrical conduction in different temperature ranges. Conductivity measurements were also made using crystals of EDN doped with  $\text{SO}_4^{2-}$  to observe the influence of dopant on the conduction mechanism.

#### 4.2 EXPERIMENTAL DETAILS

EDN was prepared by mixing solutions of distilled ethylenediamine (Glaxo Laboratories) and nitric acid (BDH Analar) in 1 : 2 mole ratio. Single crystals of pure and  $\text{SO}_4^{2-}$  doped EDN were grown from solutions of the recrystallised material as described in section 2.2. Stiochiometry of the final product was confirmed by chemical analysis. The single crystals obtained were transparent. They showed perfect cleavage along (001) plane, just as in the case of ethylenediammonium dichloride [9].

Crystals of EDN are not deliquescent. Samples of typical dimensions  $5 \times 5 \times 1 \text{ mm}^3$  were cut parallel to, and perpendicular to the cleavage plane. The two broad faces of the samples were vacuum coated with silver to render good electrical contact. The sample holder and the

chamber used for the measurement of electrical properties are described in chapter 2. The samples were annealed at 100°C in vacuum for 30 minutes before making the measurements. All the measurements were made in a dynamic vacuum of  $10^{-3}$  Torr in the temperature range 100 to 420 K. Measurements were repeated using different samples to establish reproducibility.

In the measurement of dc conductivity, a steady dc bias of 10-100 V was applied across the specimen and the current was measured using Keithley electrometer model 617. The ac conductance  $G$ , capacitance  $C$  and dielectric loss  $\tan\delta$  were measured as a function of frequency as well as temperature using Hewlett Packard LF Impedance Analyzer model 4192A. Knowing the dimensions of the sample, the specific conductance was calculated. Dielectric constant was derived from the measured values of capacitance after eliminating the lead and fringe capacitance using standard methods [14]. DSC traces were recorded using Perkin Elmer DSC-7 instrument with single crystals as well as with finely powdered samples. The temperature corresponding to the onset of thermal anomaly is reported as the transition temperature.

### 4.3 EXPERIMENTAL RESULTS

#### 4.3.1 dc electrical conductivity

Fig.4.1 shows the  $\log \sigma$  vs.  $10^3/T$  plots within the temperature range 300 to 410 K for EDN along c and c\*-axes, where  $\sigma$  is the dc conductivity. Each plot consists of two segments below 400 K. The segments fit into the equation  $\sigma = \sigma_0 \exp(-E/kT)$  where  $\sigma_0$  is a constant k is the Boltzmann's constant and E is the activation energy. The sudden jump in the conductivity resulting in a  $\Lambda$ -shaped anomaly at 404 K indicates a phase transition. The activation energy  $E_a$  and 'infinite temperature intercept'  $\log \sigma_0$  obtained by analysing different segments of the Arrhenius plots are presented in Table 4.1.

Fig.4.2 compares the conductivity of pure and  $\text{SO}_4^{2-}$  doped EDN crystals, the measurement being taken along c-axis in the temperature range 300 to 410 K. The conductivity of the doped sample is found to be slightly less than that of the pure sample in the entire temperature range. However, the activation energy is not altered significantly. The activation energy values 1.18 and 2.30 eV in the temperature range 300 to 378 K and 378 to 400 K respectively in the case of doped EDN agree well

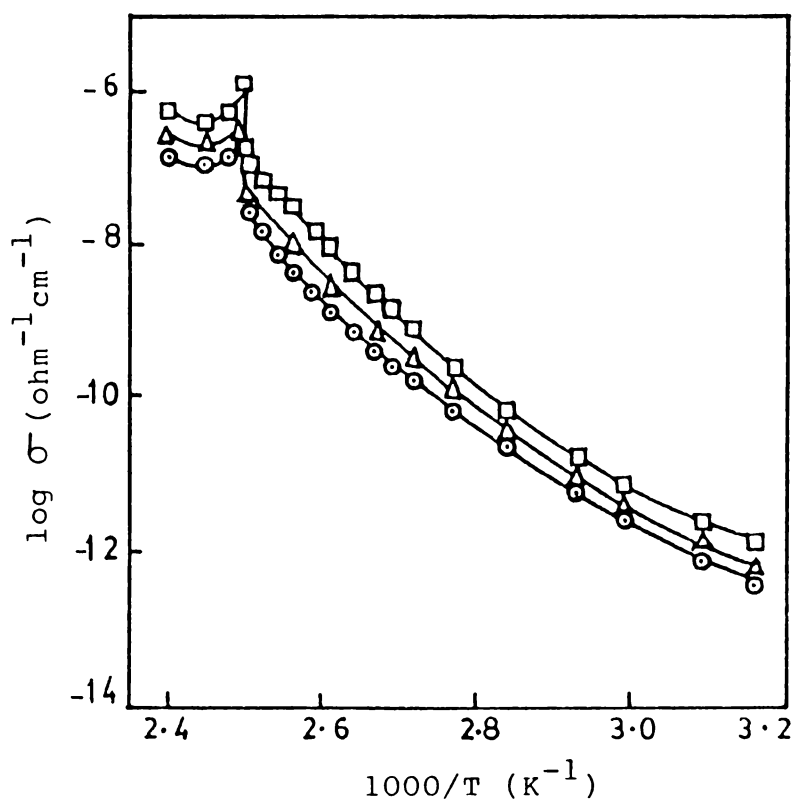


Fig.4.1  $\log \sigma_{dc}$  vs.  $1/T$  plots for EDN.  $\circ$  - along c-axis in the heating run,  $\triangle$  - cooling run,  $\square$  - along  $c^*$ -axis in the heating run.

Table 4.1: Activation energy  $E_a$  and intercept  $\log \sigma_0$  for dc conductivity of EDN single crystal along  $c$  and  $c^*$ -axes.

Axis	Temperature range (K)	Activation energy (eV)	Log $\sigma_0$
$c$	300 to 378	1.22	7.9
	378 to 400	2.12	15.8
$c^*$	300 to 378	1.11	5.2
	378 to 400	2.17	16.6

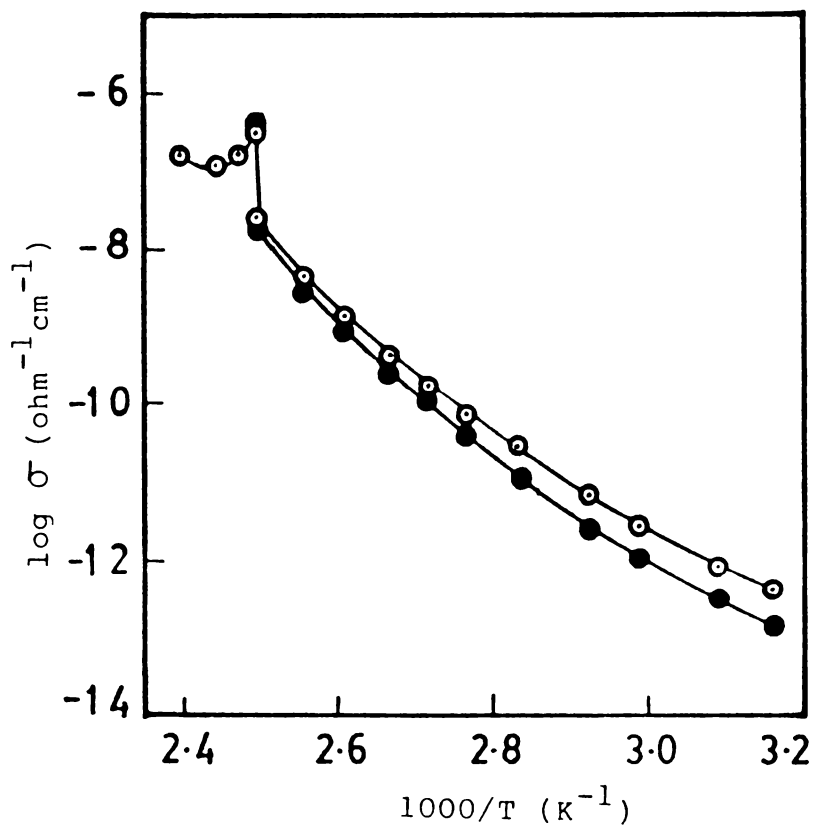


Fig.4.2:  $\log \sigma_{dc}$  vs  $1/T$  plots for EDN along c-axis.  
○ - pure sample, ● - sulphate doped sample.

with those of pure sample (Table 4.1). No shift in the phase transition temperature is observed in the doped specimen.

#### 4.3.2 ac conductivity

Fig.4.3 is a typical plot of  $\log \sigma_{ac}$  against  $10^3/T$  for EDN over the temperature range 320 to 410 K at 30 kHz, the data covering several heating and cooling runs. The abrupt change in  $\sigma_{ac}$  at 404 K indicates again the phase transition occurring in the crystal at that temperature and this is in conformity with dc measurements.

Fig.4.4 presents the Arrhenius plots ( $\log \sigma$  vs  $10^3/T$ ) for the ac and dc conductivity data obtained using pure EDN single crystals along  $c^*$ -axis. It is observed that  $\sigma_{ac}$  approaches  $\sigma_{dc}$  at higher temperatures, but deviates from  $\sigma_{ac}$  at low temperatures, the deviation being larger for higher frequencies. In the temperature range from ambient upto 378 K the plots are frequency dependent. The temperature dependence of  $\sigma_{ac}$  is not very significant below this temperature. The ac conductivity curves merge together themselves and also with the dc conductivity curve above 378 K, showing that the same conduction mechanism is operative in this high temperature region.

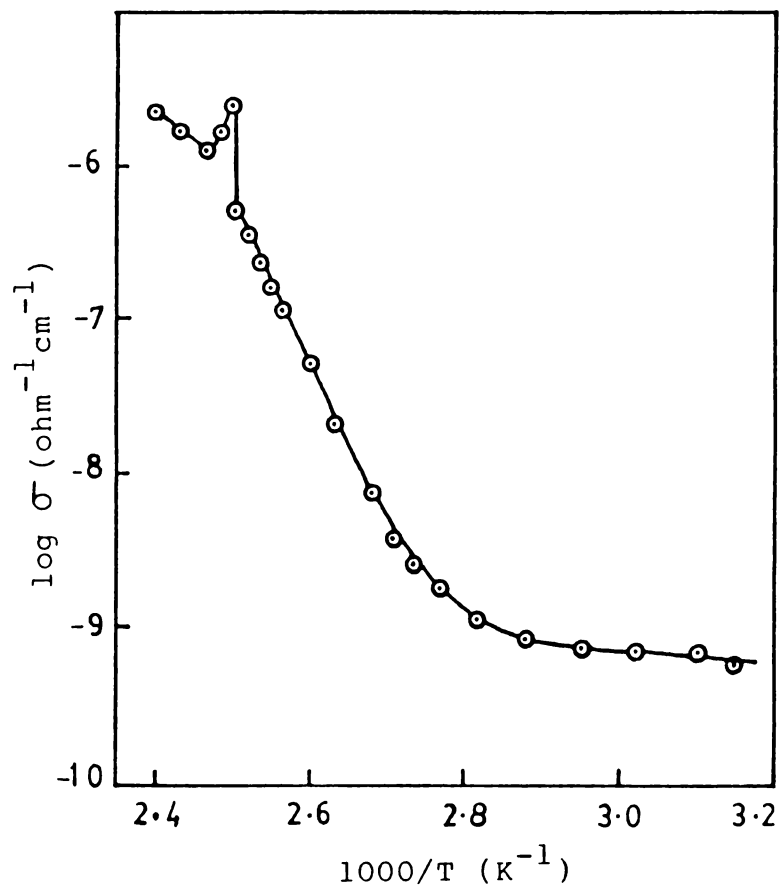


Fig.4.3  $\log \sigma_{ac}$  vs.  $1/T$  plot for EDN along c-axis at 30 kHz.

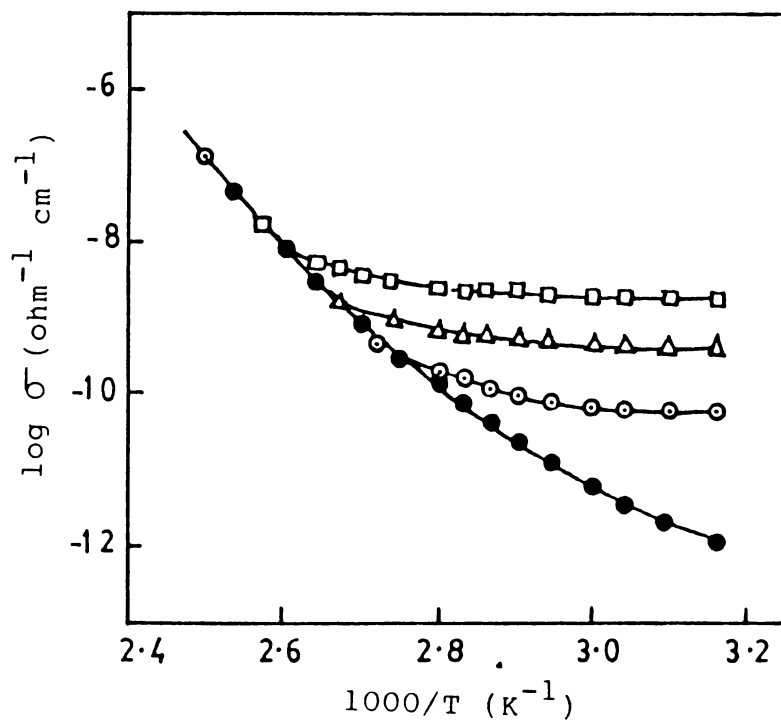


Fig.4.4: Variation of ac and dc conductivities of EDN as a function of temperature along c-axis.  $\bullet$  -  $\sigma_{dc}$ ,  $\circ$  -  $\sigma_{ac}$  at 1 kHz,  $\Delta$  -  $\sigma_{ac}$  at 30 kHz,  $\square$  -  $\sigma_{ac}$  at 100 kHz

### 4.3.3 Dielectric constant

Fig.4.5 displays the temperature dependence of dielectric constant along  $c$  and  $c^*$ -axes at different frequencies. The variation of dielectric loss along  $c^*$ -axis is represented in Fig.4.6. The dielectric constant and dielectric loss vary slowly upto 378 K. Above this temperature the variation is rapid and an abrupt change occurs at 404 K, confirming the phase transition at this temperature.

The results of the measurement of dielectric constant on single crystals of EDN in the temperature range 375 to 410 K are shown in Fig.4.7. Dielectric constant shows an abrupt increase at 404 K. In the cooling run it shows a hysteresis of 3 K. Similar results were obtained by measurements in the  $c^*$ -axis also.

## 4.4 DISCUSSION

To explain the conduction mechanism and phase transition in pure and doped specimens of EDN, an understanding of the crystal structure of this compound is necessary. Single crystal X-ray diffraction studies of EDN were carried out by Mylrajan and Srinivasan [13]. The

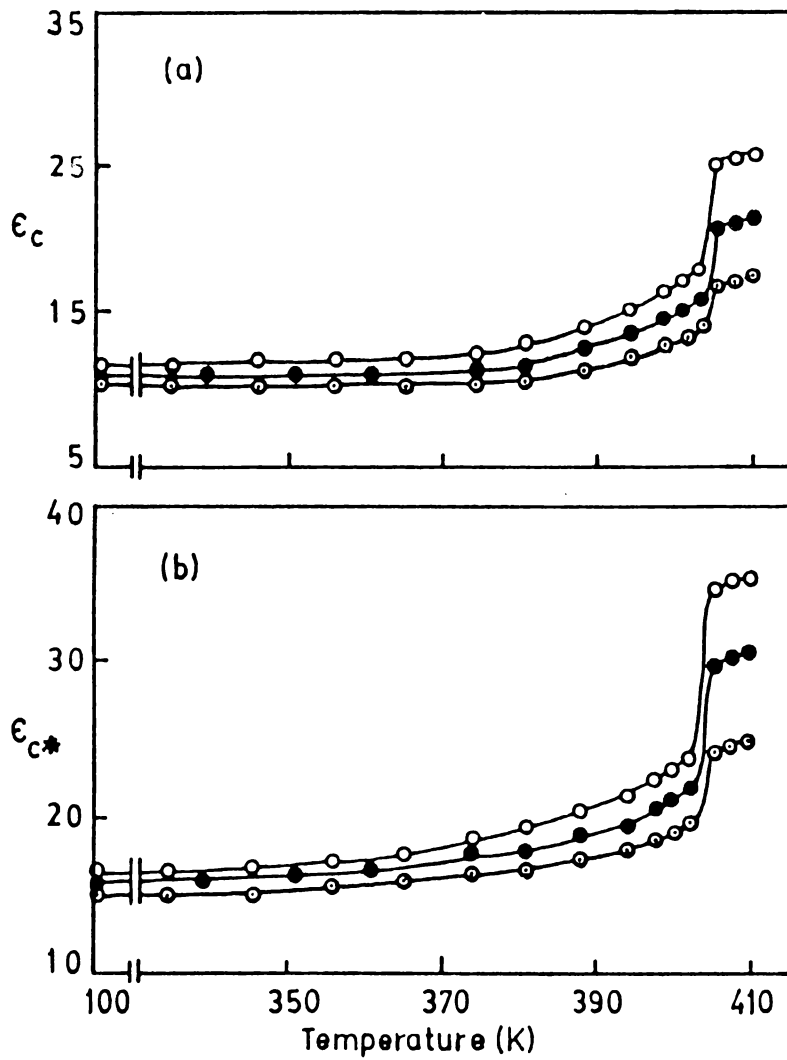


Fig.4.5 Variation of dielectric constant of EDN as a function of temperature at different frequencies. (a) - along c-axis, (b) - along c-axis, 0-1 kHz, ● - 30 kHz, ○ - 100 kHz.

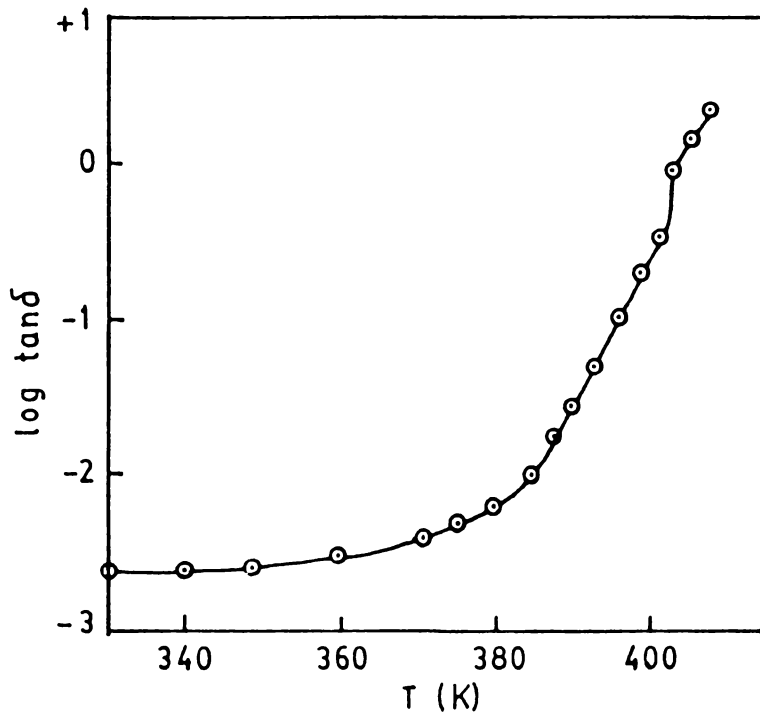


Fig.4.6 Variation of  $\tan \delta$  with temperature for EDN along c-axis.

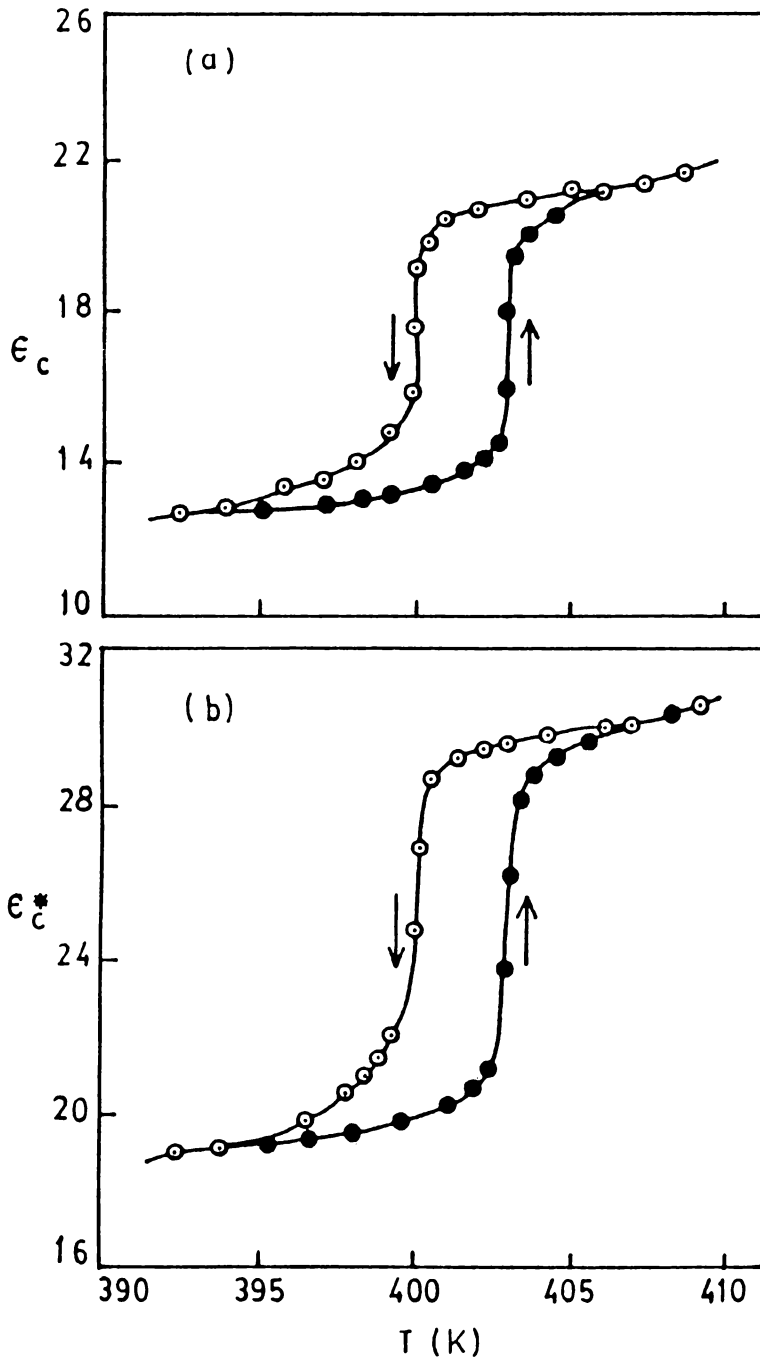
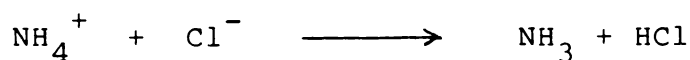


Fig.4.7 Variation of dielectric constant with temperature for EDN in the heating and cooling runs. (a) - along  $c$ -axis, (b) - along  $c^*$  axis.

structural details are the following. Fig.4.8 depicts the unit cell content of EDN. The cation occupies a centre of inversion ( $C_i$ ) at  $(0, \frac{1}{2}, \frac{1}{2})$ . The anion lies on the  $C_1$  site symmetry. Both cations and anions are held together by hydrogen bonds. The following are the bond distances: C-N = 1.474(3), C-C = 1.510(5),  $N_1-O_1 = 1.224(3)$ ,  $N_1-O_2 = 1.255(2)$ ,  $N_1-O_3 = 1.260(3)$  Å. The bond angles are:  $O_1-N_1-O_2 = 121.3(3)$ ,  $O_2-N_1-O_3 = 117.6(2)$ ,  $O_3-N_1-O_1 = 121.1(2)^\circ$ .

The electrical conduction in ammonium containing crystals has been discussed by different workers. While explaining the mechanism of conduction in ammonium chloride, Herrington and Staveley [15] have postulated that there is significant amount of dissociation in these crystals to form molecular species which may be represented by the process,



They proposed a three stage proton switch mechanism in which (i) the proton leaves the  $NH_4^+$  ion and joins the  $Cl^-$  ion forming  $NH_3$  and  $HCl$  molecules (ii) a vacancy and the appropriate molecule exchange positions and (iii) the

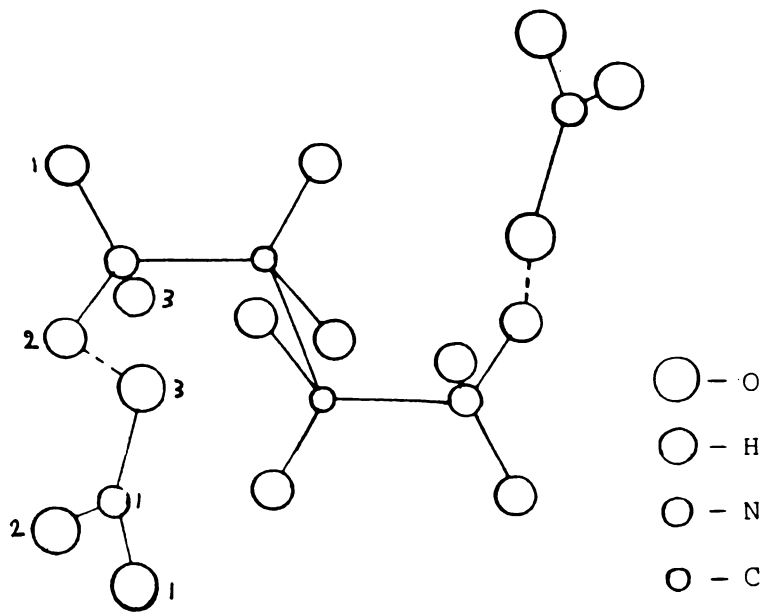


Fig.4.8 Figure showing the unit cell content of EDN.

proton jumps back to  $\text{NH}_3$  forming  $\text{NH}_4^+$  and  $\text{Cl}^-$  ions again. Thus a net displacement of charge can be accomplished by an applied electric field. The possibility of a proton switch mechanism in ammonium salts has further been supported by the work of Fuller and Patten [16]] and Taylor and Lasker [2]. The concepts put forward by Herrington and Staveley seem to be applicable to explain the mechanism of conduction in EDN also where the cations and anions are connected by hydrogen bonds. Here the initial step in the transport process can be the breaking of a hydrogen bond and the transfer of the proton directly to the neighbouring nitrate ion. Thermal disorder giving rise to fluctuations of the electrostatic field will also be in favour of such a proton transfer. Subsequently the neutral  $\text{HNO}_3$  molecules may migrate to an adjacent vacancy and in the final step a reversal of the proton switch may occur. It may be noted that the activation energy for conduction in EDN below 378 K (Table 4.1) compares very well with activation energies for proton conduction in  $\text{NH}_4\text{Cl}$  and  $\text{NH}_4\text{Br}$  [2,17,18].

A sharp demarcation into three straight line regions for the conductivity plot for c-axis is not clearly discernible in comparison with that for c\*-axis

(Fig.4.1). This could probably be due to the existence of a continuously variable barrier [19] along this direction. Also the higher value of  $\sigma_{dc}$  along  $c^*$ -axis (Fig.4.1) could be due to the higher mobility of carriers along this axis, which is parallel to the cleavage plane. The change in the slope of  $\log \sigma_{dc}$  vs  $10^3/T$  plot near 378 K indicates a change in the dominant conduction mechanism. It is also seen that the  $\log \sigma_{ac}$  vs  $10^3/T$  plots merge together and become identical with the corresponding dc conductivity plot at about 378 K. Around this temperature it is expected that the rotational reorientation of the  $-\text{NH}_3^+$  groups of EDN is initiated as indicated by a gradual shift in the  $-\text{NH}_3^+$  rocking frequencies in the infrared spectrum.

The lower value of conductivity in the doped sample indicates that either the concentration of carriers or their mobility or both are affected by doping. It is envisaged that  $(\text{H}_3\text{NCH}_2\text{CH}_2\text{NH}_3)\text{SO}_4$  occupies some of the sites in  $\text{H}_3\text{NCH}_2\text{CH}_2\text{NH}_3(\text{NO}_3)_2$  crystals and the regular chain of hydrogen bonds in the host lattice are broken by the incorporation of divalent  $\text{SO}_4^{2-}$  ions. The difference in the conformation of the EDS molecules may also be causative to this. The two  $-\text{NH}_3^+$  groups of ethylenediammonium ion are trans to each other in EDN [13] whereas they are cis to each other in EDS [12].

Though the magnitude of conductivity decreases slightly in doped samples, the activation energy for conduction is not significantly altered. This indirectly supports the fact that neither the nature of the conducting species nor the mechanism of conduction is affected by the dopant.

The magnitudes of ac and dc conductivities of EDN single crystals show a significant difference in the low temperature region (Fig.4.4). Similar behaviour was observed by Berteit et al [20] in  $\text{NH}_4\text{Br}$ . The difference can be attributed to loosely bound protons which are able to jump with the field. Thus in an ac field, the hopping probability becomes proportional to the frequency of the field and the ac conductivity shows an increase with increase in frequency.

The dielectric constant of EDN single crystals at 300 K along  $c^*$ -axis (16) is found to be greater than that along  $c$ -axis (11). Ionic crystals with non-cubic structure usually exhibit such anisotropy in dielectric properties. The abrupt changes in dc and ac conductivities, dielectric constant and dielectric loss at 404 K are certainly due to the structural phase transition

occurring at this temperature as indicated in the earlier studies. The thermal hysteresis observed in the dielectric measurement at this temperature is indicative of a first order transition. The sharp rise in conductivity can be due to the large scale availability of the mobile carriers released during the rearrangement of the ammonium group. The higher value of dielectric constant observed at the transition point arises evidently from the contribution to the orientational polarizability from the freely rotating  $-\text{NH}_3^+$  groups. The mechanism involved in this transition is analogous to those observed in many other crystals containing ammonium groups [6,7,17,21].

From the DSC and IR and Raman spectral studies, Mylrajan and Srinivasan [13] have reported the existence of three phases in EDN below its melting point at 463 K, viz.,



Their DSC thermograms indicated two peaks at 404 K and 412 K in the forward run, whereas only one broad peak was observed at 392 K in the reverse direction. They attributed the broad peak at 392 K to the merging of closely occurring phase transitions. The phase transition

at 404 K is associated with a distinct change in frequency for all the modes in the infrared spectrum. However, only the C-N stretching frequency showed slight changes at the second phase transition at 412 K. Splitting of the  $\text{-NH}_3^+$  asymmetric stretching bands was observed at 3193 and 3228  $\text{cm}^{-1}$  in the Raman spectrum at 90 K, while a single broad band at 3210  $\text{cm}^{-1}$  was seen at 420 K. The band at 58  $\text{cm}^{-1}$  at 300 K moved to lower frequencies as the temperature was increased. At 420 K it shifted to 40  $\text{cm}^{-1}$  and appeared as a shoulder of the Rayleigh wing, indicating tendency for mode softening. The infrared-active C-N stretch and  $\text{-NH}_3^+$  rocking modes appeared to be the most sensitive to the phase transitions. The  $\text{-NH}_3^+$  rocking mode at 1088  $\text{cm}^{-1}$  showed a large shift with increasing temperature. This was observed with increased half bandwidth at 1070  $\text{cm}^{-1}$  at 410 K and at 1068  $\text{cm}^{-1}$  at 420 K. These changes clearly indicate rearrangement of the skeleton. Appreciable  $\text{-NH}_3^+$  reorientation is evident from the broad and weak nature of  $\text{-NH}_3^+$  stretching, rocking and bending modes in the spectrum of the high temperature phase of this material. This is in good agreement with the results of our dielectric measurements which indicate the existence of fairly freely rotating polar groups in the high temperature phases. However, it

is to be noted that (C-N) stretching frequency showed only slight changes near 412 K. X-ray and/or neutron diffraction studies will be needed to get a clear picture regarding the crystal structure in the high temperature phase.

T  
537.226:68-911.62:661.71  
SAM

In the present investigation it is found that the samples of EDN single crystals remained transparent after the phase transition at 404 K. The reproducibility of the results was good in all runs which were terminated at 408 K. Our results suggest that if the sample is heated to a temperature too close to the reported second transition temperature of 412 K, the pattern is not well reproducible. If this temperature is exceeded, the sample turns opalescent and the electrical measurements yield erratic results.

To alleviate the vagueness regarding the nature of the reported phase transition at 412 K, we have approached the problem from two different angles: (i) What is the influence of the physical form of the sample (ie., powder or single crystal) on the phase transitions? and (ii) Does the sample undergo any transformation with loss of material in volatile form?

To ascertain the influence of the physical form of the material near this transition, DSC thermograms were recorded with single crystals as well as with finely powdered samples of nearly the same weight. The results are shown in Fig.4.9. The peak at 412 K is of pronounced intensity in single crystals while it is hardly measurable with finely powdered samples.

To check the formation of any volatile component at the transition temperature, the following methodology was used. Samples of EDN were heated to a temperature above 412 K in a tube fitted to a capillary scrubber wetted with distilled water. The vapour was flushed out in a slow stream of dry nitrogen and trapped in the scrubber. The scrubber liquid was tested with diphenylamine in sulphuric acid [22]. The results indicated the evolution of nitric acid. In a separate experiment EDN was heated to  $416 \pm 1$  K. The evolved vapours were swept in a stream of nitrogen for 30 minutes and absorbed in a trail of bulbs containing triply distilled water. The amount of nitric acid collected was determined by spectrophotometry [23]. The experiment was repeated and it was found that the sample gave out an average of 0.15 mg of  $\text{HNO}_3$  per gram of EDN.

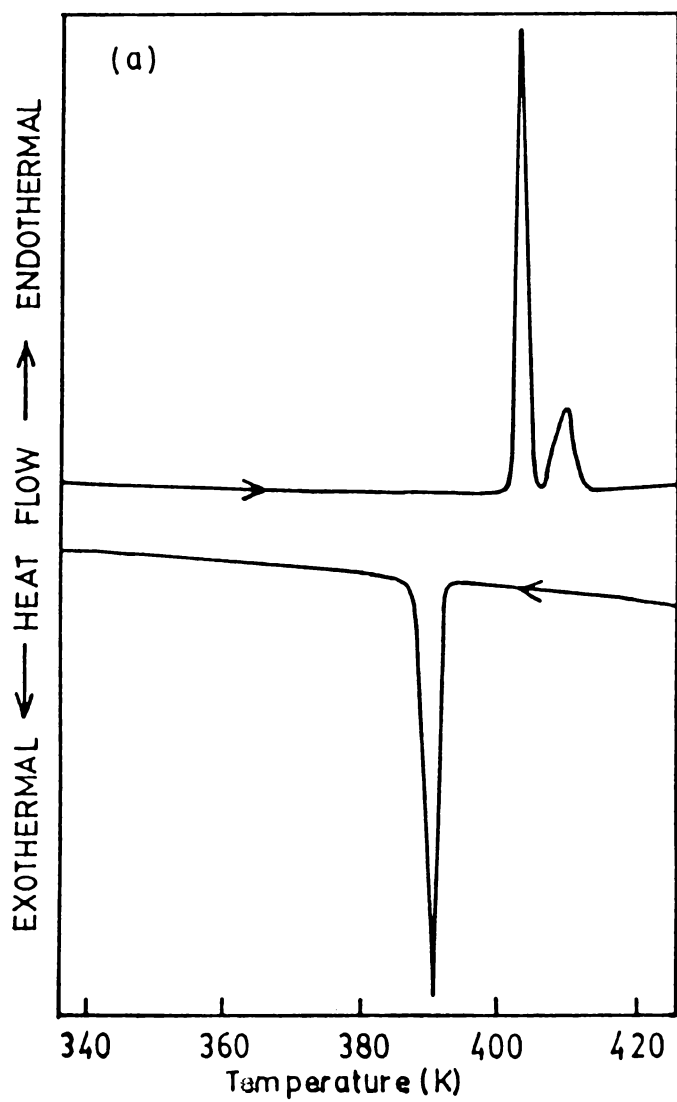


Fig.4.9(a): DSC thermogram obtained using single crystal sample of EDN.

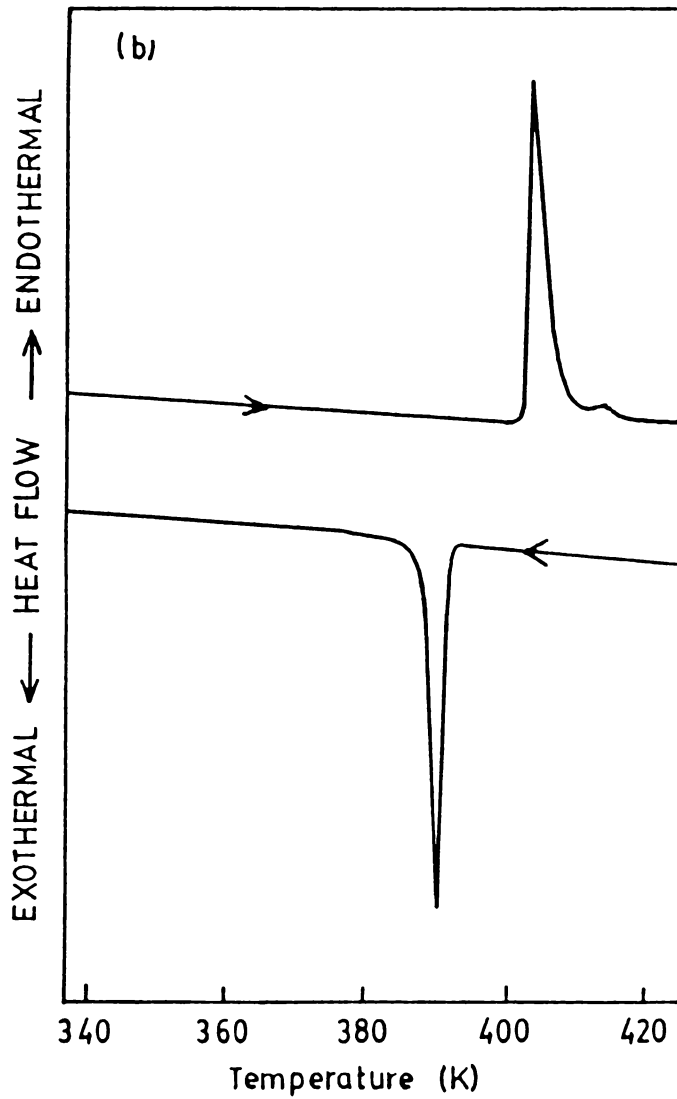


Fig.4.9(b): DSC thermogram obtained using powdered sample of EDN.

#### 4.5 CONCLUSIONS

Axis-wise measurements of dc and ac conductivities, dielectric constant and dielectric loss factor in EDN have been carried out within the temperature range 100 to 410 K using single crystals. The occurrence of a phase transition in this material is confirmed and the transition temperature has been accurately fixed at 404 K. The hysteresis shown in the dielectric behaviour indicates that the transition is of first order. The irreversible peak at 412 K in the DSC trace has been established as due to the formation of  $\text{HNO}_3$ . Protons are found to play a vital role in the conduction mechanism.

**4.6 REFERENCES**

- [1] E.J.Murphy, J. Appl. Phys. **35** (1964) 2604.
- [2] B.E.Taylor and A.L.Laskar, Phys. Stat. Sol.(b) **101** (1980) 423.
- [3] A.Devendar Reddy, S.G.Sathyanarayan and G.Sivarama Sastry, Solid State Commun. **43** (1982) 937.
- [4] U.Syamaprasad and C.P.G.Vallabhan, Phys. Lett. **89A** (1982) 37.
- [5] V.K.Subhadra, U.Syamaprasad and C.P.G.Vallabhan, J. Appl. Phys. **54** (1983) 2593.
- [6] R.Navilkumar and C.P.G.Vallabhan, J. Phys.: Condens. Matter **1** (1989) 6095.
- [7] T.Takahashi, S.Tanase, O.Yamamoto and S.Yamauchi, J. Solid State Chem. **17** (1976) 353.
- [8] T.Ashida and S.Hirokawa, Acta Cryst. **16** (1963) 841.

- [9] T.Ashida, and S.Hirokawa, Bull. Chem. Soc. Japan  
36 (1963) 704.
- [10] I.Lofving, Acta Chem. Scan. Part A 30 (1976) 715.
- [11] R.W.Berg, Spectrochim. Acta 32A (1976) 1747.
- [12] K.Sakurai, J. Phys. Soc. Japan 16 (1961) 1205.
- [13] M.Mylrajan and T.K.K.Srinivasan, Phase Transit. 12  
(1988) 285.
- [14] C.Ramasastri and Y.Syamasundara Rao., J. Phys. E:  
Sci. Instrum. 12 (1979) 1023.
- [15] T.M.Herrington and L.A.K.Staveley, J. Phys. Chem.  
Solids 25 (1964) 921.
- [16] R.G.Fuller and F.W.Patten, J. Phys. Chem. Solids  
31 (1970) 1539.
- [17] Y.V.G.S.Murti and P.S.Prasad, Physica B79 (1975)  
243.

- [18] S.Radhakrishna and B.D.Sharma, J. Appl. Phys. **44** (1973) 243.
- [19] S.Chandra and N.Singh, J. Phys. C: **16** (1983) 3081.
- [20] Y.Berteit, A.Kessler and T.List, J. Phys. **B24** (1976) 15.
- [21] U.Syamaprasad and C.P.G.Vallabhan, Solid State Commun. **38** (1981) 555.
- [22] F.Feigl and V.Anger, Spot Tests in Inorganic Analysis, Elsevier Publishing Co., Amsterdam (1972) p.360.
- [23] Encyclopaedia of Industrial Chemical Analysis, ed. by F.D.Snell and L.S.Ettre, John Wiley and Sons Inc., New York (1972) Vol.16, p.503.

## Chapter 5

### ELECTRICAL CONDUCTIVITY, DIELECTRIC PROPERTIES AND PHASE TRANSITIONS IN ETHYLENEDIAMMONIUM SULPHATE SINGLE CRYSTALS

#### Abstract

The results of dc and ac electrical conductivities, dielectric constant and dielectric loss factor in single crystals of ethylenediammonium sulphate,  $(\text{H}_3\text{NCH}_2\text{CH}_2\text{NH}_3)(\text{SO}_4)$ , measured axis-wise as a function of temperature in the range 100 to 495 K are presented in this chapter. Anomalous variations in all the above properties at 480 K indicate the occurrence of a phase transition in the material at this temperature. The existence of such a phase transition is also confirmed by DSC measurements. Electrical conductivity results are analyzed and the activation energies of conduction in different temperature ranges are evaluated from the  $\log\sigma$  vs.  $10^3/T$  plot. Deuteration of the sample lowers the conductivity in the entire temperature range. The possible mechanisms for electrical conduction and phase transition are discussed. The available results are in favour of a proton transport model.

## 5.1 INTRODUCTION

Ethylenediammonium sulphate,  $(\text{H}_3\text{NCH}_2\text{CH}_2\text{NH}_3)(\text{SO}_4)$  (EDS) is a structurally interesting material and is known for its strong optical rotatory power [1]. The crystallographic description of this material has been given by Groth [1] and Burgers [2]. The optical studies of EDS were carried out by Burkov et al. [3,4]. In order to obtain a structural basis for the interpretation of optical activity, Sakurai [5] made a detailed structural analysis of EDS by X-ray methods. Ratcliffe [6] studied the proton spin-lattice relaxation time of the ethylenediammonium ion in EDS as a function of temperature from which the activation energies for reorientation of the  $-\text{NH}_3^+$  groups were evaluated. The results also indicated a phase change setting in at 476 K on heating, with a hysteresis effect on cooling. So far, there exists no report on any studies made on the electrical properties of EDS. This chapter covers the results of the measurements of dc and ac electrical conductivities, dielectric constant and dielectric loss of single crystals of this material.

## 5.2 EXPERIMENTAL

Microcrystals of EDS were prepared by mixing freshly distilled ethylenediammine (Glaxo Laboratories)

and sulphuric acid (British Drug House, Analar grade) in 1 : 1 mole ratio and subsequent evaporation of the solution on a water bath. Large single crystals were grown by slow evaporation of the saturated solution of the material in double distilled water at ambient temperature. Doped samples were prepared in a similar manner from aqueous solution of EDS spiked with a known amount (0.1 mole %) of  $(\text{H}_3\text{NCH}_2\text{CH}_2\text{NH}_3)\text{HPO}_4$ . Deuterated samples were prepared by dissolving pure EDS in heavy water (99.5% purity, BARC, Bombay) and recrystallizing (five times) the material from the solution. The presence of deuterium in the samples was verified from the infrared spectra.

The crystals are plate-like and are not hygroscopic. They exhibit a nearly perfect cleavage parallel to (001) plane [5]. Samples in the form of rectangular plates of about  $36 \text{ mm}^2$  area and 1 mm thickness were cut with faces parallel to the cleavage plane, as well as perpendicular to it, so that measurements could be made along  $c$  and  $c^*$ -axes. Silver electrodes were vacuum deposited on to the broad faces of the samples to ensure good electrical contact and to remove the effect of any air gap between the crystal and the electrode surface.

dc electrical conductivity measurements were carried out by the two-probe method using a Keithley Electrometer model 617. The sample holder used in the present investigations has been described in Chapter 2. The dc conductivity measurements were made with voltage gradients ranging from 100 to 1000 V/cm. The measurements were made for both directions of current flow. The conductivity proved to be independent of direction and voltage gradient.

Measurement of dc conductivity in pure, doped and deuterated single crystals of EDS were carried out as a function of temperature in the range 100 to 495 K. All the measurements were made in vacuum to avoid any moisture absorption on the surface of the sample. Moreover, care was taken to anneal the sample at 100°C for 30 minutes before each experiment. The temperature dependence of conductivity was measured at a uniform heating rate of 0.1 K/min near the phase transition temperature and 1 K/min in other temperature regions. Measurements were repeated to ensure reproducibility.

The ac conductance  $G$ , capacitance  $C$ , and dielectric loss  $\tan\delta$  were measured as a function of

frequency in the temperature range 100 to 495 K.  $G$  and  $\tan\delta$  of EDS single crystals were found to be below the detection limit of the instrument (Hewlett Packard LF Impedance Analyzer model 4192 A) except in the high temperature region near the phase transition. The value of ac conductivity is calculated using the known dimensions of the sample. Dielectric constant is derived from the measured capacitance, after eliminating the lead and fringe capacitance using standard methods [8]. Differential scanning calorimetric traces were recorded using Perkin Elmer DSC-7 instrument in nitrogen atmosphere at a scanning speed of 10 K/min.

### 5.3 RESULTS

#### 5.3.1 dc electrical conductivity

Typical traces for the variation of dc electrical conductivity with temperature in pure and phosphate doped single crystals of EDS are illustrated in Fig.5.1. The increase of  $\sigma_{dc}$  with temperature is extremely small upto about 340 K. A careful analysis of the  $\log \sigma_{dc}$  vs.  $10^3/T$  plot shows that it is linear in the range 360 to 408 K. Thereafter it shows a continuous curvature upto 480 K, where a prominent conductivity anomaly, indicative of a phase transition occurs. The

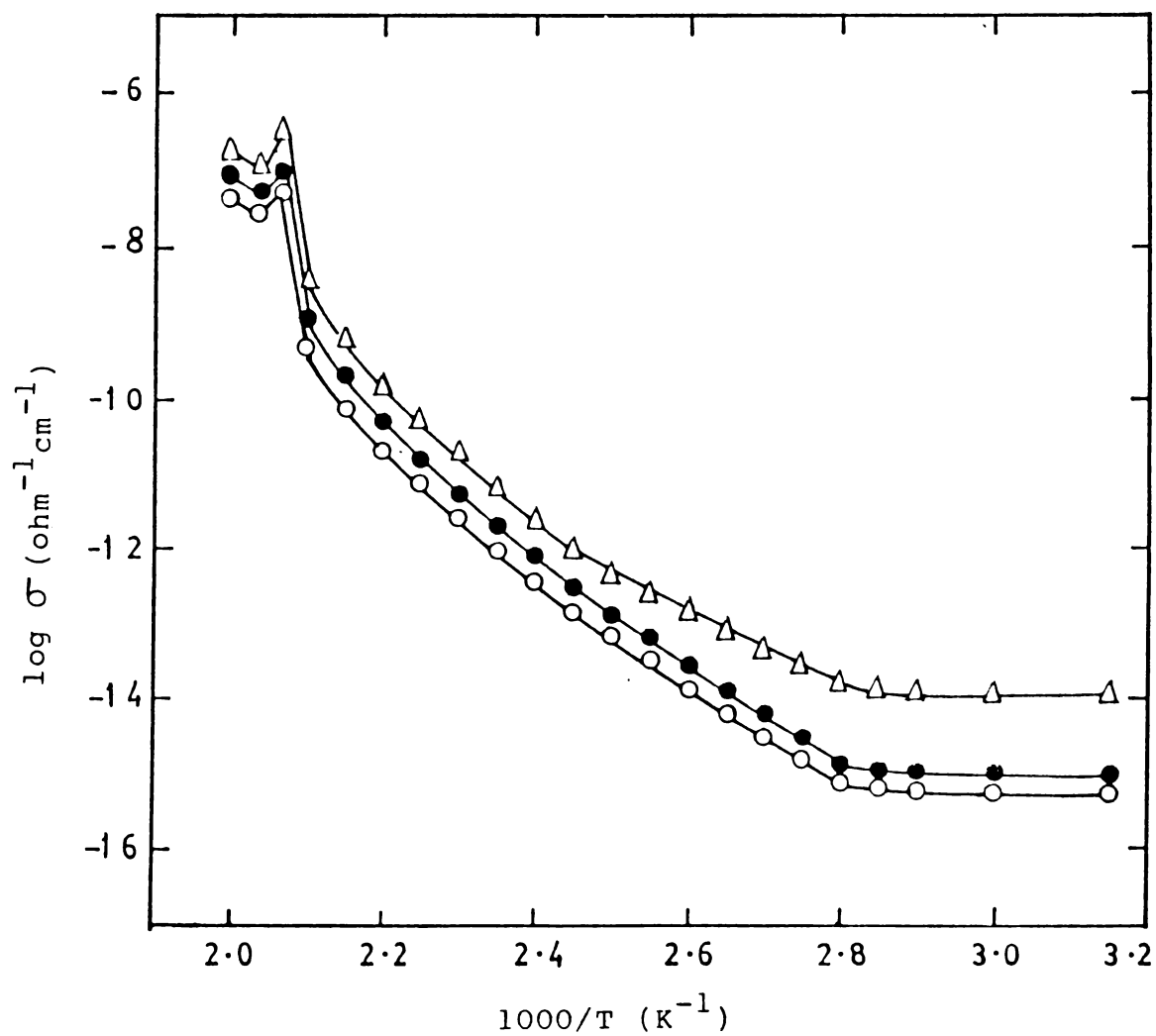


Fig.5.1:  $\log \sigma_{dc}$  vs  $1/T$  plots for EDS. O - pure EDS along c-axis, ● - phosphate doped EDS along c-axis, Δ - pure EDS along c\*-axis.

conductivity of the doped sample is found to be slightly higher than that of pure sample in the entire temperature range. Again the conductivity along  $c^*$ -axis is found to be higher than that along  $c$ -axis. The activation energy values calculated from the Arrhenius plots are given in Table 5.1. The conductivity anomalies with distinct  $\Lambda$ -shaped peaks at about 480 K are clear indications of a phase transition taking place at this temperature.

Fig.5.2 shows the  $\log \sigma$  vs.  $10^3/T$  plot for pure and deuterated single crystals, the measurement being taken along  $c$ -axis. The anomalous variations in the conductivity plot of pure and deuterated EDS show that the pure material undergoes a phase transition at 480 K while the deuterated analogue has its transition temperature shifted to 485 K. The magnitude of the electrical conductivity in the deuterated specimen is lower than that in pure EDS. The activation energy values calculated from the conductivity plot of the deuterated sample are also included in Table 5.1.

### 5.3.2 ac electrical conductivity and dielectric measurements

The temperature dependence of ac conductivity and dielectric loss in EDS single crystals along  $c$ -axis

Table 5.1: Activation energy  $E_a$  for dc conductivity of EDS single crystals along c and c\*-axes.

Sample	Axis	Temperature range (K)	Activation energy (eV)
EDS (pure)	c	360 to 408	1.25
		408 to 454	1.86
	c*	360 to 408	0.95
		408 to 454	1.71
EDS (phosphate doped)	c	360 to 408	1.36
		408 to 454	1.90
EDS (deuterated)	c	360 to 408	1.90
		408 to 454	2.13

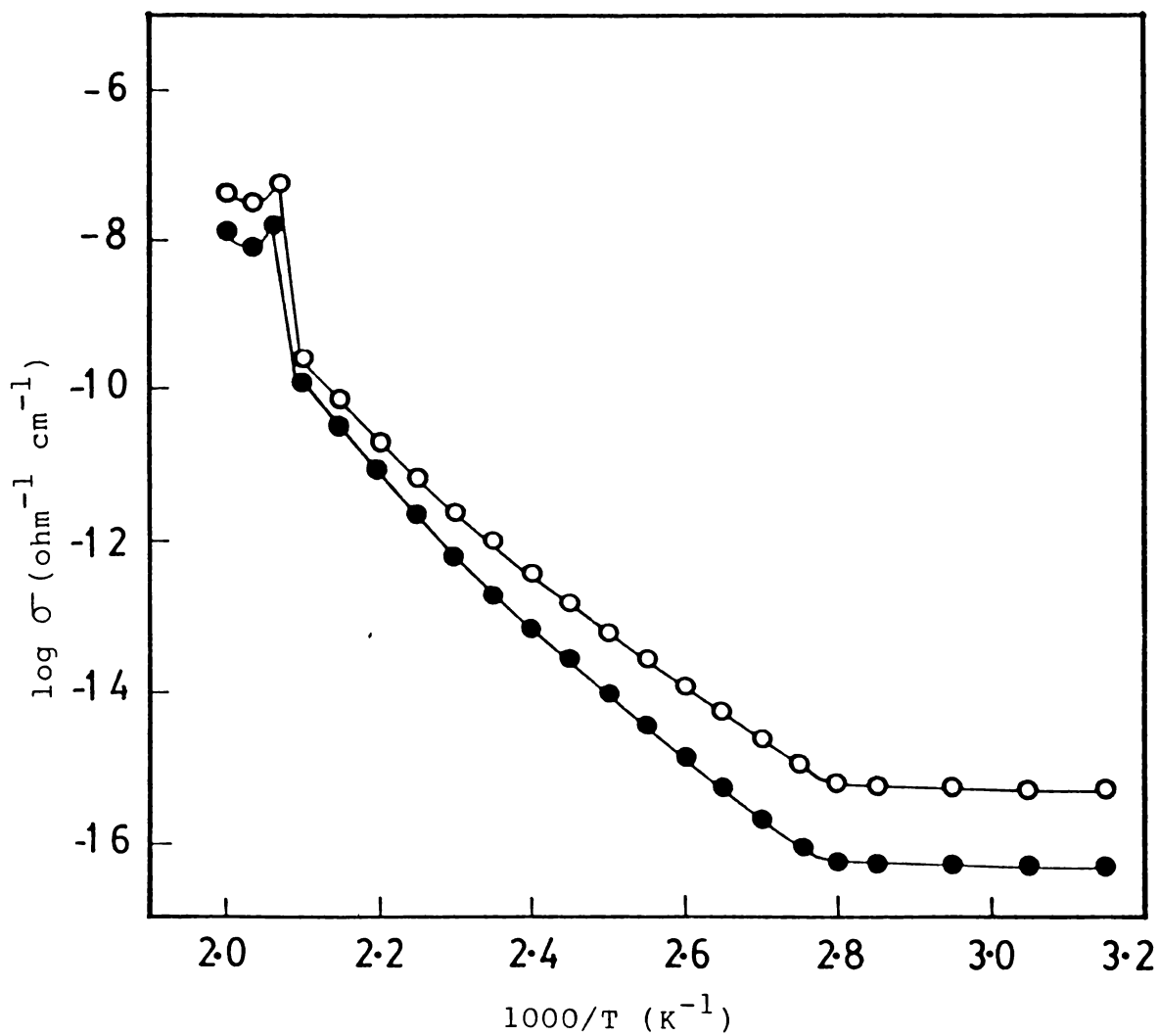


Fig.5.2:  $\log \sigma_{dc}$  vs  $1/T$  plots for EDS along c-axis.  
O - pure, ● - deuterated.

are shown in Fig.5.3. The abrupt change in  $\tan\delta$  and a  $\Lambda$ -shaped anomaly in  $\sigma_{ac}$  again indicate a phase transition at 480 K in conformity with the dc conductivity results.

Fig.5.4 illustrates the variation of dielectric constant along c and c\*-axes at different frequencies. The value of dielectric constant at 300 K is 7.29 along c-axis and 9.27 along c\*-axis (at 1 kHz). The increase in  $\epsilon_c$  and  $\epsilon_{c^*}$  is extremely small upto the phase transition temperature.  $\epsilon_c$  and  $\epsilon_{c^*}$  vs. T plots exhibit  $\Lambda$ -shaped peaks precisely at the same temperature where the conductivity anomalies occur viz., 480 K. The height of the peak notably gets suppressed for higher frequencies. Fig.5.5 shows the temperature dependence of dielectric constant along c-axis around the transition temperature recorded on heating and cooling cycles, the frequency being 10 kHz. The anomaly shows a thermal hysteresis of about 5 K, which is indicative of a first order phase transition.

### 5.3.3 Differential scanning calorimetry

Fig.5.6 shows the DSC thermograms of EDS in the heating and cooling runs. They reveal the following characteristics: The compound apparently decomposes following melting at about 554 K. The sharp peak

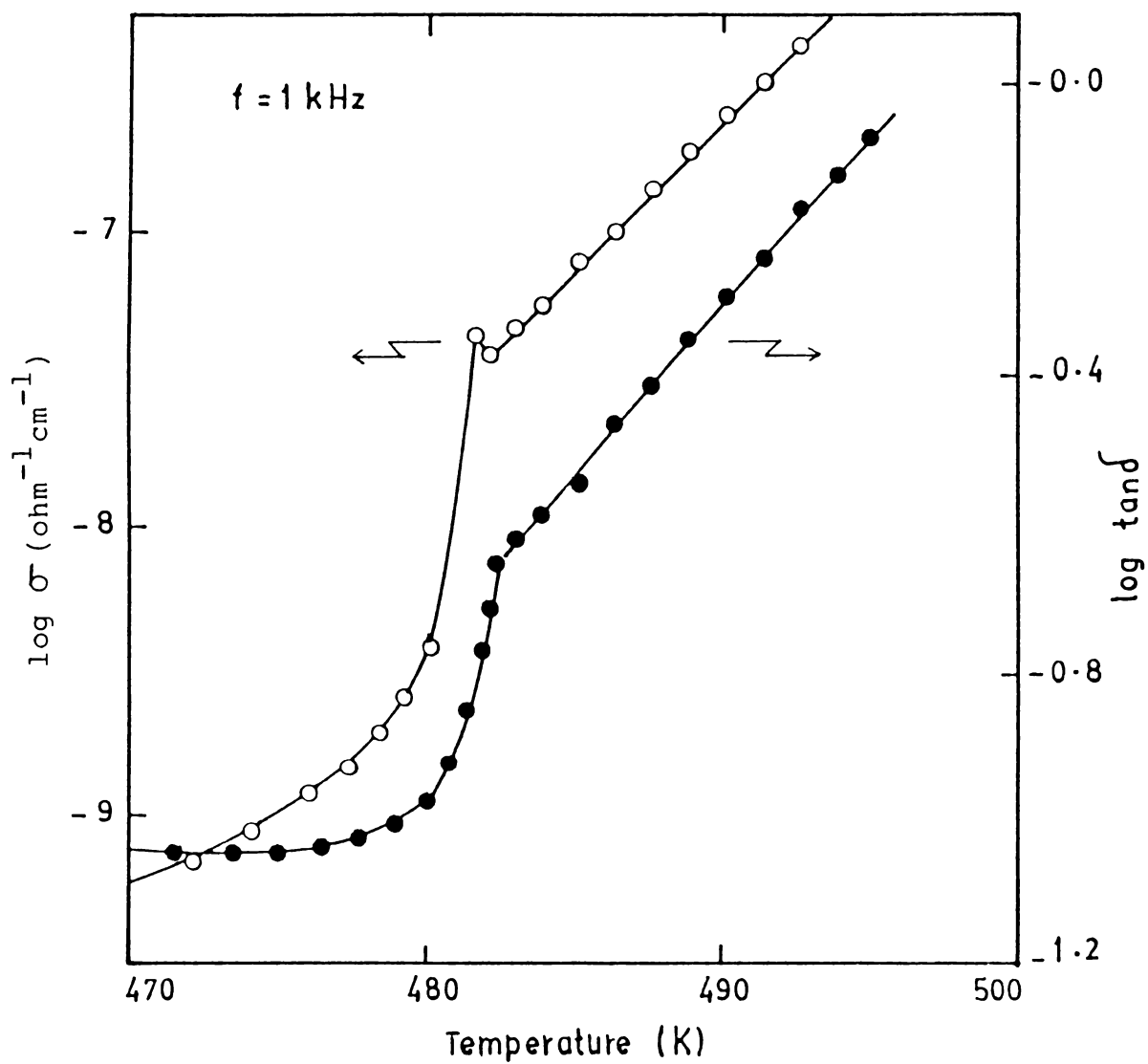


Fig.5.3: Variation of  $\sigma_{ac}$  and  $\tan \delta$  with temperature along c-axis for EDS.

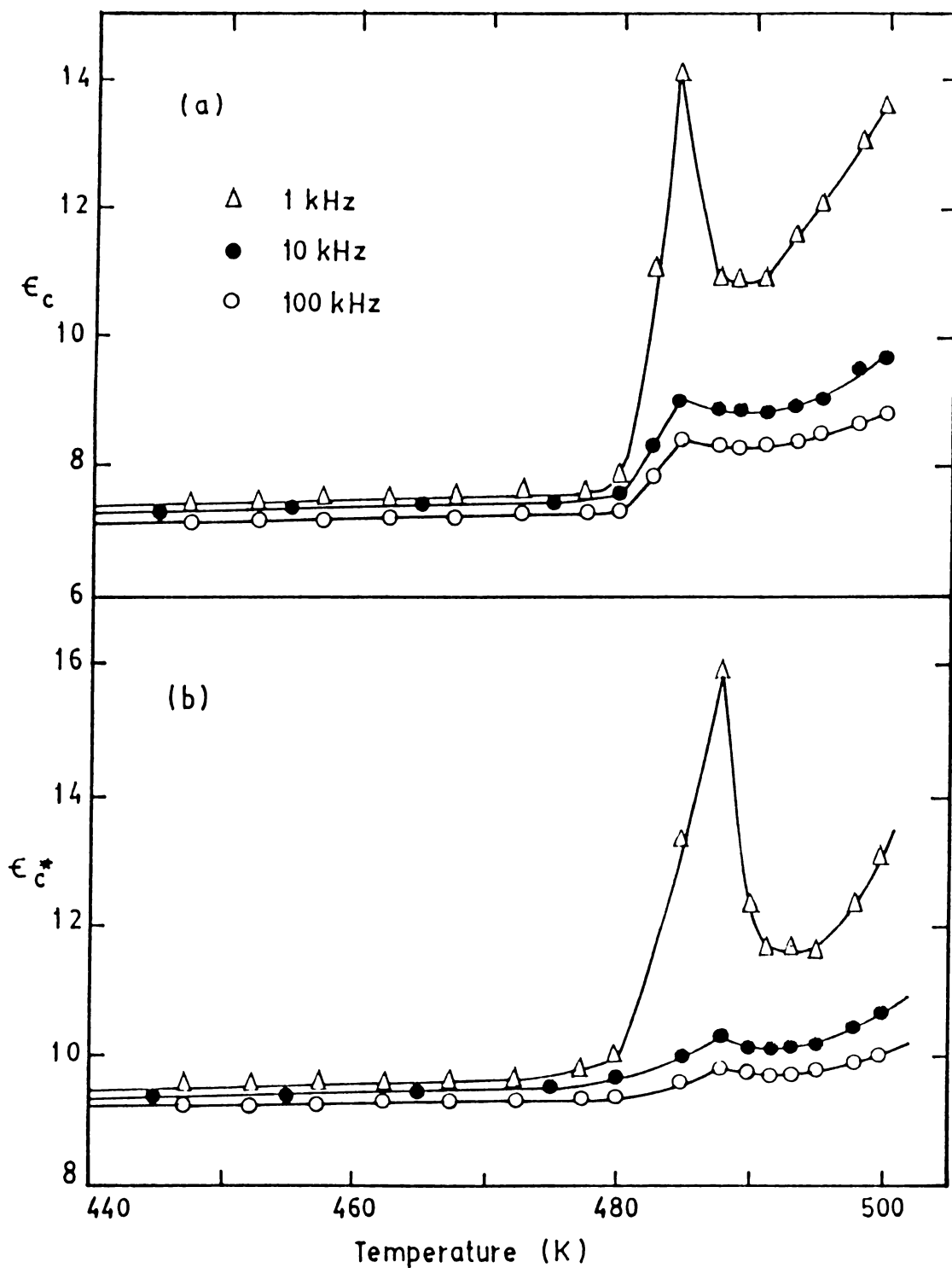


Fig.5.4: Dielectric constant of EDS as a function of temperature at different frequencies along (a) c-axis and (b) c\*-axis

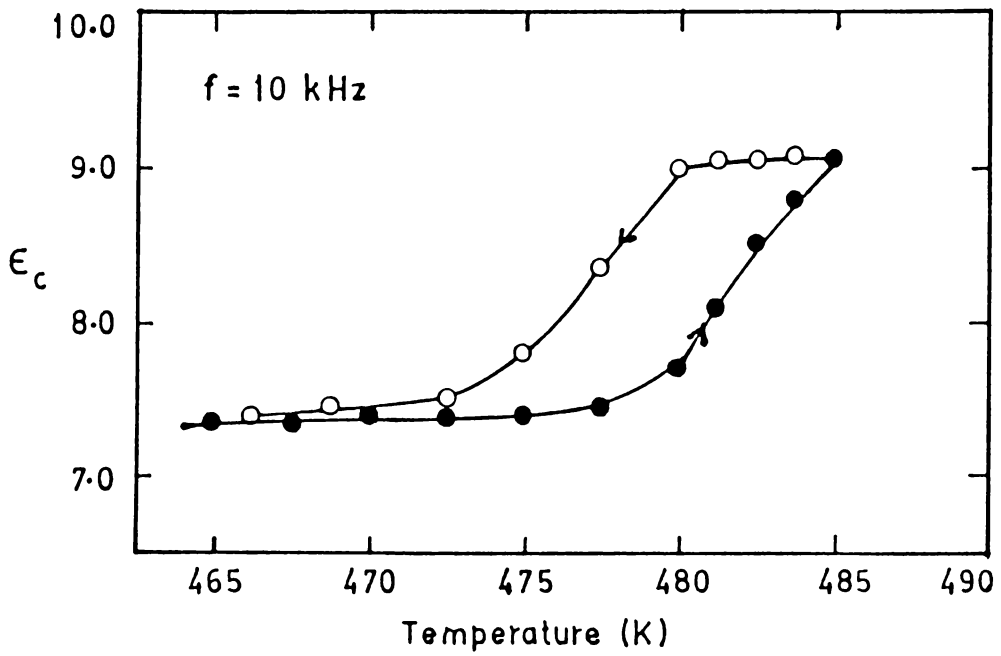


Fig.5.5: Plot of dielectric constant versus temperature for EDS along c-axis in the heating and cooling runs.

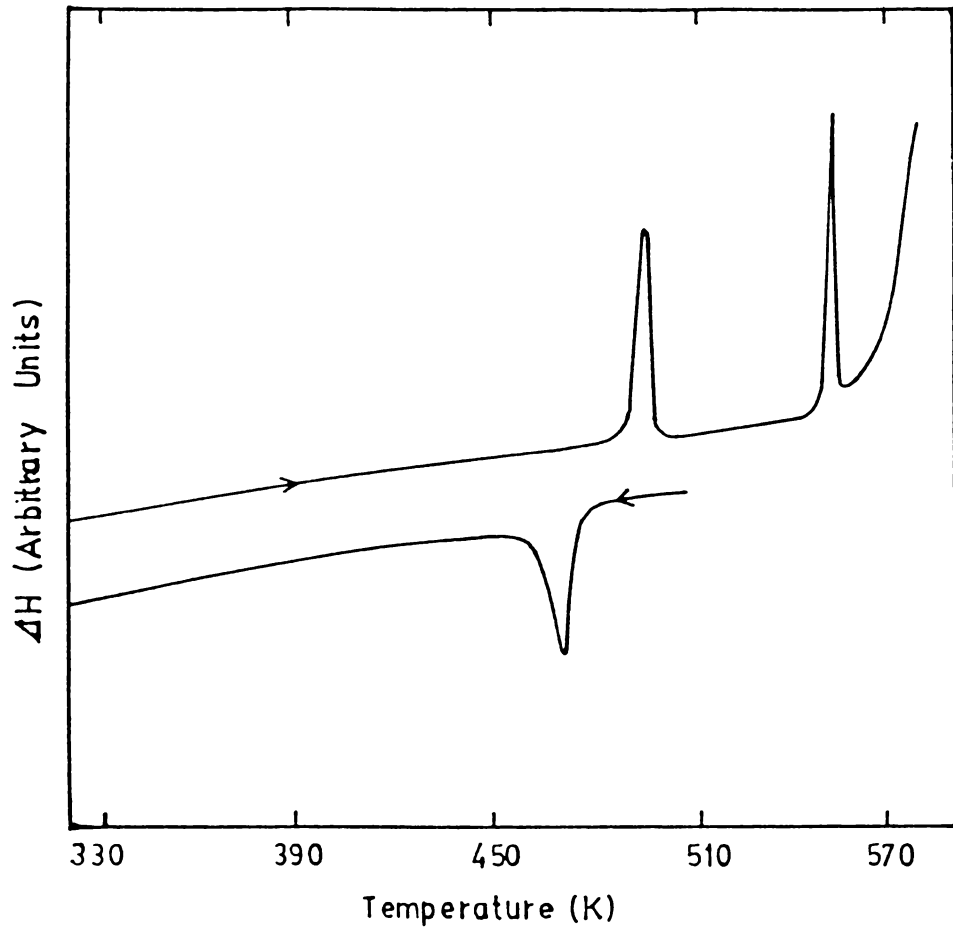


Fig.5.6 DSC traces for EDS.

preceeding decomposition is presumably due to melting of the sample. The peak with onset at 482 K is due to a phase transition. The enthalpy change ( $\Delta H$ ) for this phase transition is  $14.1 \text{ kJ mole}^{-1}$ . This transition shows a thermal hysteresis characteristics of a first order phase transition. The compound does not exhibit any transformation in the temperature range 300 to 400 K, confirming that it is not a hydrate.

#### 5.4 DISCUSSION

The mechanism of conduction in EDS single crystals can be understood by a detailed consideration of its structure [5]. A striking feature of the crystal structure is that the conformation of the ethylenediammonium group is not trans but gauche with  $C_2$  symmetry (Fig.5.7). The azimuthal angle of one half of the group with respect to the other is  $75.7^\circ$ , which is much larger than  $60^\circ$ . This large azimuthal angle may be due to the molecular repulsion between two  $\text{NH}_3^+$  groups. The C-N distance is  $1.49 \text{ \AA}$ . The average S-O distance in the sulphate group is found to be  $1.49 \text{ \AA}$ . In order to illustrate the linkage of sulphate and ethylenediammonium groups, the structure projected on (001) and (100) are shown in Figs.5.8 and 5.9 respectively. As can be seen

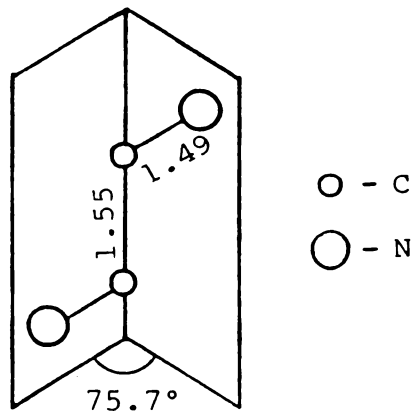


Fig.5.7 Structure of the ethylenediammonium group in EDS.

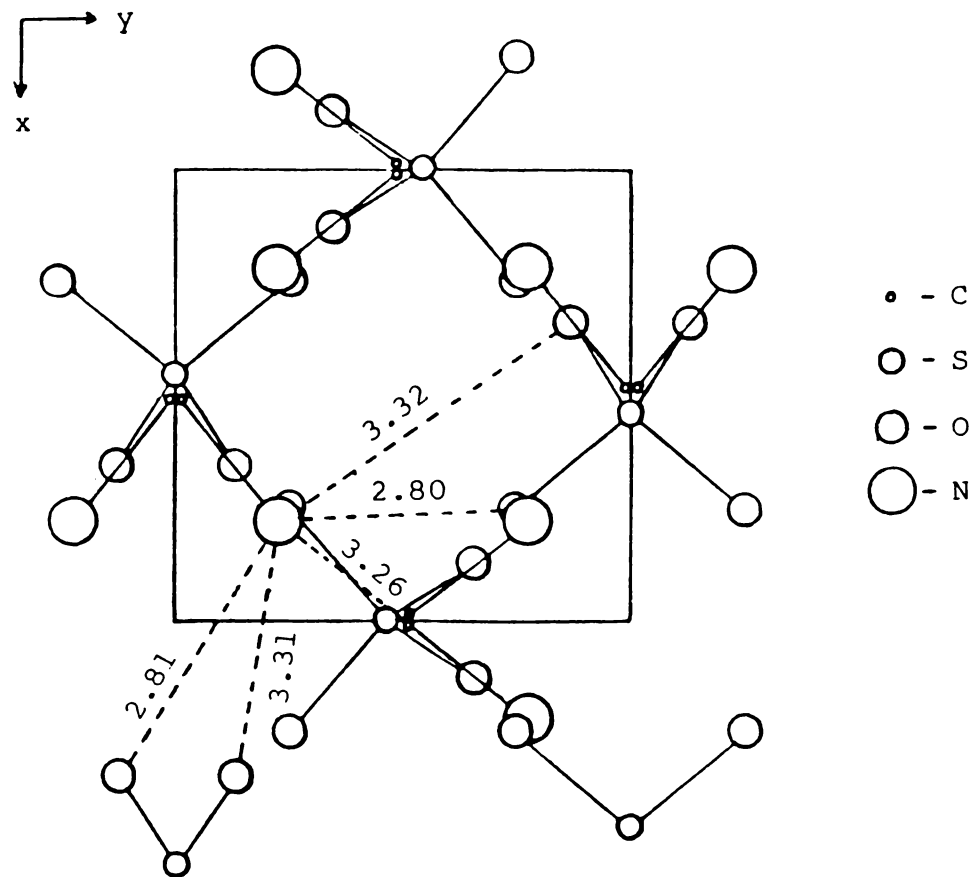


Fig.5.8 Structure of EDS projected on (001).

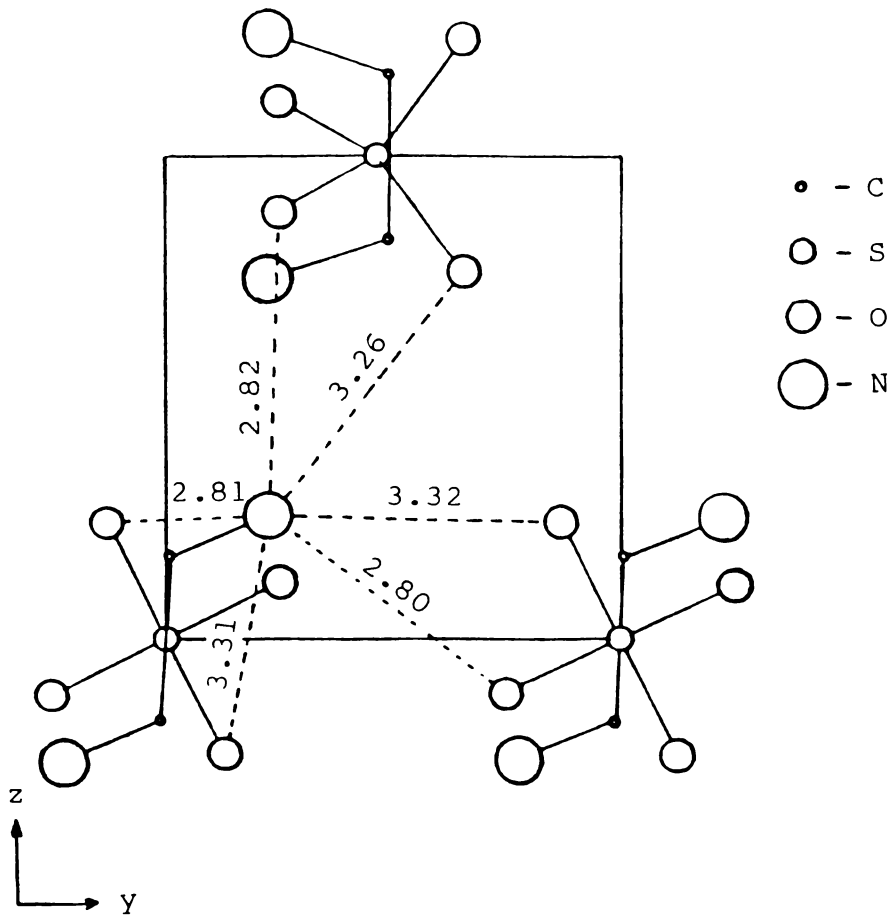


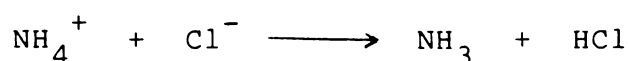
Fig.5.9 Structure of EDS projected on (100).

from Fig.5.9, the structure can conveniently be described as built up of layers, parallel to (001), containing ethylenediammonium and sulphate groups. In each layer these two groups are linked by two sets of hydrogen bonds of lengths 2.80 and 2.81 Å and N...O contacts with distances 3.31 and 3.32 Å, while these layers are held together by hydrogen bonds of length 2.82 Å and N...O contacts with a distance of 3.26 Å. As the number of linkages between layers formed by each nitrogen atom is smaller than that within a layer, a nearly perfect cleavage is observed parallel to (001). The two  $\text{-NH}_3^+$  groups of  $\text{H}_3\text{NCH}_2\text{CH}_2\text{NH}_3^{2+}$  ion are cis to each other in EDS. The structure indicates that both  $\text{-NH}_3^+$  groups have symmetrically equivalent positions in the lattice and that hydrogen bonding occurs between the  $\text{-NH}_3^+$  protons and the surrounding oxygen atoms of sulphate groups.

The rigid structure described above could be the cause for the very low, almost temperature independent conductivity from 100 K upto 340 K. Moreover, unlike typical ionic crystals, EDS has two ions of large size. On account of the large size of these ions, the probability of occurrence of interstitial ethylenediammonium and sulphate ions and their vacancies are very low. Also,

the mobilities of these defects are comparatively low. Hence ethylenediammonium and sulphate ions and their vacancies cannot contribute to the conduction process in any significant manner. As the temperature of the specimen is raised above room temperature, the hydrogen bonds become progressively weaker. At this stage it seems appropriate to conceive of a proton switch mechanism [9,10,11] to explain the conductivity of EDS single crystals above 340 K.

To explain the mechanism of conduction in ammonium chloride, Herrington and Staveley [9] have postulated that there is significant amount of dissociation in these crystals to form molecular species which may be represented,



As already described in chapter 4, they proposed a three stage proton switch mechanism in which (i) the proton leaves the  $\text{NH}_4^+$  ion and joins the  $\text{Cl}^-$  ion forming  $\text{NH}_3$  and  $\text{HCl}$  molecules (ii) a vacancy and the appropriate molecule exchange positions, and (iii) the proton jumps back to  $\text{NH}_3$  forming  $\text{NH}_4^+$  and  $\text{Cl}^-$  ions once again. The possibility of

a proton switch mechanism in ammonium salts has further been supported by the work of Fuller and Patten [10] and Taylor and Lasker [11]. The concepts put forward by Herrington and Staveley seem to be applicable to explain the mechanism of conduction in EDS also, where the cations and anions are connected by hydrogen bonds. The initial step in the transport process can be the breaking of hydrogen bonds and the transfer of the protons directly to the neighbouring sulphate ion where it is held by the Coulomb attraction of the anion. In the second step, the neutral  $\text{H}_2\text{SO}_4$  molecule may migrate to an adjacent vacancy and in the final step a reversal of proton switch may occur. Thus a net displacement of charge results in an applied electric field. The activation energy values obtained for pure, phosphate-doped and deuterated EDS in the temperature range 340 to 408 K (Table 5.1) are in very good agreement with those reported in the literature for similar materials in which the electrical conductivity is dominated by protonic contribution [11-14].

The higher magnitude of  $\sigma_{dc}$  along  $c^*$ -axis (Fig.5.1) could be due to the higher mobility of the charge carriers along this axis, which is parallel to the cleavage plane. The lower activation energy along this

axis in the temperature range 340 to 408 K also suggests a comparatively smaller barrier in this direction. The conductivity of the phosphate doped sample is found to be slightly higher than that of the pure sample in the entire temperature range, whereas the activation energy is not significantly altered (Table 5.1). When EDS is doped with ethylenediammonium phosphate,  $(\text{H}_3\text{NCH}_2\text{CH}_2\text{NH}_3)\text{HPO}_4$ , the  $\text{HPO}_4^{2-}$  ions substitute  $\text{SO}_4^{2-}$  ions. The enhancement of conductivity in the doped sample may be attributed to the contribution of the protons of the acid phosphate. This observation is also in support of the conclusion that protonic conduction is the dominant mechanism of charge transport in EDS. The results of the electrical conductivity measurements of EDS are quite similar to those obtained in our studies on ethylenediammonium dinitrate single crystals [14], in which protonic conduction was established by chemical methods.

Deuteration of EDS results in an elevation of transition temperature by about 5 K. This upward shift in transition temperature is a direct evidence of the role of  $-\text{NH}_3^+$  group in the mechanism of phase transition. The lower value of conductivity observed for the deuterated samples in the entire temperature range is in clear

support of the involvement of protons in electrical charge transport. The lower magnitude of conductivity when  $^1_1\text{H}$  of the ammonium group is substituted by  $^2_1\text{H}$  is expected to be due to the lower mobility of the heavier  $^2_1\text{H}$  atom. The slightly higher activation energy may be attributed to the minor modification in the potential well occurring in the deuterated sample. The lower vibrational amplitudes in the deuterated sample might result in a lowering of the  $\text{N}-^2_1\text{H}$  bond length compared to  $\text{N}-^1_1\text{H}$  bond length. Such a change in the bond length, in turn, can affect the potential well. The slightly higher activation energy observed can thus be due to the modification of the potential well.

In the NMR spin-lattice relaxation measurements [6], the  $T_1$  minimum of EDS is interpreted in terms of the decrease of the  $-\text{NH}_3^+$  reorientational barriers with increasing temperature because of lattice expansion and increased vibrational amplitudes. The change in slope of conductivity plots above 408 K apparently arises from the initiation of the rotational reorientation of  $-\text{NH}_3^+$  group of EDS. A varying activation energy above 408 K as observed can also result from such a gradual decrease of

the reorientational barriers. Thus some sort of a 'variable potential barrier' model [15,16] has to be invoked to explain the experimental results.

As the temperature of the sample increases further, the hydrogen bonds become progressively weaker and at about 480 K, the hydrogen bonds associated with ethylenediammonium ions can be completely broken and the  $-\text{NH}_3^+$  ions which are assumed to be in a state of torsional oscillation now change over to a state of free rotation. Such phase changes, where the barrier to  $-\text{NH}_3^+$  group orientation drops dramatically on going into the higher temperature phase, have been observed in other salts [17-19]. The onset of such a free rotation can cause a significant change in the electrical conductivity as well as dielectric constant at this temperature. Similar effects have been found to occur in a number of ammonium salts like  $(\text{NH}_4)_2\text{SO}_4$  [20],  $\text{NH}_4\text{H}_2\text{PO}_4$  [21],  $\text{LiNH}_4\text{SO}_4$  [7] and  $(\text{NH}_4)_2\text{HPO}_4$  [22].

The variation of dielectric constant with temperature in the present studies exhibit a thermal hysteresis of about 5 K. The abrupt increase in conductivity at the phase transition point and the thermal

hysteresis observed in the dielectric measurements and DSC indicate that the phase transition is of first order. The slight difference in temperature for the onset of phase transition as revealed by DSC measurement could be due to the higher heating rate employed in these experiments in contrast with conductivity and dielectric measurements.

**5.5 REFERENCES**

- [1] P.Growth, *Chemische Krystallographic Teil 3* Engelmarv, Leipzig (1910) 54.
- [2] W.G.Burgers, *Proc. Roy. Soc. London A* **116** (1927) 553.
- [3] V.I.Burkov, N.I.Guseva, V.A.Kizel, G.S.Semin and N.M.Sitnikov, *Opt. Spectrosc.* **53** (1982) 410.
- [4] V.I.Burkov, N.I.Guseva, V.A.Kizel, S.M.Postnov, G.S.Semin, G.M.Safronov and P.A.Cheltsov, *Sov. Phys. Crystallogr.* **25** (1980) 107.
- [5] K.Sakurai, *J. Phys. Soc. Japan* **16** (1961) 1205.
- [6] C.I.Ratcliffe, *J.C.S.Faraday II*, **76** (1980) 1196.
- [7] U.Syamaprasad and C.P.G.Vallabhan, *Solid State Commun.* **34** (1980) 899.
- [8] C.Ramasastri and Y.Syamasundara Rao, *J. Phys. E: Sci. Instrum.* **12** (1979) 1023.
- [9] T.M.Herrington and L.A.K.Staveley, *J. Phys. Chem. Solids* **25** (1964) 921.

- [10] R.G.Fuller and F.W.Patten, J. Phys. Chem. Solids 31 (1970) 1539.
- [11] B.E.Taylor and A.L.K.Laskar, Phys. Stat. Sol.(b) 101 (1980) 423.
- [12] Y.V.G.S.Murti and P.S.Prasad, Physica B 79 (1975) 243.
- [13] S.Radhakrishna and B.D.Sharma, J. Appl. Phys. 44 (1973) 3848.
- [14] N.C.Santhakumari and C.P.G.Vallabhan, Solid State Ionics 45 (1991) 329.
- [15] J.Bernasconi, H.U.Beryler and S.Strassler, Phys. Rev. Lett. 42 (1979) 819.
- [16] S.Chandra and N.Singh, J. Phys. C: 16 (1983) 3081.
- [17] S.Albert and J.Ripmester, J. Chem. Phys. 58 (1973) 541.
- [18] C.I.Ratcliffe and B.A.Dunell, Faraday Symp. Chem. Soc. 13 (1978) 142.

- [19] C.J.Ludman, C.I.Ratcliffe and T.C.Waddington,  
J.C.S.Faraday II, 72 (1976) 1759.
- [20] U.Syamaprasad and C.P.G.Vallabhan, J. Phys. C: Solid  
State Phys. 14 (1981) L 865.
- [21] V.K.Subhadra, U.Syamaprasad and C.P.G.Vallabhan, J.  
Appl. Phys. 54 (1983) 2593.
- [22] R.Navilkumar and C.P.G.Vallabhan, J. Phys.: Condens.  
Matter 1 (1989) 6095.

## Chapter 6

### TEMPERATURE DEPENDENT VARIATION OF ELECTRICAL PROPERTIES

#### IN ETHYLENEDIAMMONIUM ACID PHOSPHATE

##### Abstract

dc and ac conductivities, dielectric constant, and dielectric loss of single crystals of ethylenediammonium acid phosphate (EDAP) have been studied as a function of temperature in the range 100 to 415 K. At low temperatures the material is highly insulating. The Arrhenius plots for dc conductivity show two linear regions with a knee at 368 K. The observed conductivity has been explained in terms of a proton switch mechanism involving the anion and cation sublattices. ac conductivity, dielectric constant and dielectric loss measured as a function of temperature and frequency show no significant variations of these quantities upto about 368 K. Thereafter the above parameters exhibit rapid variations. Results of the studies on deuterated and doped samples are also discussed in the light of the proposed proton switch mechanism.

## 6.1 INTRODUCTION

Earlier work done on the electrical properties of ammonium salts and the work presented in the preceding chapters of this thesis have shown that the charge transport in simple and substituted ammonium salts is essentially due to protons. It is also seen that the free rotation of the ammonium moiety at a structural phase transition enhances protonic conductivity.

Ammonium dihydrogen phosphate (ADP) and potassium dihydrogen phosphate (KDP) are two well understood materials in terms of their crystal structure, electrical properties and phase transition [1-9]. In both cases protonic conduction involving hydrogen bond takes place. The possible applications of ADP are limited since it dissociates to ammonia and phosphoric acid at elevated temperatures. An advantageous combination of enhanced conductivity in acid phosphates and better thermal stability of substituted ammonium salts would result in a material of choice which has moderate protonic conductivity for low current applications.

Acid phosphates of good thermal stability and moderate electrical conductivity have been investigated in

depth by different workers in recent years [10]. The electrical transport in amorphous acid salts was first recognised by Hamlem [11]. Alberti et al [12] have studied the acid phosphates of tetravalent metals. Acid phosphates such as,  $\alpha$ -[Zr(PO<sub>4</sub>)<sub>2</sub>H<sub>2</sub>.H<sub>2</sub>O] and  $\alpha$ -[Ti(PO<sub>4</sub>)H<sub>2</sub>.H<sub>2</sub>O] even with their moderate protonic conductivity, find application in a variety of devices. Among these materials only hydrates having a layered structure in which the water molecules are sandwiched between adjacent layers exhibit good conductivity and that too, at elevated temperatures. Anhydrous acid phosphates, eventhough have a lower conductivity than the corresponding hydrates, are candidate materials for higher temperature applications, due to their superior thermal stability.

Ethylenediammonium acid phosphate (EDAP) being a substituted ammonium acid phosphate is likely to possess better thermal stability than diammonium acid phosphate, and phosphates of tetravalent metals with comparable electrical conductivity. Also, the information available on its crystal structure will be helpful to understand the mechanism of charge transport.

The crystal structure of  $(\text{H}_3\text{NCH}_2\text{CH}_2\text{NH}_3)^{2+}(\text{HPO}_4)$  was elucidated by Golubev and Kondrashev [13]. The characterizing parameters are:  $a = 7.500$ ,  $b = 8.045$ ,  $c = 11.806\text{\AA}$ ,  $\gamma = 110.13^\circ$ ,  $Z = 4$ , space group  $P2_1/b$ . The structure consists of four tetrahedral  $\text{HPO}_4^{2-}$  anions and planar ethylenediammonium cations in trans conformation. An extensive system of hydrogen bonds also exists in this material. This creates anion layers in the  $ab$  plane which are connected together by layers of ethylenediammonium ions. In this respect it is very similar to the acid phosphates of tetravalent metals [10].

## 6.2 EXPERIMENTAL

EDAP was prepared by mixing a 6 molar solution of ethylenediammine in distilled water with syrupy phosphoric acid in 1 : 1 mole ratio. The solution was cooled and filtered to collect the material. It was further purified by recrystallisation from saturated solution made with double distilled water.

Single crystals grown by isothermal evaporation gave both singular rhombohedral and twinned prisms. Large well defined crystals were grown by suspending small non-twinned crystals in a saturated solution of EDAP at

ambient temperature.  $\text{SO}_4^{2-}$  doped samples were prepared from solutions of EDAP spiked with different amounts (0.02 and 0.05 mole %) of ethylenediammonium sulphate. Deuterated single crystals were obtained by repeated recrystallisation from solutions made with heavy water of 99.5% isotopic purity.

Samples for electrical measurements were prepared by cutting specimens of typical size  $5 \times 5 \times 1 \text{ mm}^3$  with their broad faces perpendicular to and parallel to c-axis. Silver was evaporated on to the broad faces of the specimens to ensure good electrical contact. dc and ac electrical conductivity, dielectric constant and dielectric loss were measured within the temperature range 100 to 415 K, as described in Chapter 2. Within experimental error, the conductivity and dielectric constant measured along c and c\*-axes were essentially the same. All of the data to be discussed here were obtained with fields applied perpendicular to the c-axis, unless otherwise stated. DSC thermograms were recorded in a dynamic nitrogen atmosphere in the temperature range 323 to 510 K, at a scanning rate of  $10 \text{ K min}^{-1}$ .

## 6.3 RESULTS

### 6.3.1 dc conductivity

The results of dc conductivity measurements of pure, doped and deuterated single crystals of EDAP as a function of temperature are presented in Fig.6.1. At low temperatures EDAP behaves as a defect free ionic conductor. Upto about 258 K  $\sigma_{dc}$  is very low and remains almost steady. Above this temperature, the conductivity increases with temperature. The Arrhenius plots have knees at about 368 K, thus giving two distinct regions in the plots. The high temperature region (I) has an activation energy 1.99 eV and the low temperature region (II) has an activation energy 1.03 eV in the case of pure EDAP single crystals. Annealing the sample at 373 K does not alter the nature of the plot. The conductivity of the deuterated sample is found to be less than that of pure sample. However, activation energy values show only a marginal increase. Specimens of  $SO_4^{2-}$  doped material show enhanced conductivity in the whole temperature range (Fig.6.1). The magnitude of conductivity increases with dopant concentration. However, the activation energy values in the high and low temperature regions remain almost the same. The activation energy values evaluated from the slopes of conductivity plots of pure, doped and deuterated specimens of EDAP are listed in Table 6.1.

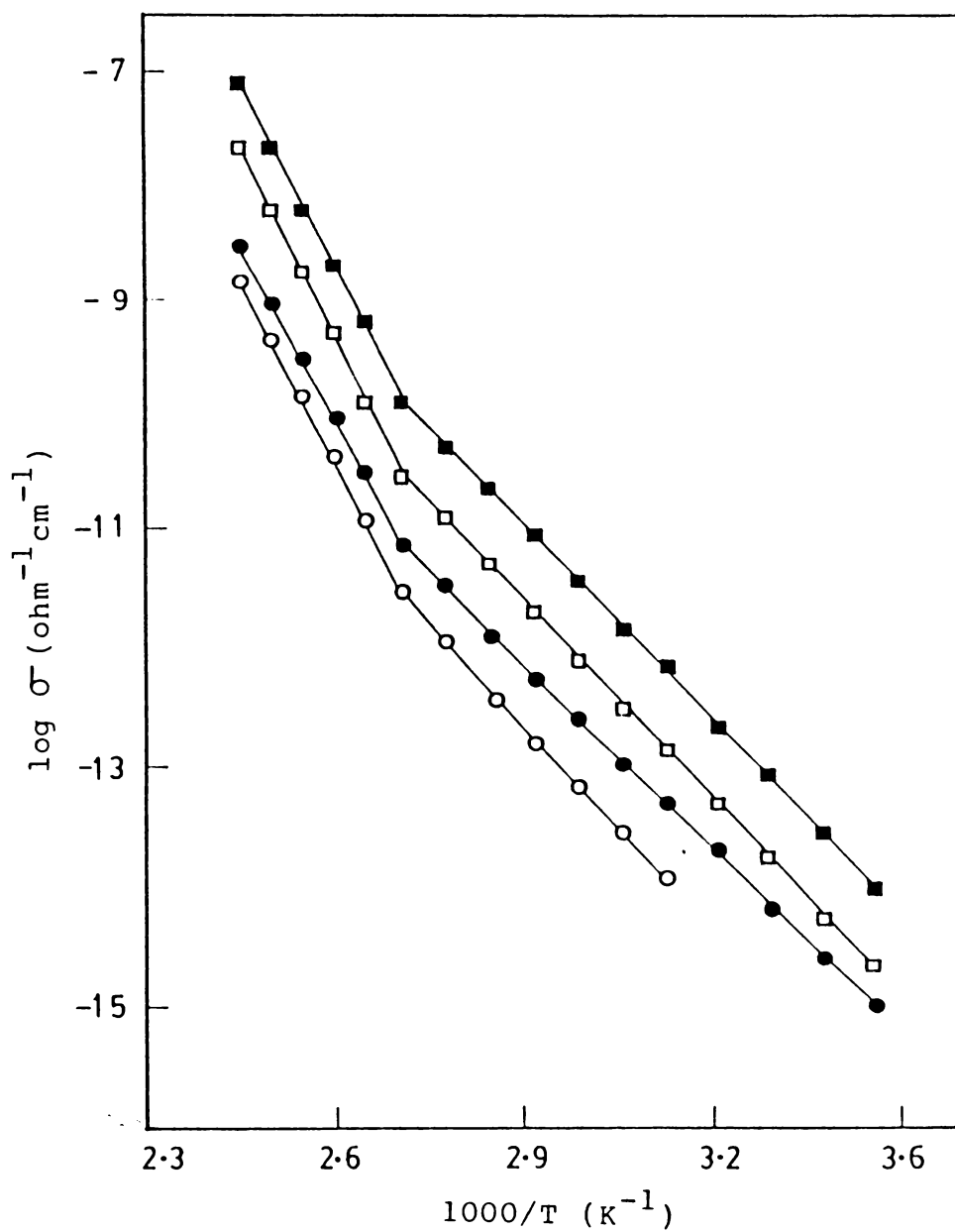


Fig.6.1  $\log \sigma_{dc}$  versus  $1/T$  plots for EDAP along c-axis.  $\circ$  - deuterated,  $\bullet$  - pure,  $\square$  - sulphate doped (0.02 mole %),  $\blacksquare$  - sulphate doped (0.05 mole %).

Table 6.1: Activation energy  $E_a$  for dc conductivity of EDAP single crystals along  $c^*$ -axis.

Sample	Temperature range (K)	Activation energy (eV)
EDAP (pure)	258 to 368	1.03
	368 to 412	1.99
EDAP (deuterated)	258 to 368	1.20
	368 to 412	2.10
EDAP ( $\text{SO}_4^{2-}$ doped, 0.02 mole %)	258 to 368	1.08
	368 to 412	2.17
EDAP ( $\text{SO}_4^{2-}$ doped, 0.05 mole %)	258 to 368	1.09
	368 to 412	2.19

The magnitude of dc conductivity of pure, doped and deuterated single crystals of EDAP at 300 K are compared in Table 6.2.

### 6.3.2 ac conductivity

The results of ac conductivity measurements of EDAP as a function of temperature at various frequencies is presented in Fig.6.2. At low temperatures  $\sigma_{ac}$  is frequency dependent and increases with increase in the applied frequency. However, the temperature dependence of ac conductivity is extremely small upto about 368 K. As the temperature is raised further the plots of  $\log \sigma_{ac}$  against reciprocal temperature merge together. The activation energy evaluated from the ac conductivity plot above 368 K is found to be 2.34 eV.

### 6.3.3 Dielectric constant

Dielectric constant of EDAP at 300 K is 7.33 at 1 kHz. The value of  $\epsilon$  increases only very slightly with temperature in the range 100 to 368 K, as can be seen from Fig.6.3. Dielectric constant has dependence on frequency at all temperatures, but it becomes more pronounced at higher temperatures. The variation of dielectric loss factor with temperature (Fig.6.4) is analogous to that of dielectric constant.

Table 6.2:  $\sigma_{dc}$  of EDAP samples at 300 K

Sample	$\log \sigma_{dc}$ (300 K)
EDAP (pure)	-14.20
EDAP ( $\text{SO}_4^{2-}$ doped, 0.02 mole %)	-13.80
EDAP ( $\text{SO}_4^{2-}$ doped, 0.05 mole %)	-13.10
EDAP (deuterated)	-14.90

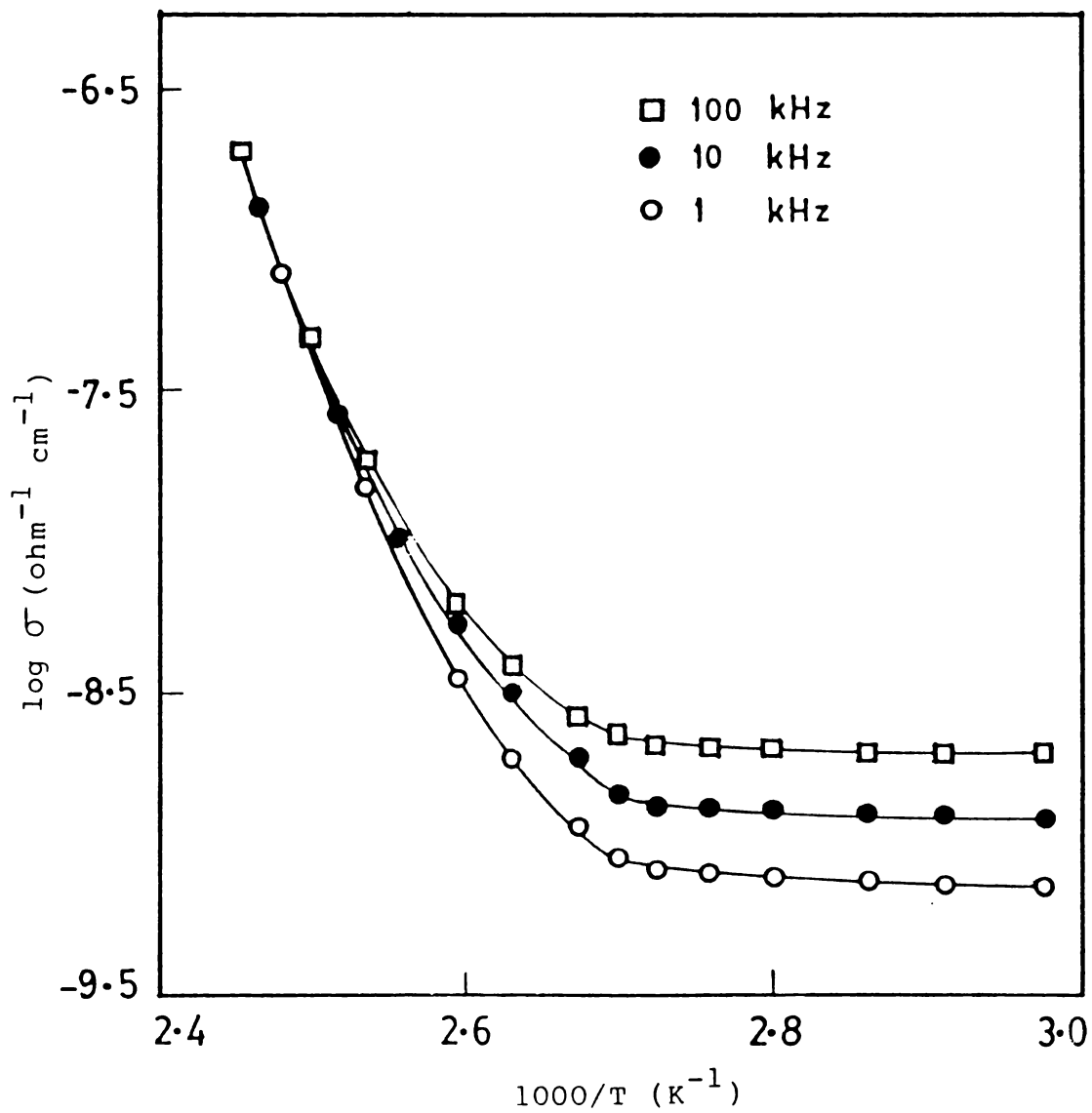


Fig.6.2  $\log \sigma_{ac}$  versus  $1/T$  plots for EDAP along c-axis.

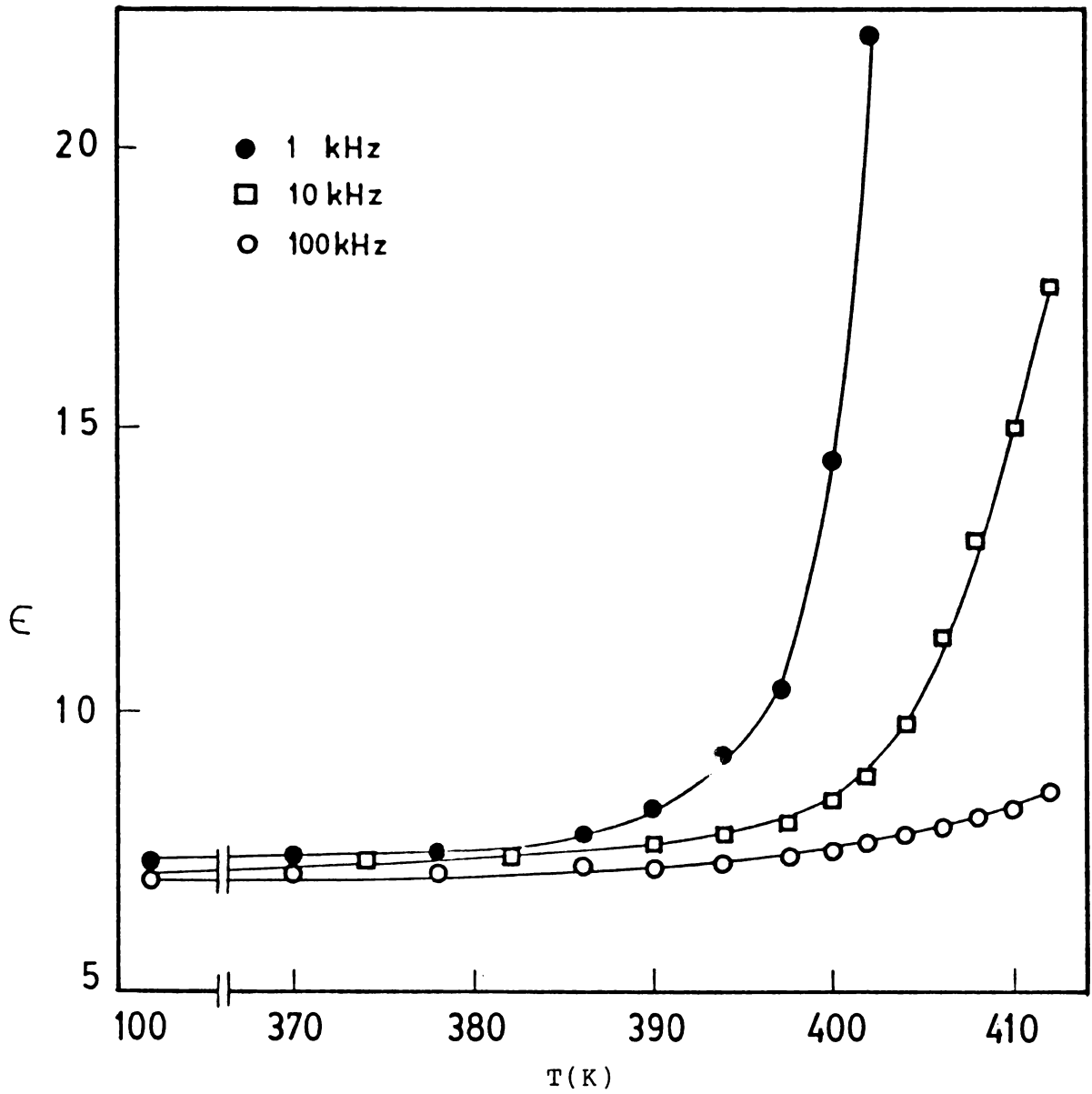


Fig.6.3 Variation of dielectric constant with temperature for EDAP.

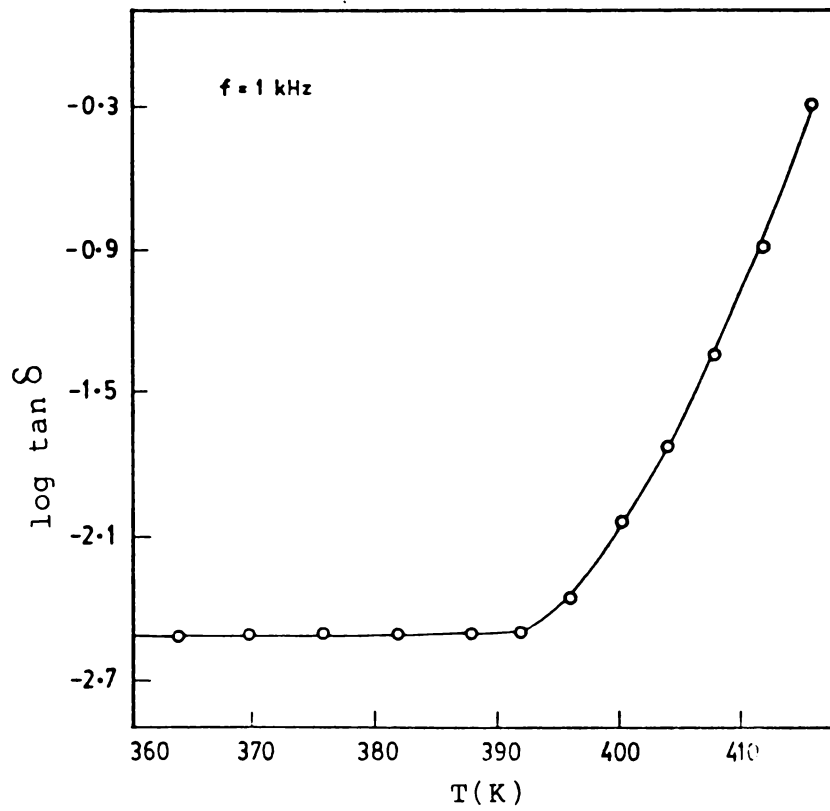


Fig.6.4: Variation of  $\tan \delta$  with temperature for EDAP along c-axis.

#### 6.3.4 Differential scanning calorimetry

The DSC thermograms of EDAP (Fig.6.5) do not indicate any phase transformation upto 480 K. Thereafter it shows a continuous endothermic transformation, probably due to decomposition.

#### 6.4 DISCUSSION

A detailed consideration of the crystal structure of EDAP will be helpful in understanding the mechanism of charge transport process in this material. The structure of ions, bond lengths and bond angles are illustrated in Fig.6.6. The planar ethylenediammonium ion exists in a trans conformation.

The three P-O bonds in the tetrahedral phosphoric acid ion are very similar and have an average bond length of  $1.526(7) \text{ \AA}$ . The fourth P-O bond which corresponds to the OH group is longer ( $1.585 \text{ \AA}$ ). Such bond inequality is characteristic of acid anions [14]. The arrangement of the ions in the lattice is illustrated in Fig.6.7. The anion layers in the bc plane alternate with the cation layers. The structure contains an extensive hydrogen bond network. The  $\text{HPO}_4^{2-}$  anions are connected to

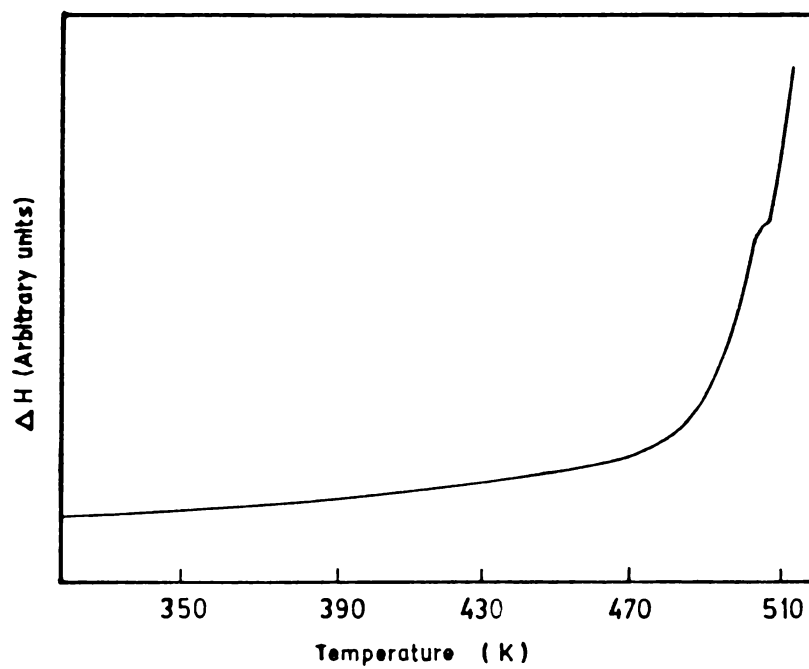


Fig.6.5 DSC thermogram of EDAP; heating rate  $10 \text{ K}^{-1}$ .

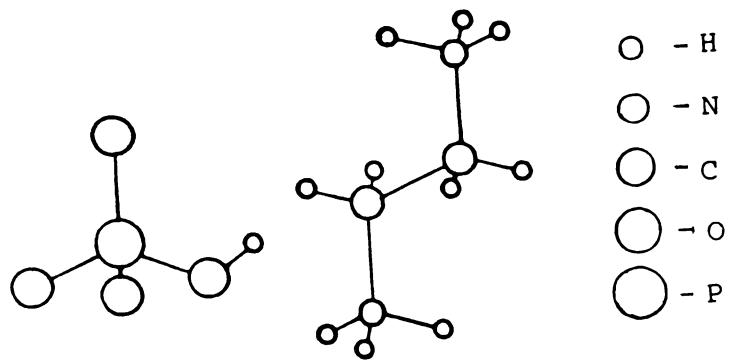


Fig.6.6 Structure of constituent ions of EDAP.

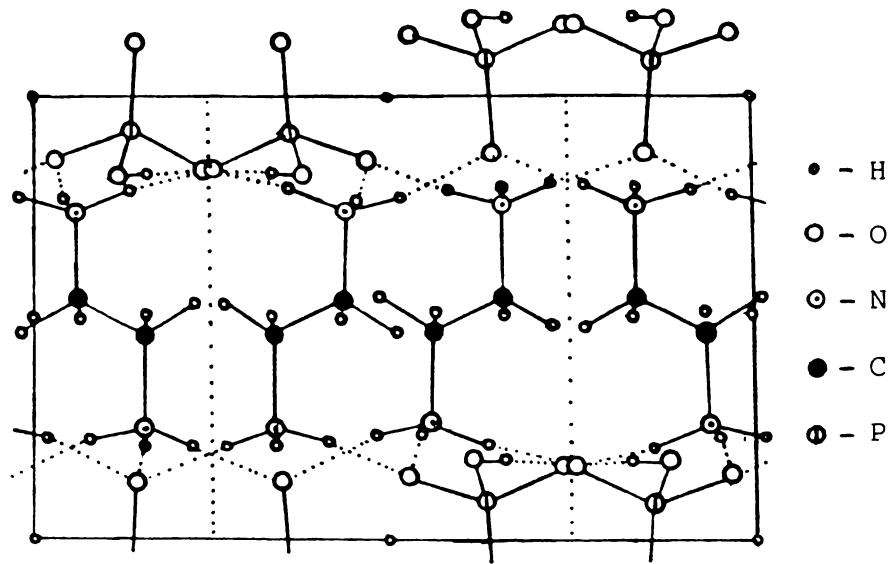


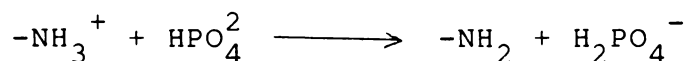
Fig.6.7: Projection of the structure of EDAP along  $c^*$ -axis.

each other by hydrogen bonds in chains typical of acid salts [14,15]. The N-H...O hydrogen bonds in which all the hydrogen atoms of the ammonium groups are involved, connect these chains into layers. They also connect these layers into a three dimensional framework. The hydrogen bonds have a shortened H...O distance relative to the Van der Waals' distance. The anion oxygen atoms form several hydrogen bonds.

The two distinct regions shown in the Arrhenius plots for dc conductivity (Fig.6.1) have activation energies 1.03 eV below 368 K and 1.99 eV above it. The activation energy values observed are very close to those in EDC, EDN and EDS. These, in turn, are in good agreements with the activation energies reported for protonic conduction in simple ammonium salts [16-19]. Harris and Vella [4] explained the electrical conduction in ADP on the basis of the model put forth by Herrington and Staveley [17] for  $\text{NH}_4\text{Cl}$ . It was considered that the proton migration in ADP crystal occurs in the  $\text{NH}_4^+$  sublattice in addition to that in the  $\text{H}_2\text{PO}_4^-$  sublattice [2]. In the case of EDAP, if we consider the two sublattices, both can independently contribute to protonic conduction just as in the case of ADP. The acid phosphate

sublattice can contribute to protonic conductivity by a migration of proton across P-O-H....O-P which is in effect an intrabond jump. This leads to a rearrangement of the already existing P-O...H hydrogen bond on a receiving anion segment resulting in an interbond jump of hydrogen atom. In terms of the P-O bond lengths this is equivalent to a rearrangement of three equivalent and one non-equivalent P-O bonds.

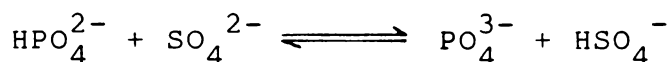
Another form of proton transport involving the ammonium sublattice can also be operative. The ammonium sublattice dissociates transferring a proton to the anion sublattice.



Such a dissociation has been experimentally demonstrated in ammonium dihydrogen phosphate [4]. The proton transfer mechanisms in the two sublattices envisaged here are in effect equivalent to the proton switch mechanism described in the preceding chapters. At higher temperatures the overall conductivity of EDAP might be the sum of the contributions of the anion and cation sublattices.

The magnitude of dc conductivity observed along  $c$  and  $c^*$ -axes are close to each other. This is in contrast to the observation with EDC, EDN and EDS. A probable explanation can be linked with their crystal structure. EDC, EDN and EDS have layered structures, the anion and cation layers being held together by weak van der Waals' forces. In EDAP a strong three dimensional framework of hydrogen bonds exists. Hence it is reasonable to assume that there is no preferential direction for proton migration.

Doping of EDAP with EDS leads to noticeable increase in conductivity (Table 6.2). At the same time, the activation energy values are not affected to any significant extent. This testifies that doping leads to the generation of more carriers without affecting the activation energy barrier. O'Keefee and Perrino [8] encountered a similar effect when potassium dihydrogen phosphate was doped with potassium hydrogen sulphate. They accounted for the observed increase in conductivity to an exchange of hydrogen ions between host and dopant anions. A similar argument can be put forth to explain the increase in conductivity due to doping of EDAP with sulphate ions.



In effect, this is equivalent to a proton switch operating between the host and dopant anions. The frequency of such a proton switch depends on the concentration of the dopant in the host sublattice. Hence an increase in dopant concentration leads to an increase in conductivity which is precisely the observation made here.

The fact that the deuterated samples have lower conductivity values compared to the undeuterated samples is a clear and direct evidence for the predominance of protonic conduction in the crystal, in the entire temperature region studied.

The  $\log \sigma_{ac}$  vs.  $1/T$  plot has a plateau in the low temperature region followed by a continuously rising portion. At higher temperatures the ac conductivity curves merge together among themselves and also with the dc conductivity curve. It may be noted that in the low temperature region ac and dc conductivities differ considerably in magnitude. Berteit [18], and Taylor and Laskar [19] have observed similar differences between dc and ac conductivities in ammonium salts. They attributed

this difference to the presence of loosely bound protons which can jump in tune with the ac field. The same concept is applicable here also since the only mobile ion present in the lattice is the proton. The probable phenomenon which can cause a difference in ac and dc conductivities are blocking and space charge effects. The absence of these were confirmed by noting that the current is independent of time at an applied potential. Also, upon reversing the polarity of the dc field, the magnitude of current remains the same. These along with the good reproducibility of data supports the validity of measurements.

Dielectric constant and dielectric loss factor for EDAP do not show any significant change with temperature up to 368 K, which is typical of ionic crystals [20]. However, above this temperature these parameters increase slowly up to about 392 K and thereafter rapidly. In the high temperature region, the weakening of the hydrogen bonds in the lattice and consequent change in the polarisability of ions may be responsible for this rapid increase in dielectric constant.

The DSC thermogram of EDAP is in sharp contrast to those of EDC, EDN and EDS. No phase transition was observed in the temperature range 323 to 480 K. Above 480 K the samples starts melting with decomposition. The decomposition peak masks the peak due to melting.

**6.5 REFERENCES**

- [1] W.P.Mason, *Piezoelectric Crystals and their Applications to Ultrasonics* (Van Nostrand, New York, 1950) p.140.
- [2] E.J.Murphy, *J. Appl. Phys.* **35** (1964) 2609.
- [3] J.M.Pollock and M.Sharan, *J. Chem. Phys.* **51** (1969) 3604.
- [4] L.B.Harris and G.J.Vella, *J. Chem. Phys.* **58** (1971) 4550.
- [5] V.K.Subhadra, U.Syamaprasad and C.P.G.Vallabhan, *J. Appl. Phys.* **54** (1983) 2593.
- [6] J.K.Rath and S.Radhakrishna, *J. Mater. Sci. Lett.* **6** (1987) 929.
- [7] V.H.Schmidt and E.A.Uehling, *Phys. Rev.* **126** (1962) 447.
- [8] M.O'Keefee and C.T.Perrino, *J. Phys. Chem. Solids*, **28** (1967) 211.

- [9] J.K.Rath and S.Radhakrishnan, *J. Mater. Sci. Lett.* **6** (1987) 334.
- [10] J.B.Goodenough, J.Jensen, A.Potier (ed.) *Solid State Protonic Conductors III*, Odense University Press, Odense, Denmark (1985).
- [11] R.P.Hamlem, *J. Electrochem. Soc.* **109** (1962) 726.
- [12] G.Alberti and E.Torracca, *J. Inorg. Nucl. Chem.* **30** (1968) 1093.
- [13] S.M.Golubev and Yu D.Kondrashev, *J. Struct. Chem.* **25** (1984) 471.
- [14] D.E.Corbridge, *Bull. Soc. Fr. Miner, Cristallogr.* **94** (1971) 271.
- [15] T.Leban, L.Golic and J.C.Speakman, *J. Chem. Soc., Perkin Trans. II*, (1973) 703.
- [16] R.Navilkumar and C.P.G.Vallabhan, *J. Phys.: Condens Matter* **1** (1989) 6095.

- [17] T.M.Herrington and L.A.K.Staveley, *J. Phys. Chem. Solids* 25 (1964) 921.
- [18] Y.Berteit, A.Kessler and T.List, *Z. Phys. B* 24 (1976) 15.
- [19] B.E.Taylor and A.L.Laskar, *Phys. Stat. Sol.(b)* 101 (1980) 423.
- [20] C.P.Smith, *Electrical Behaviour of Solids*, p.132. McGraw-Hill, New York (1955).

## Chapter 7

### A COMPARATIVE STUDY OF EXPERIMENTAL RESULTS FOR ETHYLENEDIAMMONIUM SALTS AND CONCLUSIONS

#### 7.1 CHOICE OF MATERIALS

The choice of the four ethylenediammonium salts, viz., ethylenediammonium dichloride (EDC), ethylenediammonium dinitrate (EDN), ethylenediammonium sulphate (EDS) and ethylenediammonium acid phosphate (EDAP) selected for the present study was prompted by the following considerations:

- i) Investigations by earlier workers on simple ammonium salts have established protonic conduction and to some extent the influence of the counter ion on their electrical properties.
- ii) Ethylenediammonium salts investigated here have well established crystal structure [1-4]. A comparative study of their electrical properties and phase transitions would shed new light on the role of the environment of the hydrogen atoms on protonic conduction.

- iii) The anions chosen have varying polarizabilities. This could influence the environment of the mobile protons and its consequences may be reflected in the experimental results.
- iv) Protonic conductors of moderate conductivity are assuming greater significance due to their technological application in devices such as hydrogen ion detectors, fuel cells and batteries.

An overview of the crystal structure of these materials will be helpful in discussing the mechanism of charge transport in them. The features of their crystal structure are presented in Table 7.1.

## 7.2 dc CONDUCTIVITY

It has been seen in the preceding chapters that essentially protonic conduction occurs in all the four materials. The nature of  $\log \sigma_{dc}$  vs  $1/T$  plots for all of them are similar. There are three distinct regions in the plots prior to the phase transition temperature in EDC, EDN and EDS. Apparently EDAP does not exhibit any

Table 7.1: Features of the crystal structure of ethylene-diammonium salts studied

Material	Space group	Morphology	Values of a, b, c Å	Number of formula units in unit cell
EDC	$P2_1/a$	monoclinic	9.95±0.01 6.89±0.01 4.42±0.01	2
EDN	$PT(c'_i)$	triclinic	5.068 (2) 5.514 (3) 7.174 (3)	1
EDS	$P4_1 2_1$ or $P4_3 2_1$	tetragonal	8.47±0.02 8.47±0.02 18.03±0.04	8
EDAP	$P2_1/b$	monoclinic	7.500 8.045 11.806	4

indication of a phase transition. For the sake of convenience these regions may be named as region I, II and III in the order of decreasing temperature.

All the four ethylenediammonium salts have low electrical conductivities at ambient and subambient temperatures. Region III of the Arrhenius plots is almost flat. In this region the temperature dependence of  $\sigma_{dc}$  is extremely small. In region II dc conductivity increases with temperature. Region I of the plots in the case of EDC, EDN and EDS show a continuous curvature. In the conductivity plot of EDAP region I is also a straight line region, showing an increase of  $\sigma_{dc}$  with temperature. The summary of dc conductivity data is given in Table 7.2.

It is seen from Table 7.2 that eventhough the temperature limits of the regions vary from material to material, the activation energies for the same region in different materials along the same axis remains more or less the same. The difference in the temperature limits of different regions and the difference in the magnitude of conductivity and slight difference in activation energies can be explained in the light of the crystal structure and nature of bonding in these materials. Also

Table 7.2: Summary of dc conductivity data of EDC, EDN, EDS and EDAP

Material	Axis of measure- ment	$\log \sigma_{dc}$ ( $^{-1} \text{cm}^{-1}$ ) at 300 K	Temperature range of region II (K)	Activation energy $E_a$ (eV) <sup>a</sup>	Temperature range of region I (K)	Activation energy $E_a$ (eV)
EDC	c	-15.95	320 to 369	1.27	369 to 403	1.37
	c*	-15.05	320 to 369	0.98	369 to 403	1.28
EDN	c	-13.44	316 to 378	1.22	378 to 400	2.12
	c*	-12.82	316 to 378	1.11	378 to 400	2.17
EDS	c	-14.65	357 to 408	1.25	408 to 476	1.86
	c*	-13.95	357 to 408	0.95	408 to 476	1.71
EDAP	c	-14.26	258 to 368	1.02	368 to 415	1.98
	c*	-14.15	258 to 368	1.00	368 to 415	1.94

it is observed that in EDC, EDN and EDS, which have layered structures, the conductivity is higher along the axis parallel to the cleavage plane than that in the direction perpendicular to it.

The environment of the mobile hydrogen atoms influences the nature of the activation barrier for conduction. Hence it is necessary to have a look at the bonding environment of the N-H hydrogen atoms in all the materials, and also that of the OH hydrogen in EDAP. The two  $-\text{NH}_3^+$  groups of ethylenediammonium ion may be either trans to each other as in EDC [1] or cis, as in EDS [3]. These conformations indicate that in each case both  $-\text{NH}_3^+$  groups have symmetrically equivalent positions in the lattice and that hydrogen bonding occurs between the  $-\text{NH}_3^+$  protons and the surrounding halide ions or oxygens of the sulphate group.

The higher activation energy and higher upper temperature limit of region III for EDS may be explained as follows: It is reasonable to assume that the internal barriers will be fairly constant for all cases where the  $\text{ED}^{2+}$  ion is in the trans conformation or for cases in the cis conformation. There may be some difference between

the internal barriers for the two conformations since in the cis form the two  $-\text{NH}_3^+$  groups are close enough that they must interact to some extent. The cause of the difference in the energy barriers becomes clear when the four known crystal structures are inspected closely.

In the light of the known crystal structures, it has been possible to link the magnitude of the observed activation energies with the environment of the  $-\text{NH}_3^+$  group. It is seen that the hydrogen bond length as well as the distance between the layers vary depending upon the size of the counter ion, i.e., the environment of the mobile protons are different in all the four cases. The intact structures naturally would lead to a very low conductivity at low temperatures as observed in all the four ethylenediammonium salts studied here. As temperature increases, thermal activation of the lattice enhances proton mobility. The activation energy in region II in all of these materials lie very close to one another. This is also a qualitative indication of the occurrence of similar mechanism for charge transport that is dominant in this temperature range.

The increase in conductivity at phase transition has been attributed to the release of protons during the

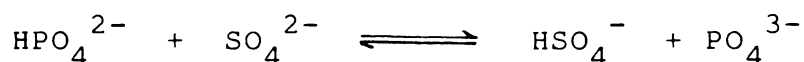
rotational reorientation of the ammonium group. The continuous curvature in the Arrhenius plot, observed prior to the onset of phase transition is an indication of the existence of a continuously varying activation energy barrier arising from the loosening of the crystal lattice. This is especially true of EDC, EDN and EDS. The higher activation energy at elevated temperatures may probably be due to the higher energy input required to loosen the stronger hydrogen bonds.

When EDC and EDN are doped with EDS, a decrease in conductivity is observed. However, when EDS is doped with EDAP or vice-versa an increase in conductivity occurs. In EDC, EDN and EDS, the change in conductivity due to doping is only very slight. Appreciable increase in conductivity is exhibited only in the case of EDAP doped with EDS.

The activation energy values in different temperature ranges are not affected significantly by doping in all the four salts. This directly points to the fact that the activation barriers are not modified to any large extent by doping. Indirectly it points to the fact that the mechanism of conduction is also not affected by doping.

The slight decrease in conductivity in EDC and EDN upon doping may be explained as follows: When the impurity ion enters the host lattice substitutionally, it disturbs the uniform structure of the lattice and creates local distortion. When the interaction of the impurity with the lattice increases the barrier height it is exhibited as a change in the activation energy. A modification in the environment of the carrier brought about in this manner can change the mobility of the same. However, at the levels of doping employed here such effects are only very slight.

The enhancement of conductivity when EDS is doped with EDAP or vice-versa may be explained on the same line, but with an additional factor operating as indicated below. The proton of the acid phosphate can exchange with a sulphate ion as shown below:



$\text{HSO}_4^-$  is a stronger acid than  $\text{HPO}_4^{2-}$ , i.e., the proton of  $\text{HSO}_4^-$  has higher mobility and as a consequence the doped sample has a higher conductivity.

Deuteration of all the samples leads to lowering of conductivity in the whole temperatures range. This provides a direct clue to the fact that proton is the effective charge transport agent [5-9]. Substitution of hydrogen atoms with deuterium leads to a decrease in mobility and hence a decrease in conductivity. This is also reflected as a slight increase in the activation energy values resulting from the slight modification of the lattice dimensions.

### 7.3 ac CONDUCTIVITY

In all the materials  $\log \sigma_{ac}$  vs  $1/T$  plots show the same pattern. At low temperatures the values are small and are independent of temperature. At higher temperatures  $\sigma_{ac}$  increases with temperature. Also such plots show anomalies at phase transitions.

### 7.4 DIELECTRIC CONSTANT

The dielectric constant represents a contribution of the polarizability of the species in the crystal lattice. Depending upon the frequency of the field, different types of dielectric relaxations can set in. At a fixed frequency the variation of dielectric response with

temperature indicates the temperature-dependent contribution of dipolar species. Ethylenediammonium salts behave typical ionic solids. The value of  $\epsilon'$  is low at subambient temperatures and increases only very slightly with increasing temperature. However, at higher temperatures the crystal lattice loosens, and the contribution from the orientational polarization increases. This causes a rapid increase in dielectric constant. This is evident in all the cases studied.

#### 7.5 PHASE TRANSITION IN ETHYLENEDIAMMONIUM SALTS

The phase transition occurring in ED salts were clearly revealed in both the electrical measurements and DSC thermograms. EDC, EDN and EDS which have layered structures show phase transitions with onset at 403, 404 and 480 K respectively. At the phase transition point dc conductivity curves show  $\lambda$ -shaped anomalies. ac measurements (ac conductivity, dielectric constant and dielectric loss) also show anomalies at the same temperature at which these occur in  $\sigma_{dc}$ . In many ammonium salts such anomalous variations at the high temperature phase transitions have been attributed to rotational reorientation of the

ammonium group [10-18]. In solid ED salts the only reorientations which can occur preserving the symmetry of the lattice are  $C_3$  reorientations of the  $-\text{NH}_3^+$  groups, or a  $C_2$  reorientation of the whole ion. The barrier for the latter motion is likely to be extremely high considering the shape and bulk of the ion and the hydrogen bonding at both ends. It is anticipated that reorientational barriers decrease with increasing temperature, because of lattice expansion and increased vibrational amplitudes [19]. It then seems very reasonable to suggest that the observed anomaly may be explained in terms of the rotational reorientation of both the  $-\text{NH}_3^+$  groups of the  $\text{ED}^{2+}$  ion. Such phase changes where the barrier to  $-\text{NH}_3^+$  group reorientation drops dramatically on going into the higher temperature phase have also been observed using NMR spin lattice relaxation measurements [20-22].

## 7.6 CONCLUSIONS

The observations discussed in the preceding sections make it clear that protonic conduction occurs in all the four ethylenediammonium salts studied.  $\sigma_{\text{dc}}$ ,  $\sigma_{\text{ac}}$ ,  $\epsilon$  and  $\tan\delta$  measurements as a function of temperature have shown that anomalous variation occurs to these parameters

at a phase transition. This is attributed to the rotational reorientation of the  $\text{-NH}_3^+$  ion with simultaneous release of protons at the phase transition. The migration of protons with relatively low activation energies in all the materials can be linked with rearrangement of  $\text{-N-H...X}$  hydrogen bonds and/or  $\text{O-H...X}$  hydrogen bonds through a proton switch mechanism.

**7.7 REFERENCES**

- [1] T.Ashida and S.Hirokawa, Bull. Chem. Soc. Jpn. 36 (1963) 704.
- [2] M.Mylrajan and T.K.K.Srinivasan, Phase Transitions 12 (1988) 285.
- [3] K.Sakurai, J. Phys. Soc. Jpn. 16 (1961) 1205.
- [4] S.M.Golubev and Yu K.Kondrashev, J. Struct. Chem. 25 (1984) 471.
- [5] L.Glasser, Chem. Rev. 75 (1975) 21.
- [6] U.Syamaprasad and C.P.G.Vallabhan, Solid State Commun. 41 (1982) 169.
- [7] U.Syamaprasad and C.P.G.Vallabhan, Phys. Lett. 89A (1982) 37.
- [8] V.K.Subhadra, U.Syamaprasad and C.P.G.Vallabhan, J. Appl. Phys. 54 (1983) 2593.
- [9] R.Navilkumar and C.P.G.Vallabhan, Phys. Stat. Sol. (a) 112 (1989) K 113.

- [10] Y.V.G.S.Murti and P.S.Prasad, *Physica B* **79** (1975) 243.
- [11] U.Syamaprasad and C.P.G.Vallabhan, *Solid State Commun.* **34** (1980) 899.
- [12] U.Syamaprasad and C.P.G.Vallabhan, *J. Phys. State Commun.* **14** (1980) 899.
- [13] R.Navilkumar and C.P.G.Vallabhan, *J. Phys.: Condens. Matter* **1** (1989) 6095.
- [14] C.I.Ratcliffe, *J. C. S. Faraday II*, **76** (1989) 1196.
- [15] S.Albert and J.Ripmeester, *J. Chem. Phys.* **58** (1973) 541.
- [16] C.I.Ratcliffe and B.A.Dunell, *Faraday Symp. Chem. Soc.* **13** (1978) 142.
- [17] C.J.Ludman, C.I.Ratcliffe and T.C.Waddington, *J. C. S. Faraday II*, **72** (1976) 1759.

PART II

STUDIES ON THE ELECTRICAL PROPERTIES OF POLY(META-TOLUIDINE)  
AND POLY(ANILINE CO-META-TOLUIDINE)

## Chapter 8

### CONDUCTING POLYMERS--AN OVERVIEW

#### Abstract

Conducting polymers have turned out to be a material reality in recent years. This chapter gives a review of the development of conducting organic polymers covering the techniques used to make them conductive and some of their more important uses. The various theories put forward to explain the charge transport in conducting polymers are discussed briefly. The conducting polymers derived from aniline have been reviewed exhaustively and some of the disparities observed in their properties are highlighted.

## 8.1 INTRODUCTION

One of the salient features of most polymers, which distinguishes them from metals, is their inability to carry electrical current. This insulating property is the first and foremost advantage in the context of conventional applications of polymers. For example, coatings of polymers are used for insulating electrical wires. This creates a general impression that plastics and electrical conductivity are mutually exclusive.

During the last two decades a novel class of organic polymers with remarkable electrical conductivity has been synthesised. In fact, they form a major section of a general class of materials termed synthetic metals. Initially these remained only as a laboratory curiosity. But the enormous potentials they offer for various applications make them materials of choice in many applications.

## 8.2 TYPE OF CONDUCTING POLYMERS

Among the many polymers studied for their conductivity polyacetylene, polyaniline, polypyrrole, polythiophene, poly(phenylene sulphide) poly(phenylene-

vinylene) are the best studied so far. Of these, polyaniline has been known ever since 1862 when H. Letheby [1] prepared it for the first time by the anodic oxidation of aniline in sulphuric acid. However, the study of conducting polymers took an exciting turn when it was demonstrated that polyacetylene can assume metallic conduction under proper conditions of doping [2]. Polyacetylene is a simple macromolecule of formula  $(CH)_n$ . Polyacetylene as such is an infusible highly insulating solid. It was the combined efforts of Shirakawa, MacDiarmid, Heeger and others [2] that revealed the surprising fact that partial oxidation of polyacetylene enhances its conductivity by nine orders of magnitude.

Three other polymers studied subsequently are polypyrrole [3], polythiophene [4], and polyaniline [5]. Diaz et al. [3] have shown that polypyrrole, which normally occurs as an intractable black powder could be rendered conductive by electrolytic oxidation. Later, Tourillon et al. [4] showed that thiophene also can give a conductive polymer by electrochemical oxidation.

Polyaniline has been described by English and French chemists [6,7] at the turn of this century. It can exist in different oxidation states of varying conducti-

vity from  $10^{-11}$  to  $10 \text{ ohm}^{-1} \text{ cm}^{-1}$ . Different oxidation states of polyaniline have different colours and electrical properties. The order of conductivity and nature of dopant related to various conducting polymers are given in Table 8.1.

The ease of preparation, manipulation of advantageous properties by simple chemical treatments, and the wide range of conductivity that can be attained by doping with acids make polyaniline one of the most attractive materials.

### 8.3 POLYANILINE - AN OVERVIEW

Eventhough polyaniline was known for a century in the form of 'aniline black' it was Jozefowicz and coworkers who showed that the conductivity of polyaniline could be varied by doping with acid [7]. They also recognised the potential of PA as an electrode material in batteries. In the 1980's PA was subjected to intense synthetic, structural and physical characterisation by various groups [5,8-17]. Wudl et al. [15] and Baughman and Shacklette [16] have shown that it was a general structure which may be schematically represented as given in Fig.8.1.

Table 8.1: Some more common conducting polymers reported

Polymer	Dopants	Approximate conductivity ( $\text{ohm}^{-1}\text{cm}^{-1}$ )
Polyacetylene	$\text{I}_2$ , $\text{Br}_2$ , Li, Na, $\text{AsF}_5$	10,000
Polypyrrole	$\text{BF}_4^-$ , $\text{ClO}_4^-$ , tosylate	500-7500
Polythiophene	$\text{BF}_4^-$ , $\text{ClO}_4^-$ , tosylate, $\text{FeCl}_4^-$	1000
Poly(3-alkylthiophene)	$\text{BF}_4^-$ , $\text{ClO}_4^-$ , $\text{FeCl}_4^-$	1000-10,000
Poly(phenylene sulphide)	$\text{AsF}_5$	500
Poly(phenylenevinylene)	$\text{AsF}_5$	10,000
Poly(thienylenevinylene)	$\text{AsF}_5$	2700
Polyphenylene	$\text{AsF}_5$ , Li, K	1000
Poly(isothianaphthene)	$\text{BF}_4^-$ , $\text{ClO}_4^-$	50
Polyazulene	$\text{BF}_4^-$ , $\text{ClO}_4^-$	1
Polyfuran	$\text{BF}_4^-$ , $\text{ClO}_4^-$	100
Polyaniline	HCl	200

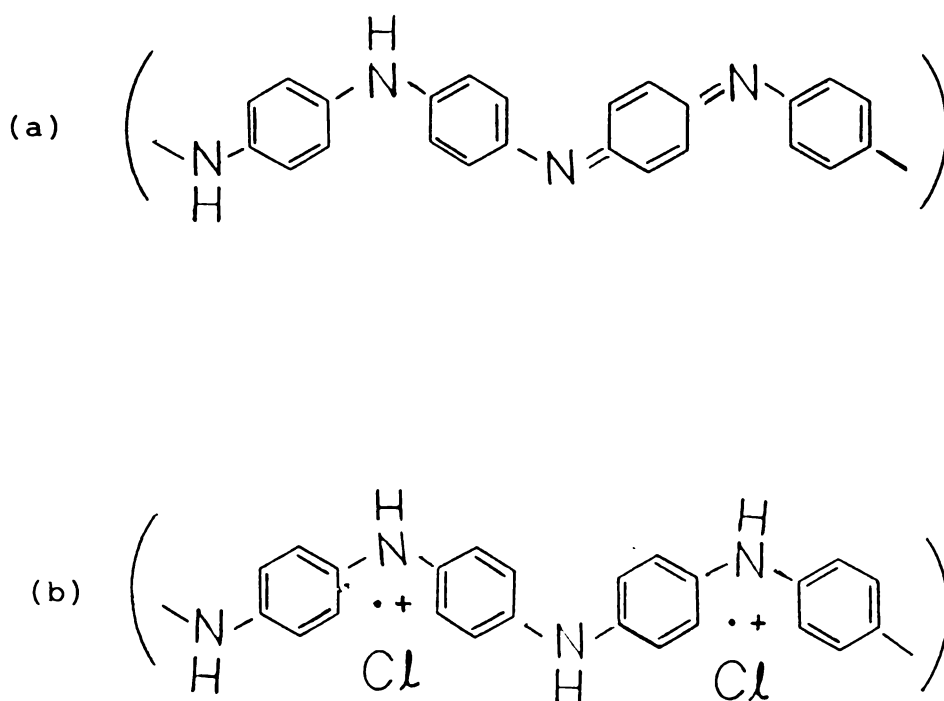


Fig.8.1: Schematic illustration of the structure of  
 (a) polyaniline (emeraldine) base  
 (b) protonated polyaniline (emeraldine salt)

The form represented here is known as emeraldine, in which the oxidation of polyaniline is carried out to an extent of 50%. Higher and lower oxidised forms do not show the high degree of conductivity observed in emeraldine. It is also seen that emeraldine treated with a base such as caustic soda or ammonia turns out to be a strong insulator [5]. It is evident that partially oxidised aniline (emeraldine) which is protonated, alone shows good conductivity.

The polyaniline family of conducting polymers differs from other conducting polymers in several aspects:

Firstly, the quasi-one dimensional polyaniline is not charge conjugation symmetric, i.e., Fermi level and band gap are not formed in the centre of the band so that the valence and conduction bands are asymmetric. Consequently, the energy level positions of doping induced [18,19] and photon induced [20,21] absorptions differ substantially from those in charge conjugation symmetric polymers such as polyacetylene, polypyrrole and polythiophene [22,23].

Secondly, both carbon rings and nitrogen atoms are within the conjugation path forming a generalized A-B polymer [24].

Thirdly, the emeraldine base form of polyaniline can be converted from the insulating to the metallic state by adding protons to the imine ( $-N=$ ) sites, while the number of electrons associated with the emeraldine chain is unaltered [5,8,19,25,26].

Various theories have been proposed to explain the conductivity observed in doped polyaniline. Electrical conductivity studies on protonated emeraldine salt have given evidence for the formation of a "granular" polymeric metal [27], ie., within the protonation regime the charge conduction is dominated by phase segregation into protonated and unprotonated regions. In such cases it is likely that a charging energy limited tunneling mechanism exists [28]. It is also found that the conductivity of protonated emeraldine is sensitive to humidity [29-33]. There have been only limited studies [34-36] on the conduction process in less conducting forms of polyaniline.

#### 8.4 SUBSTITUTED POLYANILINE

A perusal of literature shows that the conditions of chemical synthesis of polyaniline vary from one study to another [37-47]. These variables include

reaction medium, type and concentration of acid, oxidant, washing agents and drying temperature. These, in turn, affect chemical structure, composition, oxidation state, thermal stability and electrical properties of the resulting material. However, most of these studies were centered around materials derived from aniline. The influence of substitution on aniline has rarely been studied in any detail.

Shenglong et al. [48] synthesized substituted polyanilines from *m*-toluidine, *o*-chloroaniline and nitroaniline by chemical polymerization. They characterized the resulting polymers by DSC, X-ray, IR, XPS and dc conductivity. The results revealed that the substituent affects the regularity of the polymer chain.

Copolymerization of 2-chloroaniline and 2-iodoaniline individually with aniline in different monomer feed ratios showed that the properties of the resulting material depended on the monomer feed ratio [49]. An increase in the fraction of substituted aniline beyond 0.5 decreased the extent of protonation drastically. The polymers derived from substituted anilines invariably show lower electrical conductivity.

Studies carried out by Langer [50] on poly-(N-methylaniline) and copolymers of N-methylaniline with aniline showed that the electrical properties depended upon the method of preparation, doping level, molecular conformation and residual oligomeric impurities. The role of oligomeric impurities have also been observed by different workers [51-53].

It is clear that the results reported by various workers on polyaniline as well as on substituted polyanilines differ in the quantitative aspects presumably due to subtle variations in the molecular aspects, and due to the presence of oligomeric impurities. It was thought worthwhile to investigate in detail the electrical characteristics of copolymer of aniline with m-toluidine after careful purification.

#### 8.5 THEORIES OF ELECTRICAL CONDUCTION IN CONDUCTING POLYMERS

The electrical conductivity  $\sigma$  represents the transport of net charge through a medium in an applied electric field  $E$ ,

$$\text{ie., } \sigma \equiv \frac{j}{E} \quad (8.1)$$

where  $j$  is the current density

As the solitons, polarons and bipolarons may exert considerable effect on the electronic states accessible to electrons, these may dramatically affect transport properties. At this point, it will be helpful if some of the predictions for ac and dc conductivities in model systems are considered. As most of the conducting polymers have crystalline orders over a segment of about 200 Å and as this reduces to a few tens of Angstrom after doping, it is reasonable to compare this with the electronic structure of disordered semiconductors.

In dc conductivity studies the net charge transported across the entire sample is measured. In ac conductivity measurements, the electrical conductivity is measured as a function of the frequency of an alternating electric field. A difference in the behaviour of  $\sigma(f)$  is likely to occur when conduction takes place by the motion of charge carriers in the extended states by hopping in localized states, hopping among soliton, polaron or bipolaron states, or by transport between small "metallic" particles embedded in an insulating polymer matrix. The density of states  $N(e)$  determines to a large extent the transport mechanism. When carriers are in extended states as in a metal, the conductivity does not depend upon

frequency. When carriers are excited across the band gap of a crystalline semiconductor or across the mobility edge into extended states in a disordered semiconductor, the conductivity is independent of frequency. Here  $\sigma$  is proportional to the product of density of excited charge carriers and the temperature dependent mobility of the excited charge carriers. However, when carriers are not in excited states as in a disordered or inhomogeneous system, the conductivity at higher frequency is usually larger than the dc conductivity.

The frequency dependence of conductivity is common to disordered semiconductors and insulators [54]. Diverse physical mechanisms [55,56] including variable-range-hopping and the presence of surface barriers and ionic dipoles may be invoked to explain these observations. The observed conductivity is commonly expressed as,

$$\sigma_{\text{Tot}} = \sigma_{\text{dc}} + \sigma_{\text{ac}}(f, T) \quad (8.2)$$

In all treatments dealing with hopping in a manifold of states near the Fermi level, it is assumed that ac and dc conductivities are only weakly dependent

on  $T$ . A typical case is the variable-range-hopping model suggested by Mott [55]. According to this model, hopping of a charge carrier in three dimensions produces a conductivity given by,

$$\sigma_{(T)} = \left\{ 0.39 [N(E_F) / \alpha kT]^{1/2} \nu_0 e^2 \right\} \exp[-(T_0/T)^{1/2}] \quad (8.3)$$

where  $T_0 = 16 \alpha^3 / kN(E_F)$ ,  $\alpha^{-1}$  is the decay length of the localized state,  $\nu_0$  a hopping attempt frequency,  $N(E_F)$  the density of states at the Fermi energy  $E_F$ , 'e' the electronic charge, and  $k$  the Boltzman constant. Similarly, the Austin-Mott [57] analysis of pairwise hopping between localized states near the Fermi energy predicts a linear temperature dependence for the ac conductivity:

$$\sigma_{ac} = 2 \pi^2 / 3) e^2 k T N^2(E_F) \alpha^{-5} f [\ln(\nu_0 / 2 \pi f)]^4 \quad (8.4)$$

For moderate frequencies ( $10^2 < f < 10^8$  Hz) and  $\nu_0$  of the order of about  $10^{12}$  Hz, this model [55] gives,

$$\sigma_{ac} \propto T f^5 \quad (8.5)$$

A strong  $T$  dependence of  $\sigma_{ac}$  can result from thermal activation of charge carriers from localized states in the

gap to localized states in the valence or conduction band tails. Here the temperature dependence of  $\sigma_{dc}$  and  $\sigma_{ac}$  is determined largely by the number of charge carriers excited to the band tails [56]. Thus,

$$\sigma_{dc} \propto \exp(-E'_a/kT) \quad (8.6)$$

$$\sigma_{ac} \propto f^{ST} \exp(-E'_a/kT) \quad (8.7)$$

with  $E'_a < E_a$ . Here  $E_a$  is the energy for activation to extended states.

Hopping of polarons can also lead to a strong T dependence for  $\sigma_{dc}$  and  $\sigma_{ac}$  [56,58]. Kivelson proposed [59] a phenomenological model for hopping conduction based on the separation of energy (temperature) and spatial dependence of the rate of hopping among states. The corresponding expression simplifies to the form,

$$\sigma_{ac} = K^{-1}(f/T)[\ln(Df/T^{n+1})]^4 \equiv K'x \quad (8.8)$$

where  $K'$  and  $D$  are constants.

The hopping mechanism is characterized by a log-normal distribution of hopping rates. Hence all such hopping mechanisms exhibit some common features.

A high frequency limit is reached when frequency is greater than the maximum hopping rate (attempt frequency  $\Gamma_0$ ). The ratio of  $\sigma(f=0)/\sigma(f \gg \Gamma_0)$  is a useful quantity since it is a measure of the distribution of site energies. Also it is independent of the detailed considerations of hopping mechanism [60]. For two extreme cases of isoenergetic hopping where the distribution of site energies is narrow compared with  $kT$  and variable range hopping in which distribution is much broader than  $kT$ , the ratio obtained is very different in the two limits. This ratio is a useful diagnostic of the charge conduction mechanism. The arguments can be summarised in the relationship derived by Kivelson and Epstein. For isoenergetic hopping,

$$\frac{\sigma(\infty)}{\sigma(0)} = \frac{9D}{32\pi A} \left(\frac{\xi}{R_0}\right)^4 F\left(\frac{2BR_0}{\xi}\right) \exp(2BR_0/\xi) \quad (8.9)$$

where  $A = 0.45$ ,  $B = 1.39$ ,  $D \approx 1$  and  $F(x)$  is given by,

$$F(x) = (1 + x^{-1} + 7x^{-2} + 12x^{-3} + 12x^{-4} - x^2 e^{-x})^{-1}$$

and is equal to 1 for large  $x$ .

For variable-range-hopping [55],

$$\frac{\sigma(\infty)}{\sigma(0)} = \frac{3\pi(2.3)}{0.2} \left(\frac{T}{T_0}\right)^{3/2} G \exp\left[\left(\frac{T_0}{T}\right)^{1/4}\right] x \left\{1 + 0 \left[\left(\frac{T}{T_0}\right)^{1/4}\right]\right\} \quad (8.10)$$

where  $G \approx 1$ .

In both mechanisms  $\sigma(f)$  is an increasing function of  $f$  and approaches its infinite frequency value when  $f > \Gamma_0$ . The composite metal-insulator systems also show a decrease in dc conductivity with decreasing temperature. A frequency dependence occurs from capacitive coupling between conducting metallic regions. The effective medium theory put forth by Springett [61] predicts that the frequency dependence of measured conductivity  $\sigma_m$  emerges at some frequency, depending upon the relative conductivities of the metal and insulating regions and their volume fractions.

## 8.6 APPLICATIONS OF CONDUCTING POLYMERS [62]

### (i) Batteries

Majority of the conducting polymers developed so far are the oxidised forms of extended conjugation polymers. These find use as active electrodes in rechargeable batteries. All solid state batteries based on conductive polymers have been developed by Hitachi, and Bridgestone in Japan, Allied Signal in USA, and Varta in Germany. The button type polyaniline cathode/Li-Al anode 3-Volt battery developed by Bridgestone is characterized by high cycle life and energy density several times higher

than that of CdNi and Pb/acid batteries. Varta has commercialised a Li-Al/polypyrrole battery in collaboration with BASF. These batteries are excellent for applications where low power, long life, and reliable operation are required. Examples are back-up sources for static random access memories, intelligent telephones and timers, for video cassette recorders, and as batteries for calculators and television remote controls.

(ii) Electronic devices

Certain conducting polymers like polyaniline show a wide range of colours as a result of change in the oxidation state and protonation. The electrochromic properties of such polymers are exploited to produce devices like displays and thermal 'smart windows'. These can be fabricated in large areas and unlimited visual angles. Because these do not change colour after the applied voltage has been switched off, the electrochromic device exhibits a memory function (bistability) and can be used to store information.

(iii) Gas separation membranes

An unusual application of polyaniline is in gas separation. Kaner and Heiss have discovered that conductive polyaniline membrane which is subjected to

repeated doping-undoping cycles, becomes porous and can act as a medium for the separation of gases, eg., separation of oxygen from nitrogen.

(iv) Conducting textiles and surface coatings

A textile with amazing electrical conductivity has been produced by impregnating the fabric with polypyrrole and polyaniline. These textiles have the same strength as their commercial counterparts. Such conductive fabrics incorporated into the plastic composites when used to cast aeroplane frames, dissipate charge during lightning strikes preventing any damage to the aeroplane. Such fabrics distort radar signals. When incorporated into the aircraft surface finish they mislead the enemy radar. Latex compositions containing colloidal polyaniline, polyathiophene and polypyrrole when sprayed onto surfaces conductive coatings capable of electromagnetic shielding are formed, thus preventing electronic eavesdropping.

Eventhough tremendous progress has been made in this field, challenges still remain. Materials with higher carrier mobilities are needed. Structural

modifications can lead to more desirable properties and a correlation of the structure with properties will help to develop better materials.

(v) Semiconductor applications

As semiconductors, conducting polymers find use in electronic and electro-optic devices. The formation of unipolar devices such as Schottky diodes, metal-insulator-semiconductor diodes and metal-insulator-semiconductor field effect transistors have been fabricated using polyacetylene, polypyrrole and polythiophene. Bipolar devices suffer from the diffusion of dopant across the p-n junction.

(vi) Optical applications

The interest in conducting polymers in electro-optical devices is multifold. The non-linear response of a polymer chain results in a field dependent modulation of the  $\pi - \pi^*$  absorption spectrum. This gives a large induced absorption. Trans-polyacetylene and poly(phenylene-vinylene) have been used as optical modulators. Very recently electro-optic devices especially electroluminescent ones have been reported.

In spite of the fact that a large volume of work has been reported on the properties of polyaniline, the properties of its derivatives are little known. In the ensuing chapters of this thesis the results of the investigations carried out on poly(meta-toluidine) and the copolymers of aniline with meta-toluidine are presented.

**8.7 REFERENCES**

- [1] H.Letheby, *J. Chem. Soc.* **15** (1962) 161.
- [2] C.K.Chiang, C.R.Fincher, Y.W.Park, A.J.Heeger, H.Shirakawa, E.J.Louis, S.C.Gau and A.G.MacDiarmid, *Phys. Rev. Lett.* **39** (1977) 1098.
- [3] A.F.Diaz, K.K.Kanazawa and G.P.Gardini, *J. Chem. Soc. Chem. Commun.* (1979) 635.
- [4] G.Tourillon, D.Gourier, F.Garnier, D.Vivien, *J. Phys. Chem.* **88** (1984) 1049.
- [5] J.C.Chiang and A.G.MacDiarmid, *Synth. Met.* **13** (1986) 193.
- [6] A.G.Green and A.E.Woodhead, *J.Chem. Soc.* (1910) 2388.
- [7] R de Surville, M.Josefowicz, L.T.Yu, J. Perichon and R.Buvet, *Electrochim. Acta.* **13** (1968) 1451.
- [8] A.G.MacDiarmid, J.C.Chiang, W.S.Huang, B.D.Humphrey, N.L.D.Somasiri, W.Wu and S.I.Yaniger, *Mol. Cryst. Liq. Cryst.* **121** (1985) 173.

- [9] D.S.Boudreaux, R.R.Chance, J.F.Wolf, L.W.Shacklette, J.L.Bredas, B.Themans, J.M.Andre and R.Silbey, *J. Chem. Phys.* **85** (1986) 4584.
- [10] M.Nechtschein, C.Santier, J.P.Travers, J.Chroboczek, A.Alix and M.Ripert, *Synth. Met.* **18** (1987) 1311.
- [11] J.P.Travers, M.Nechtschein, *Synth. Met.* **21** (1987) 135.
- [12] T.Hagiwara, T.Demura and K.Iwata, *Synth. Met.* **18** (1987) 317.
- [13] E.M.Genies, M.Lapkowski, C.Santier and E.Vieil, *Synth. Met.* **18** (1987) 631.
- [14] W.R.Salaneck, I.Lundstrom, T.Hjertberg, C.B.Duke, E.M.Conwell, A.Paton, A.G.MacDiarmid, N.L.D.Somasiri, W.S.Huang and A.F.Richter, *Synth. Met.* **18** (1987) 291.
- [15] F.Wudl, R.O.Angus, Jr., F.L.Lu, P.M.Allemand, D.F.Vachon, M.Novak, Z.X.Liu and A.J.Heeger, *J. Am. Chem. Soc.* **109** (1987) 3677.

- [16] L.W.Shacklette, J.F.Wolf, S.Gould, R.H.Baughman, J. Chem. Phys. **88** (1988) 3955.
- [17] B.Wehrle, H.H.Limbach, J.Mortensen and J.Heinze, Angew. Chem. Int. Ed. Engl. Adv. Mater. **28** (1989) 1741.
- [18] S.Stafstrom, J.L.Bredas, A.J.Epstein, H.S.Woo, D.B.Tanner, W.S.Huang and A.G.MacDiarmid, Phys. Rev. Lett. **59** (1987) 1464.
- [19] A.J.Epstein, J.M.Ginder, F.Zuo, R.W.Bigelow, H.S.Woo, D.B.Tanner, A.F.Richter, W.S.Huang, A.G.MacDiarmid, Synth. Met. **18** (1987) 303.
- [20] A.J.Epstein, J.M.Ginder, M.G.Roe, T.L.Gustafson, M.Angelopoulos and A.G.MacDiarmid, in Materials Research Society Conference Proceedings, (ed.) A.J.Heeger, J.Orenstein and D.R.Ulrich (MRS, Pittsburgh, 1988), Vol.109, p.313.
- [21] R.P.McCall, M.G.Roe, J.M.Ginder, T.Kusumoto, A.J.Epstein, G.E.Asturias, E.M.Scherr and A.G.MacDiarmid, Synth. Met. **29** (1989) 433.

- [22] Handbook of Conducting Polymers, (ed.) T.Skotheim (Dekker, New York, 1986), Vol.1 and 2.
- [23] Proceedings of the International Conference on Synthetic Metals, Albano Terme, 1984; Proceedings of the International Conference on Synthetic Metals, Kyoto, 1986; Proceedings of the International Conference on Synthetic Metals, Santa Fe, 1988.
- [24] J.A.Pople and S.H.Walmsley, Mol. Phys. 5 (1962) 15.
- [25] A.G.MacDiarmid, J.C.Chiang, M.Halpern, W.S.Huang, J.R.Krawczyk, R.J.Mammone, S.L.Mu, N.L.D.Somasiri and W.Wu, Polym. Prepr. 25 (1984) 248.
- [26] J.M.Ginder, A.F.Richter, A.G.MacDiarmid and A.J.Epstein, Solid State Commun. 63 (1987) 97.
- [27] F.Zuo, M.Angelopoulos, A.G.MacDiarmid and A.J.Epstein, Phys. Rev. B 36 (1987) 3475.
- [28] B.Abeles, P.Sheng, M.D.Coults and Y.Arie, Adv. Phys. 24 (1975) 407; Phys. Rev. Lett. 31 (1973) 44.

- [29] M.Angelopoulos, A.Ray, A.G.MacDiarmid and A.J.Epstein, *Synth. Met.* 21 (1987) 21.
- [30] P.Travers and N.Nechtschein, *Synth. Met.* 21 (1987) 135.
- [31] M.Nechtschein, C.Santier, J.P.Travers, J.Chroboezek, A.Alix and M.Ripert, *Synth.Met.* 18 (1987) 311.
- [32] H.H.S.Javadi, F.Zuo, M.Angelopoulos, A.G.MacDiarmid and A.J.Epstein, *Mol. Cryst. Liq. Cryst.* 160 (1988) 225.
- [33] H.H.S.Javadi, M.Angelopoulos, A.G.MacDiarmid and A.J.Epstein, *Synth. Met.* 26 (1988) 1.
- [34] M.Angelopoulos, G.E.Asturias, S.P.Ermer, A.Ray, E.M.Scherr, A.G.MacDiarmid, M.Akhtar, Z.Kiss and A.J.Epstein, *Mol. Cryst. Liq. Cryst.* 160 (1988) 151.
- [35] M.X.Wan, A.G.MacDiarmid and A.J.Epstein, *Solid State Sci.* 76 (1987) 216.
- [36] T.Hayashi, Y.Hirai, H.Tanaka and T.Nishi, *Jpn. Phys.* 26 (1987) L1800.

- [37] A.G.Green and A.E.Woodhead, *J. Chem. Soc.* **97** (1910) 2388.
- [38] A.G.Green and A.E.Woodhead, *J. Chem. Soc.* **101** (1912) 1117.
- [39] T.Hagiwara, M.Yamura and K.Iwata, *Synth. Met.* **25** (1988) 243.
- [40] V.G.Kulkarni, L.D.Campbell and W.R.Mathew, *Synth. Met.* **30** (1989) 321.
- [41] A.G.MacDiarmid, J.C.Chang, M.Halpern, W.Huang, S.Mu and N.L.D.Somasiri, *Mol. Cryst. Liq. Cryst.* **121** (1985) 173.
- [42] A.Pron, F.Genoud, C.Menardo and M.Nechtschein, *Synth. Met.* **24** (1988) 193.
- [43] A.Andreatta, Y.Cao, J.Chiang and A.J.Heeger, *Synth. Met.* **26** (1988) 383.
- [44] J.P.Travers, J.Chroboczek, F.Devreux, F.Genoud, M.Nechtschein, A.Syed, E.M.Genies and C.Tsintavis, *Mol. Cryst. Liq. Cryst.* **121** (1985) 195.

- [45] J.Tang, X.Jing, B.Wang and F.Wang, Synth. Met. 24 (1988) 231.
- [46] Y.Furukawa, T.Hara, Y.Hyodo and I.Harada, Synth. Met. 16 (1986) 189.
- [47] M.Inoue, E.R.Navarro and M.B.Inoue, Synth. Met. 30 (1989) 199.
- [48] W.Shenglong, W.Fosong and G.Xiaohui, Synth. Met. 16 (1986) 99.
- [49] K.G.Neoh, E.T.Kang and K.L.Tan, Eur. Polym. J. 26 (1990) 403.
- [50] J.J.Langer, Synth. Met. 35 (1990) 295.
- [51] J.C.Chiang and A.G.MacDiarmid, Synth. Met. 13 (1986) 193.
- [52] J.J.Langer, Synth. Met. 20 (1987) 35.
- [53] J.J.Langer, Mater. Sci. 14 (1988) 41.

- [54] Handbook of Conducting Polymers, (ed.) T.Skotheim (Dekker, New York, 1986) Vol.2, Ch.29.
- [55] N.F.Mott and E.A.Davis, Electronic Processes in Non-crystalline Materials, Clarendon Press, Oxford(1979).
- [56] P.Nagels, in Amorphous Semiconductors, Vol.36, Topics in Applied Physics, (ed.) M.H.Brodsky (Springer Verlag, Berlin, 1979).
- [57] I.G.Austin and N.F.Mott, Adv. Phys. 18 (1969) 41.
- [58] D.Emin, in Electronic and Structural Properties of Amorphous Semiconductors (ed.) P.G.LeComber and J.Mort, Academic Press, New York, 1973.
- [59] S.Kivelson, Phys. Rev. 15 (1982) 3798; Mol. Cryst. Liq. Cryst. 77 (1983) 65; Phys. Rev. Lett. 46 (1981) 1344.
- [60] S.Kivelson and A.J.Epstein, Phys. Rev. 29 (1984) 3336.
- [61] B.E.Springett, Phys. Rev. Lett. 31 (1973) 1463.
- [62] M.G.Kanatzidis, Chem. Engg. News (1990) 36.

## Chapter 9

### EXPERIMENTAL METHODS ADOPTED FOR THE STUDY OF CONDUCTING POLYMERS

#### Abstract

This chapter summarises the experimental methods employed for preparing poly(meta-toluidine) and poly-(aniline co-meta-toluidine) and for characterising them by optical, thermal and electrical methods. The techniques employed include uv-visible and infrared spectroscopy, differential scanning calorimetry, ac and dc conductivity, and dielectric constant measurements.

## 9.1 INTRODUCTION

The results reported on the properties of polyaniline considerably differ depending on the method of preparation [1-12]. Various factors contribute to such discrepancies. In chemically prepared samples factors like the oxidant used to bring about polymerization, the ratio of monomer to oxidant, the temperature at which oxidation is carried out, the post-treatment given to the crude material like washing, doping and drying, and exposure to humidity influence the properties. Sometimes, samples prepared by the same method also significantly differ in properties. One of the factors which invariably affects the electrical properties is the retention of moisture by doped samples. The chemical polymerization also leaves some oligomeric impurities [13]. The oligomeric compounds being low molecular weight quino-  
neimines, their salts will have a higher electrical conductivity.

It was also observed during our preliminary studies that, when polyaniline samples in the form of compacted pellets were maintained at  $10^{-6}$  Torr for depositing silver electrodes, a violet component was

deposited inside the dome of the vacuum system. This is perhaps due to the presence of low molecular weight compounds which can sublime under reduced pressure and elevated temperature.

In the experimental procedures followed here, meticulous care was exercised to purify the monomers, to remove the oligomeric residues from the crude polymer and to maintain identical conditions for post-preparative treatment.

## 9.2 SYNTHESIS OF POLYMERS

### 9.2.1 Purification of aniline

Commercially available aniline contains traces of aromatic hydrocarbons and nitrobenzene. On storing aniline develops a dark colour probably due to air oxidation. Hence aniline was purified by recommended methods [14].

Aniline was dissolved in 6 M HCl. Any precipitate of aniline hydrochloride was dissolved by stirring with more of water. The solution was extracted with toluene to remove neutral and acidic impurities present.

The aniline hydrochloride solution was rendered alkaline with 40% caustic soda. The contents were cooled. The oily liquid that separated out was removed, dried over solid sodium hydroxide and distilled. The middle fraction which distilled out at 184 to 186°C was collected.

### 9.2.2 Purification of meta-toluidine

m-toluidine (CDC, Bombay) was dark in colour. It was subjected to the same treatment described in the previous section for aniline. The fraction distilling out at 200 to 202°C was collected.

### 9.2.3 Preparation of polymers

The purified monomer or a mixture of monomers (0.1 mole) was dissolved in 500 ml of 2 molar  $H_2SO_4$ . The solution was cooled to 5°C and flushed with nitrogen gas. Ammonium persulphate (0.1 mole, 22.8 g) dissolved in a minimum quantity of water was added slowly with stirring. The reaction mixture was stirred further for 4 hrs. The solid product was collected by filtration and washed with 2 molar  $H_2SO_4$  and then with copious amount of distilled water. The solid was dried in air.

#### 9.2.4 Preparation of polymer base

The crude polymer salt obtained from the above step was powdered and stirred with excess of ammonium hydroxide solution for 2 hrs. The base so formed was filtered under suction and washed with distilled water till the washings were free of ammonia. The base was dried in an air oven at 80°C and stored in a vacuum dessicator.

#### 9.3 PURIFICATION OF POLYMER BASE

Polyaniline base and its salts are insoluble in water, dilute acid, alkali and in common organic solvents. However, it was found that methanol and acetonitrile leach out a coloured component from the crude polymer base. Since methanol is readily available, it was chosen for extracting the soluble portion, which is probably the oligomer.

The oligomer is only slightly soluble in methanol. Hence the powdered sample was taken in a filter paper thimble and extracted in a Soxhlet extractor on a water bath for about 200 hrs. The progress of extraction was monitored by withdrawing nascent extract periodically

from the Soxhlet apparatus and recording the uv-visible spectrum. Extraction was assumed to be complete when the extract did not give any absorption band in the 300-700 nm range of the spectrum.

#### 9.4 DOPING

It has been observed by earlier workers [12,15] that doping of polyaniline from moderately concentrated HCl results in the incorporation of chlorine atom to the aromatic ring. For this reason, the purified base was doped with HCl of upto one molar concentration. Finely powdered base (1 g) was shaken with 200 ml of hydrochloric acid of appropriate concentration for 24 hrs. The protonated material formed was filtered without the aid of solvent, sucked dry by drawing air using a water pump. It was dried in an air oven at 80°C, and then stored in a vacuum dessicator.

The pH of the equilibrium solution was measured using a pH meter (Systronics model 335). A combination of glass and calomel electrode was used, and was calibrated with standard buffers.

## 9.5 CHARACTERIZATION OF THE MATERIAL

The samples of polymer prepared were characterized by the IR spectrum, uv-visible spectrum, differential scanning calorimetry and electrical properties.

### 9.5.1 Infrared spectra

The infrared spectra of the samples were recorded by nujol mull technique on a Perkin-Elmer model 683 infrared spectrophotometer.

### 9.5.2 UV-Visible spectra

UV-Visible spectra of solutions were recorded using Shimatzu uv-visible spectrophotometer model 160 A. UV-Visible spectra of finely powdered solids were recorded by Quagliano's method using Hitachi model 340 uv-visible-NIR spectrophotometer. A paste of finely powdered sample was mulled with nujol and uniformly spread over a strip of whatman No.40 filter paper. A strip of filter paper smeared with nujol was used as blank.

### 9.5.3 DSC

Differential scanning calorimetric traces were recorded using Perkin-Elmer DSC 7 instrument as described in 2.5.

#### 9.5.4 Electrical properties

Finely powdered, dried samples of about 250 mg were pressed to circular discs in a pelletizer [Perkin-Elmer] at a pressure of 4 tons/cm<sup>2</sup>. Both broad faces of the pellet were vacuum deposited with silver to provide good electrical contact and measurements were taken on the same day.

The instruments and their configuration used in the electrical measurements were the same as those employed in section 2.4. The specimens were preheated to 80°C in a dynamic vacuum of 10<sup>-3</sup> Torr for 30 minutes prior to the experimental runs. The samples were then cooled to the initial temperature of the runs. dc and ac electrical conductivity, dielectric constant and dielectric loss were measured as a function of temperature as well as frequency. The experiments were repeated with different samples to ensure reproductivity of results.

## 9.6 REFERENCES

- [1] A.G.Green and A.E.Woodhead, J. Chem. Soc. 97 (1910) 2388.
- [2] J.Langer, Solid State Commun. 26 (1978) 839.
- [3] A.G.MacDiarmid, L.S.Yang, W.S.Huang and B.D.Humphrey, Synth. Met. 18 (1987) 393.
- [4] T.Hagiwara, M.Yamura and K.Iwata, Synth. Met. 25 (1988) 243.
- [5] V.G.Kulkarni, L.D.Campbell and W.R.Mathew, Synth. Met. 30 (1989) 321.
- [6] A.G.MacDiarmid, J.C.Chiang, M.Halpern, W.Haugng, S.Mu, and N.L.D.Somasiri, Mol. Cryst. Liq. Cryst. 121 (1985) 173.
- [7] A.Pron, F.Genoud, C.Menardo and M.Nechtschein, Y. Synth. Metl 24 (1988) 193.
- [8] A.Andreatta, Y.Cao, J.Chaing and A.J.Heeger, Synth. Met 26 (1988) 383.

- [9] J.P.Travers, J.Chroboczek, F.Devreux, F.Genoud, M.Nechtschein, A.Syed, E.M.Genies and C.Tsintavis, *Mol. Cryst. Liq. Cryst.* 12 (1985) 195.
- [10] J.Tang, X.Jing, B.Wang and F.Wang, *Synth. Met.* 24 (1988) 231.
- [11] W.R.Salaneck, I.Landstrom, T.Hjertberg, C.B.Duke, E.Conwell, A.Paton, A.G.MacDiarmid, N.L.D.Somasiri, W.S.Huang and A.F.Richtrer, *Synth. Met.* 18 (1987) 291.
- [12] K.L.Tan, B.T.G.Tan, S.H.Khor, K.G.Neoh and E.T.Kang, *J. Phys. Chem. Solids* 52 (1991) 673.
- [13] J.J.Langer, *Synth. Met.* 35 (1990) 295.
- [14] D.D.Perrin, W.L.F.Armarego and D.R.Perrin, *Purification of Laboratory Chemicals*, 2nd edn. Pergamon Press, S.R.(1980), p.108.
- [15] Mirrezaei H.S.Munro and D.Parker, *Synth. Met.* 26 (1988) 169.

## Chapter 10

### ELECTRICAL CONDUCTIVITY AND DIELECTRIC CONSTANT OF POLY(META-TOLUIDINE)

#### Abstract

The dc and ac conductivities and dielectric constant of poly(meta-toluidine) prepared by chemical oxidation have been measured after careful purification. The dc conductivity at 300 K for the pristine base increases from  $5.7 \times 10^{-11}$  to  $3.24 \times 10^{-9} \text{ ohm}^{-1} \text{ cm}^{-1}$  upon doping with 1 M HCl. Its conductivity does not reach the metallic regime. Temperature and frequency dependence of electrical properties were analysed using various formats to elucidate the possible mechanism of electrical conduction. In the base and lightly doped materials conduction is a thermally activated process. In heavily doped materials conduction takes place by a variable-range-hopping mechanism.

## 10.1 INTRODUCTION

The details on the synthesis of substituted polyaniline have appeared only scarcely in the literature. Bingham and Ellis [1] synthesised substituted polyanilines. Shenglong et al. [2] have investigated the polymerization reactions of meta-toluidine, ortho-chloroaniline and ortho-nitro-aniline. Of these, nitro-aniline does not yield a polymer. They characterised poly(meta-toluidine) and poly(chloroaniline) by DSC, X-ray, IR, XPS and room temperature dc conductivity measurements. Snauwaert et al. [3] have observed that partial dechlorination occurs during the synthesis of poly(chloroaniline). In all these cases the results reported are on the as-prepared polymers. No special procedure was employed to remove the oligomeric impurities which are present in the as-prepared material.

Meta-toluidine is aniline with a methyl substituent on the meta-position of the benzene ring. Para-position is free and can participate in a head-to-tail linkage with another molecule as in the case of aniline, thus forming poly(meta-toluidine) (Fig.10.1).

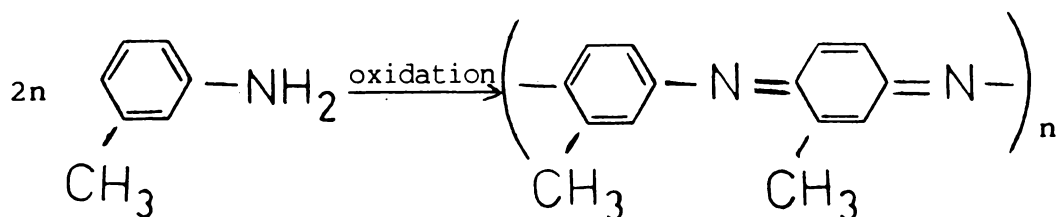


Fig.10.1 Schematic illustration of the formation of poly(meta-toluidine).

The resulting poly(meta-toluidine) base differs from polyaniline only for the methyl group present on the benzene ring. This substituent can lead to a twisting of the planar structure of this quasi-one dimensional molecule, thus modifying its electrical properties.

It is therefore worthwhile to undertake a detailed experimental study of the electrical properties of this material. We have here carried out a systematic investigation of the electrical properties of oligomer free pristine poly(meta-toluidine) base and its HCl-doped forms. The oligomer-containing material has a low melting point and was not further investigated.

## 10.2 EXPERIMENTAL

### 10.2.1 Preparation of poly(m-toluidine)

Meta-toluidine (CDH, Bombay) was purified as described in section 9.2.2. Pure meta-toluidine (0.1 mole, 10.7 g) was dissolved in 500 ml of 2 molar sulphuric acid. The solution was flushed with nitrogen gas and cooled to 5°C. To this solution, 0.1 mole (22.8 g) of ammonium persulphate dissolved in a minimum quantity of water was added with slow stirring. The solution was kept stirred for 4 hrs. The crude material was filtered and washed with water. The crude polymer containing oligomers was dried in an air oven at 80°C. A portion of this product was finely ground and equilibrated with excess of ammonium hydroxide solution to convert it to the base. It was stirred for 2 hrs., filtered and washed with distilled water till the washings were free of ammonia.

### 10.2.2 Removal of oligomers

Poly(m-toluidine) so prepared contained oligomeric impurities soluble in methanol. These were removed by continuous extraction with methanol in a Soxhlet extractor for about 200 hrs. Progress of

extraction was monitored by taking out fresh extract and recording the UV-Visible spectrum. Extraction was continued till the extract did not give any absorption in the visible spectrum.

### 10.2.3 Doping

Finely powdered poly(meta-toluidine) sample (1 g) was shaken with 200 ml of HCl of appropriate concentration for 24 hrs. The material was filtered without the aid of any solvent. pH of the filtrate was determined. The solid was dried at 80°C in an air oven.

### 10.2.4 Preparation of specimen for electrical measurements

About 200 mg of powdered dry poly(m-toluidine) free of oligomers (PT) and doped materials derived from these (PTD) were pressed to circular discs of 12 mm diameter and thickness about 1.3 mm using a hydraulic press at a pressure of 4 tons  $\text{cm}^{-2}$ . Broad faces of the discs were vacuum deposited with silver to provide good electrical contact. The samples were kept in an evacuated desiccator and used for the electrical measurements on the same day.

### 10.2.5 Measurement of electrical properties

dc electrical conductivity as a function of temperature, and ac conductivity and dielectric constant as functions of temperature and frequency were measured as described in section 9.5 of this thesis.

### 10.2.6 Thermal and spectral characterization

Differential scanning calorimetric measurements were made as described in section 9.4. UV-Visible spectra of the solid samples were recorded after mulling with nujol and smearing on a strip of filter paper.

## 10.3 EXPERIMENTAL RESULTS AND DISCUSSION

### 10.3.1 UV-Visible spectrum of the oligomer extract

Extraction of the crude polymer gives a highly coloured solution. As can be seen from Fig.10.2, the complex nature of the spectrum indicates the presence of a variety of compounds in the initial stages. In later stages of extraction, the absorption in the visible range disappears. At this stage it is assumed that the material is free of soluble oligomers.

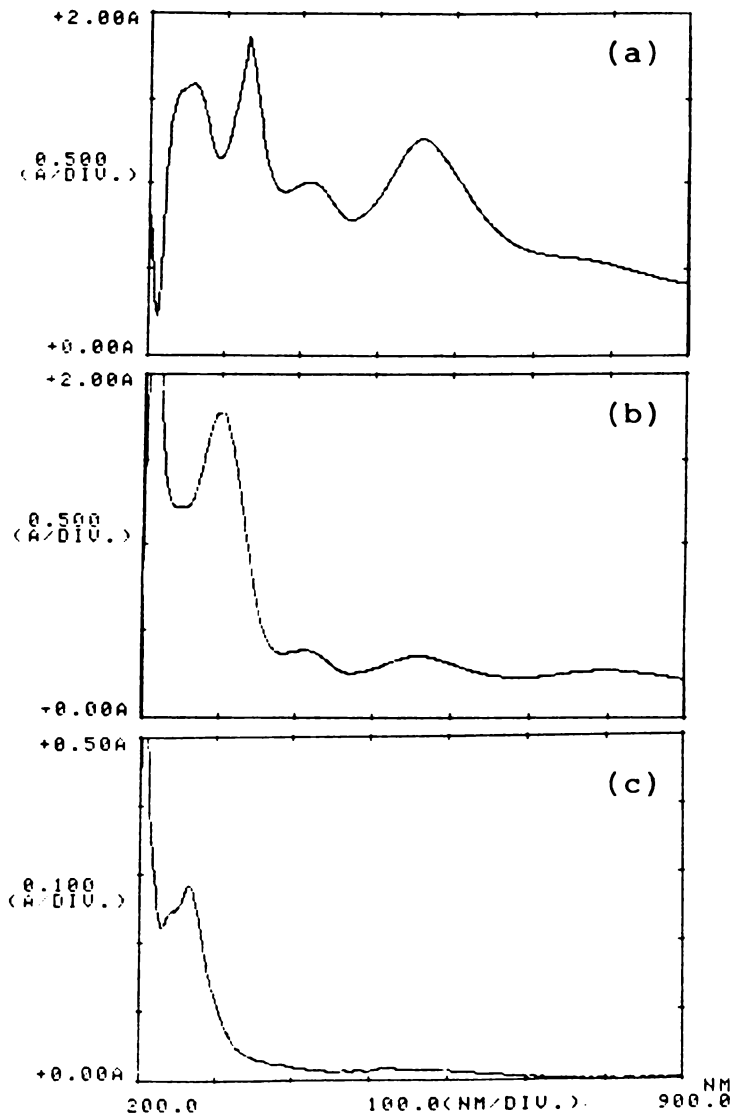


Fig.10.2: UV-Visible spectrum of the methanolic extract of PT (a) after 1 hour of extraction (diluted 10 times) ; (b) after 4 days ; (c) after 7 days.

### 10.3.2 Infrared spectrum

The infrared spectrum of the purified base (PT) gives absorptions at 2970, 2865, 2820, 1480, 1375, 810 and 720  $\text{cm}^{-1}$ . The band at 1375  $\text{cm}^{-1}$  confirms the presence of methyl group in the material. In  $\text{PTD}_4$  (ie., PT base doped in 1 M HCl) a weak band occurs at 1145  $\text{cm}^{-1}$  which is characteristic of protonated polyaniline.

### 10.3.3 Effect of doping

Protonation of polyaniline is known to modify its electronic spectrum. In PT, the effect of doping is very slight as can be seen from Fig.10.3. This is perhaps due to the inability of the polyaniline backbone in PT to get protonated. This is further reflected in the electrical properties.

### 10.3.4 Electrical properties

Poly(meta-toluidine) contains only one type of repeat unit viz., meta-toluidine (Fig.10.1). It is known that substituents present on quasi-one-dimensional molecules forming conjugate double bonds can restrict the long range planarity. For a polymeric conductor it is

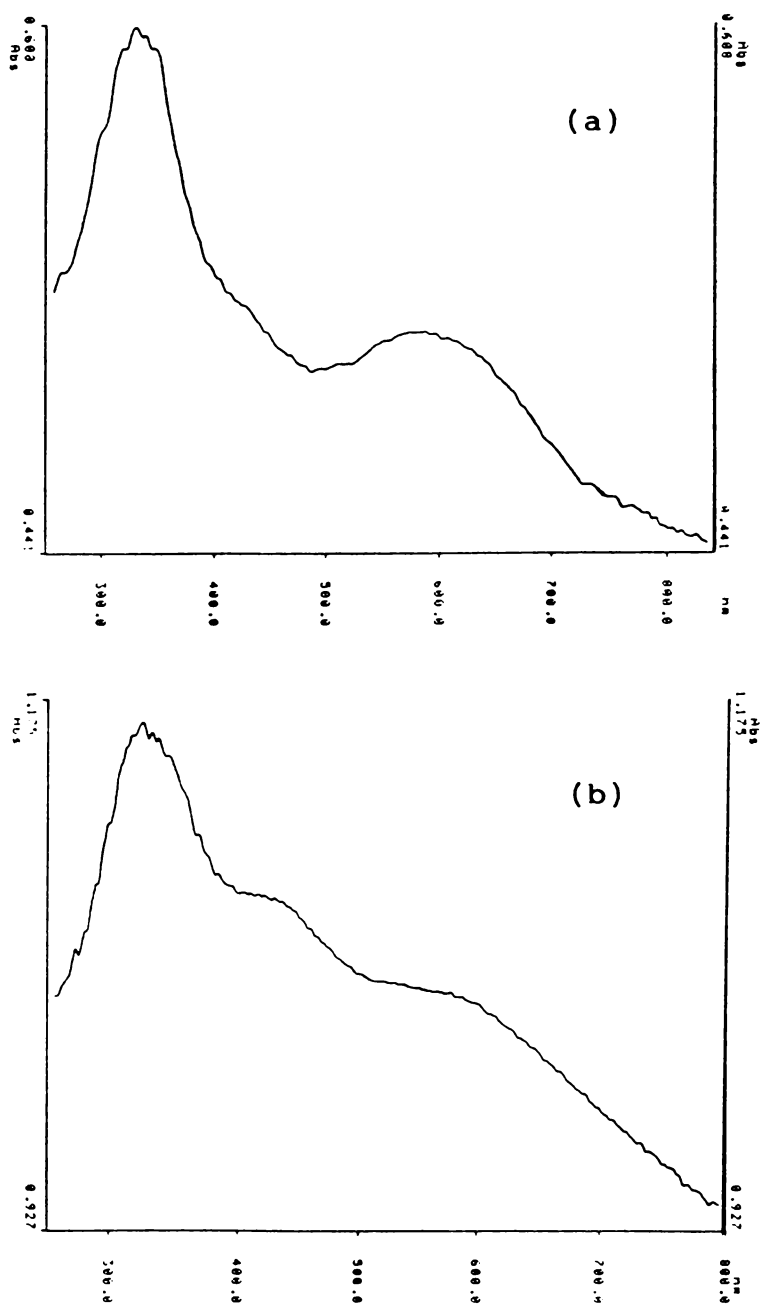


Fig.10.3: Solid state electronic spectrum of PT.  
(a) base ; (b) doped in 1 M HCl

essential that the double bonds are extensively conjugated. The lack of extended conjugation of  $\pi$ -bond might be the reason for the very low conductivity in PT. Even doping in 1 M HCl does not improve its conductivity significantly (Table 10.1) compared to that in polyaniline.

#### 10.3.5 dc conductivity

The dc conductivity of PT shows strong dependence on T. Also its magnitude increases with increasing concentration of the dopant. In order to facilitate the comparison of various models of transport in disordered materials, the available dc conductivity data are presented in different formats.

The Arrhenius plot for the dc conductivity data for pristine PT base and acid doped PT base are presented in Fig.10.4. With increasing protonation the degree of curvature of the plots in the low temperature region increases. For various protonation levels, the slope of the Arrhenius plots i.e., the activation energy in the temperature region 210 to 370 K decreases with increasing degree of protonation. As can be seen from Table 10.1, the activation energy shows only slight variations with increase in the degree of doping.

Table 10.1: Dependence of  $\sigma_{dc}$  data for poly(meta-toluidine) on the equilibrium pH of dopant HCl

Material	Equilibrium pH of HCl dopant solution	$\log \sigma_{ac}$ ( $\text{ohm}^{-1} \text{cm}^{-1}$ ) at 300 K	Activation energy in the temperature range 210-370 K $E_a$ (eV)	$T_o^{**}$ (K)	n
PT	7.00*	-10.24	0.41	--	--
PTD <sub>1</sub>	0.56	-9.58	0.43	--	--
PTD <sub>2</sub>	1.32	-8.93	0.42	$2.90 \times 10^8$	17.70
PTD <sub>3</sub>	2.24	-8.67	0.39	$2.13 \times 10^8$	16.22
PTD <sub>4</sub>	2.87	-8.49	0.38	$2.07 \times 10^8$	16.18

\* distilled water

\*\* see formula (10.1)

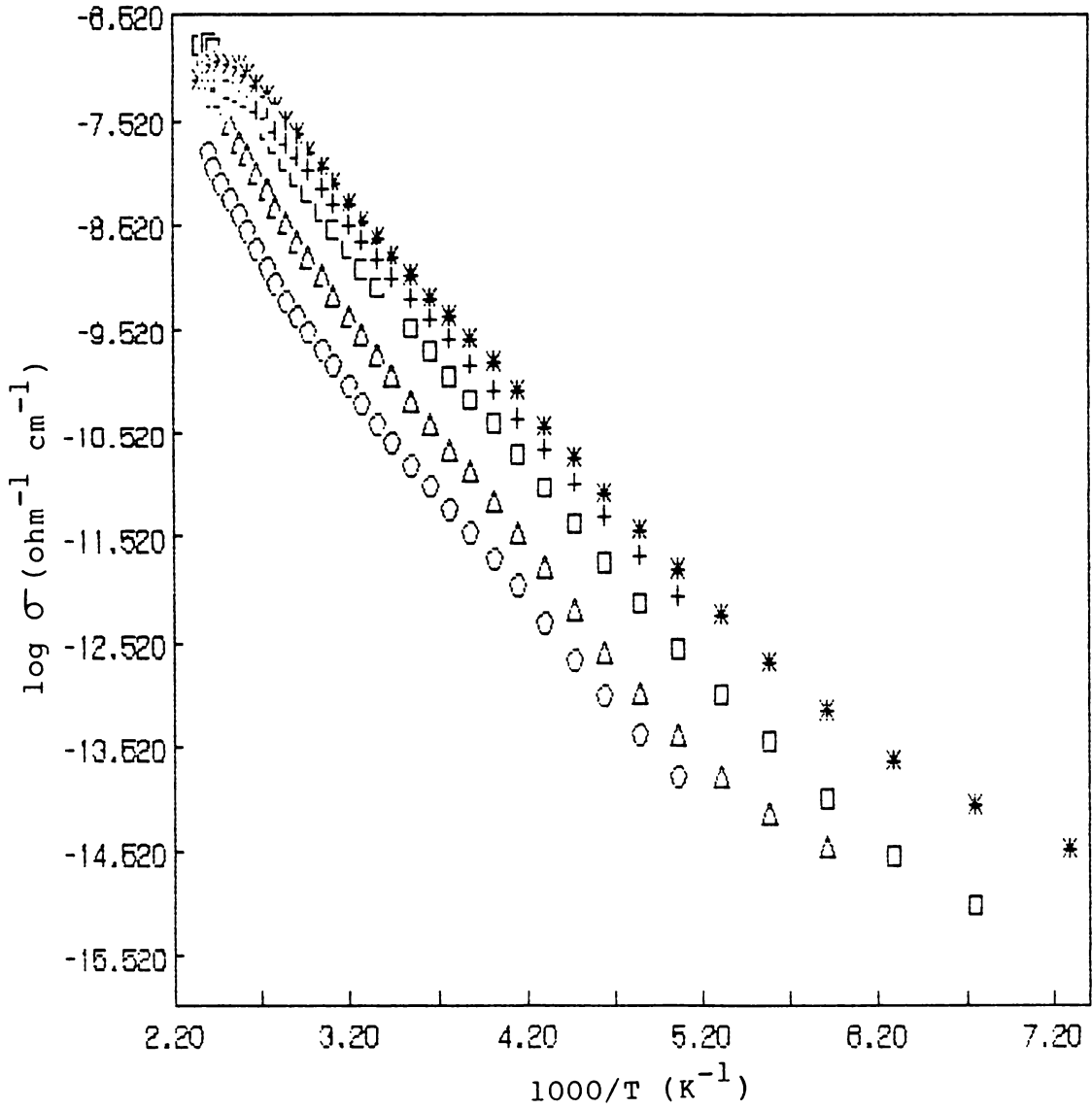


Fig.10.4 Plot of  $\log \sigma_{dc}$  versus  $1000/T$  for poly(meta-toluidine) base and its protonated forms

○ - PT ; △ - PTD<sub>1</sub> ; □ - PTD<sub>2</sub> ; + - PTD<sub>3</sub> ;  
\* - PTD<sub>4</sub>

The dc conductivity data when plotted as  $\log \sigma$  vs  $\log T$  (Fig.10.5) loosely fit into a power law behaviour

$$\sigma_{dc} = AT^n$$

$n$  varies only slightly with the degree of doping.

The plot of  $\log \sigma T^{\frac{1}{2}}$  vs  $T^{-\frac{1}{4}}$  is shown in Fig.10.6. It gives a better linear fit than the  $\log \sigma$  vs  $T^{-1}$  plot. This observation is in agreement with the variable-range-hopping model [4,5] for which  $\sigma_{dc}$  can be written,

$$\sigma_{dc} = 2 \left[ \frac{9 \propto N_0}{8\pi kT} \right]^{\frac{1}{2}} \nu_{ph} \exp[-(T_0/T)^{\frac{1}{4}}] \quad (10.1)$$

where  $T_0 = \frac{16}{kN_0 \propto^3}$

Here  $N_0$  is the density of states at the Fermi level,  $\nu_{ph}$  is the phonon attempt frequency and  $\propto$  is the three-dimensionally averaged characteristic decay length for the localized sites involved in variable-range-hopping. A good fit to this plot is in agreement with a composition dependent  $T_0$  as given in Table 10.1.

The dc conductivity data treated in accordance with the theory for various mechanisms for conduction show

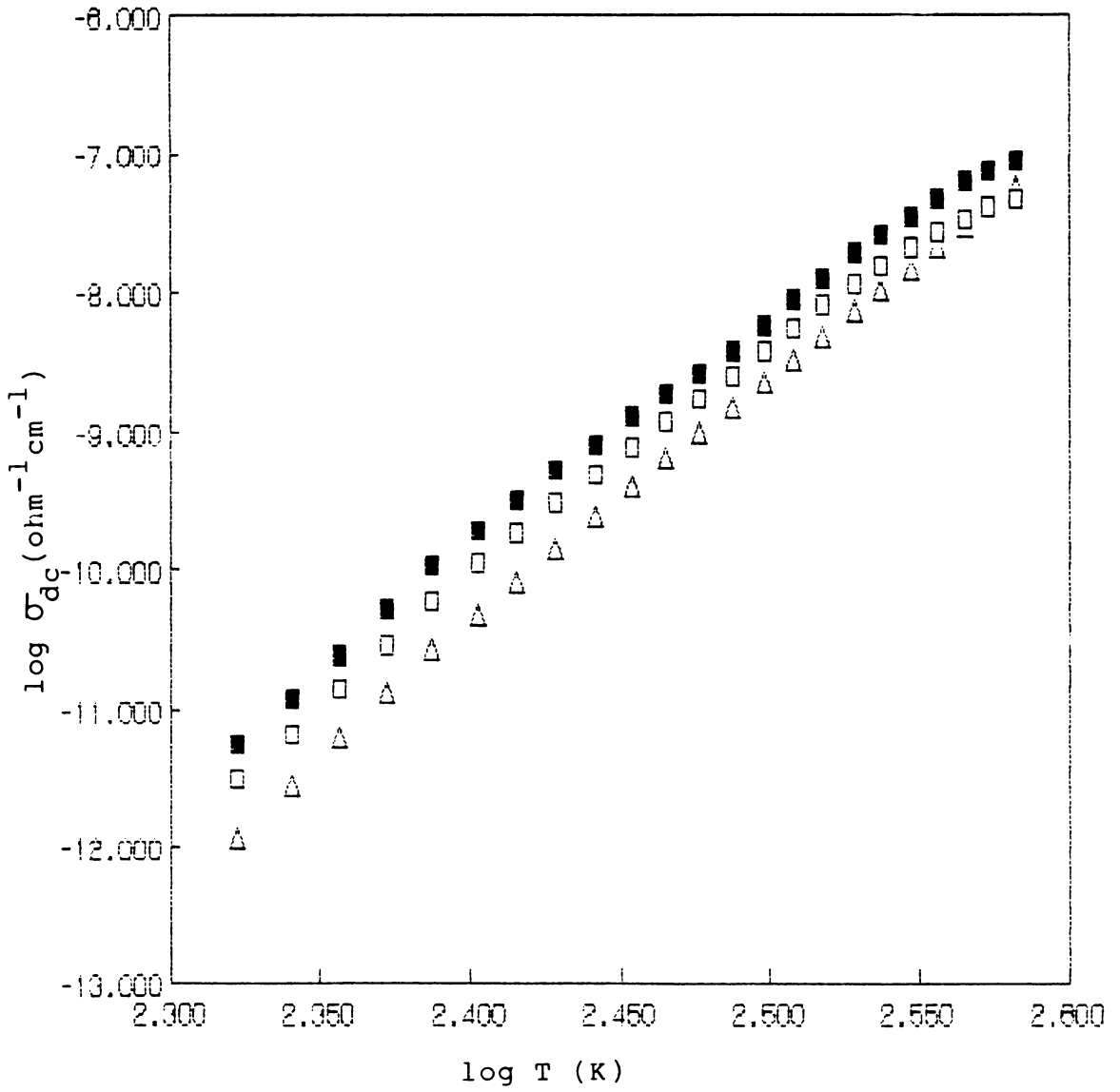


Fig.10.5: Plot of  $\log \sigma_{dc}$  vs.  $\log T$  for PT.

Δ - PTD<sub>2</sub> ; □ - PTD<sub>3</sub> ; ■ - PTD<sub>4</sub>

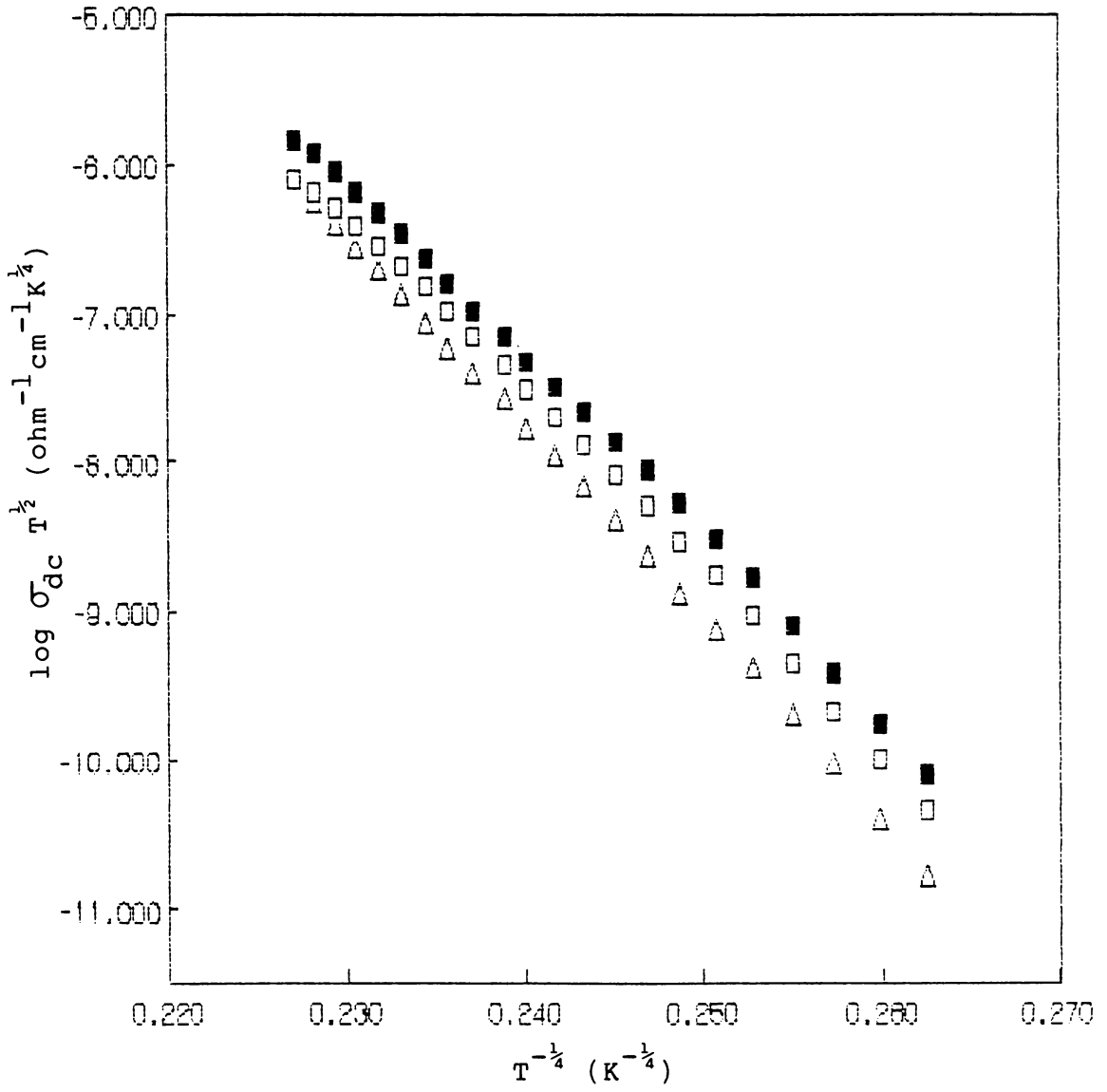


Fig.10.6: Plot of  $\log \sigma_{dc} T^{\frac{1}{2}}$  vs.  $T^{-\frac{1}{4}}$  for PT.

$\Delta$  - PTD<sub>2</sub> ;  $\square$  - PTD<sub>3</sub> ;  $\blacksquare$  - PTD<sub>4</sub>

that the best fit is obtained for a variable-range-hopping model. Though doping enhances conductivity in PT, the increase is much less than that in polyaniline.

### 10.3.6 ac conductivity

The experimental results for ac conductivity of PT base and that doped in 1 M HCl are presented in Fig.10.7 and 10.8. Measurements were made on PT and PT doped with HCl at different concentrations of dopant represented in Table 10.2. However, typical plots for PT and PTD<sub>4</sub> alone are presented in the figures. For all the materials studied the ac conductivity versus frequency plots are linear at very low temperatures. As the temperature rises, the low frequency contribution of ac conductivity increases. Also the conductivity increases with increasing degree of doping. The dependence of ac conductivity on the degree of doping is listed in Table 10.2. At all temperatures the conductivity at higher frequencies varies as,

$$\sigma_{ac} \propto f^s \quad (10.2)$$

where  $s \sim 0.42$ .

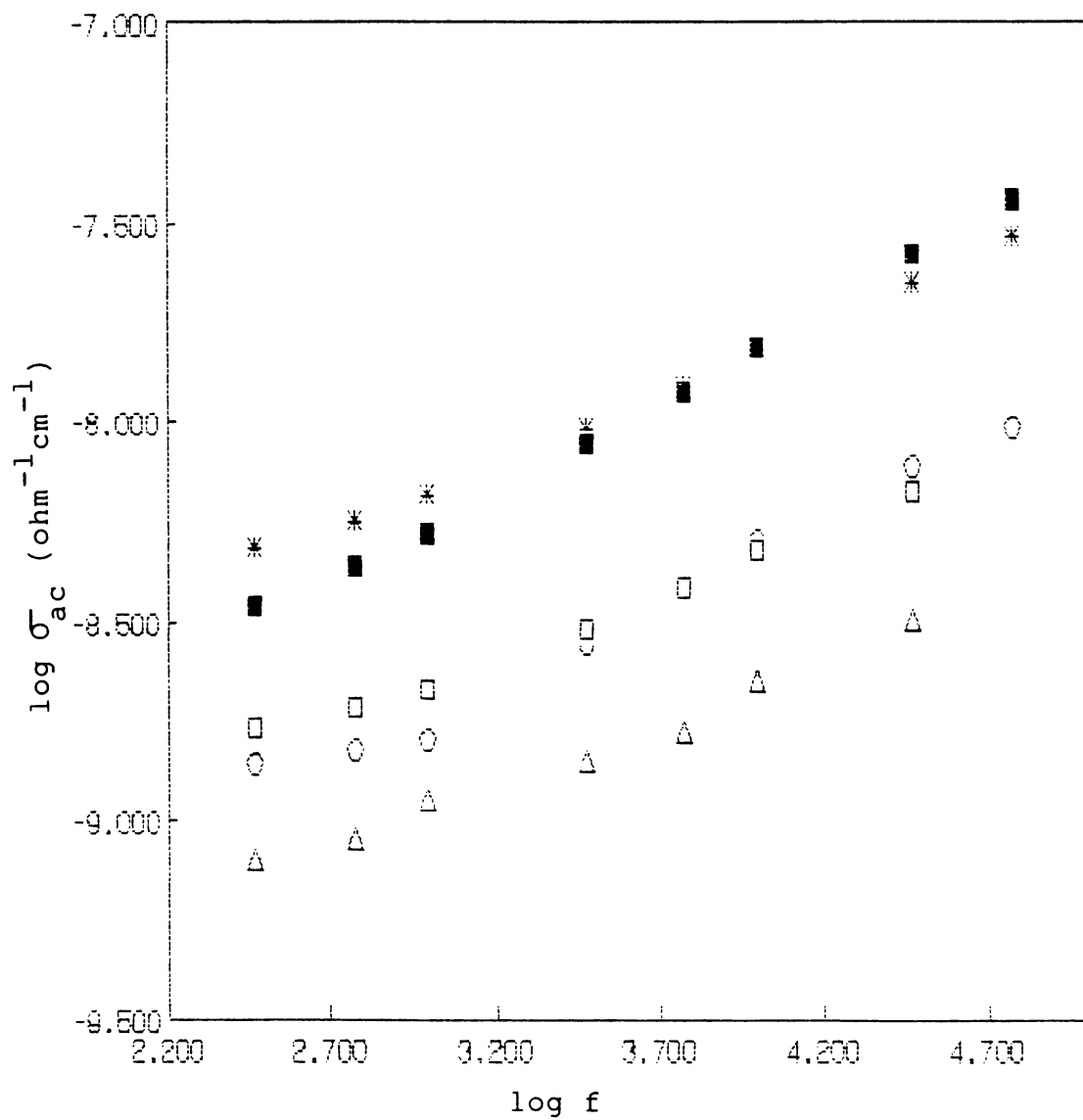


Fig.10.7: Plot of  $\log \sigma_{ac}$  ( $\text{ohm}^{-1}\text{cm}^{-1}$ ) vs.  $\log f$  for PT

$\Delta$  - 230 K ;     $\circ$  - 260 K ;     $\square$  - 290 K  
 $\blacksquare$  - 320 K ;     $*$  - 350 K

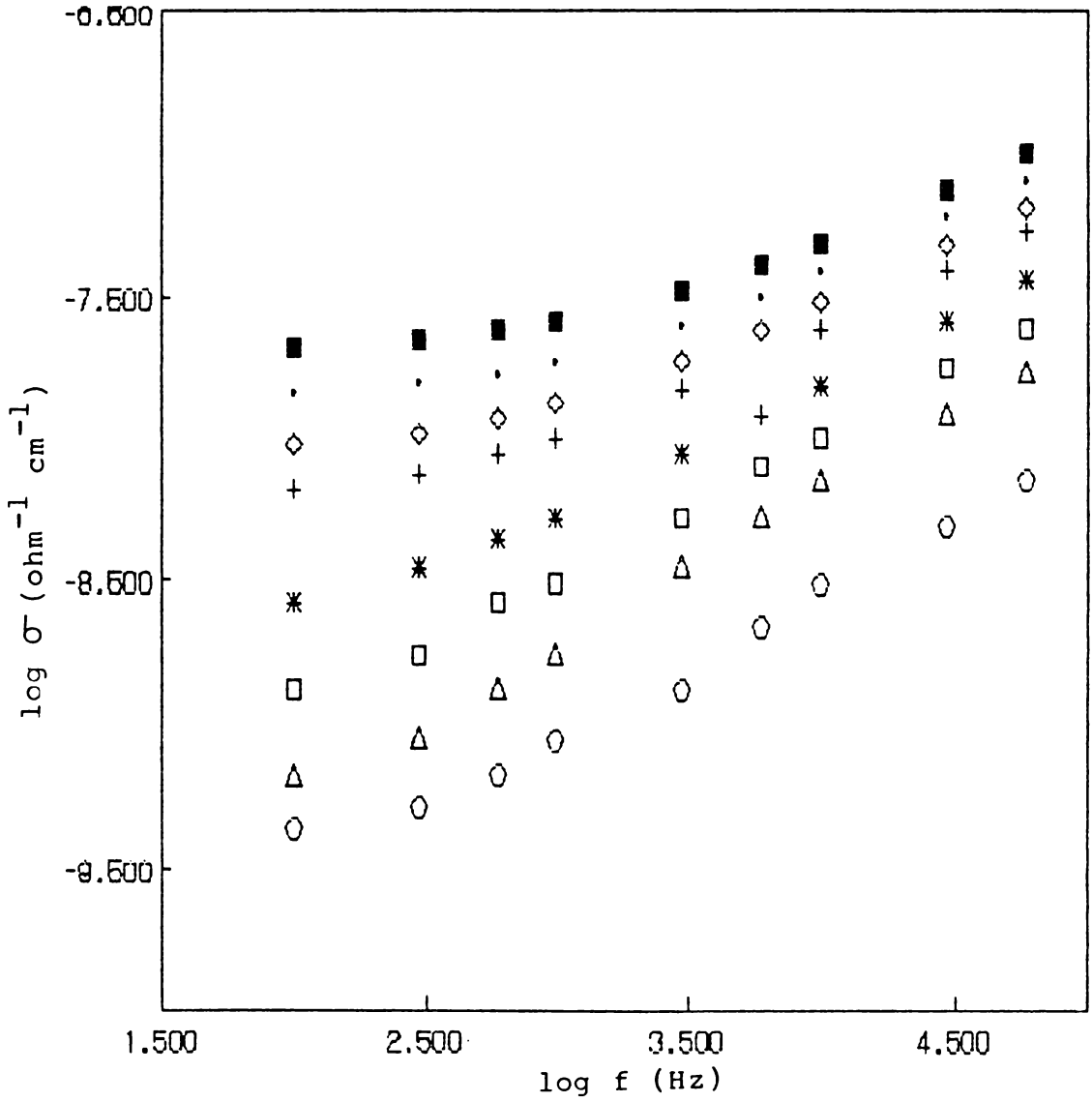


Fig.10.8: Plot of  $\log \sigma_{ac}$  vs.  $\log f$  for  $\text{PTD}_4$ .

○ - 140 K ; △ - 170 K ; □ - 200 K ;  
 \* - 230 K ; + - 260 K ; ◇ - 290 K ;  
 • - 320 K ; ■ - 350 K

Table 10.2: Dependence of ac conductivity and dielectric constant of poly(meta-toluidine) on the equilibrium concentration of dopant HCl.

Material	Equilibrium pH of doping solution	$\log[\sigma (\text{ohm}^{-1}\text{cm}^{-1})]$ (300 K, 1kHz)	(300 K, 1 kHz)
PT	7.0*	-8.85	6.87
PTD <sub>1</sub>	0.56	-8.79	6.93
PTD <sub>2</sub>	1.32	-8.66	7.08
PTD <sub>3</sub>	2.24	-8.28	11.85
PTD <sub>4</sub>	2.87	-8.12	12.85

\* distilled water

### 10.3.7 Dielectric constant

Fig.10.9 and 10.10 show the variation of dielectric constants of pristine and doped PT as a function of frequency at different temperatures. The dielectric constant of doped PT, (PTD<sub>4</sub>, Fig.10.10), has a higher value than the pristine base (Table 10.2). In all these materials, the dielectric constant is almost frequency independent at low temperatures. At low frequencies there is an increasing temperature contribution to the dielectric constant.

### 10.3. 8 Differential scanning calorimetry

DSC thermograms of the samples presented in Fig.10.11 show a broad hump which starts at about 50°C and levels off around 120°C. Thereafter they show a plateau up to 240°C. This is followed by a continuous endothermic process probably due to conformational rearrangement of the chain or due to decomposition. The endothermic process between 50 and 120°C is due to the loss of adsorbed moisture [6,7]. The electrical data presented above were measured after annealing the sample at 80°C in a dynamic vacuum for 30 min. This explains the absence of any spurious conductivity or dielectric variation due to adsorbed moisture in the results given above.

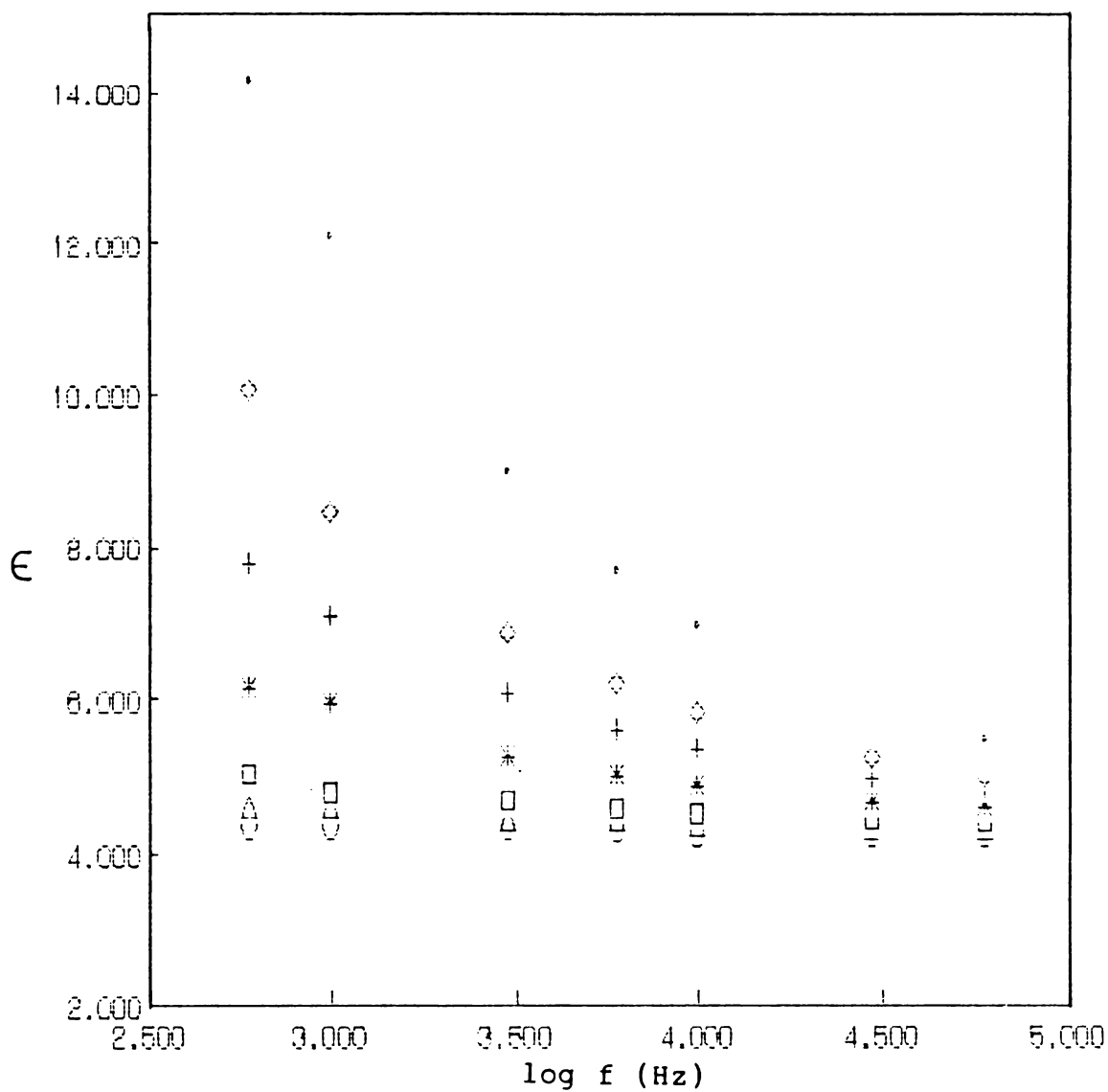


Fig.10.9: Plot of dielectric constant vs. log f for PT.

○ - 170 K ; △ - 200 K ; □ - 230 K ; \* - 260 K  
 + - 290 K ; ◇ - 320 K ; • - 350 K

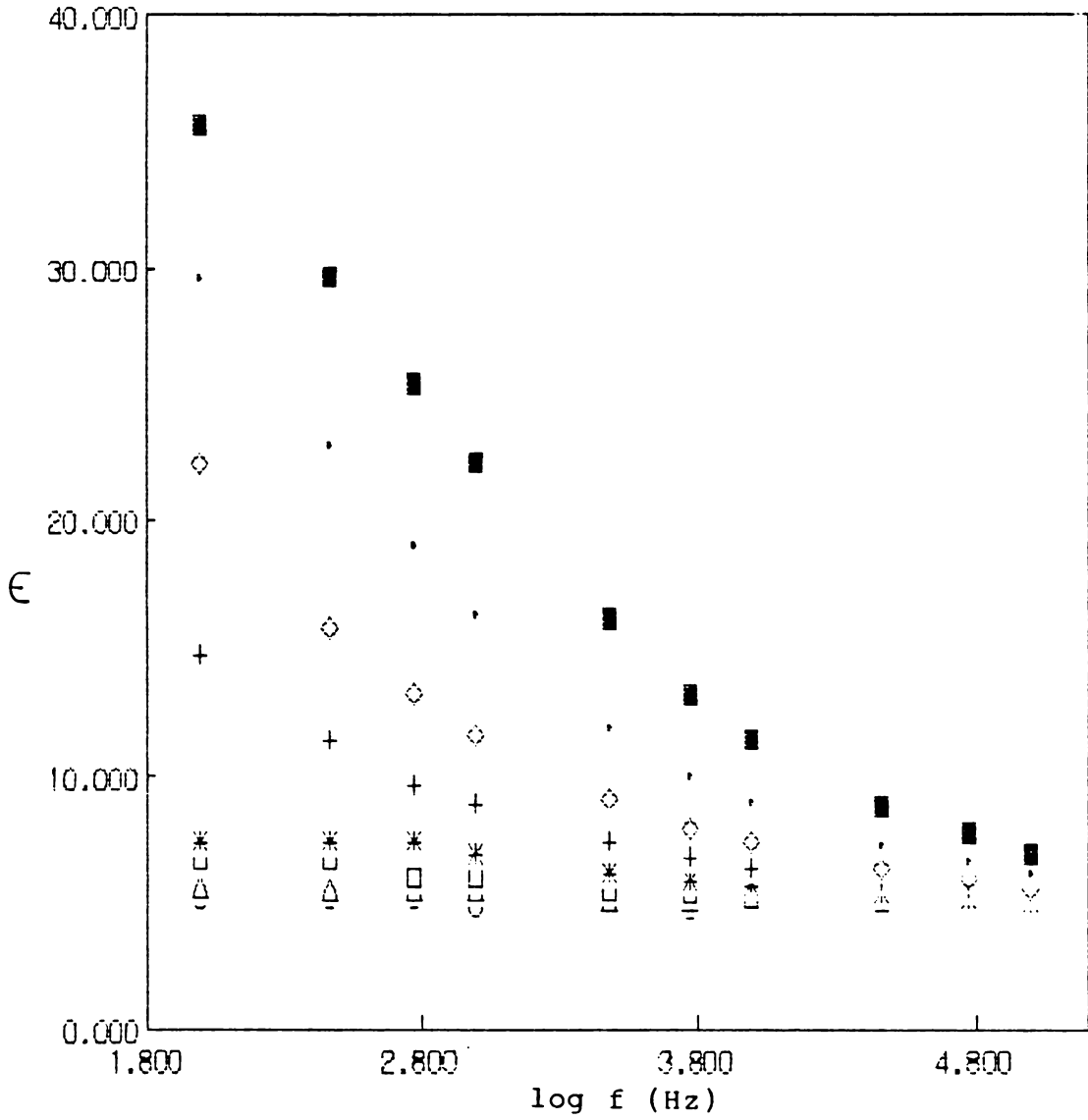


Fig.10.10: Plot of dielectric constant vs.  $\log f$  for  $\text{PTD}_4$

○ - 140 K ; △ - 170 K ; □ - 200 K ; \* - 230 K  
 + - 260 K ; ◇ - 290 K ; • - 320 K ; ■ - 350 K

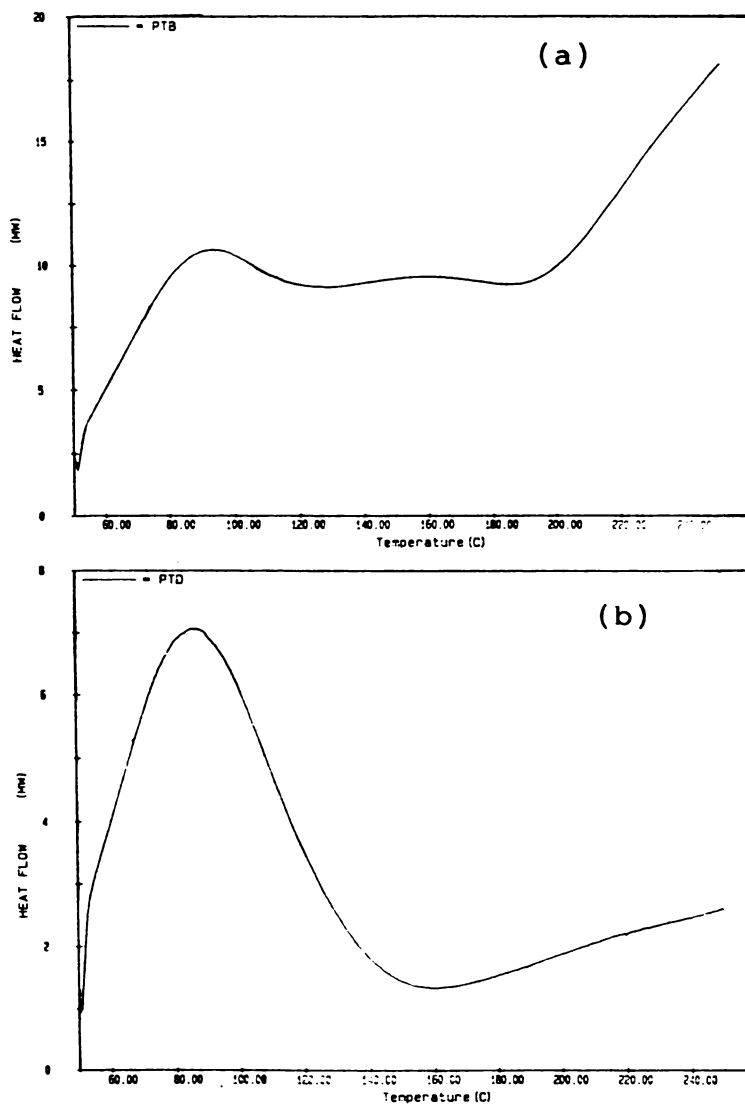


Fig.10.11: DSC thermograms for (a) PT ; (b)  $PTD_4$

#### 10.4 REFERENCES

- [1] A.Bingham and B.Ellis, *J. Polym. Sci.* (1969) 3229.
  
- [2] W.Shenglong, W.Fosong and G.Xiaohui, *Synth. Met.* (1986) 99.
  
- [3] P.Snauwaert, R.Lazzaroni, J.Riga and J.J.Verbist, *Synth. Met.* (1986) 245.
  
- [4] N.F.Mott and E.A.Davis, *Electronic Processes in Non-Crystalline Materials* (Clarendon, Oxford, 1979).
  
- [5] P.Nagles, in *Amorphous Semiconductors*, Vol.36 of *Topics in Applied Physics*, edited by M.H.Brodsky (Springer-Verlag, Berlin, 1979).
  
- [6] K.L.Tan, B.T.G.Tan, S.H.Khor, K.G.Neoh and E.T.Kang, *J. Phys. Chem. Solids* (1991) 673.
  
- [7] K.G.Neoh, E.T.Kang, S.H.Khor and K.L.Tan, *Polym. Degrad. Stab* (1990) 107.

## Chapter 11

### ELECTRICAL PROPERTIES OF POLY(ANILINE CO-META-TOLUIDINE)

#### Abstract

Poly(aniline co-meta-toluidine) was prepared using different mole ratios of aniline to meta-toluidine. ac and dc electrical conductivities and dielectric constant were measured for the as-prepared material, which contains oligomers, as well as for oligomer-free samples. Studies were also conducted with these materials doped to different levels with protonic acid. The oligomer-containing material shows higher conductivity as well as dielectric constant. Doping enhances conductivity and dielectric constant in all the materials. Dependence of conductivity as well as frequency was studied in detail and analysis was made using different mechanistic formats. The activation parameters thus derived indicate that conduction is a thermally activated process in pristine base and lightly doped materials. In heavily doped materials a variable-range-hopping mechanism applicable to disordered semiconductors is prevalent. However, the substitutional effect exerted by the meta-toluidine repeat units inhibits conductivity and in spite of heavy doping, it never reaches the metallic conductivity shown by polyaniline.

## 11.1 INTRODUCTION

The work presented in the preceding chapter reveals some interesting differences in the properties of poly(meta-toluidine) from polyaniline. The most striking difference is with regard to electrical properties, especially the electrical conductivity. Conductivity of polyaniline can be raised to metallic regime by simple proton doping, whereas poly(meta-toluidine), which is nothing but polyaniline with a methyl substituent on each repeat unit, attains only a conductivity about six orders of magnitude less. This points to the interesting results that may be anticipated if one investigates the electrical properties of copolymers of aniline with meta-toluidine in different mole ratios of the monomers.

The chemical structure and electrical characteristics of polyaniline prepared under various conditions have been exhaustively studied [1-26]. However, studies directed to reveal the influence of substituents on the properties of polyaniline have been scarce [27-28].

The copolymers of aniline with 2-chloroaniline and 2-iodoaniline have been reported by Neoh et al. [28]. The composition of the copolymers could be effectively

controlled by varying the monomer feed ratio. These studies were essentially confined to a simple measurement of dc electrical conductivity along with investigations on the structural elucidation by IR and X-ray photoelectron spectroscopy.

This chapter summarises the experimental methods employed in the synthesis of poly(aniline co-meta-toluidine), its purification, doping technique and physicochemical and electrical characterisation of the resulting materials. The conduction mechanism in samples treated by different techniques are also discussed.

## 11.2 EXPERIMENTAL

### 11.2.1 Preparation of poly(aniline co-meta-toluidine)

Aniline and meta-toluidine were purified as described in section 9.2. Copolymers were prepared by taking the monomer in the feed ratios shown in Table 11.1.

Aniline and meta-toluidine were taken in appropriate mole ratios and dissolved in 800 ml of 2 molar  $H_2SO_4$ . The solution was cooled to 5°C. Ammonium persulphate dissolved in a minimum quantity of water was

slowly added to the amine solution with stirring. Stirring was continued for 2 hrs. The precipitate was filtered and washed with water and dried at 80°C.

Poly(aniline co-meta-toluidine) base (PAT) was prepared by stirring finely powdered salts with excess of ammonia. The base so obtained was thoroughly washed with distilled water till all traces of sulphate were removed and the washings were free of ammonia. The base was dried at 80°C in an air oven.

#### 11.2.2 Removal of oligomers

PAT prepared as described in the above section contained a fraction which readily dissolved in methanol. Removal of the soluble fraction, which is probably the oligomer, was rather slow in the latter stages of extraction. Hence the samples were continuously extracted for about 200 hrs. in a Soxhlet extractor using methanol. Portions of nascent extract were withdrawn and the UV-visible spectrum was recorded. The extraction of oligomer was assumed to be complete when the spectrum of the extract did not show any peak in the visible region.

### 11.2.3 Doping

Finely powdered sample (1 g) was shaken with 100 ml hydrochloric acid of appropriate strength for 24 hrs. The solid was filtered off without the aid of solvent. The pH of the filtrate was also noted (Table 11.1).

### 11.2.4 Measurement of electrical properties

The electrical properties of the samples were measured on compacted pellets. Silver electrodes were vacuum deposited on the broad faces to provide good electrical contact. dc conductivity as a function of temperature and ac conductivity and dielectric constant as a function of frequency as well as temperature were measured as described in section 9.5.4.

### 11.2.5 Differential scanning calorimetry

DSC traces were recorded using a Perkin Elmer DSC instrument in flowing nitrogen atmosphere. Details are presented in section 2.5.

Table 11.1: Reagent feed ratio employed in the preparation of poly(aniline co-meta-toluidine)

Material	Aniline- m-toluidine mole ratio	Weight of aniline (g)	Weight of m-toluidine (g)	Weight of (NH <sub>4</sub> ) <sub>2</sub> S <sub>2</sub> O <sub>8</sub> (g)
PAT <sub>1</sub>	2 : 1	12.4	7.1	45.6
PAT <sub>2</sub>	1 : 1	9.3	10.7	45.6
PAT <sub>3</sub>	1 : 2	6.2	14.3	45.6

### 11.3 EXPERIMENTAL RESULTS AND DISCUSSION

#### 11.3.1 Removal of oligomer

It is observed that chemically prepared copolymers contain a considerable proportion of methanol soluble fraction [29-31]. This fraction is insoluble in aqueous mineral acids and bases. Extraction of PAT with methanol gives a blue-violet solution. The absorption spectrum of the initial extract has an absorption maximum at 542 nm (Fig.11.1). This absorption maximum changes gradually as extraction proceeds. Such a shift in the absorption maximum in a conjugated  $\pi$ -system is characteristic of increasing extent of conjugation. In the present case the shift in the absorption maximum of the extract as extraction proceeds may be due to the increasing proportion of higher molecular weight fraction in the extract.

#### 11.3.2 Influence of oligomer

The influence of low molecular weight oligomer fraction on the electrical properties of high molecular weight polymers is likely to be pronounced. The relaxation phenomena associated with conformational reorganisation of long chain molecules are reflected in the temperature

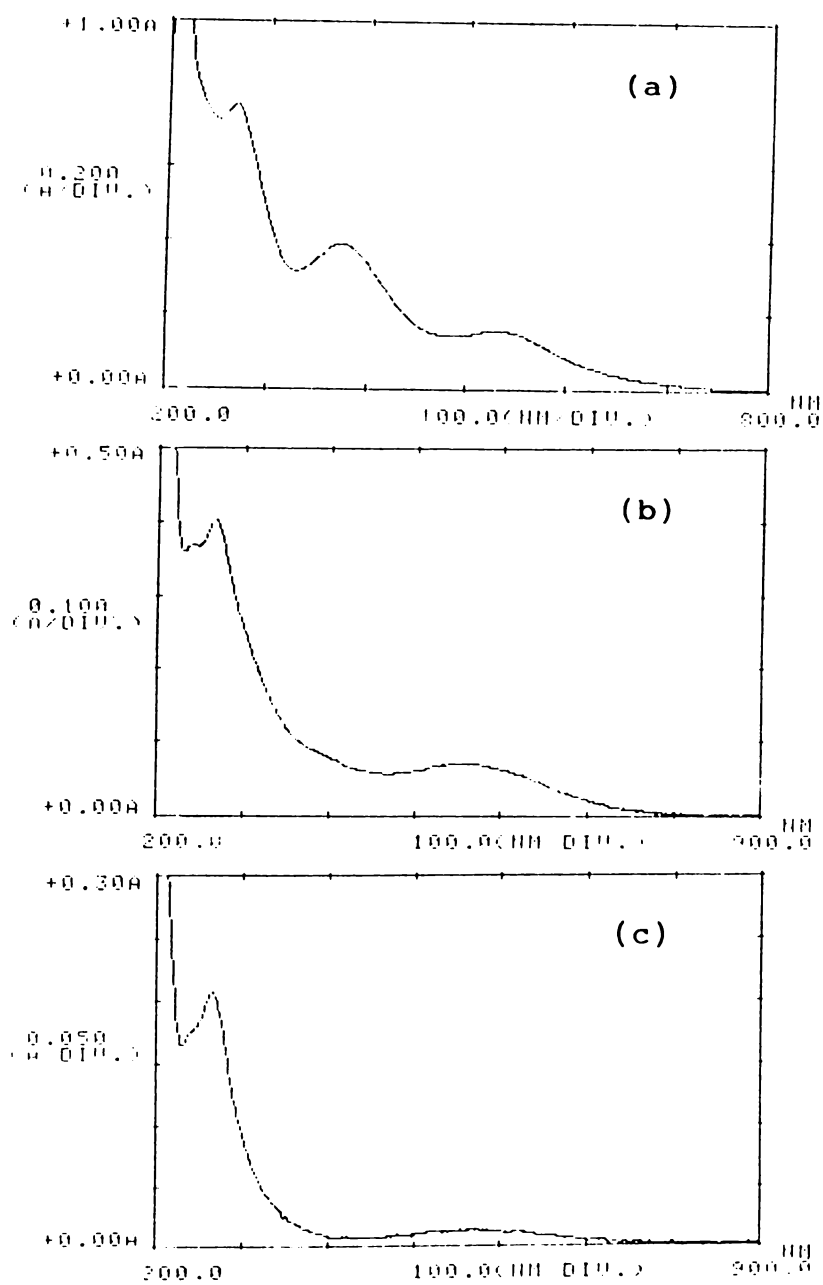


Fig.11.1: UV-Visible spectrum of the methanolic extract from  $PAT_2$ . (a) after one hour (diluted 50 times); (b) after four days (c) after seven days.

and frequency dependence of ac conductivity and dielectric constant [19(b)]. It has been conclusively shown [29-31] that low molecular weight species are present in polyaniline prepared under various conditions. Yet majority of the studies have not considered the influence of oligomers. In this study it is observed that the as-obtained co-polymers contain methanol soluble material which is probably the oligomer.

The marked influence of oligomer on the electrical properties can be assessed from the data given in Tables 11.2 and 11.3. The presence of oligomer imparts a higher conductivity and dielectric constant to all the materials studied.

### 11.3.3 Nature of the copolymer

The incorporation of meta-toluidine units in the polymer is conclusively evidenced by the appearance of an infrared absorption band at  $1370\text{ cm}^{-1}$  due to a substituent methyl group. Other characteristic peaks of the polyaniline system i.e., those at 1580, 1490, 1380, 1330, 880 and  $810\text{ cm}^{-1}$  also appear in the spectrum [28]. The weak band appearing at  $1140\text{ cm}^{-1}$  is characteristic of the HCl doped material [32].

Table 11.2.1: dc conductivity data for poly(aniline co-meta-toluidine (PAT<sub>1</sub>))

Material**	Equilibrium pH of dopant HCl solution	$\log \sigma_{dc}^{-1}$ (ohm <sup>-1</sup> cm <sup>-1</sup> ) at 300 K	Activation energy in the temper- ature range 280-360 K (eV)
PAT <sub>1</sub>	7.00*	-12.03	0.61
PAT <sub>1</sub> D <sub>1</sub>	3.26	-10.90	0.58
PAT <sub>1</sub> D <sub>2</sub>	2.10	-9.75	0.52
PAT <sub>1</sub> D <sub>3</sub>	1.13	-7.34	0.35
PAT <sub>1</sub> D <sub>4</sub>	0.41	-6.84	0.31
PAT <sub>1</sub> O	7.00	-11.49	0.53
PAT <sub>1</sub> OD <sub>4</sub>	0.45	-4.82	0.26

\* distilled water

\*\* Legend: PAT<sub>1</sub> - aniline to m-toluidine feed ratio 2:1  
D - dopant level  
O - oligomer-containing

Table 11.2.2: dc conductivity data for poly(aniline co-meta-toluidine) (PAT<sub>2</sub>)

Material** dopant solution	Equilibrium pH of HCl	$\log \sigma_{dc}^{-1} \text{ cm}^{-1}$ at 300 K	Activation energy in the temperature range 210-370 K $E_a$ (eV)	$T_o$ (K)	n
PAT <sub>2</sub>	7.00*	-12.96	0.67	--	--
PAT <sub>2</sub> D <sub>1</sub>	3.02	-12.84	0.62	--	--
PAT <sub>2</sub> D <sub>2</sub>	2.00	-12.01	0.60	$6.86 \times 10^8$	22.24
PAT <sub>2</sub> D <sub>3</sub>	1.14	-9.07	0.48	$3.06 \times 10^8$	18.07
PAT <sub>2</sub> D <sub>4</sub>	0.28	-7.25	0.36	$1.13 \times 10^8$	13.96
PAT <sub>2</sub> O	7.00*	-10.40	0.53	$3.85 \times 10^7$	21.50
PAT <sub>2</sub> OD <sub>4</sub>	0.39	-5.04	0.26	$6.02 \times 10^8$	10.56

\* distilled water

\*\* Legend: PAT<sub>2</sub> - aniline to meta-toluidine ratio 1:1

D - dopant level

O - oligomer-containing

Table 11.2.3: dc conductivity data for poly(aniline  
co-meta-toluidine (PAT<sub>3</sub>))

Material**	Equilibrium pH of dopant HCl solution	$\log \sigma_{dc}$ (ohm <sup>-1</sup> cm <sup>-1</sup> ) at 300 K	Activation energy in the temper- ature range 280-360 K (eV)
PAT <sub>3</sub>	7.00*	-13.60	0.59
PAT <sub>3</sub> D <sub>1</sub>	2.73	-13.36	0.58
PAT <sub>3</sub> D <sub>2</sub>	1.59	-12.88	0.59
PAT <sub>3</sub> D <sub>3</sub>	1.01	-11.74	0.58
PAT <sub>3</sub> D <sub>4</sub>	0.36	-11.10	0.58
PAT <sub>3</sub> O	7.00*	-10.79	0.50
PAT <sub>3</sub> OD <sub>4</sub>	0.42	-5.85	0.26

\* distilled water

\*\* Legend: PAT<sub>3</sub> - aniline to meta-toluidine feed ratio 1:2  
D - dopant level  
O - oligomer-containing

Table 11.3.1: ac conductivity and dielectric constant data for poly(aniline co-meta-toluidine) (PAT<sub>1</sub>)

Material**	Equilibrium pH of dopant HCl solution	$\log \sigma_{ac}$ (ohm <sup>-1</sup> cm <sup>-1</sup> ) 1 kHz, 300 K	Dielectric constant (1 kHz, 300 K)
PAT <sub>1</sub>	7.00*	-9.33	3.64
PAT <sub>1</sub> D <sub>1</sub>	3.02	-9.26	3.84
PAT <sub>1</sub> D <sub>2</sub>	2.00	-9.17	3.93
PAT <sub>1</sub> D <sub>3</sub>	1.14	-6.74	40.42
PAT <sub>1</sub> D <sub>4</sub>	0.28	-6.75	40.42
PAT <sub>1</sub> O	7.00*	-9.28	5.26
PAT <sub>1</sub> OD <sub>4</sub>	0.39	-4.96	3745.0

\* distilled water

\*\* Legend: PAT<sub>1</sub> - aniline to meta-toluidine feed ratio 2:1  
D - dopant level  
O - oligomer-containing

Table 11.3.2: ac conductivity and dielectric constant data  
for poly(aniline co-meta-toluidine) (PAT<sub>2</sub>)

Material**	Equilibrium pH of dopant HCl solution	$\log \sigma_{ac}$ (ohm <sup>-1</sup> cm <sup>-1</sup> ) (1 kHz, 300 K)	Dielectric constant (1 kHz, 300 K)
PAT <sub>2</sub>	7.00*	< -9.50	4.72
PAT <sub>2</sub> D <sub>1</sub>	3.26	< -9.50	4.81
PAT <sub>2</sub> D <sub>2</sub>	2.10	< -9.50	4.88
PAT <sub>2</sub> D <sub>3</sub>	1.13	-7.38	22.08
PAT <sub>2</sub> D <sub>4</sub>	0.41	-2.21	22.51
PAT <sub>2</sub> O	7.00*	-9.59	4.78
PAT <sub>2</sub> OD <sub>4</sub>	0.45	-4.68	1939.45

\* distilled water

\*\* Legend: PAT<sub>2</sub> - aniline to meta-toluidine feed ratio 1:1  
D - dopant level  
O - oligomer-containing

Table 11.3.3: ac conductivity and dielectric constant data  
for poly(aniline co-meta-toluidine) (PAT<sub>3</sub>)

Material**	Equilibrium pH of dopant HCl solution	$\log \sigma_{ac}$ (ohm <sup>-1</sup> cm <sup>-1</sup> ) (1 kHz, 300 K)	Dielectric constant (1 kHz, 300 K)
PAT <sub>3</sub>	7.00*	< -9.50	4.29
PAT <sub>3</sub> D <sub>1</sub>	2,73	< -9.50	4.42
PAT <sub>3</sub> D <sub>2</sub>	1.59	< -9.50	4.63
PAT <sub>3</sub> D <sub>3</sub>	1.01	< -9.50	5.14
PAT <sub>3</sub> D <sub>4</sub>	0.36	< -9.50	6.01
PAT <sub>3</sub> O	7.00*	-8.61	7.01
PAT <sub>3</sub> OD <sub>4</sub>	0.42	-5.58	134.00

\* distilled water

\*\* Legend: PAT<sub>3</sub> - aniline to meta-toluidine feed ratio 1 : 2  
D - dopant level  
O - oligomer-containing

#### 11.3.4 Solid state electronic spectrum

In the case of heavily doped copolymers it is seen that the electronic spectra differ slightly from those of the base material (Fig.11.2). However, such changes are not so pronounced as with polyaniline [33].

#### 11.3.5 dc conductivity

The copolymers prepared from different monomer ratios of aniline and meta-toluidine and their doped forms show that dc conductivity increases with increasing proportion of aniline in the copolymer. Also dc conductivity rises with decreasing equilibrium pH of dopant HCl (ie., increasing acid concentration) as can be seen from Table 11.2. The Arrhenius plots of dc conductivity for various dopant levels, assuming that the incorporation of dopant is proportional to the equilibrium concentration of dopant in solution, are presented in Fig.11.3, 11.4 and 11.5. For the pristine base as well as for the lightly doped forms, the Arrhenius plots give straight lines. This indicates that a single activation process is responsible for conductivity in these materials for the whole temperature range. At very low temperatures the base and lightly doped materials are highly insulating and

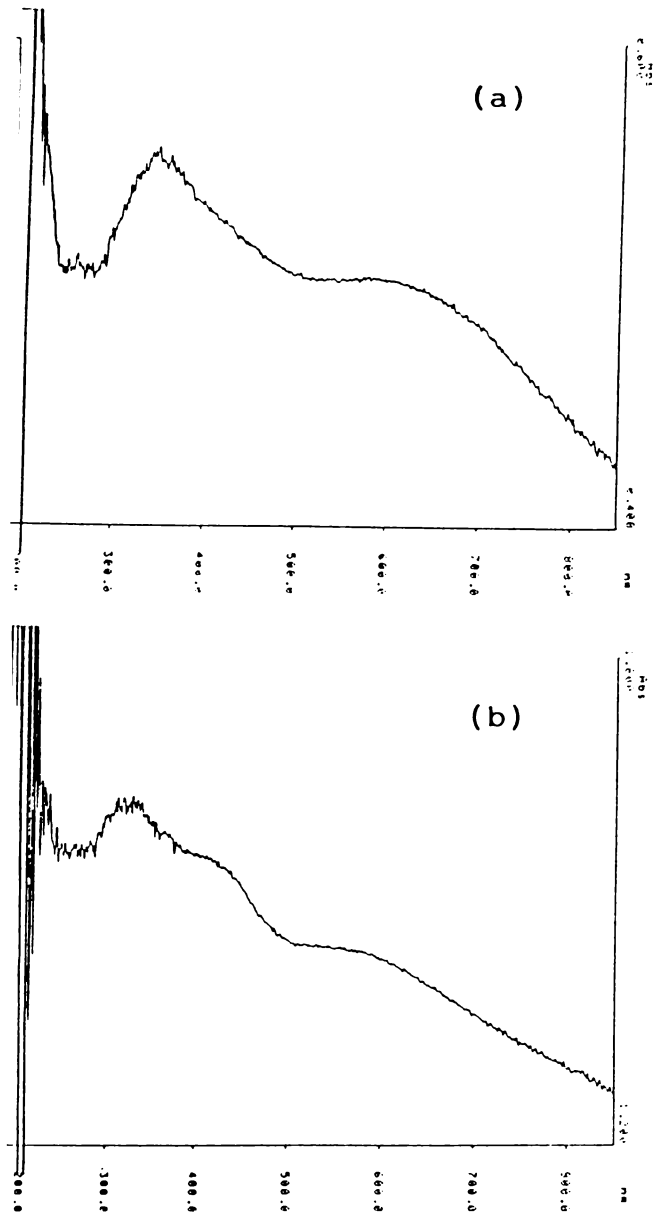


Fig.11.2.1: Effect of doping on the solid state electronic spectrum of PAT<sub>1</sub>.  
(a) PAT<sub>1</sub> base ; (b) PAT<sub>1</sub>D<sub>4</sub> (doped in 1 M HCl).

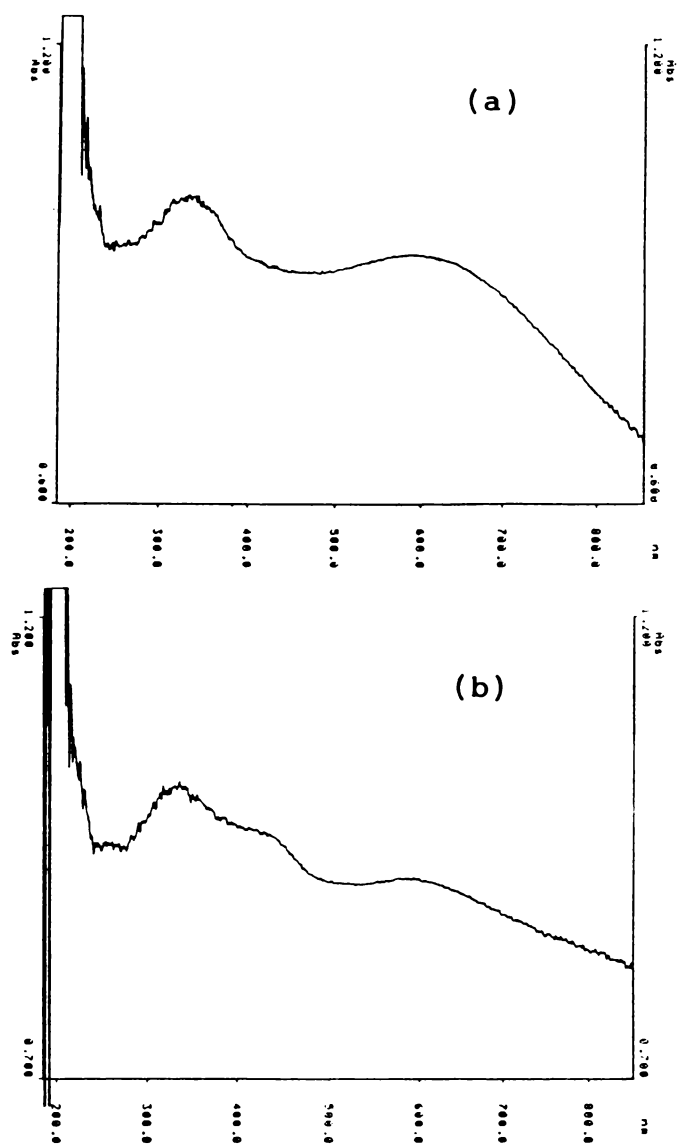


Fig.11.2.2: Effect of doping on the solid state electronic spectrum of  $\text{PAT}_2$ .  
(a)  $\text{PAT}_2$  base ; (b)  $\text{PAT}_2\text{D}_4$  (doped in 1 M HCl)

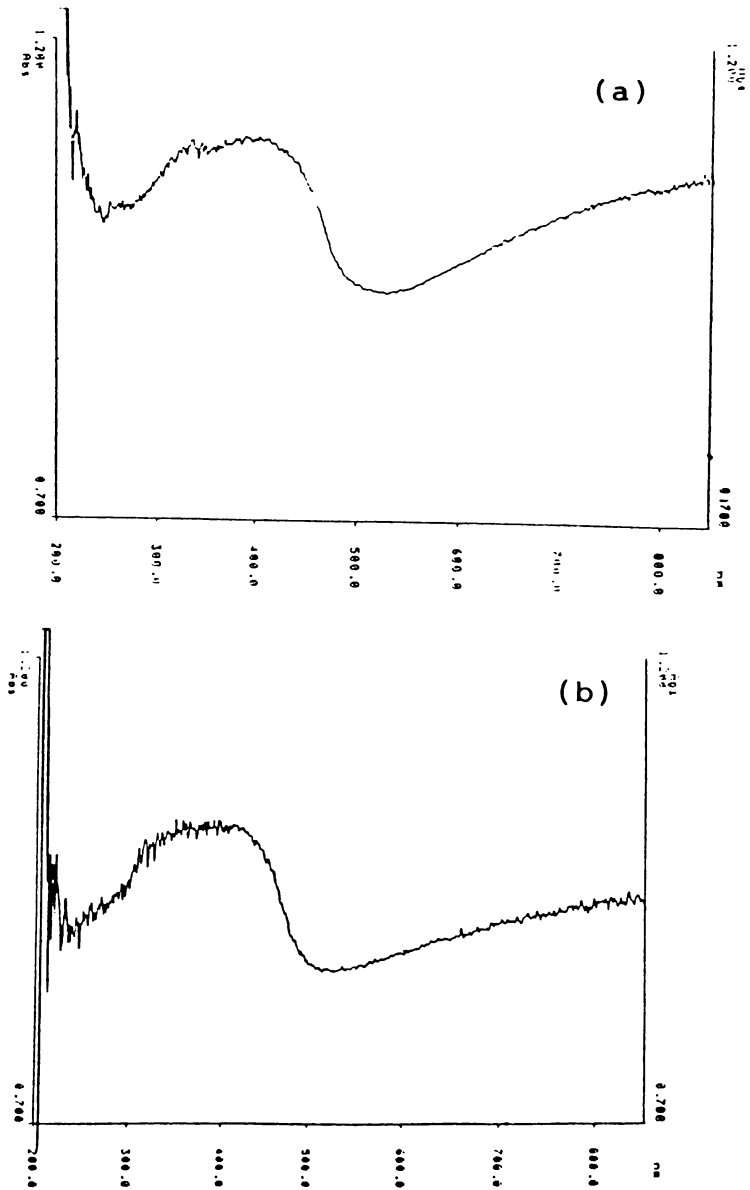


Fig.11.2.3: Effect of doping on the solid state electronic spectrum of  $PAT_3$ . (a)  $PAT_3$  base (b)  $PAT_3D_4$  (doped in 1 M HCl)

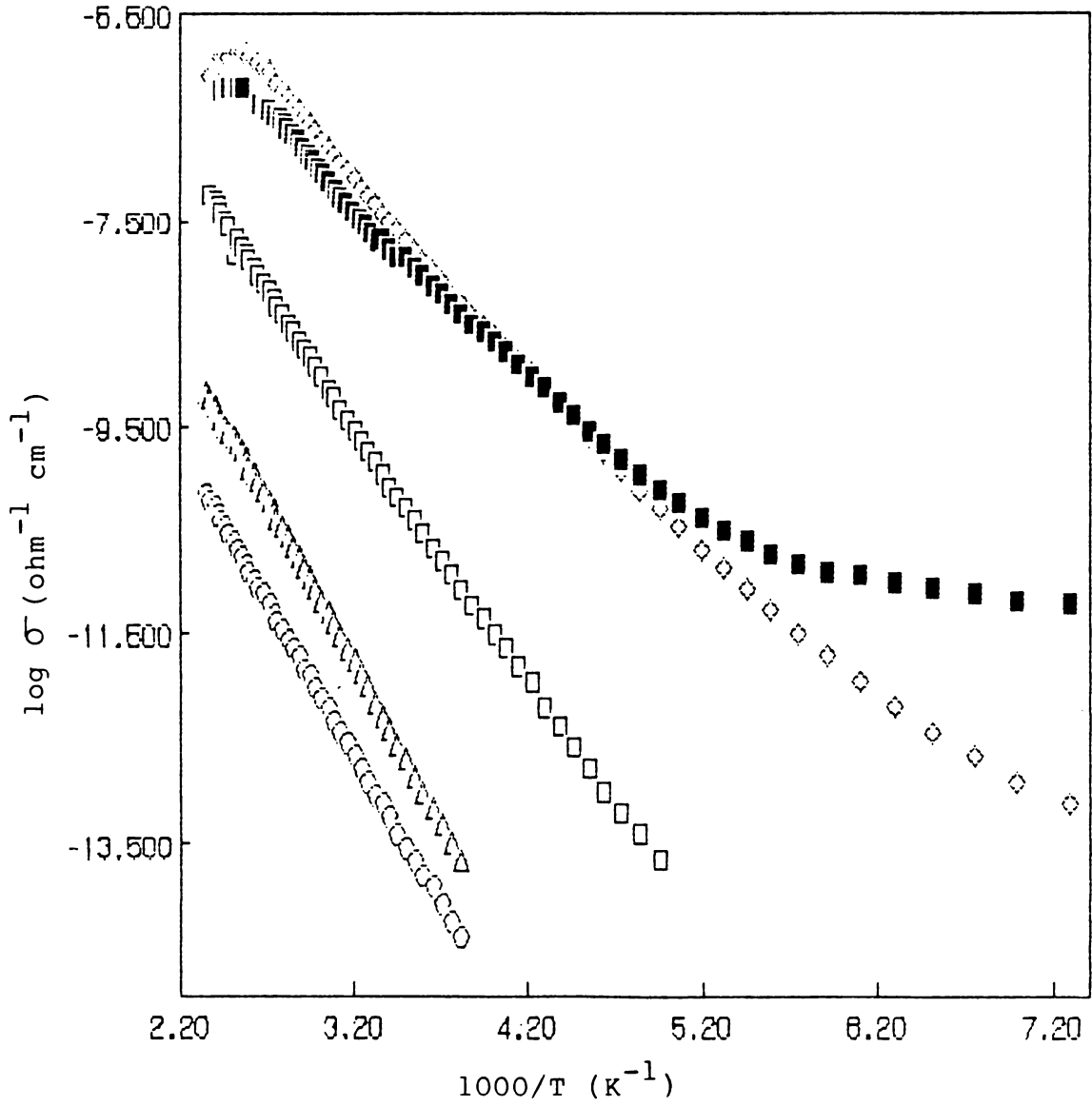


Fig.11.3.1: Arrhenius plots for the dc conductivity of PAT<sub>1</sub>.

○ - PAT<sub>1</sub> base ;    △ - PAT<sub>1</sub>D<sub>1</sub> ;    □ - PAT<sub>1</sub>D<sub>2</sub> ;  
 ◇ - PAT<sub>1</sub>D<sub>3</sub> ;    ■ - PAT<sub>1</sub>D<sub>4</sub>

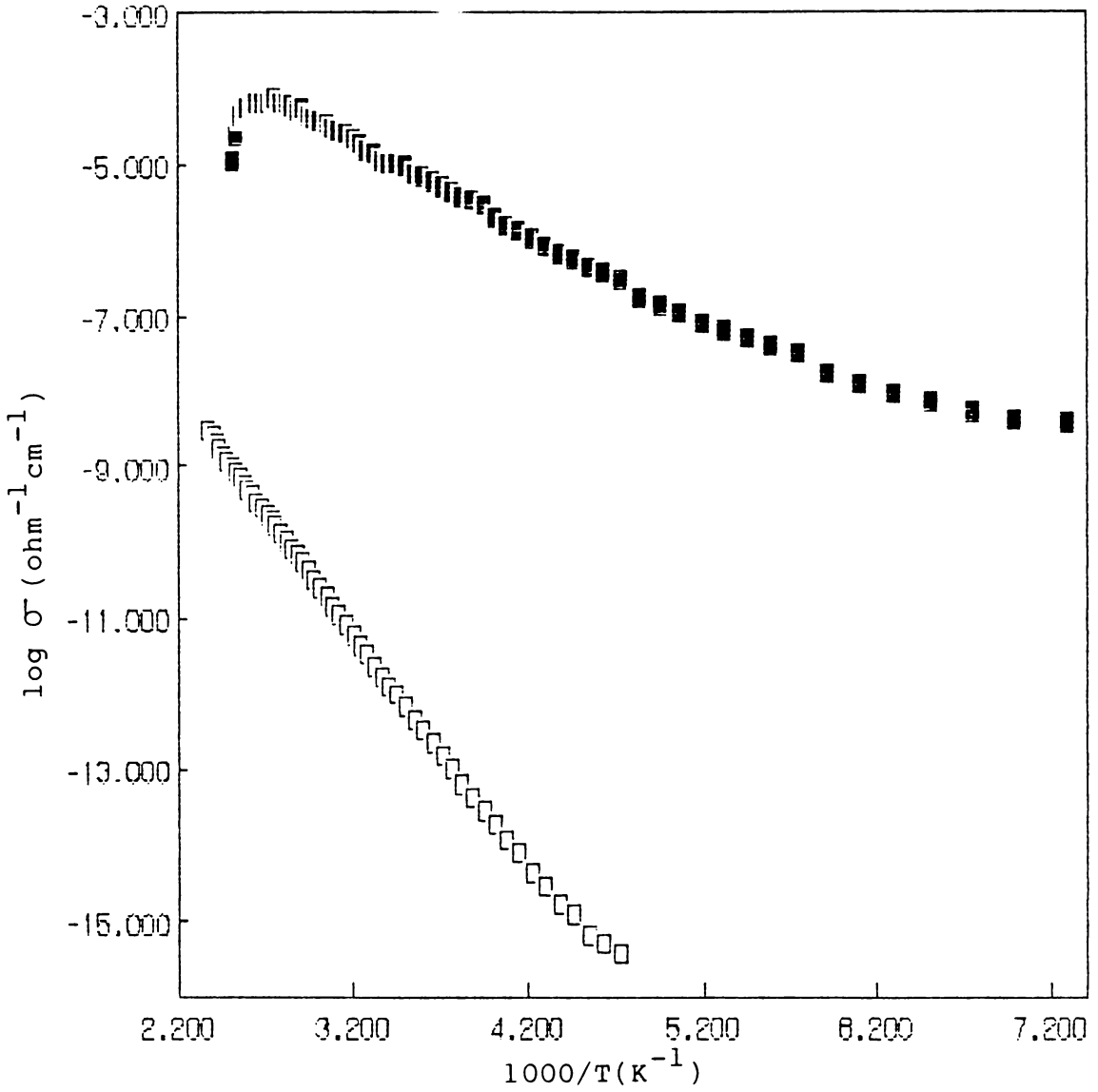


Fig.11.3.2: Arrhenius plots for the dc conductivity of  $\text{PAT}_1\text{O}$ .  $\square$  -  $\text{PAT}_1$  base ;  $\blacksquare$  -  $\text{PAT}_1\text{OD}_4$

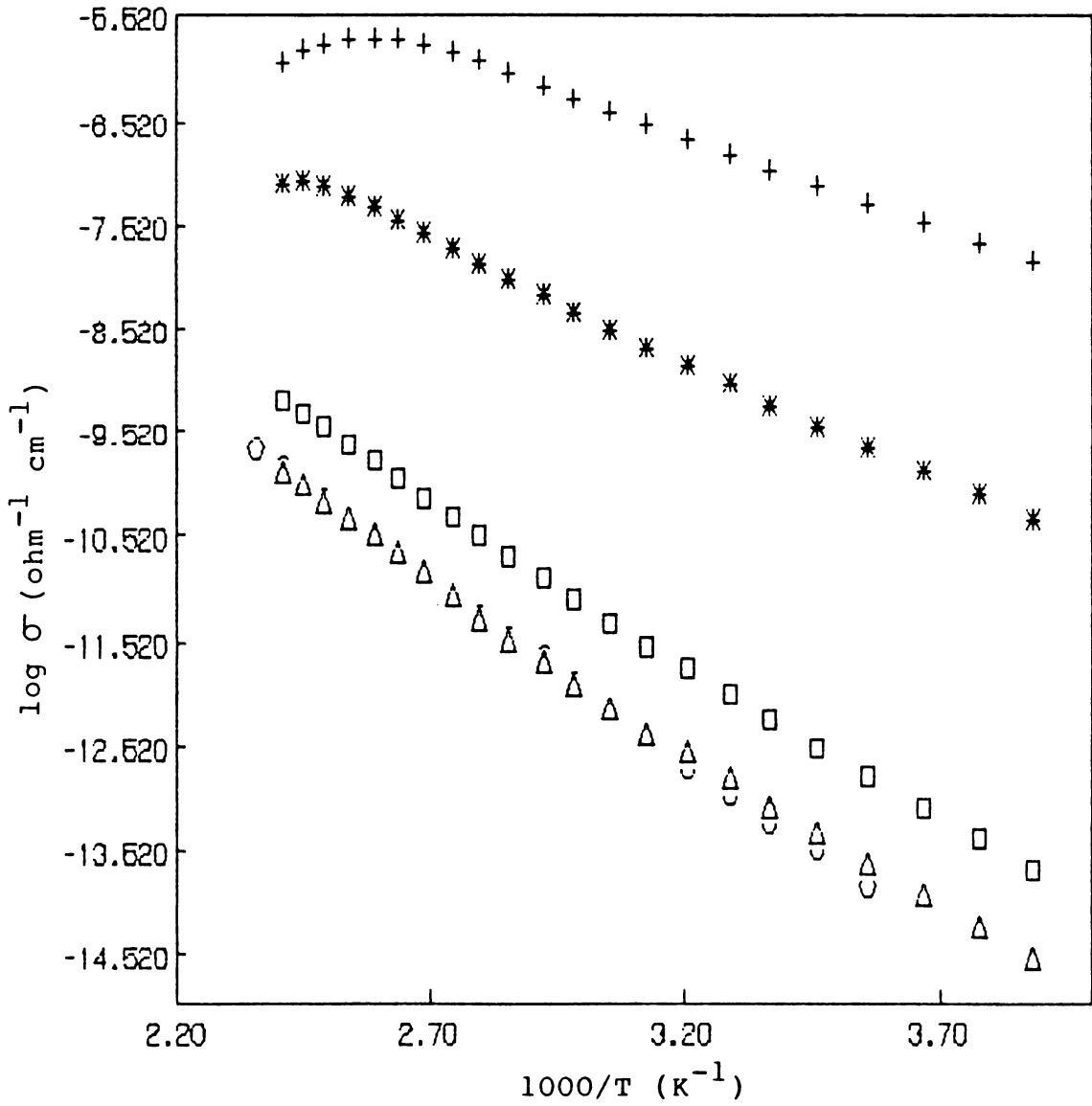


Fig.11.4.1: Arrhenius plots for the dc conductivity of PAT<sub>2</sub>.  
 ○ - PAT<sub>2</sub> base ;    Δ - PAT<sub>2</sub>D<sub>1</sub> ;    □ - PAT<sub>2</sub>D<sub>2</sub>  
 \* - PAT<sub>2</sub>D<sub>3</sub> ; + - PAT<sub>2</sub>D<sub>4</sub>

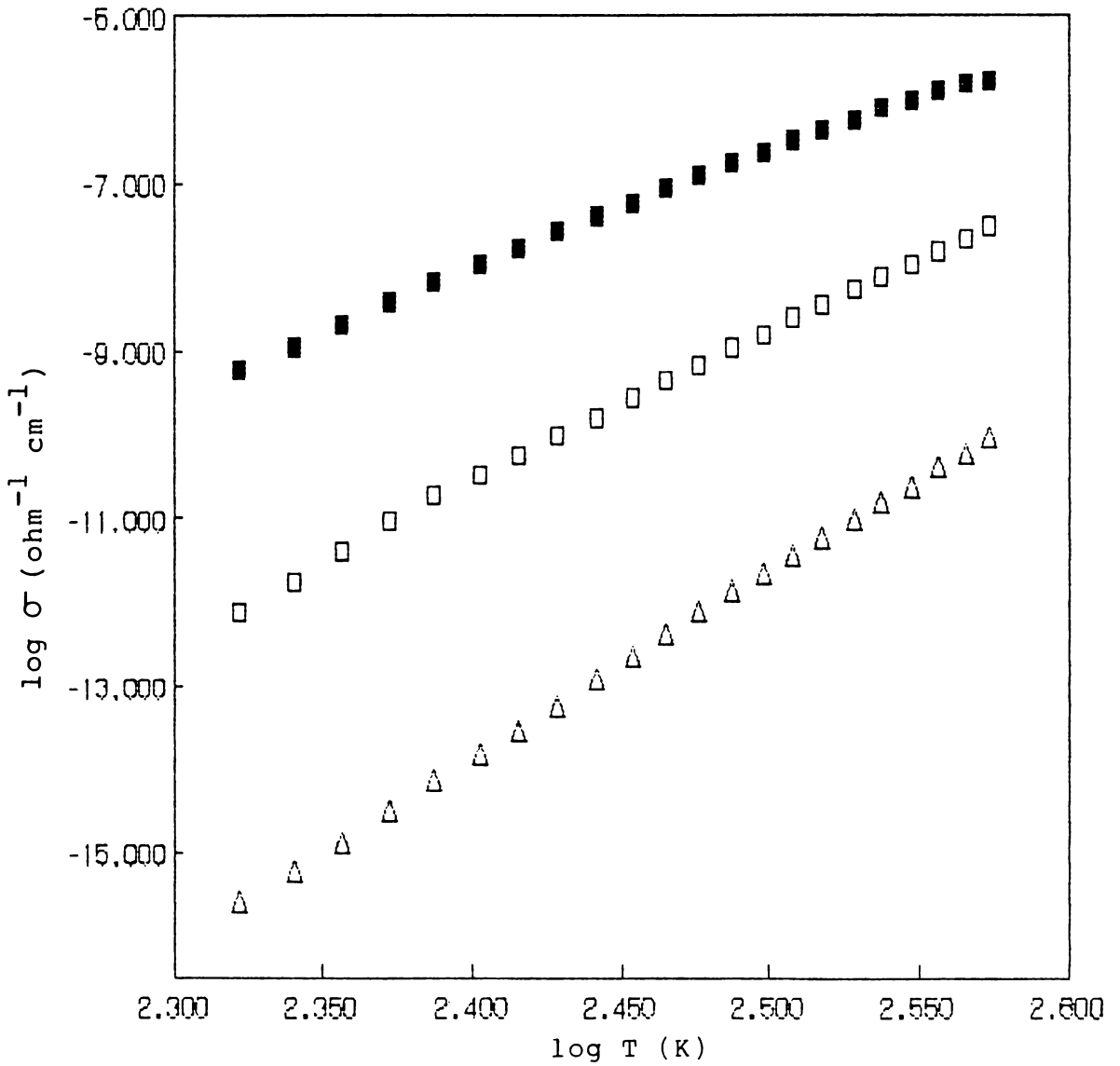


Fig.11.4.2: Plot of  $\log \sigma_{dc}$  versus  $\log T$  for  $PAT_2$   
 $\Delta$  -  $PAT_2D_2$  ;  $\square$  -  $PAT_2D_3$  ;  $\blacksquare$  -  $PAT_2D_4$

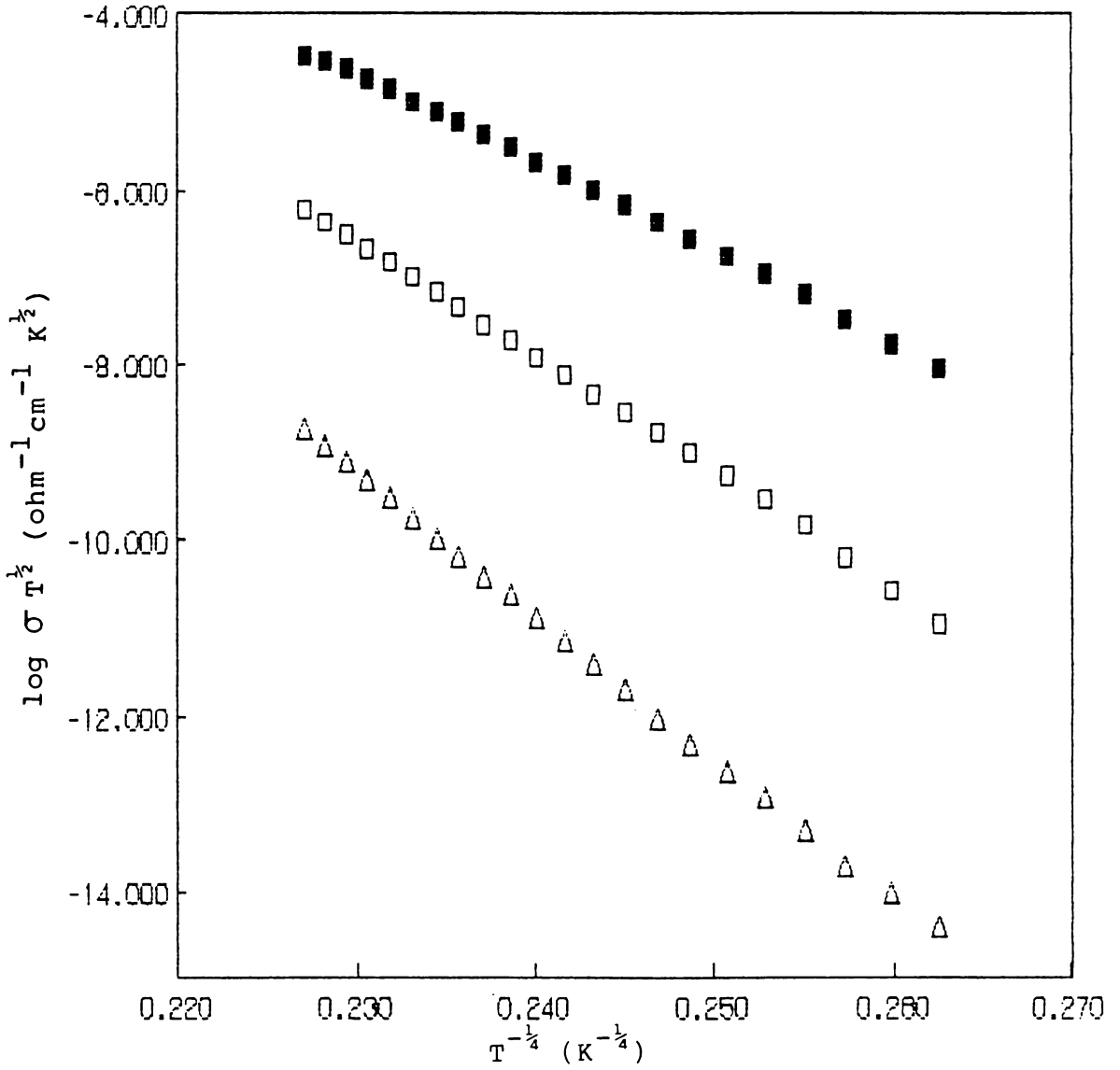


Fig.11.4.3: Plot of  $\log \sigma_{dc} T^{1/2}$  versus  $T^{-1/4}$  for PAT<sub>2</sub>.

$\Delta$  - PAT<sub>2</sub>D<sub>2</sub> ;  $\square$  - PAT<sub>2</sub>D<sub>3</sub> ;  $\blacksquare$  - PAT<sub>2</sub>D<sub>4</sub>

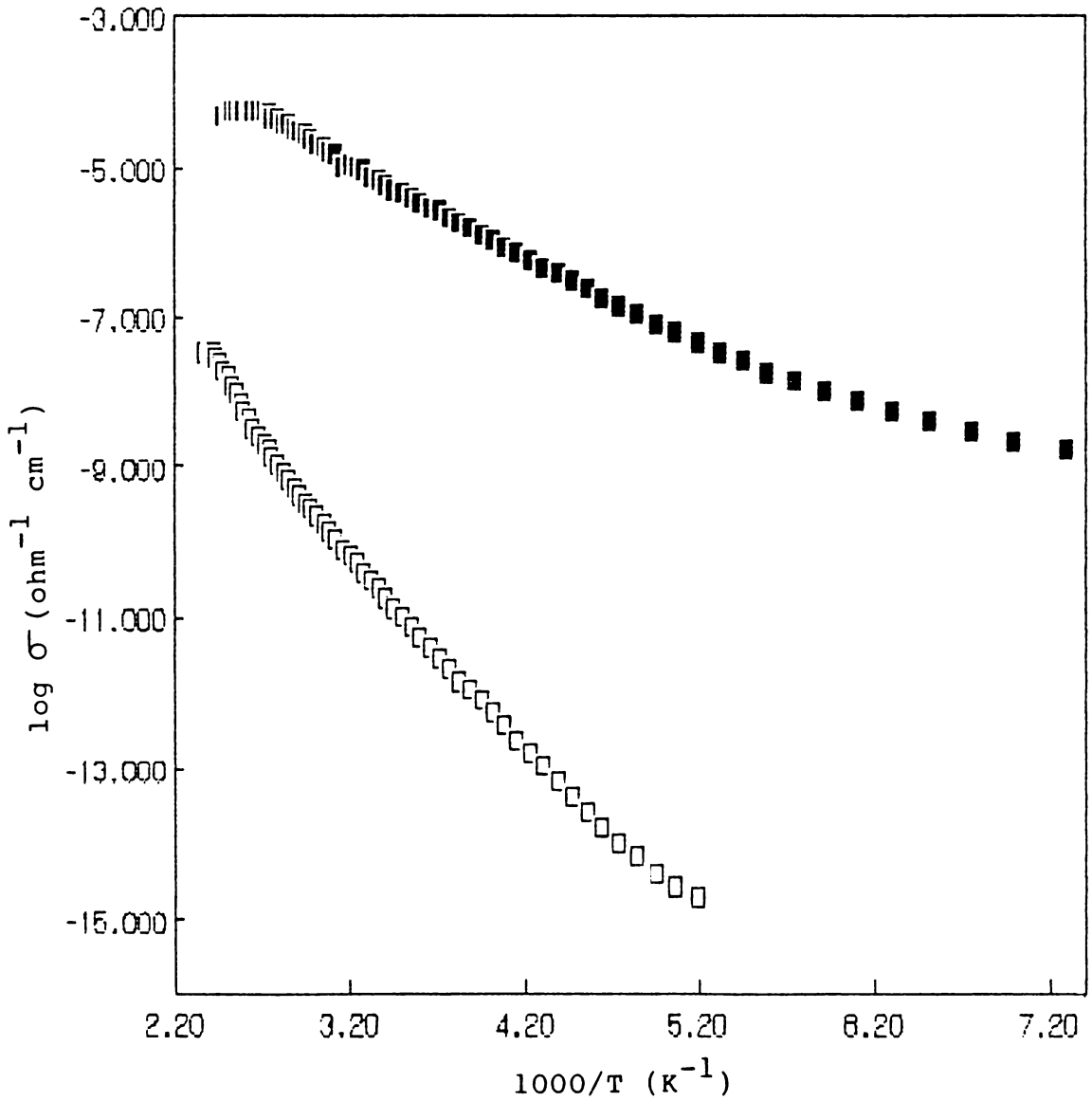


Fig.11.4.4: Arrhenius plots for the dc conductivity of  $\text{PAT}_2\text{O}$ .  $\square$  -  $\text{PAT}_2\text{O}$  base ;  $\blacksquare$  -  $\text{PAT}_2\text{D}_4$  (doped in 1 M HCl)

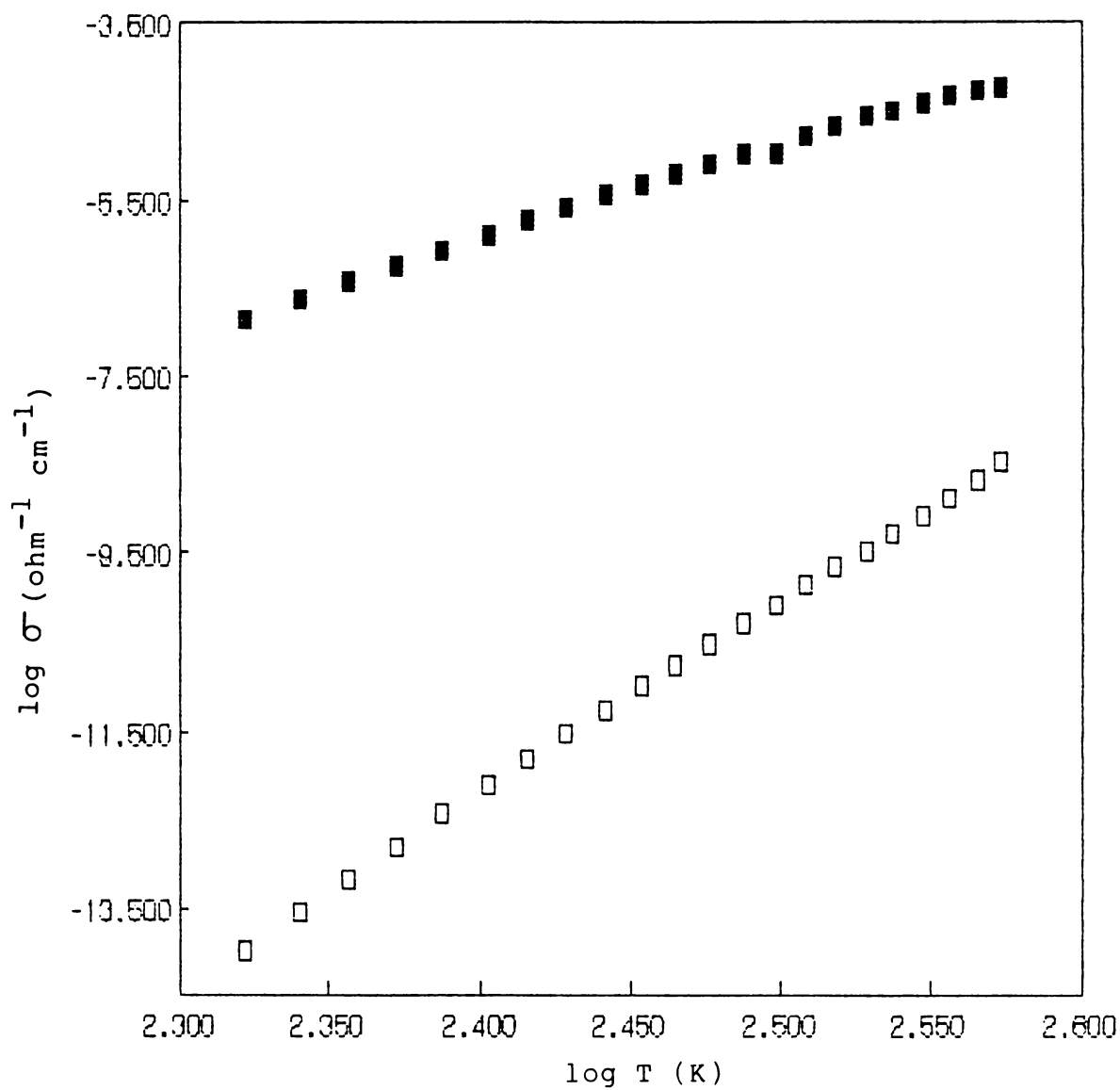


Fig.11.4.5: Plot of  $\log \sigma_{dc}$  versus  $\log T$  for  $\text{PAT}_2\text{O}$ .  
 □ -  $\text{PAT}_2\text{O}$  base ; ■ -  $\text{PAT}_2\text{OD}_4$  (doped in 1 M HCl)

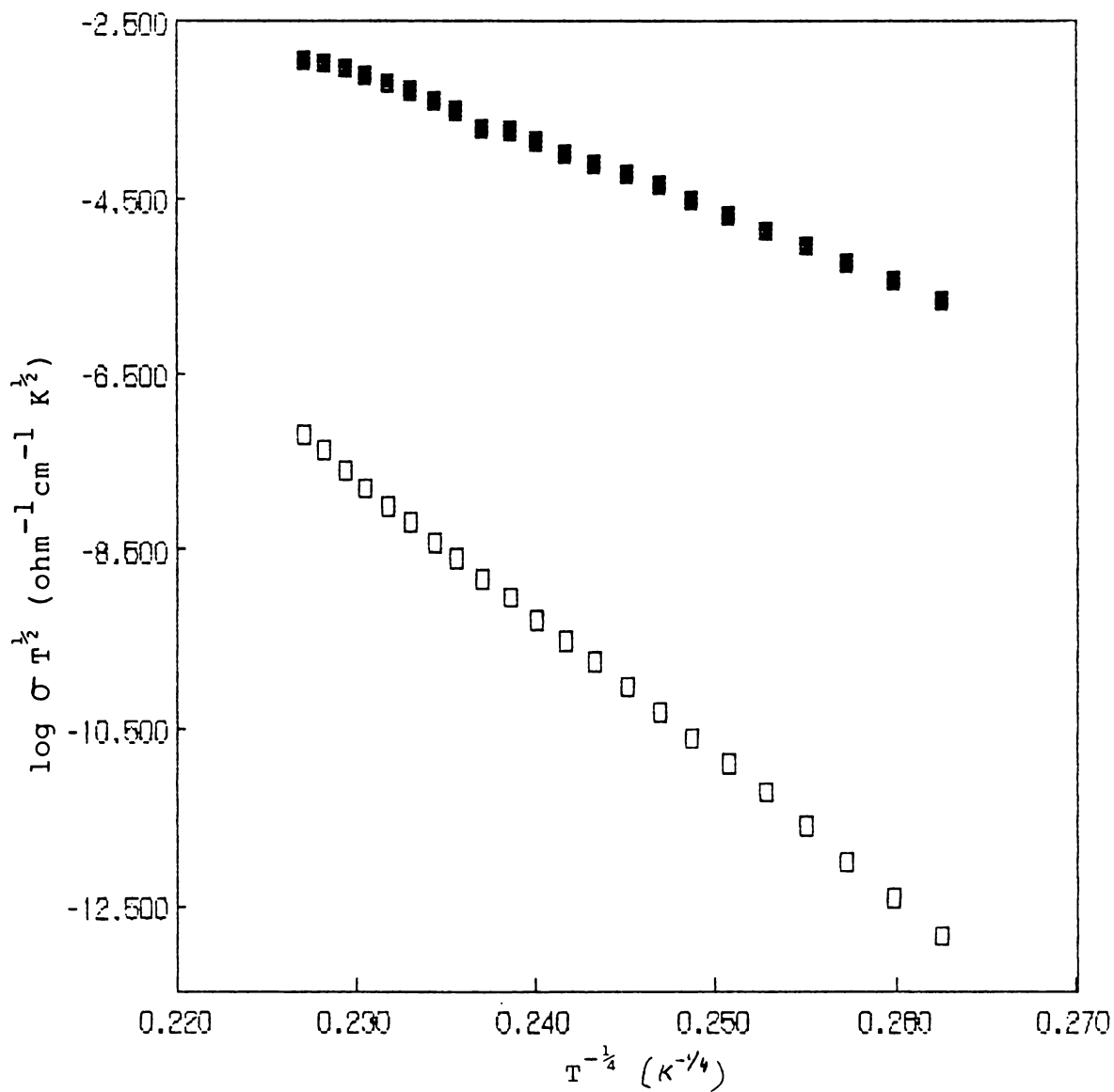


Fig.11.4.6: Plot of  $\log \sigma_{dc} T^{1/2}$  versus  $T^{-1/4}$  for  $PAT_2O$ .  
 □ -  $PAT_2O$  base ; ■ -  $PAT_2OD_4$  (doped in 1 M HCl)

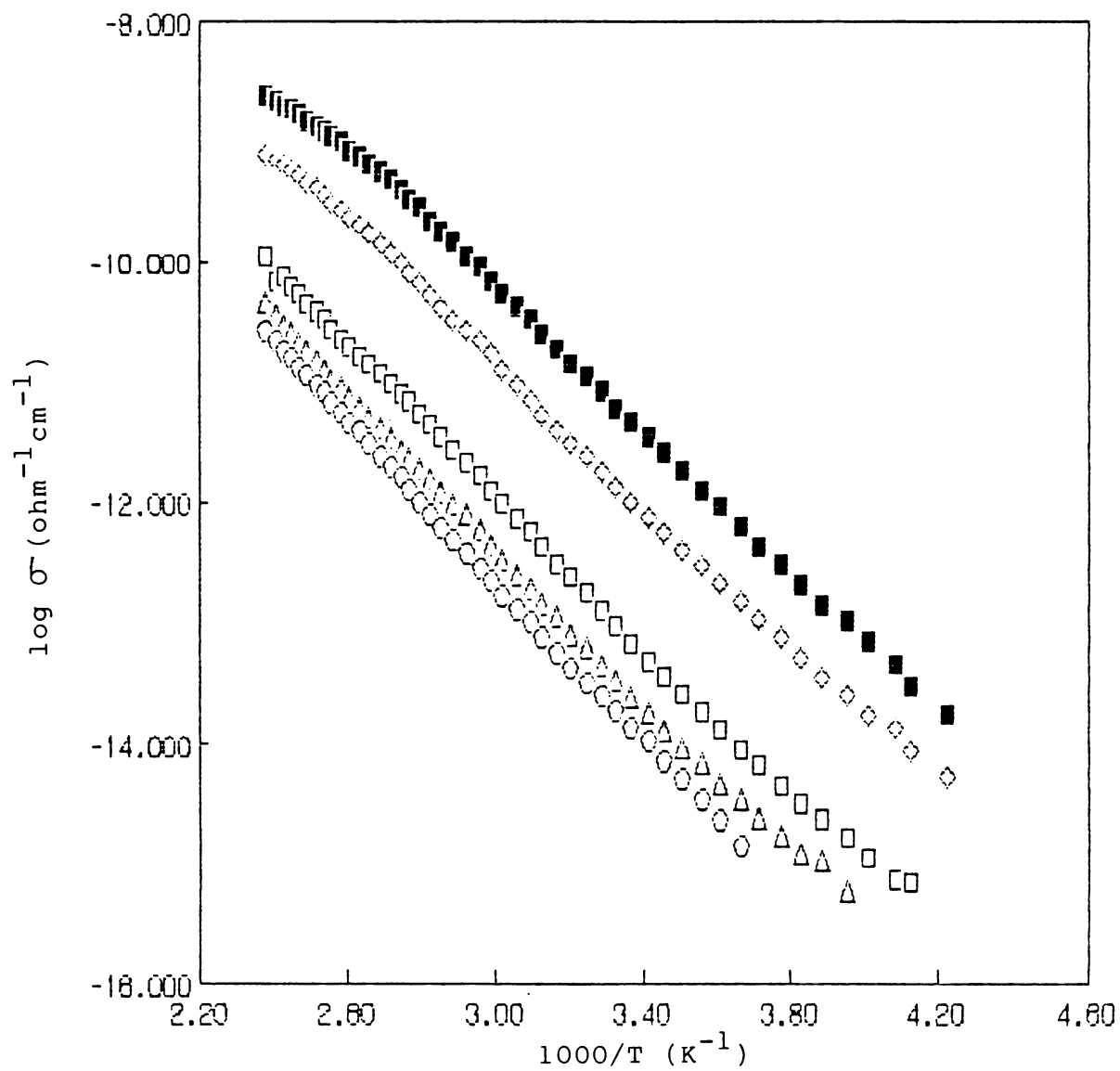


Fig.11.5.1: Arrhenius plots for the dc conductivity of PAT<sub>3</sub>.

○ - PAT<sub>3</sub> base ;    △ - PAT<sub>3</sub>D<sub>1</sub> ;    □ - PAT<sub>3</sub>D<sub>2</sub> ;  
 ◇ - PAT<sub>3</sub>D<sub>3</sub> ;    ■ - PAT<sub>3</sub>D<sub>4</sub>

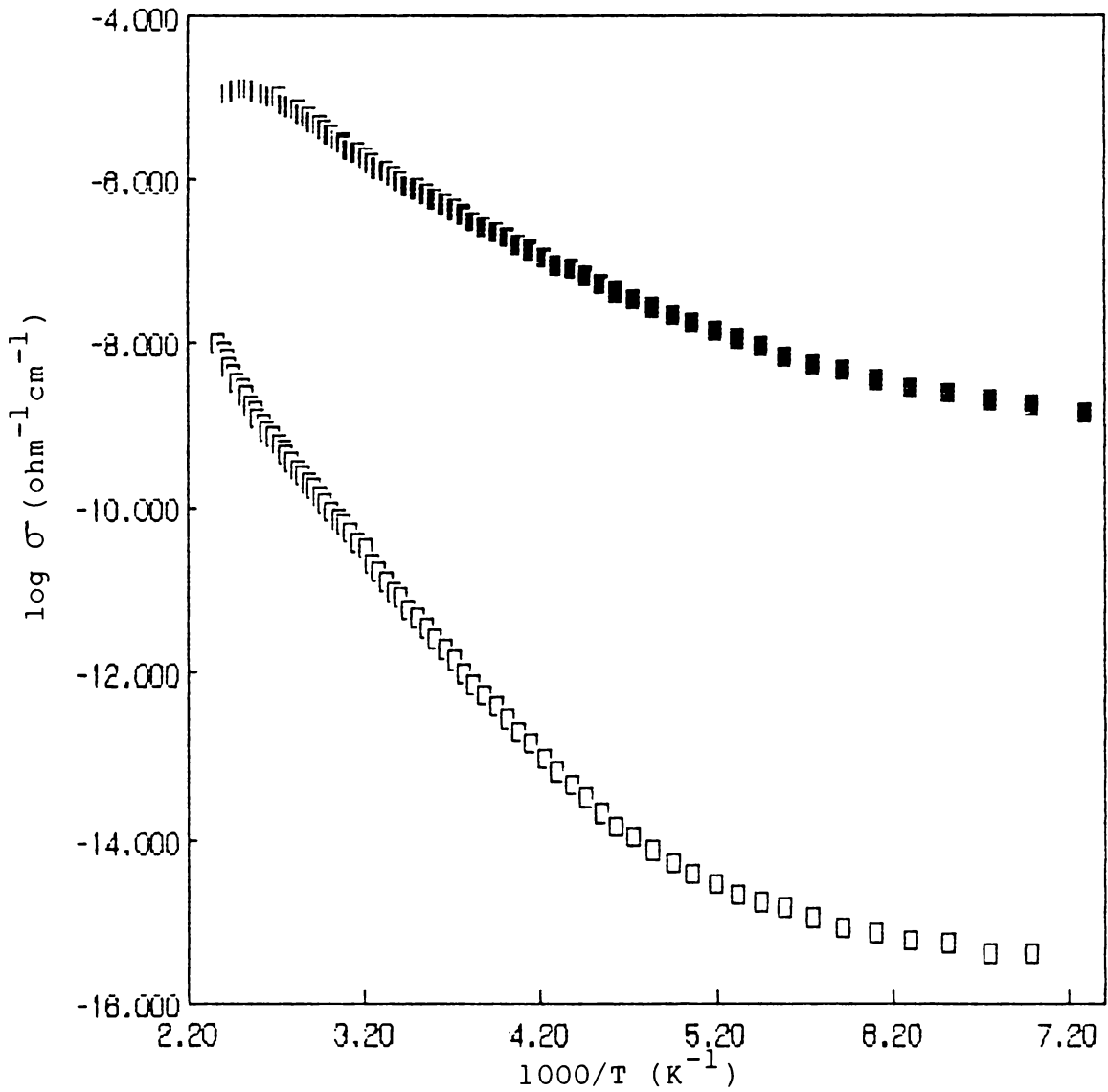


Fig.11.5.2: Arrhenius plots for the dc conductivity of PAT<sub>3</sub>O.  
 □ - PAT<sub>3</sub>O base ; ■ - PAT<sub>3</sub>OD<sub>4</sub> (doped in 1 M HCl)

the reliability of conductivity measurements decreases. In heavily doped materials, the Arrhenius plots show a curvature at low temperatures. The activation energy measured from the linear portion of the Arrhenius plots are given in Table 11.2. It is seen that the activation energy decreases with increasing degree of protonation. In this respect it is similar to polyaniline base as reported by Zuo et al. [19(b)]. One of the distinct features observed in these studies is that the dc conductivity of the materials decreases with increasing proportion of meta-toluidine in the copolymer.

As is evident from Figs.11.3-11.5 that dc conductivity data do not give a precise linear fit for  $\log \sigma$  vs  $1/T$  plots for heavily doped forms in the whole temperature range. Therefore, the dc conductivity data were plotted in  $\log \sigma$  vs  $\log T$  and  $\log \sigma T^{\frac{1}{2}}$  vs  $T^{-\frac{1}{4}}$  formats. The behaviour of these plots is similar for all the three copolymers. Hence the plots for  $PAT_2$  which are typical alone are depicted in Figs.11.4.2 and 11.4.3. It is clear that the  $\log \sigma T^{\frac{1}{2}}$  vs  $T^{-\frac{1}{4}}$  plots give a better fit especially in the case of heavily doped materials. For the base as well as lightly doped forms, the conduction seems to be a thermally activated process. Doping leads to the

formation of conductive segments dispersed in an insulating matrix. The enhanced conductivity observed with oligomer-containing materials may be due to the formation of oligomer salts of higher conductivity.

### 11.3.6 ac conductivity

The ac conductivity of oligomer-containing samples is higher than that for purified samples in the pristine as well as doped forms.

#### (a) Copolymer base

The base forms of the copolymers, oligomer-containing as well as oligomer-free, show very low ac conductivity (Table 11.2). Also, the frequency and temperature dependence of  $\sigma_{ac}$  for all samples of the base are very small. A typical representation of frequency and temperature dependence of  $\sigma_{ac}$  is given in Fig.11.6.

#### (b) Doped copolymers

As the extent of doping increases, the magnitude of ac conductivity in doped copolymers also increases. The frequency and temperature dependence of  $\sigma_{ac}$  for all samples listed in Table 11.2 were studied. Of these the

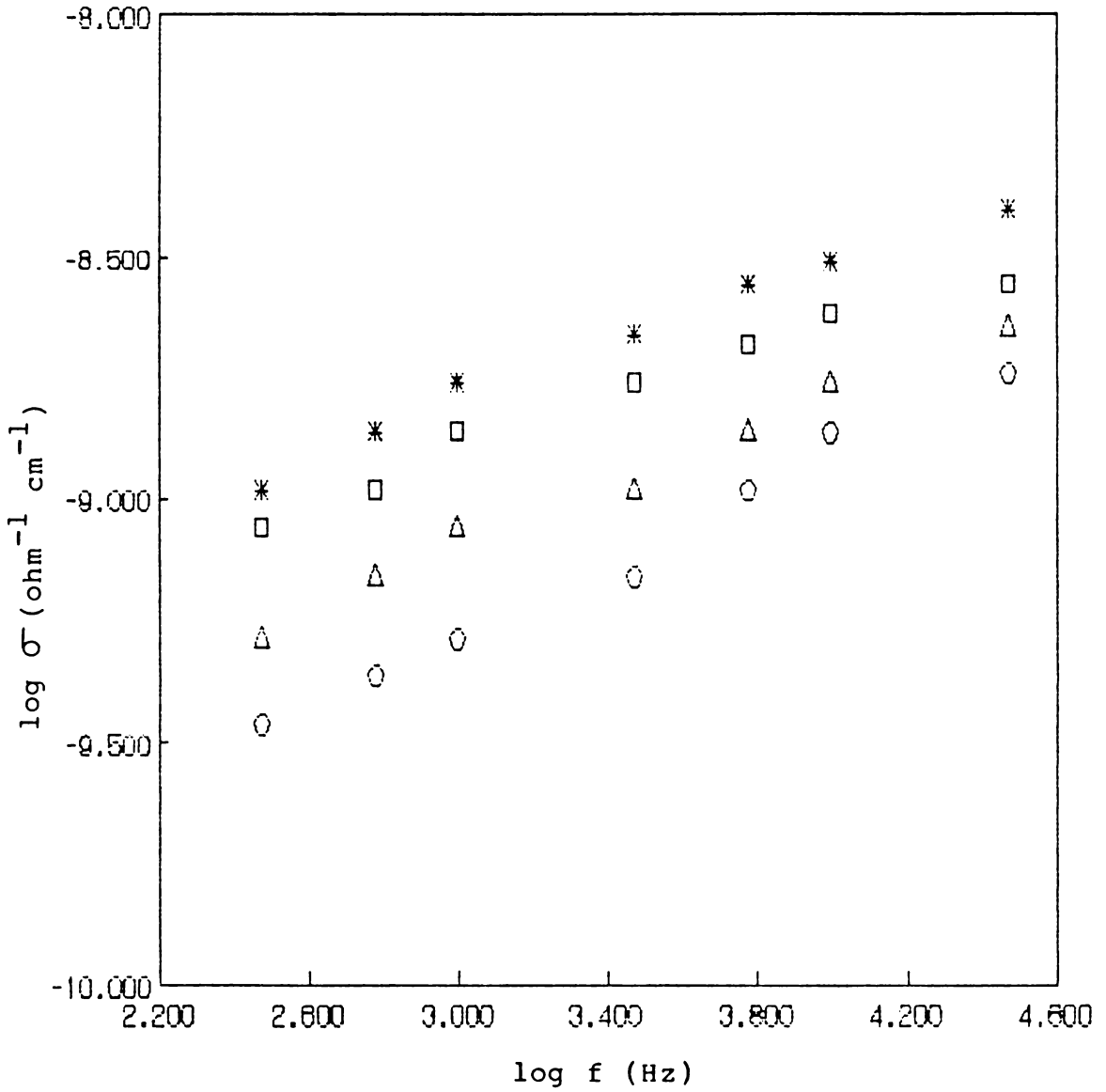


Fig.11.6: A typical plot of  $\log \sigma_{ac}$  versus  $\log f$  for poly(aniline co-meta-toluidine) base. ○ - 260 K, △ - 290 K, □ - 320 K  
\* - 350 K.

copolymer containing the highest proportion of aniline shows maximum values for conductivity ( $1.8 \times 10^{-7}$  and  $2.1 \times 10^{-5} \text{ ohm}^{-1} \text{ cm}^{-1}$  for  $\text{PAT}_1\text{D}_4$  and  $\text{PAT}_1\text{OD}_4$  respectively, at 300 K and 1 kHz). Fig.11.7 to 11.9 illustrate the temperature and frequency dependence of  $\sigma_{ac}$  for the fully doped forms (doped with 1 M HCl) of the polymers, viz.,  $\text{PAT}_1\text{D}_4$ ,  $\text{PAT}_1\text{OD}_4$ ,  $\text{PAT}_2\text{D}_4$ ,  $\text{PAT}_2\text{OD}_4$ ,  $\text{PAT}_3\text{D}_4$  and  $\text{PAT}_3\text{OD}_4$ . Though the value of ac conductivity at a fixed frequency at a particular temperature varies from material to material, the general pattern of the plots are quite similar i.e., the nature of frequency and temperature dependence is the same in all the samples. This indicates that the same conduction mechanism is operative in all the copolymers.

At low temperatures the ac conductivity of samples of oligomer-containing and oligomer-free copolymer doped with 1 M HCl ( $\text{PAT}_2$ ) conforms to the relationship,

$$\sigma_{ac} = Bf^s$$

with the value of  $s \sim 0.52$  and  $\sim 0.47$  for  $\text{PAT}_2\text{D}_4$  and  $\text{PAT}_2\text{OD}_4$  respectively. The corresponding values of  $s$  for the base forms ( $\text{PAT}_2$  and  $\text{PAT}_2\text{O}$ ) are  $\sim 0.24$  and  $\sim 0.19$ .

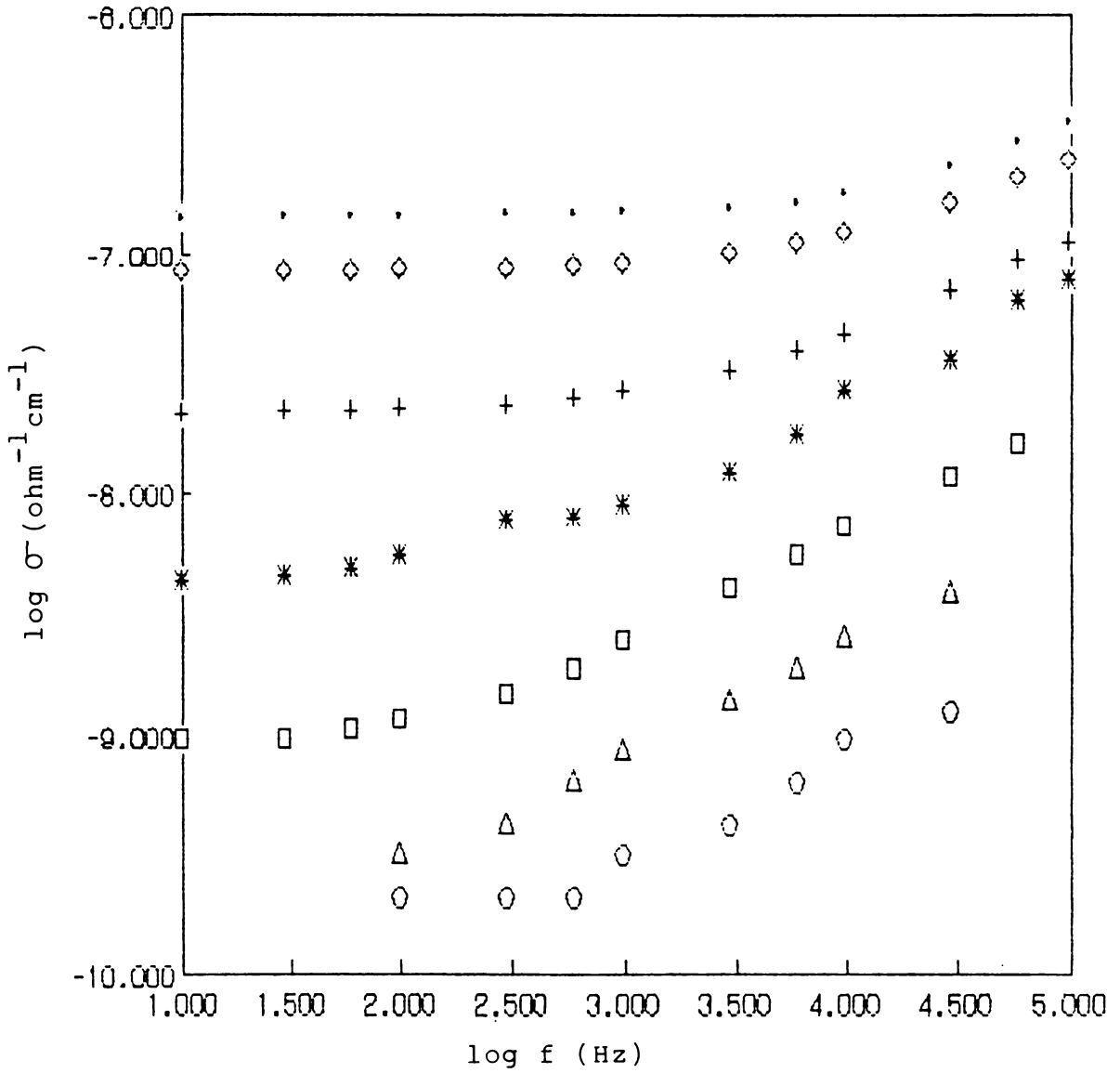


Fig.11.7.1: Plot of  $\log \sigma_{ac}$  versus  $\log f$  for  $\text{PAT}_1\text{D}_4$ . ○ - 170 K ;  
 △ - 200 K ; □ - 230 K ; \* - 260 K ; + - 290 K ;  
 ◇ - 320 K ; • - 350 K.

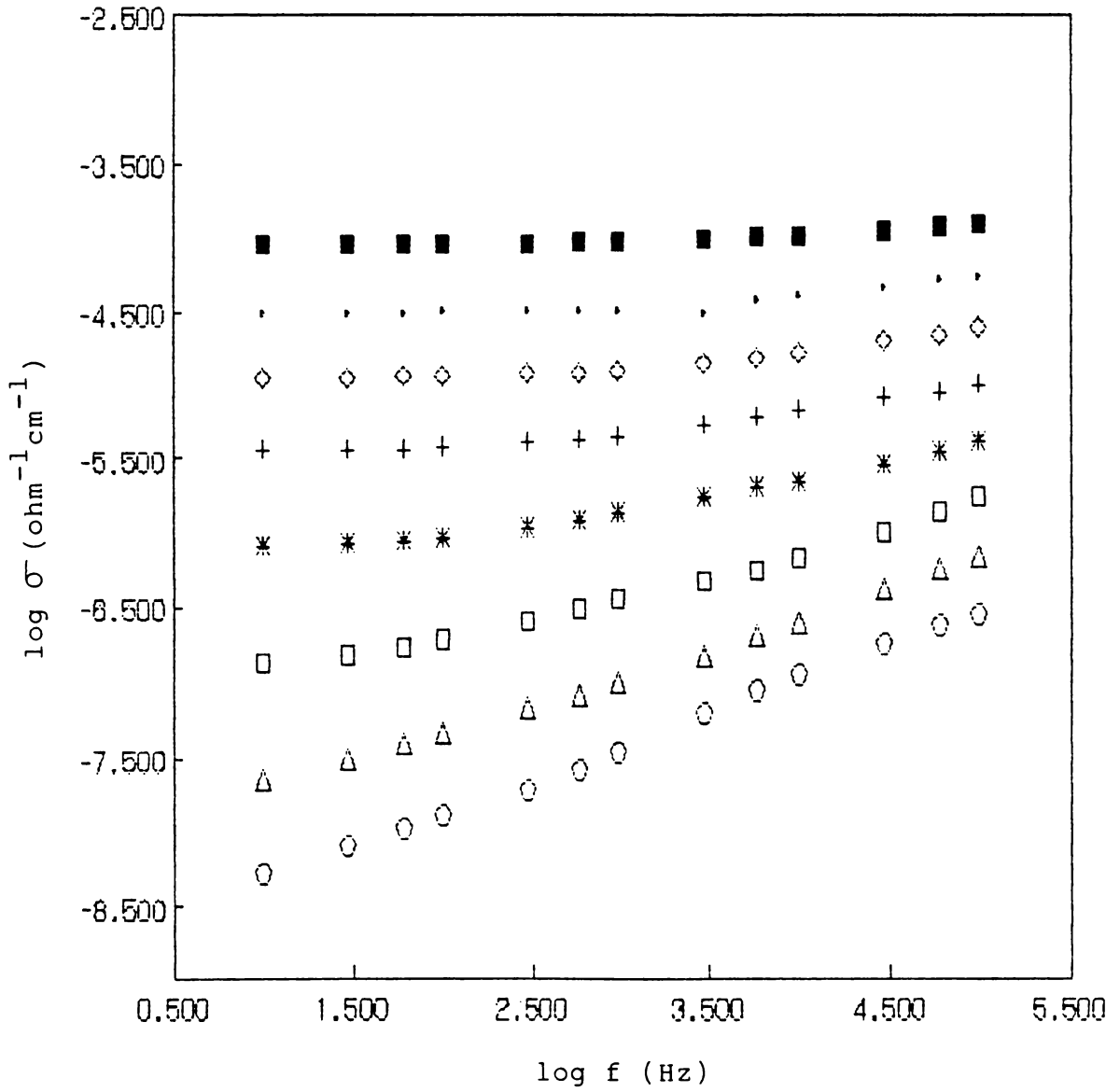


Fig.11.7.2: Plot of  $\log \sigma_{ac}$  versus  $\log f$  for  $\text{PAT}_1\text{OD}_4$ .

○ - 140 K ; △ - 170 K ; □ - 200 K ; \* - 230 K  
 + - 260 K ; ◇ - 290 K ; • - 320 K ; ■ - 350 K

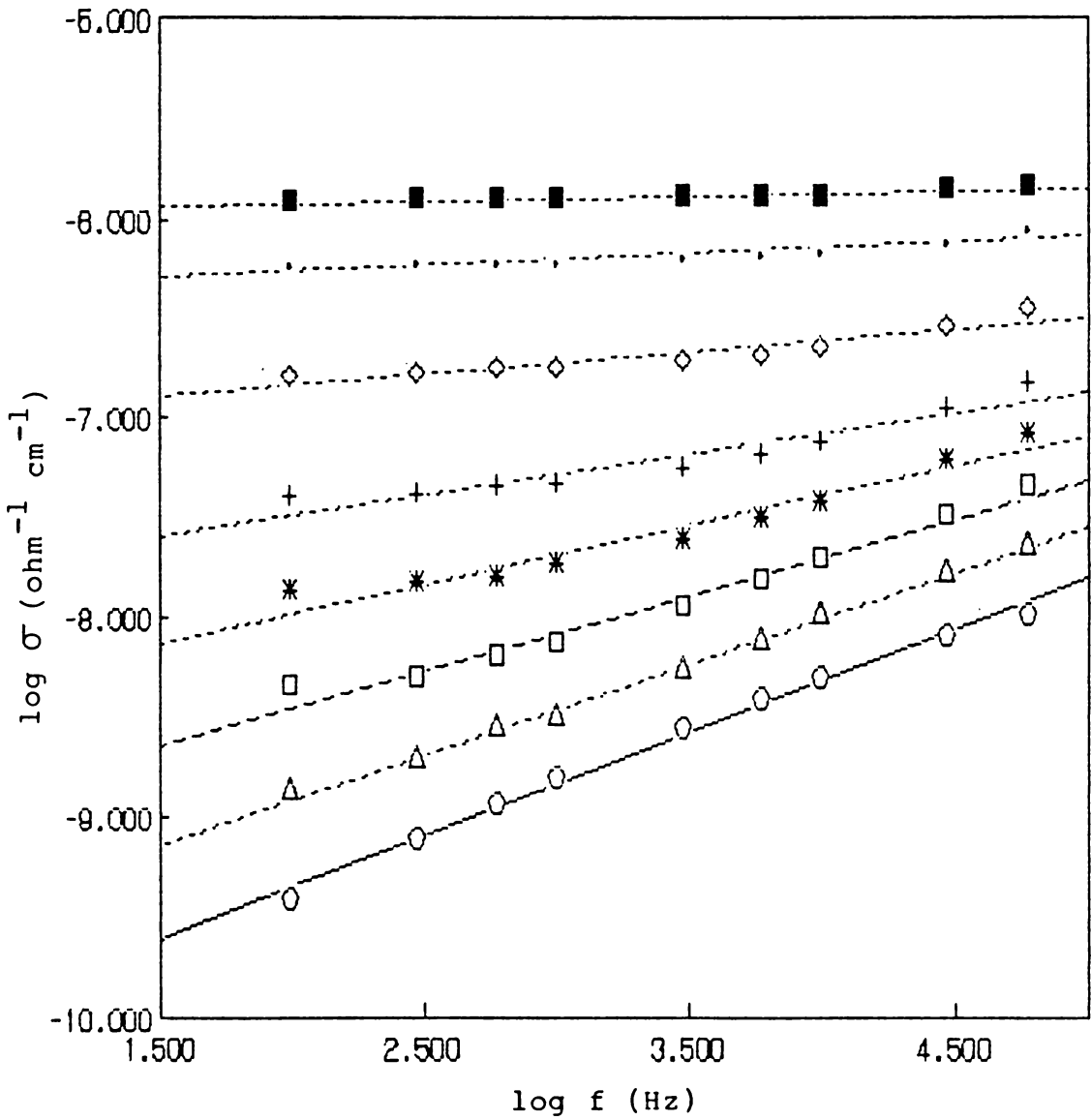


Fig.11.8.1: Plot of  $\log \sigma_{ac}$  versus  $\log f$  for  $\text{PAT}_2\text{D}_4$

○ - 140 K ; △ - 170 K ; □ - 200 K ; \* - 230 K  
 + - 260 K ; ◇ - 290 K ; · - 320 K ; ■ - 350 K

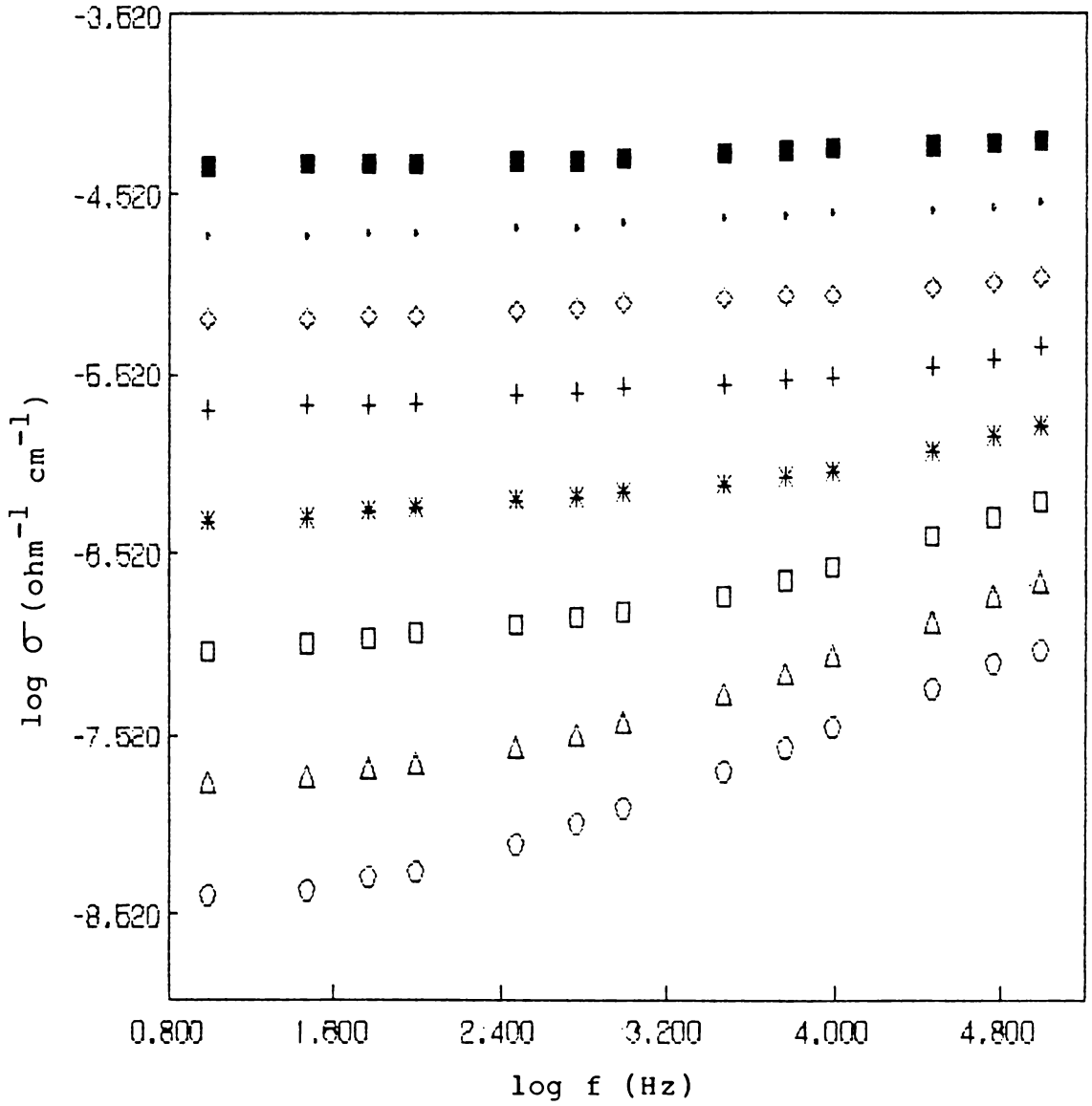


Fig.11.8.2: Plot of  $\log \sigma_{ac}$  versus  $\log f$  for  $\text{PAT}_2\text{OD}_4$ .

○ - 140 K ; △ - 170 K ; □ - 200 K ; \* - 230 K  
 + - 260 K ; ◇ - 290 K ; • - 320 K ; ■ - 350 K

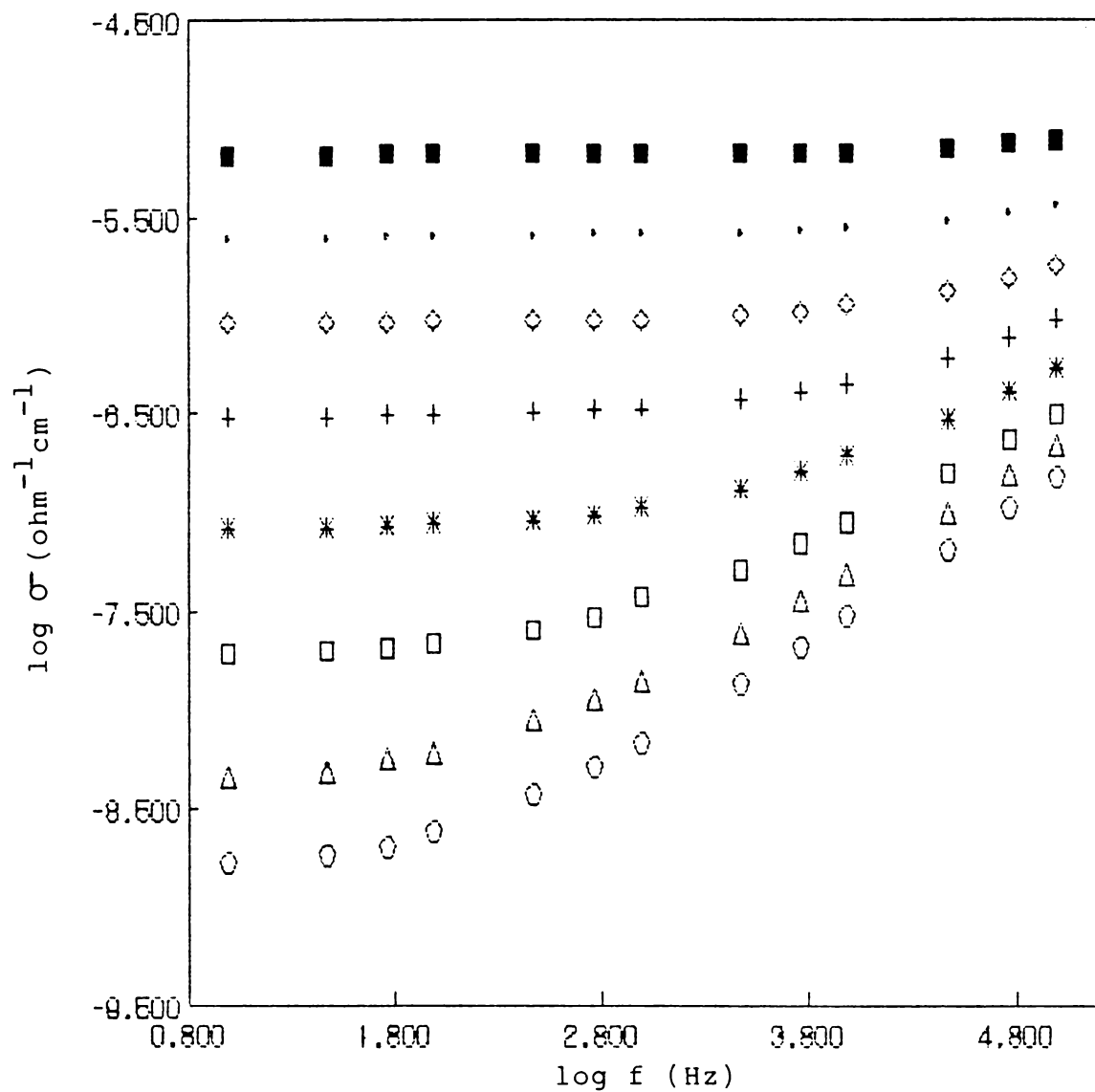


Fig.11.9: Plot of  $\log \sigma_{ac}$  versus  $\log f$  for  $\text{PAT}_3\text{OD}_4$

○ - 140 K ; △ - 170 K ; □ - 200 K ; \* - 230 K  
 + - 260 K ; ◇ - 290 K ; · - 320 K ; ■ - 350 K

It is also seen that the value of  $\sigma$  increases with increasing level of doping. Other copolymers also show similar behaviour with regard to ac conductivity, the value of  $\sigma$  slightly varying with the nature of the copolymer.

### 11.3.7 Dielectric constant

The variation of dielectric constant as a function of frequency and temperature were studied in the case of all the copolymer samples (Table 11.3). Only the plots for the base and heavily doped (doped with 1 M HCl) forms are presented in Fig.11.10 to 11.13.

The general pattern of the plots for the samples remains the same. At the lowest temperatures studied the dielectric constant does not vary significantly with frequency. As the temperature is raised, the low frequency contribution of dielectric constant increases. The dielectric constant of the base forms are relatively small at all temperatures. At 300 K its value varies from 5 to 8 (at 1 kHz). The value of dielectric constant increases with increasing level of doping. The doped forms of the copolymers show abnormally high values of dielectric constant at elevated temperatures.

The high temperature and low frequency dielectric constants of the copolymers increase with increasing level of protonation. For  $PAT_1OD_4$ , i.e., the oligomer containing copolymer of highest aniline ratio protonated with 1 M HCl, the value of dielectric constant is about 3800 at 1 kHz (300 K). For the corresponding oligomer-free material ( $PAT_1D_4$ ) the value is only 40. The 'giant' dielectric constant is perhaps due to the contribution of the substituent present on the benzene ring and of the charge carriers generated by doping. Of all the copolymers studied the oligomer-containing materials have higher dielectric constant compared to purified materials.

### 11.3.8 Thermal behaviour

The DSC thermograms of the poly(aniline co-meta-toluidine) samples in the base and doped forms are presented in Fig.11.14.1 to 11.16.2. An analysis of the shapes of these thermograms reveals some important features. The oligomer-free pristine bases,  $PAT_1$  and  $PAT_2$  show a broad endothermic hump in the temperature range 50-180°C. With  $PAT_3$  and the heavily doped forms of all the pure copolymers (i.e.,  $PAT_1D_4$ ,  $PAT_2D_4$  and  $PAT_3D_4$ ) a more defined endothermic peak is observed with a maximum at about 90°C. All the oligomer-containing samples and

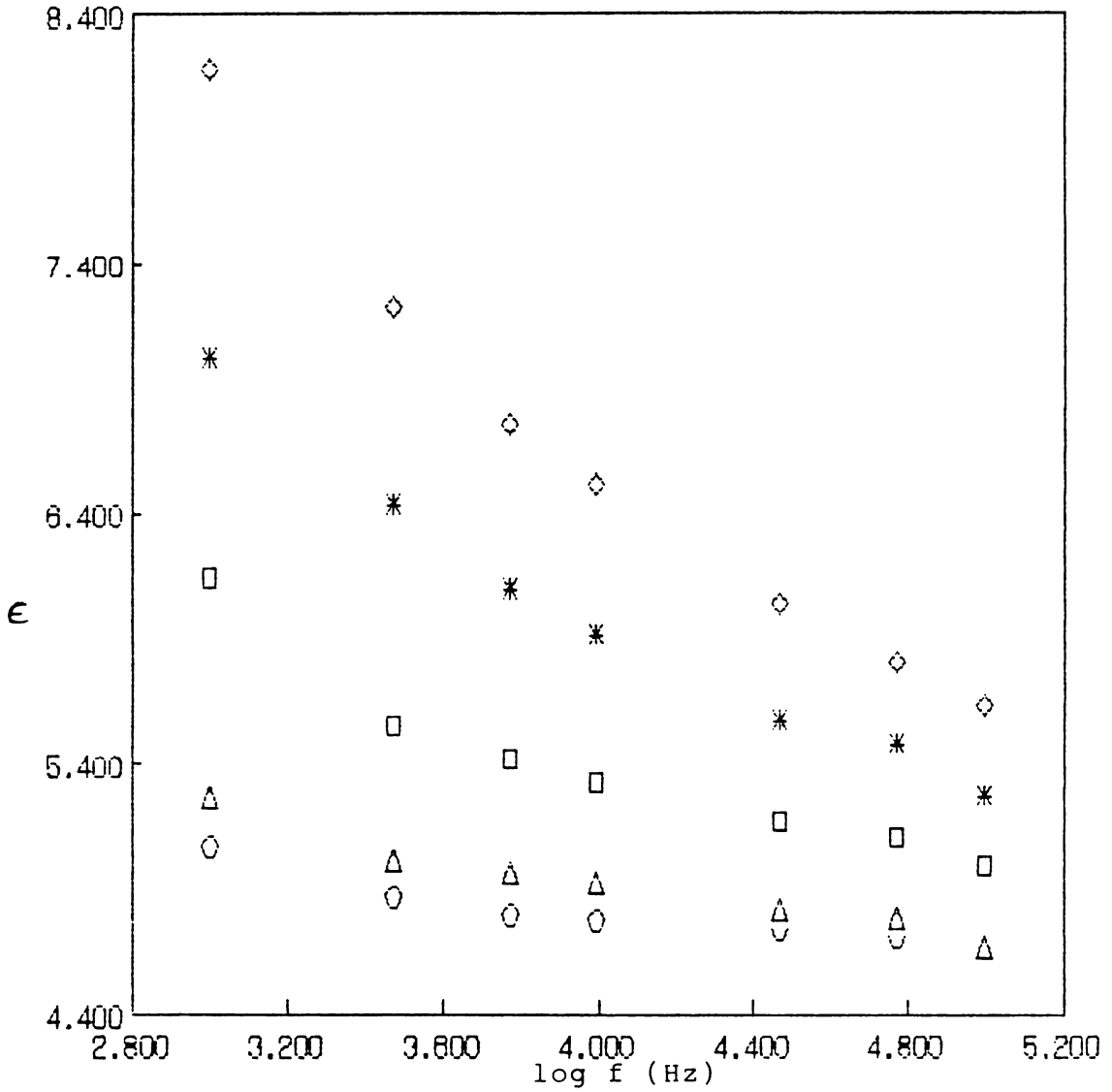


Fig.11.10: A typical plot for dielectric constant versus log f for poly(aniline co-meta-toluidine) base.

○ - 230 K ; △ - 260 K ; □ - 290 K ; \* - 320 K  
 ◇ - 350 K

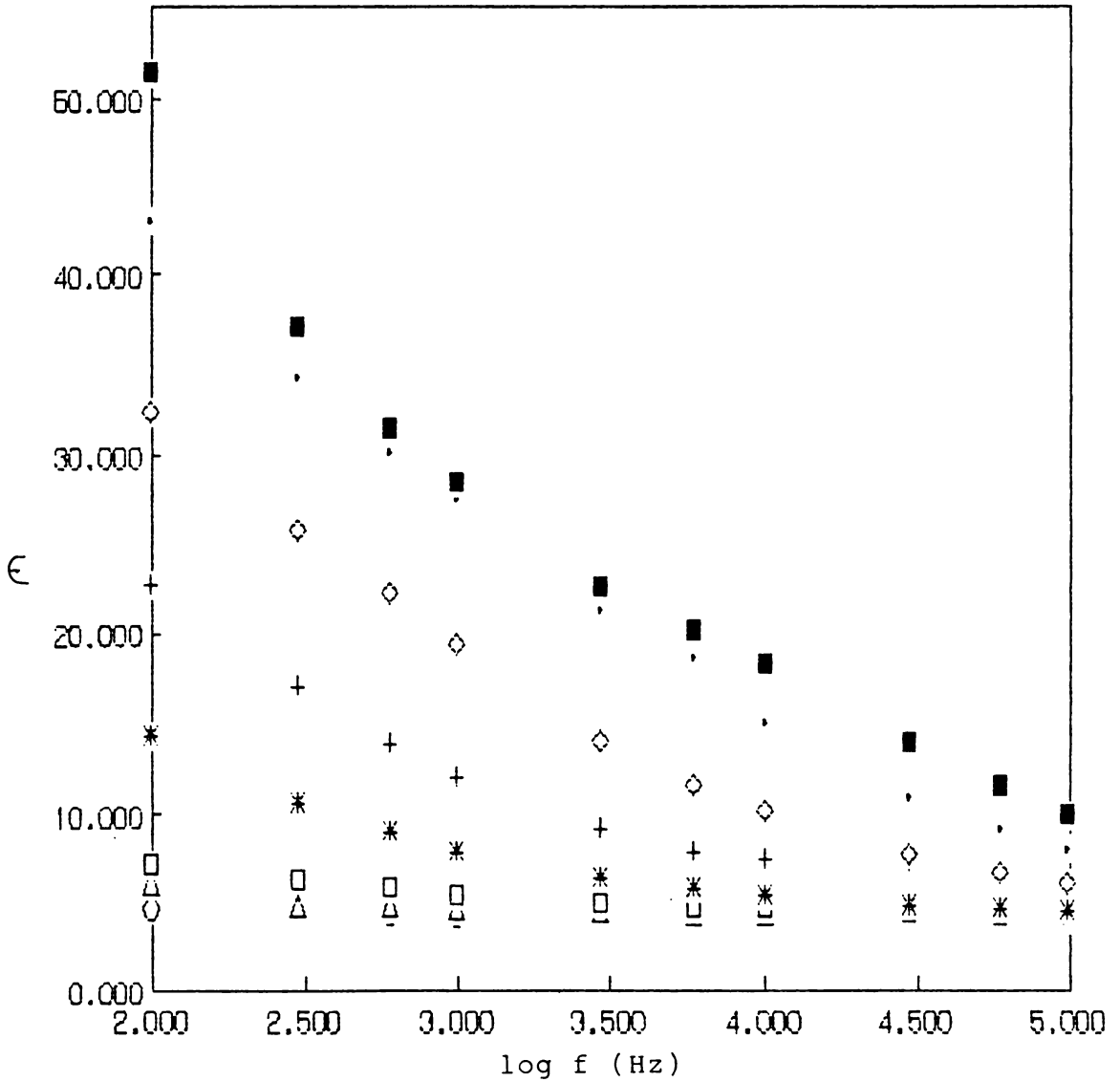


Fig.11.11.1: Plot of dielectric constant versus log f for  $PAT_1D_4$ .

○ - 140 K ; △ - 170 K ; □ - 200 K ; \* - 230 K  
 + - 260 K ; ◇ - 290 K ; • - 320 K ; ■ - 350 K

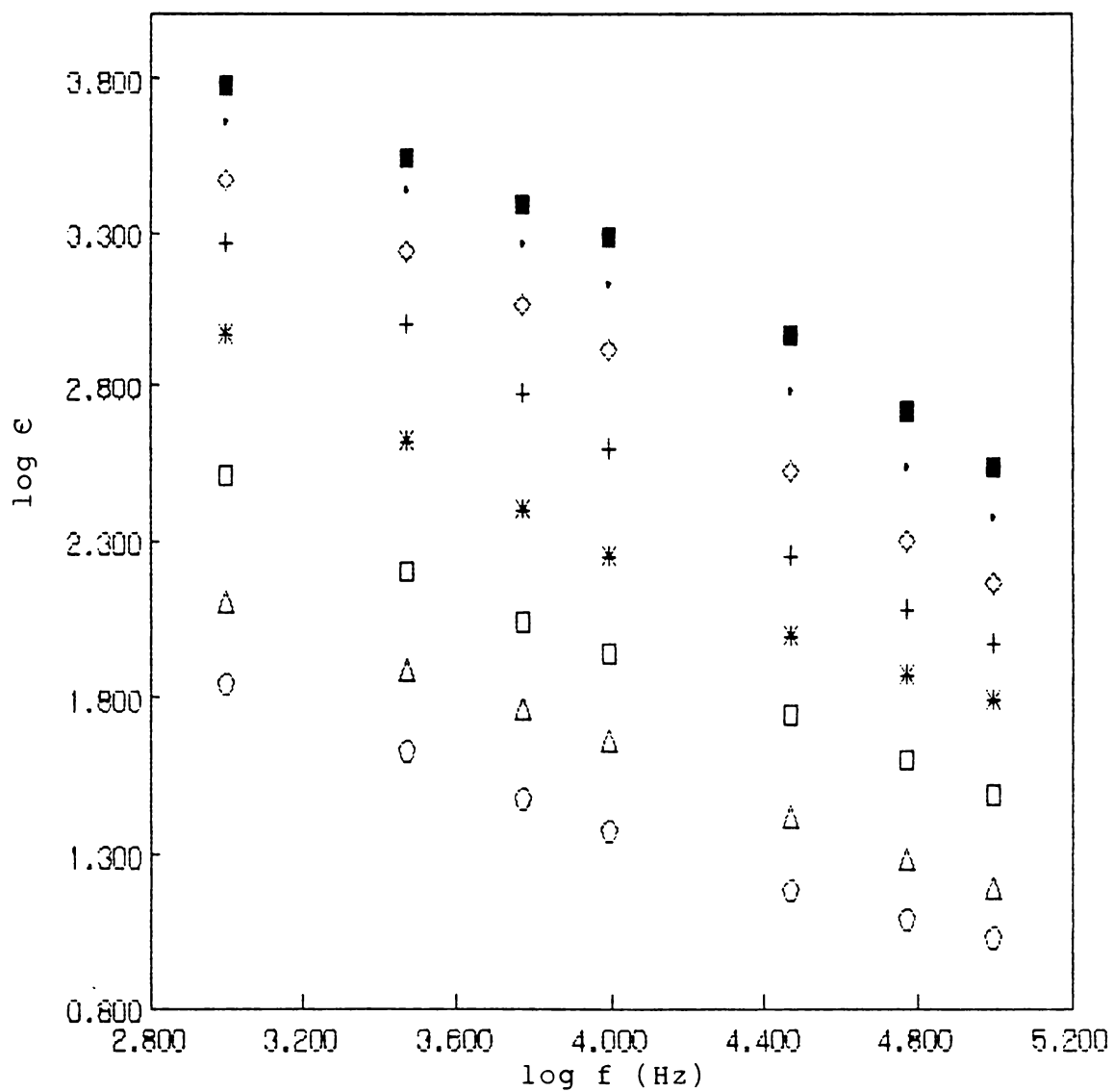


Fig.11.11.2: Plot of log of the dielectric constant versus log f for  $\text{PAT}_2\text{OD}_4$

○ - 140 K ; △ - 170 K ; □ - 200 K ; \* - 230 K  
 + - 260 K ; ◇ - 290 K ; · - 320 K ; ■ - 350 K

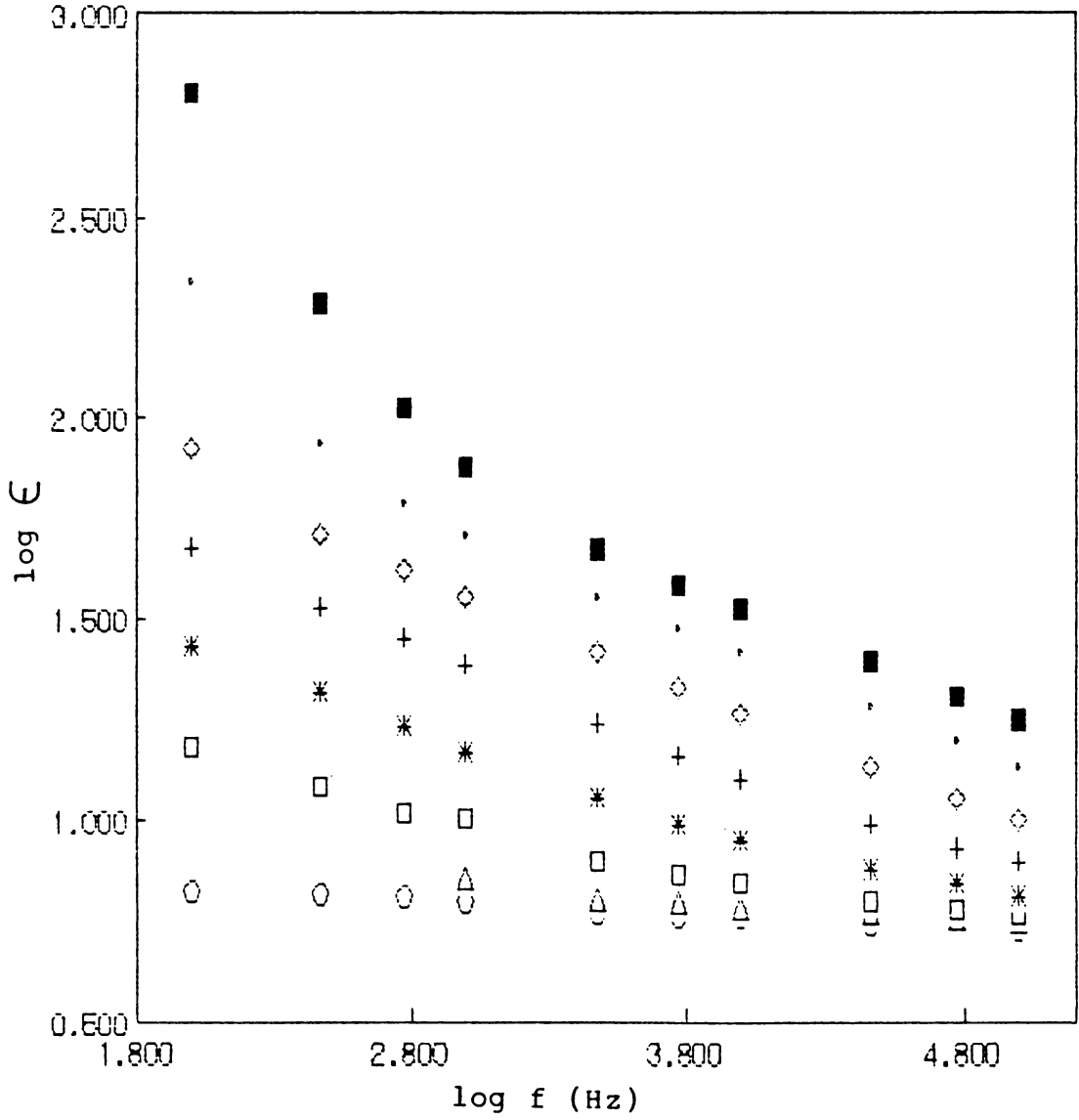


Fig.11.12.1: Plot of log of the dielectric constant versus log f for PAT<sub>2</sub>D<sub>4</sub>.

○ - 140 K ; △ - 170 K ; □ - 200 K ; \* - 230 K  
 + - 260 K ; ◇ - 290 K ; · - 320 K ; ■ - 350 K

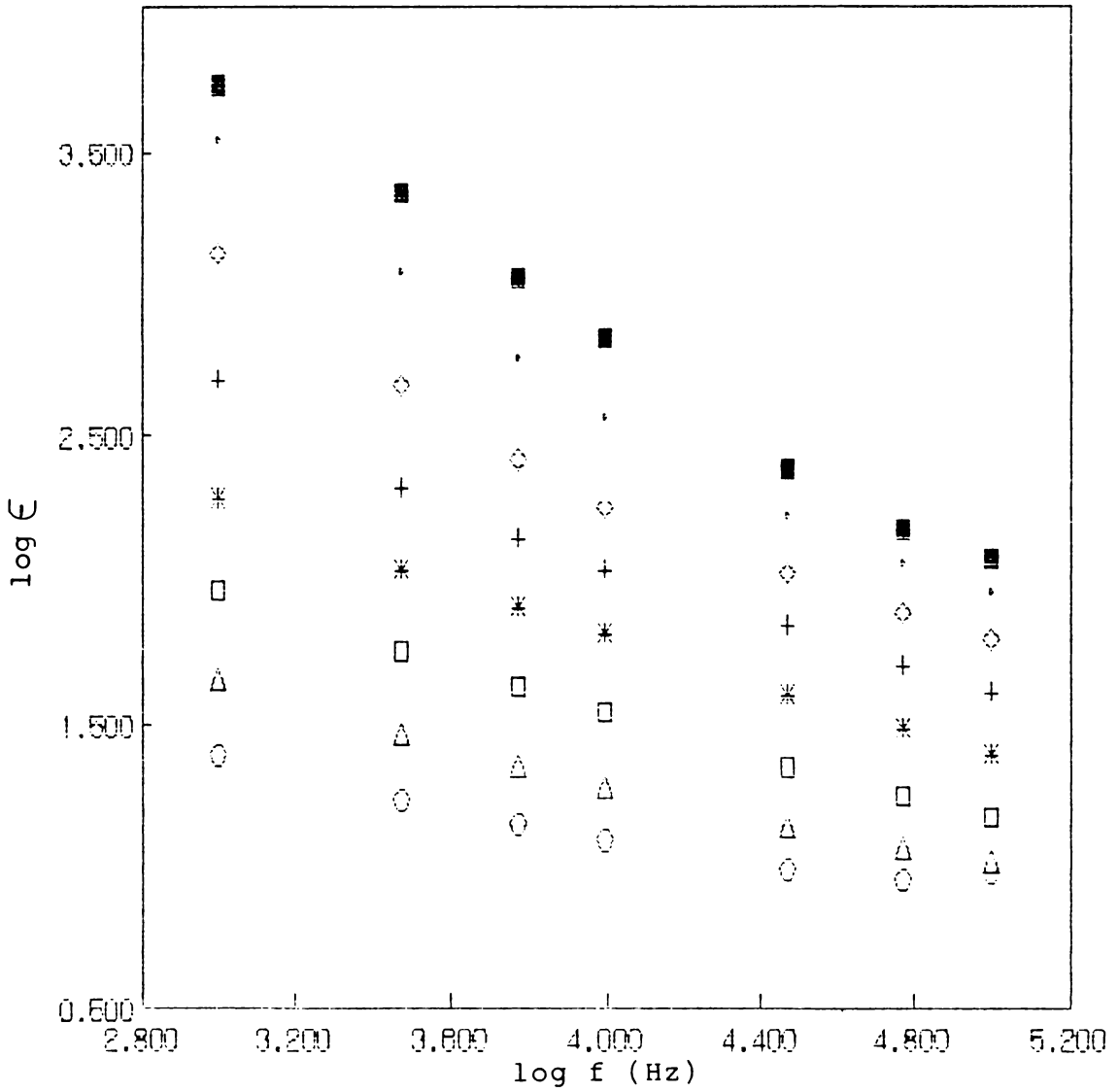


Fig.11.12.2: Plot of log of the dielectric constant versus log f for  $\text{PAT}_2\text{OD}_4$ .

○ - 140 K ; △ - 170 K ; □ - 200 K ; \* - 230 K  
 + - 260 K ; ◇ - 290 K ; • - 320 K ; ■ - 350 K

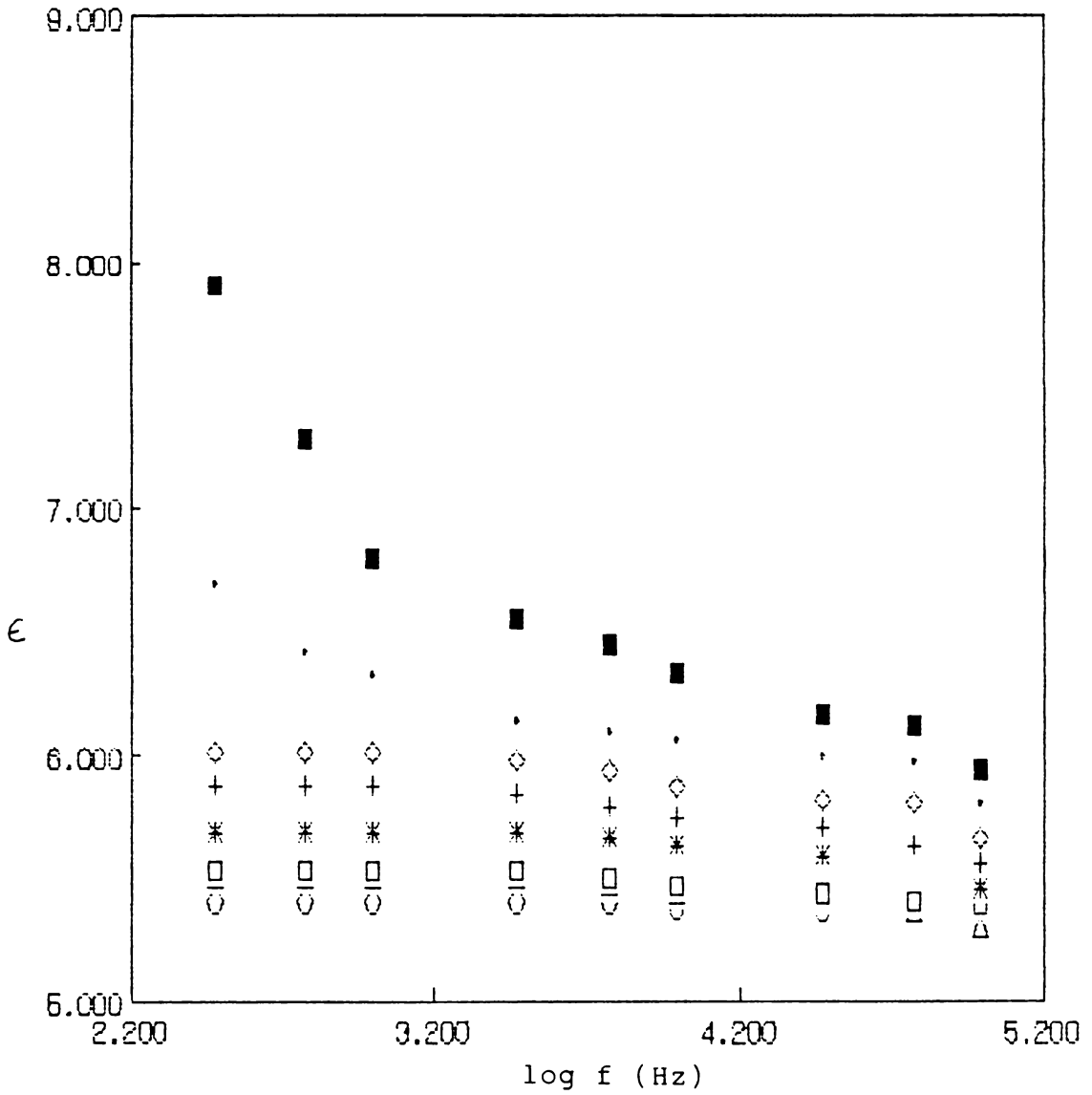


Fig.11.13.1: Plot of log of dielectric constant versus log f for  $\text{PAT}_3\text{D}_4$ .

○ - 140 K ; △ - 170 K ; □ - 200 K ; ✱ - 230 K  
 + - 260 K ; ◇ - 290 K ; • - 320 K ; ■ - 350 K

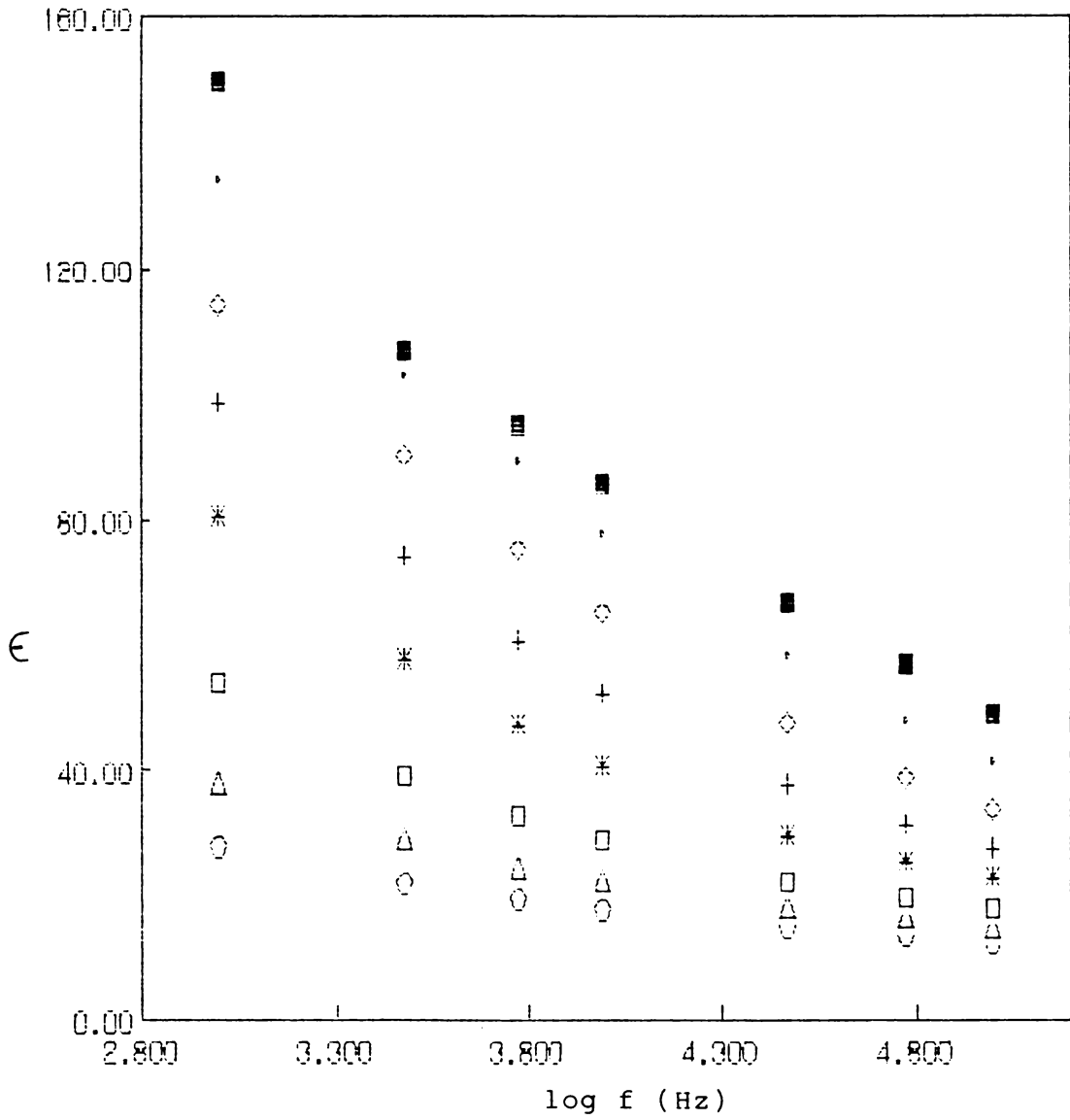


Fig.11.13.2: Plot of dielectric constant versus log f for  $\text{PAT}_3\text{OD}_4$

○ - 140 K ; △ - 170 K ; □ - 200 K ; \* - 230 K

+ - 260 K ; ◇ - 290 K ; • - 320 K ; ■ - 350 K

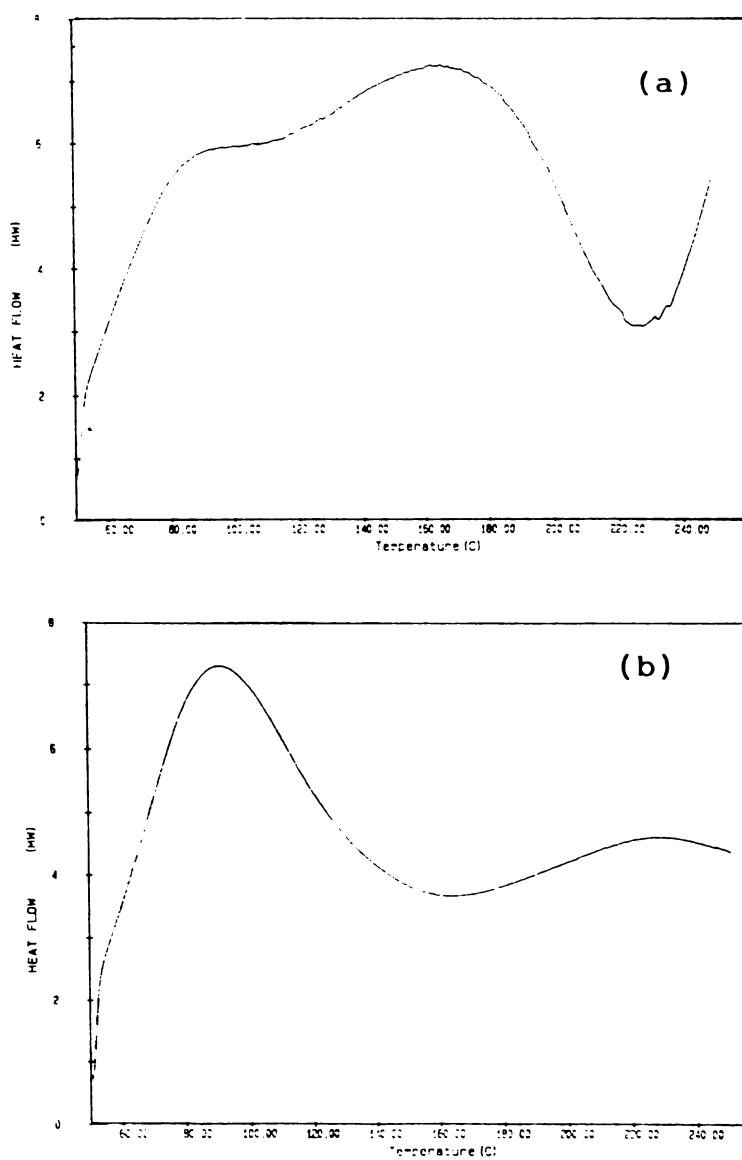


Fig.11.14.1: Effect of doping on the DSC thermogram of  $PAT_1$ .  
(a)  $PAT_1$  ; (b)  $PAT_1D_4$

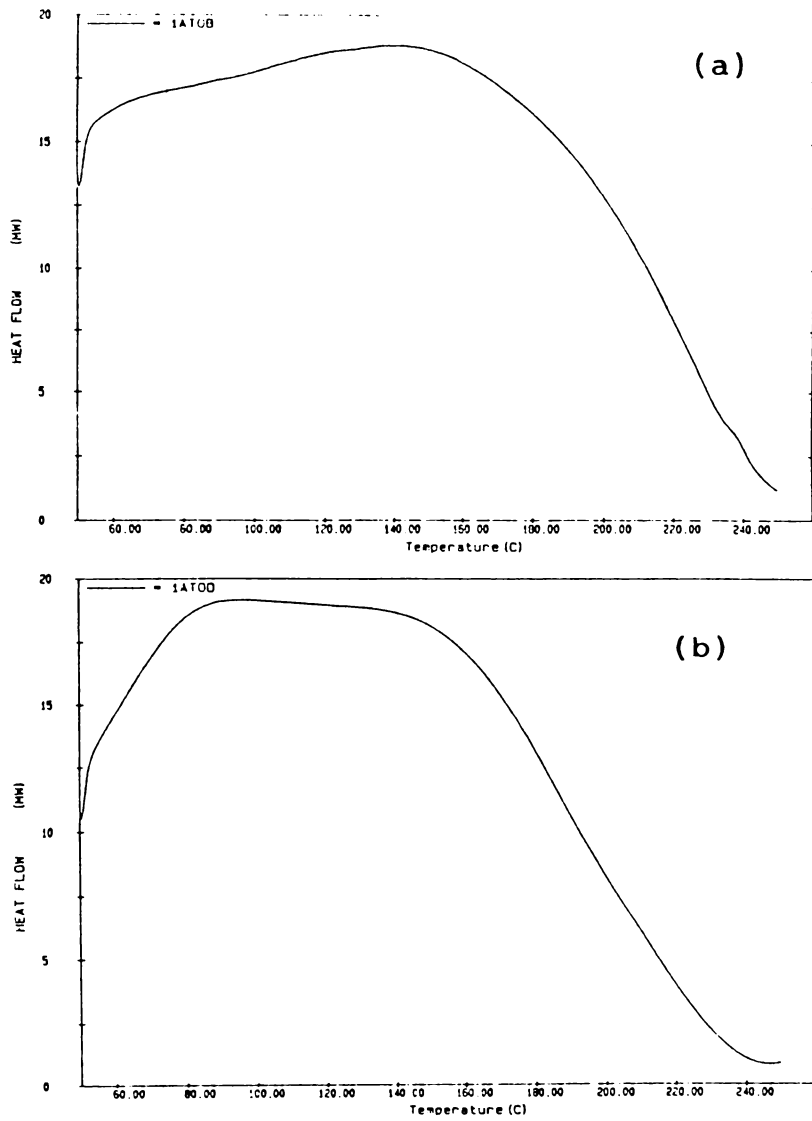


Fig.11.14.2: Effect of doping on the DSC thermogram of  $\text{PAT}_1\text{O}$ .

(a)  $\text{PAT}_1\text{O}$  ; (b)  $\text{PAT}_1\text{OD}_4$

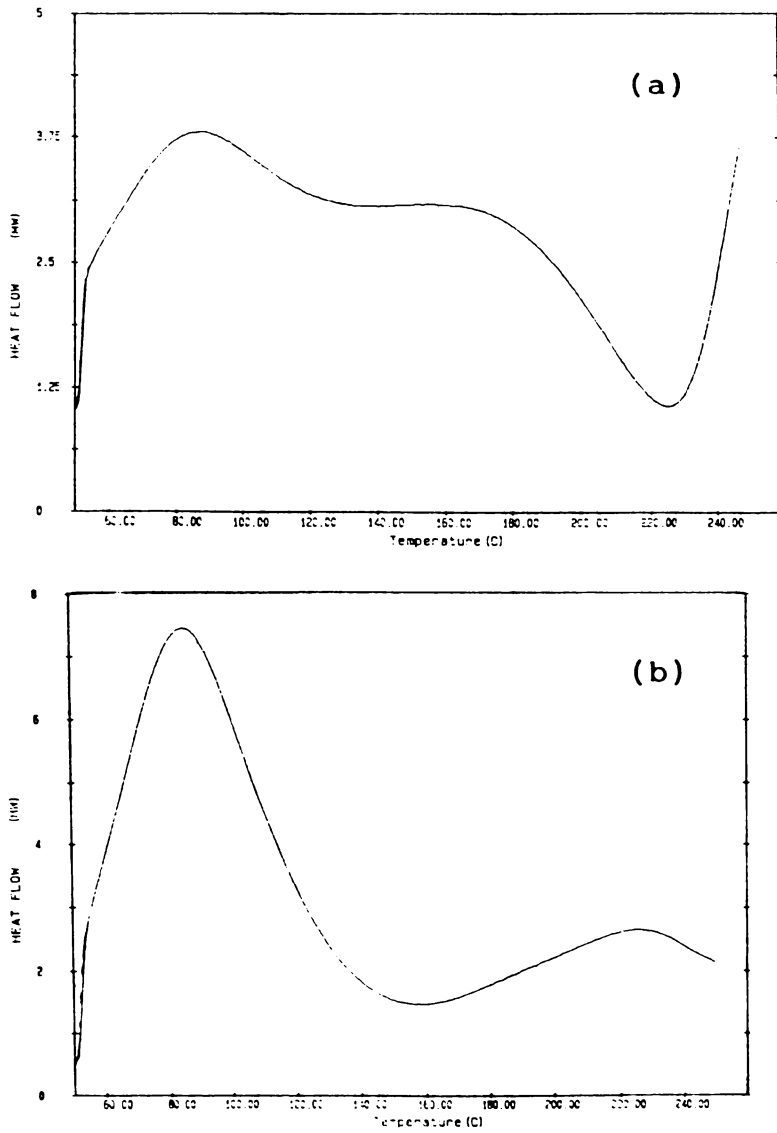


Fig.11.15.1: Effect of doping on the DSC thermogram of  $PAT_2$ .

(a)  $PAT_2$  ; (b)  $PAT_2D_4$

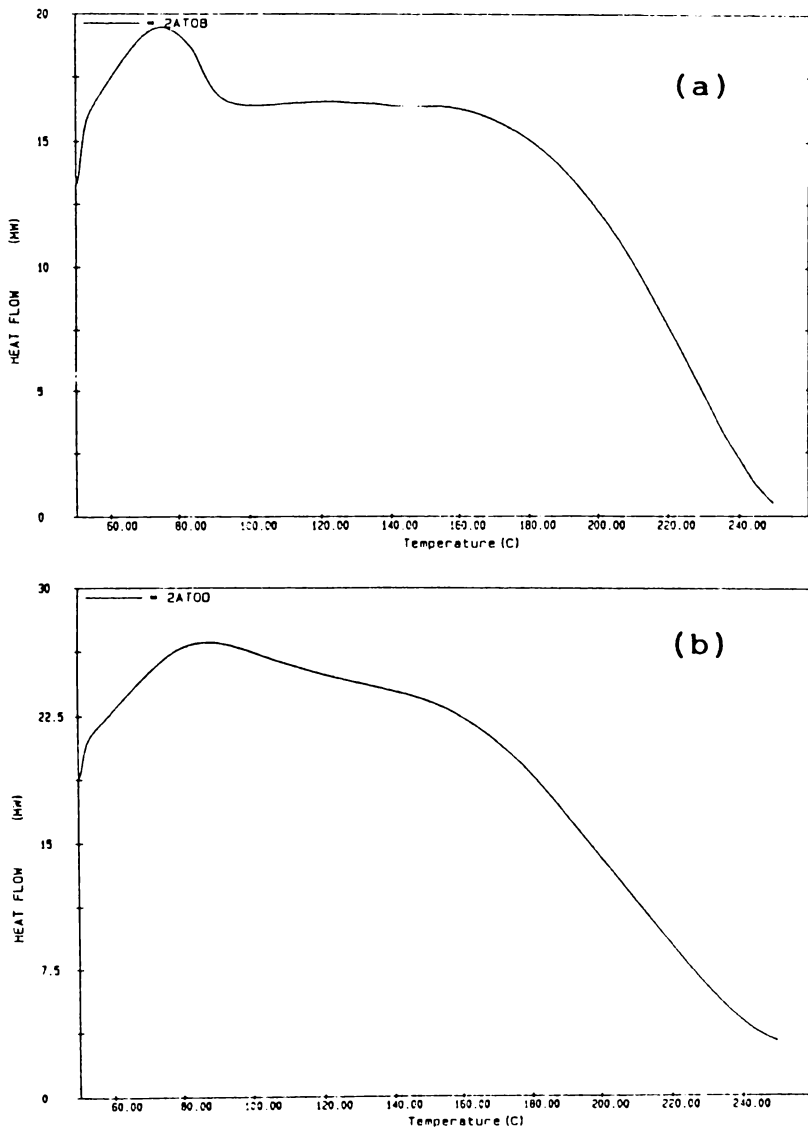


Fig.11.15.2: Effect of doping on the DSC thermogram of  $PAT_2O$ .  
(a)  $PAT_2O$  ; (b)  $PAT_2OD_4$

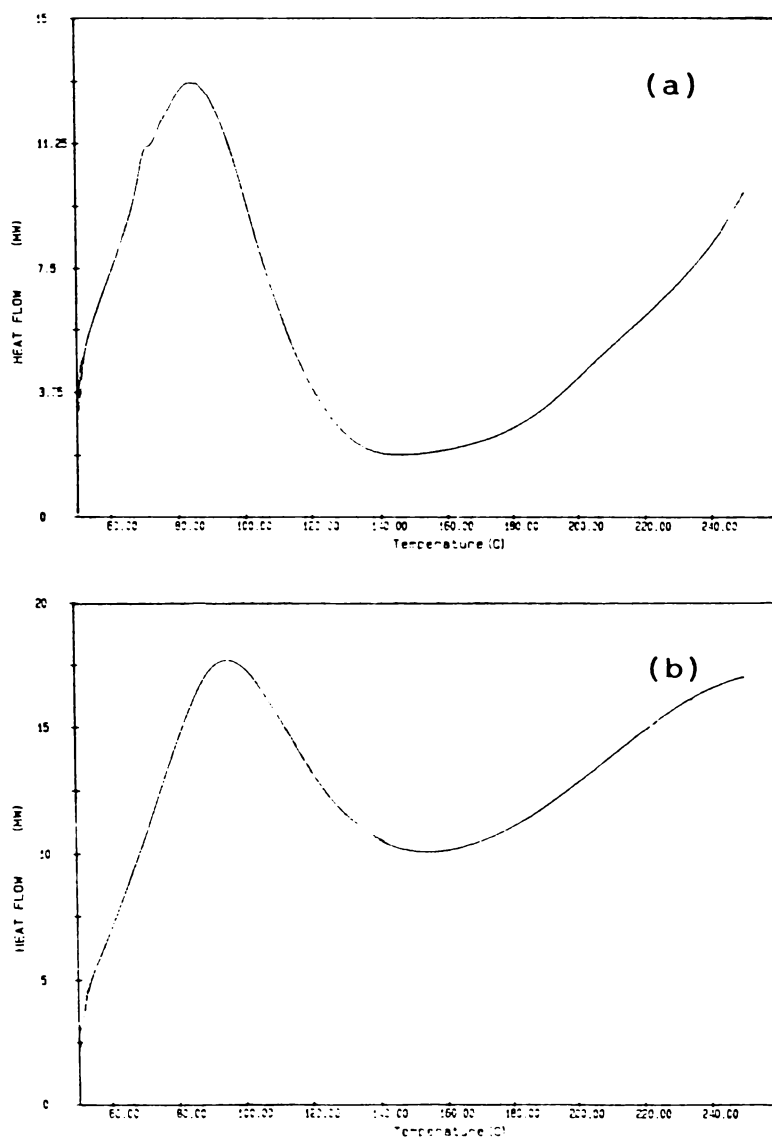


Fig.11.16.1: Effect of doping on the DSC thermogram of  $PAT_3$ .  
(a)  $PAT_3$  ; (b)  $PAT_3D_4$

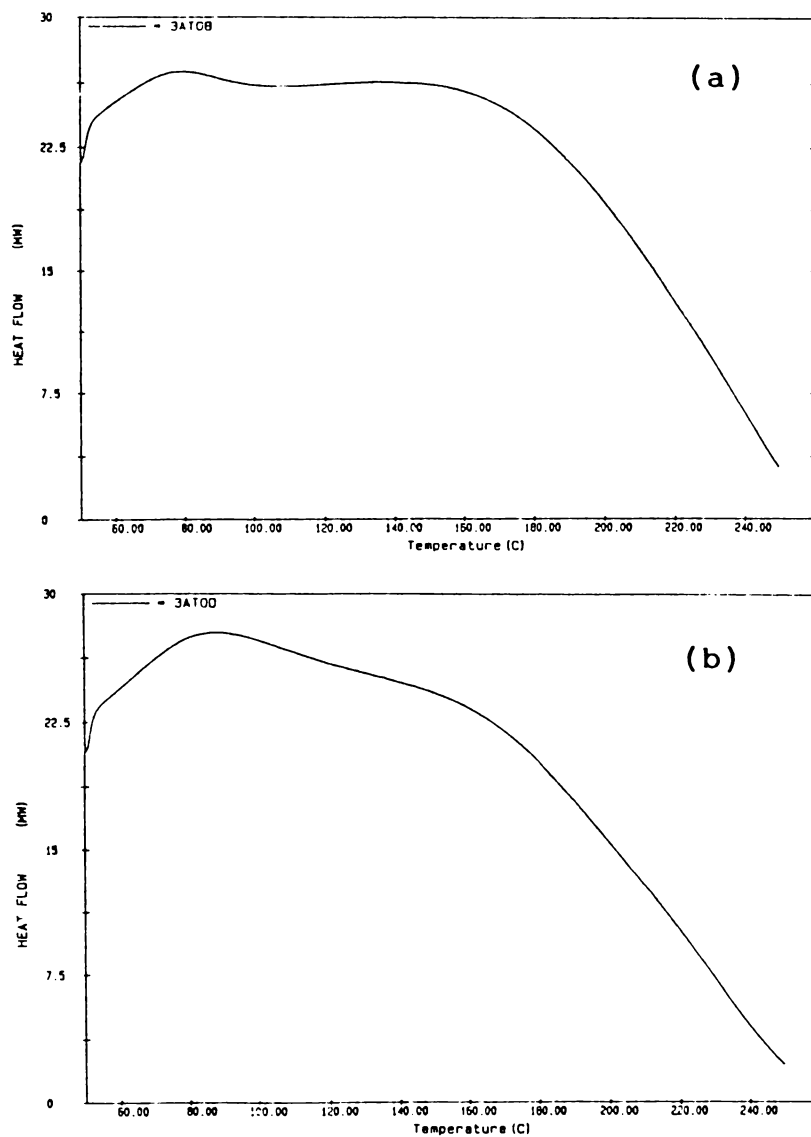


Fig.11.16.2: Effect of doping on the DSC thermogram of  $\text{PAT}_3\text{O}$ .

(a)  $\text{PAT}_3\text{O}$  ; (b)  $\text{PAT}_3\text{OD}_4$

their heavily doped forms show only a very broad hump with onset at about 50°C and spanning over a wide temperature range. The pronounced influence of the oligomers on the characteristics of the copolymers is well evidenced by these thermograms. They also clearly show that the nature of the pristine base is modified by the incorporation of the dopant.

#### 11.4 CONCLUSIONS

The oligomer-containing copolymers show higher values for conductivity and dielectric constant compared to the corresponding oligomer-free compounds. The magnitudes of conductivity and dielectric constant for the copolymers depend on the proportion of aniline repeat units in the copolymer. As the ratio of the aniline repeat units in the copolymer increases the conductivity and dielectric constant also increase.

Analysis of the temperature dependence of dc conductivity and the frequency as well as temperature dependence of ac conductivity and dielectric constant observed in this study shows that it is appropriate to consider charge hopping among fixed polaron sites to explain the charge transport in the heavily doped copolymers whereas a thermal activation mechanism is appropriate for conduction in the pristine bases.

**11.5 REFERENCES**

- [1] D.Vachon, R.O.Angus, Jr., F.L.Lu, M.Nowak, Z.X.Liu, H.Schaffer, F.Wudl and A.J.Heeger, *Synth. Met.* **18** (1987) 297.
- [2] A.G.MacDiarmid, J.C.Chiang, A.F.Ritcher and A.J.Epstein, *Synth. Met.* **18** (1987) 285.
- [3] A.F.Diaz and J.A.Logan, *J. Electroanal. Chem. Interfacial Electrochem.* **111** (1980) 111.
- [4] J.C.Chiang and A.G.MacDiarmid, *Synth. Met.* **13** (1986) 193.
- [5] T.Ohsaka, Y.Ohnuki, N.Oyama, G.Katagiri and K.Kamisako, *J. Electroanal. Chem. Interfacial Electrochem.* **161** (1986) 305.
- [6] Y.Cao, S.Li, Z.Xue and D.Guo, *Synth. Met.* **16** (1986) 305.
- [7] J.Tang, X.Jing, B.Wang and F.Wang, *Synth. Met.* **24** (1988) 231.

- [8] K.L.Tan, B.T.G.Tan, E.T.Kang, and K.G.Neoh, *Phys. Rev. B* **39** (1989) 8070.
- [9] B.Wehrle, H.H.Limbach, J.Mortensen and J.Heinze, *Angew. Chem Int. Ed. Engl. Adv. Mater.* **28** (1989) 1741.
- [10] J.P.Travers, J.Chroboczek, F.Devreux, F.Genoud, M.Nechtschein, A.Syed, E.M.Genies and C.Tsintavis, *Mol. Cryst. Liq. Cryst.* **121** (1985) 195.
- [11] J.Linger, *Solid State Commun.* **26** (1978) 839.
- [12] F.Wudl, R.O.Angus, Jr., F.L.Lu, P.M.Allemand, D.J.Vachon, M.Nowak, Z.X.Liu and A.J.Heeger, *J. Am. Chem. Soc.* **109** (1987) 3677.
- [13] Y.W.Park, Y.S.Lee, C.Park, L.W.Shacklette and R.H.Baughman, *Solid State Commun.* **63** (1987) 1063.
- [14] G.E.Wnek, *Polymer Prepr.* **26** (1985) 277.
- [15] P.M.McManus, S.C.Yang and R.J.Cushman, *J. Chem. Soc. Chem. Commun.* (1985) 1156.

- [16] P.M.McManus, R.J.Cushman and S.C.Yang, *J. Phys. Chem.* **91** (1987) 744.
- [17] R.J.Cushman, P.M.McManus and S.C.Yang, *Makromol. Chem. Rapid Commun.* **8** (1987) 69.
- [18] A.P.Monkman, D.Bloor, G.C.Stevens and J.C.H.Stevens, *J. Phys. B* **20** (1987) 1337.
- [19] F.Zuo, M.Angelopoulos, A.G.MacDiarmid and A.J.Epstein  
(a) *Phys. Rev. B* **36** (1987) 3475; (b) *Phys. Rev. B* **39**  
(1989) 3570.
- [20] M.Angelopoulos, A.Ray, A.G.MacDiarmid and  
A.J.Epstein, *Synth. Met.* **21** (1987) 21.
- [21] J.P.Travers and N.Nechtschein, *Synth. Met.* **21** (1987)  
135.
- [22] M.Nechtschein, C.Santier, J.P.Travers, J.Chroboczek,  
A.Alix and M.Ripert, *Synth. Met.* **18** (1987) 311.
- [23] H.H.S.Javadi, F.Zuo, M.Angelopoulos, A.G.MacDiarmid  
and A.J.Epstein, *Mol. Cryst. Liq. Cryst.* **160**  
(1988) 225.

- [24] H.H.S.Javadi, M.Angelopoulos, A.G.MacDiarmid and A.J.Epstein, *Synth. Met.* **26** (1988) 1.
- [25] M.Angelopoulos, G.E.Asturias, S.P.Ermer, A.Ray, E.M.Scherr, A.G.MacDiarmid, M.Akhtar, Z.Kiss and A.J.Epstein, *Mol. Cryst. Liq. Cryst.* **160** (1988) 151.
- [26] M.X.Wan, A.G.MacDiarmid and A.J.Epstein, *Solid State Sci.* **76** (1987) 216.
- [27] T.Hayashi, Y.Hirai, H.Tanaka and T.Nishi, *Jpn. Phys.* **26** (1987) L1800.
- [28] K.G.Neoh, E.T.Kang and K.L.Tan, *Eur. Polym. J.* **26** (1990) 403.
- [29] J.C.Chiang and A.G.MacDiarmid, *synth. Met.* **13** (1986) 193.
- [30] J.J.Langer, *Synth. Met.* **20** (1987) 35.
- [31] J.J.Langer, *Mater. Sci.* **14** (1988) 41.
- [32] J.Tang, X.Jing, B.Wang and F.Wang, *Synth. Met.* **24** (1988) 231.
- [33] Y.Furukawa, T.Hara, Y.Hyodo and I.Harada, *Synth. Met.* **16** (1986) 189.

## Chapter 12

### SUMMARY AND CONCLUSIONS

The electrical characteristics of poly(meta-toluidine), copolymers of aniline with meta-toluidine in various ratios and their acid-doped forms have been studied. The materials in as-prepared form invariably contain oligomeric substances which can be extracted with methanol. To ascertain the influence of oligomeric impurities, studies were carried out with oligomer-free as well as with oligomer-containing materials. The retention of moisture by the oligomer-containing polymer is higher than that by the purified material as can be seen from the DSC thermograms. The retained moisture is released by the materials slowly above the ambient temperature, becomes very rapid above 60°C and is almost complete above 100°C. The variation in dc and ac electrical conductivity and dielectric constant effected by the presence of oligomeric impurities are quite noticeable.

The incorporation of meta-toluidine in the copolymer is confirmed by the IR spectrum. Meta-toluidine modifies the electrical properties significantly. All the

polymer bases are strong insulators. Doping with acid enhances the electrical conductivity as well as dielectric constant in all the polymer samples. However, the influence of dopant varies depending on the nature of the polymer. It is also found that as the ratio of meta-toluidine in the copolymer increases, the electrical conductivity as well as dielectric constant decreases. The effect of dopant concentration on the properties of poly(meta-toluidine) and the copolymers are illustrated in Fig.12.1, 12.2 and 12.3. It can be seen from these figures that the values for electrical properties reach a saturation when the concentration of the dopant is increased.

Depending on the degree of doping, the conduction mechanism registers a change. In pristine copolymer bases and their lightly doped forms the conduction seems to be by thermal activation. At higher concentrations of dopant a variable-range-hopping mechanism is proposed as revealed from the analysis of the conductivity data. The large value of dielectric constant observed at high dopant levels may be due to the contributions of the structural units as well as of the charge

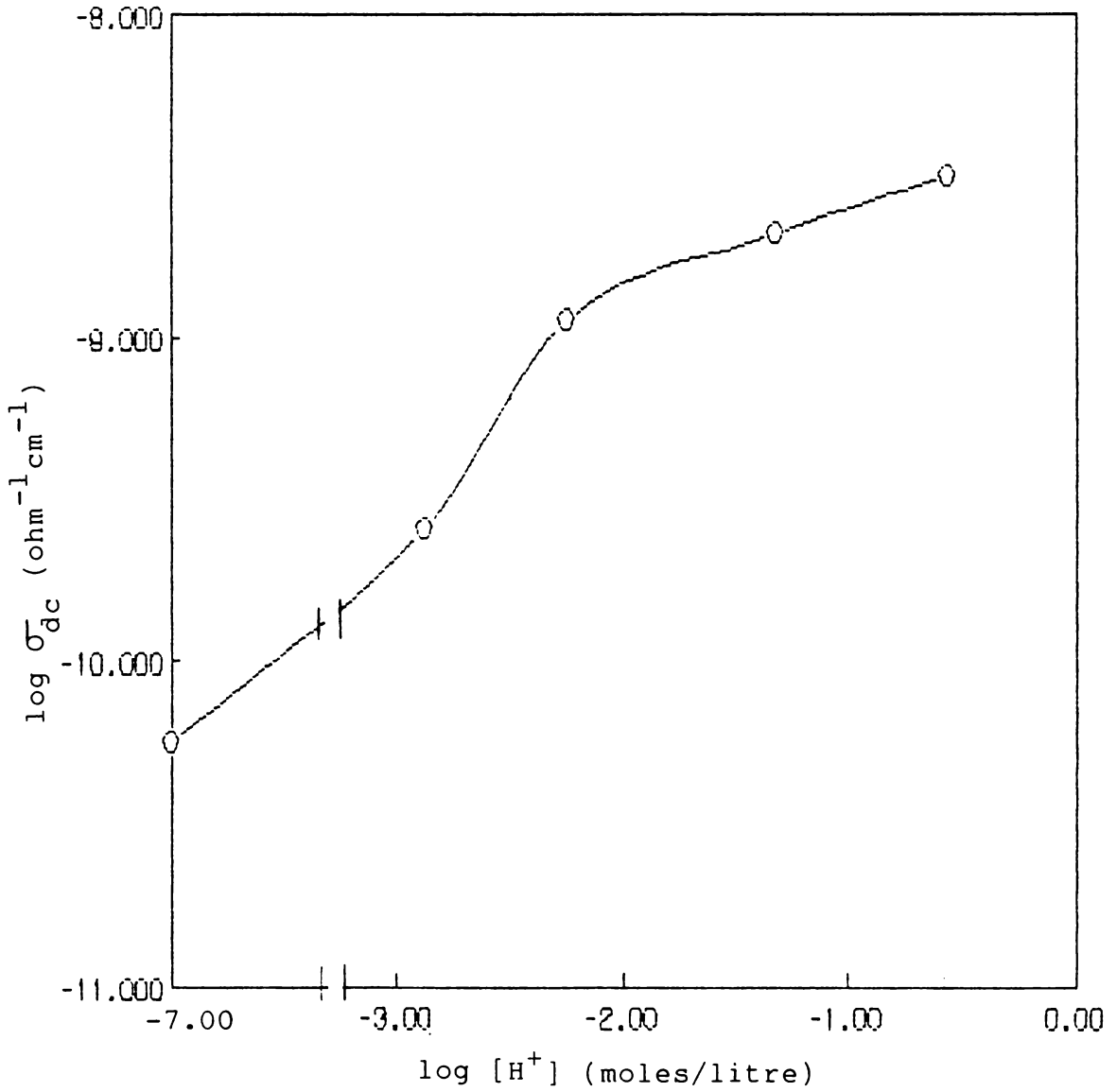


Fig.12.1: Plot of dc conductivity versus dopant acid concentration for PT.

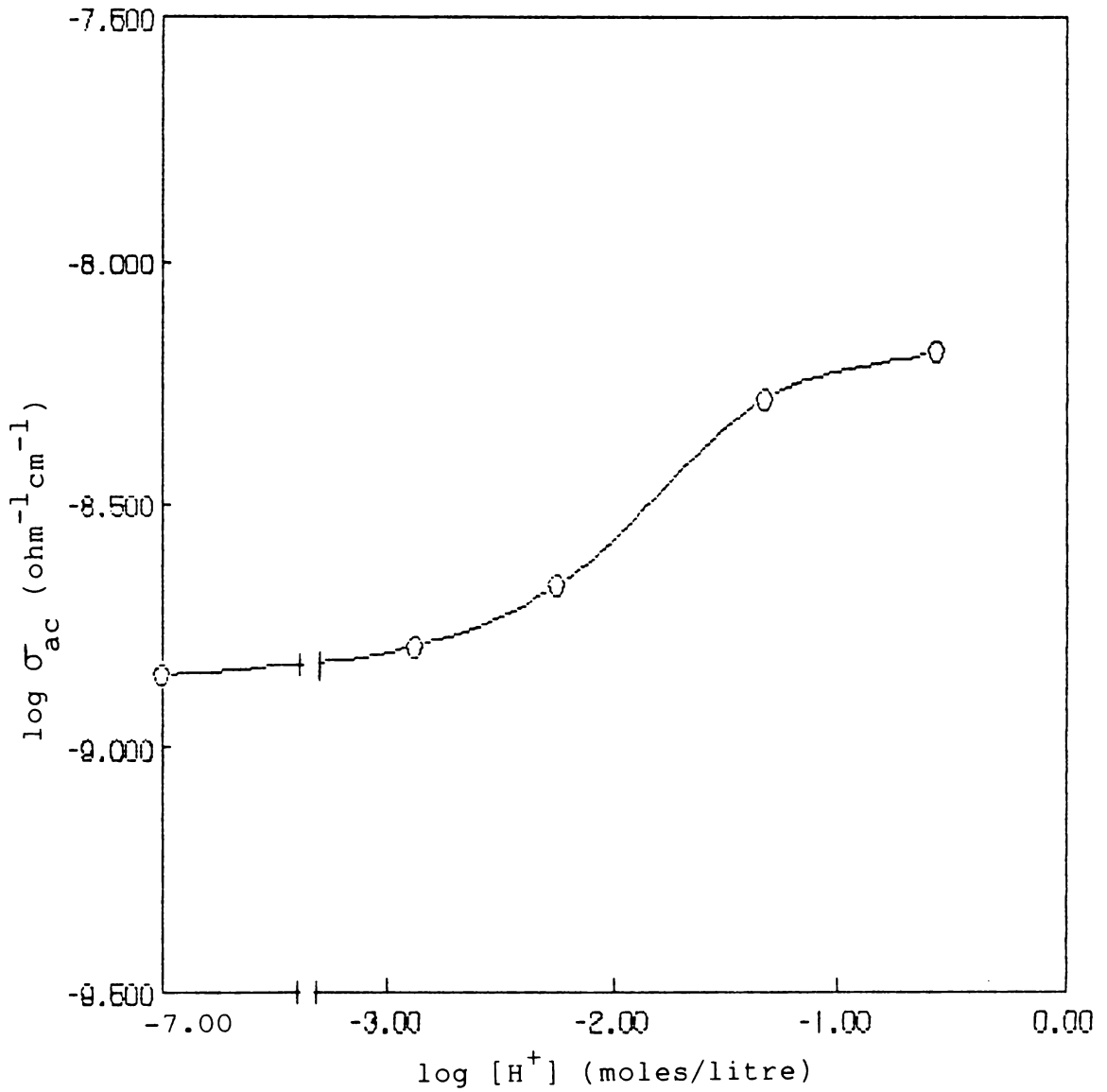


Fig.12.2: Plot of ac conductivity versus dopant acid concentration for PT.

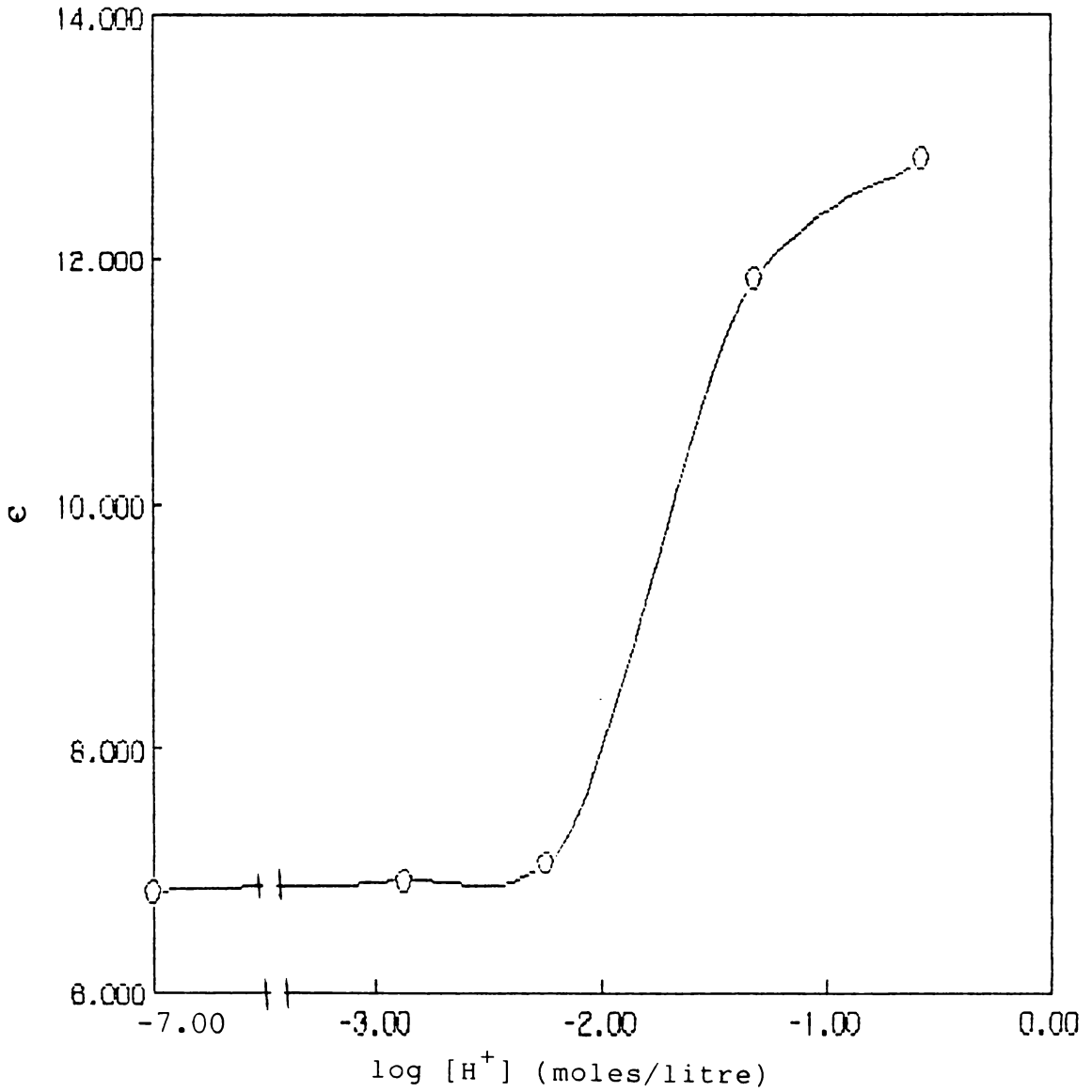


Fig.12.3: Plot of dielectric constant versus dopant acid concentration for PT.

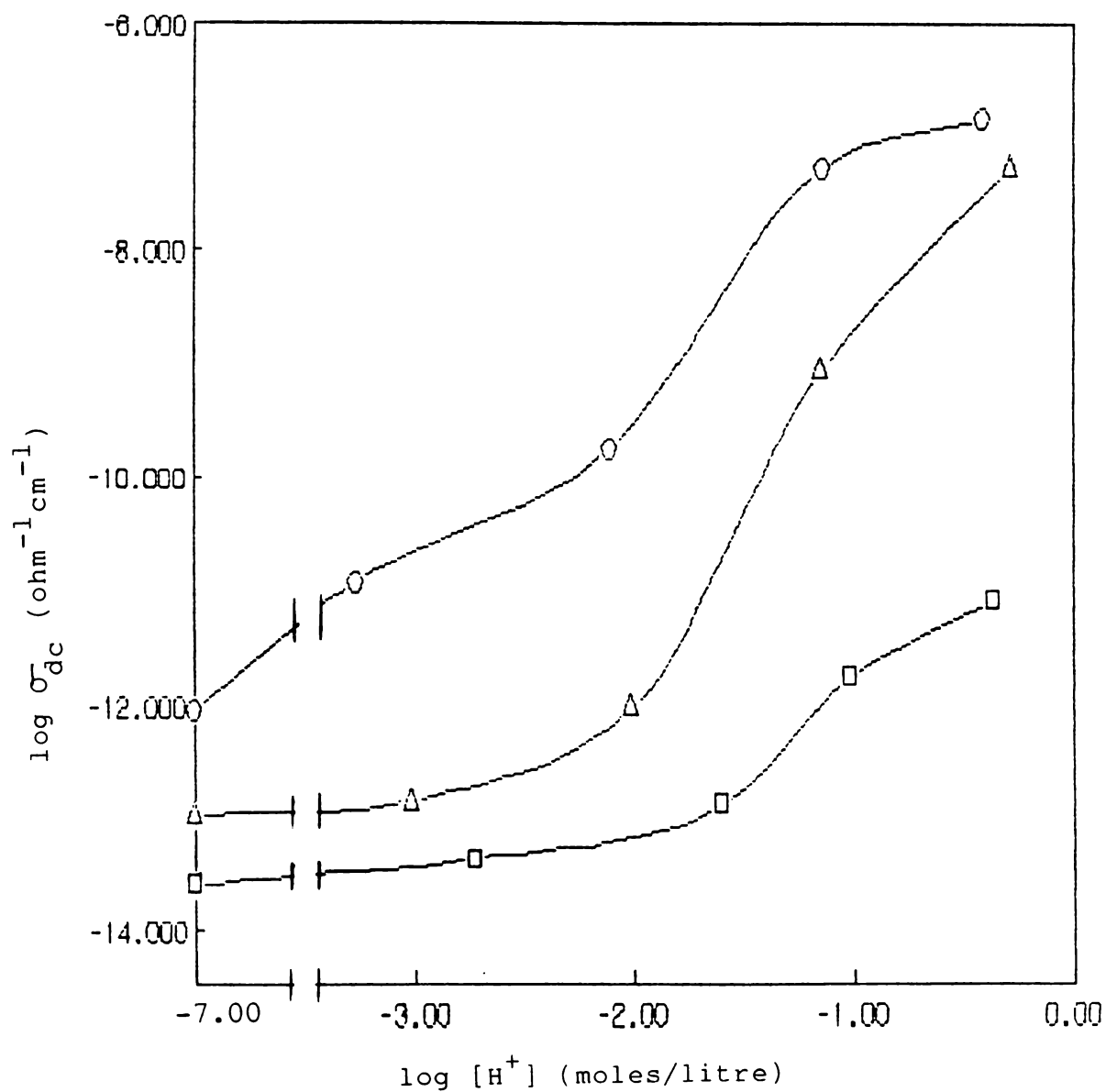


Fig.12.4: Plot of dc conductivity versus dopant acid concentration for PAT<sub>1</sub>, PAT<sub>2</sub> and PAT<sub>3</sub>.

○ , △ , □

carriers generated by doping. The large dielectric constant associated with the doped forms of  $PAT_1$  and  $PAT_2$  apparently makes them suitable candidates for charge storage applications.

\* \* \*